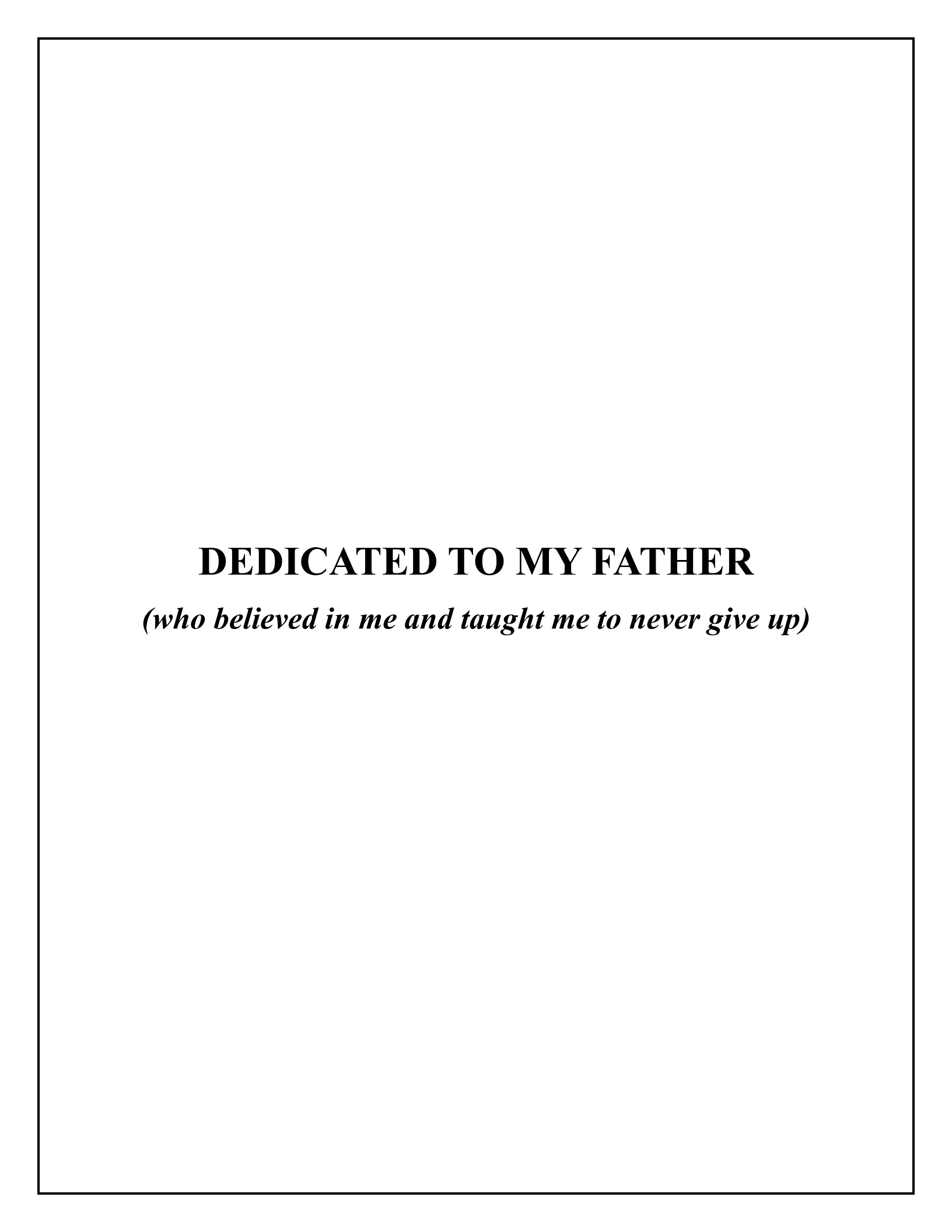
INVESTIGATING THE ROLE OF AtHMGB15 IN DIFFERENTIATION INDUCED PROGRAMMED CELL DEATH DURING POLLEN DEVELOPMENT

Thesis submitted for the degree of Doctor of Philosophy (Sc.) in Biotechnology

by RUBY BISWAS

UNIVERSITY OF CALCUTTA
2024



ACKNOWLEDGEMENT

Today as I look back to the day I began my journey, I cannot be anything but grateful to all the experiences and people I have had and met in these 6 years. Ma and Baba thank you for always believing in me and encouraging me to do what I love. Dr. Ritu Biswas, without you I wouldn't be prepared for any challenges of the world.

I express my sincere gratitude to my supervisor Prof. Shubho Chaudhuri for his enthusiasm, encouragement, knowledge and guidance in both academics and life. His patience to hear my half-baked ideas and then guiding me to transform them into refined forms. This would have never been possible without his unwavering support and supervision.

The Integrated MSc-PhD program of Bose Institute allowed me to explore the depths of science and prepared me with the skills I needed for my PhD project. I owe so much to the faculty members of Bose Institute who were instrumental in designing such a wonderful program. I am grateful to the Director of Bose Institute and DST for providing me with the fellowship while pursuing my research work. I would also like to take an opportunity to thank Prof. Gaurab Gangopadhyay and Prof. Pallob Kundu for their insightful queries, suggestions and comments on my work as well as their encouragement.

I am thankful to Dr. Biplab Majhi and Dr. Koushik Sarkar at IISER Kolkata for allowing and assisting me to use their GC-MS facility for my research work.

I would like to extend my gratitude to Dr. Adrita Roy, Dr. Dipan Roy, Dr. Amit Paul, Dr. Rwitie Mallik, Dr. Pratiti Dasgupta, Dr. Jinia Chakrabarty, Dr. Sambit Dutta and Dr. Anindya Kundu for their invaluable advices. My heartfelt gratitude to my lab mates Sonal Sachdev, Sabini Basu, Vishal Roy, Ayantika Nandi and Rukshar Parveen for their cooperation, care, sympathy and patience.

My earnest appreciation goes out to Bapi Bose, Nadiram Kayal, Binod Turi, Uttam Das, Mrinal Das, Sheolee Ghosh Chakraborty, and Asim Kumar Nath for their technical assistance.

I am thankful to Mouli Naskar, Rijhdyuti Dutta and Suchismita Chowdhury for sincerely working under my supervision. Their contributions are appreciated and gratefully acknowledged.

I am truly thankful to my friends Samrat Mitra, Nilanjana Hazra, Debopriya Bose, Dr. Koustav Bhakta, Dr. Tushar Chakraborty and Dr. Prateek Chawla for their unflinching generosity and support. Dr. Mousumi Bhattacharyya for her insight and kind advices whenever required. Sangeeta Chatterjee for her warmth and encouragement. Arpan Dutta for keeping me inspired with his well-timed share of humour, and advices in these past months.

Ruby Biswas

ABBREVIATIONS

ARID AT Rich Interaction Domain

HMG High Mobility Group

dPCD Developmental Programmed Cell Death

DNA Deoxynucleic acid

RNA Ribonucleic acid

DEPC Diethyl pyrocarbonate

q-RTPCR Quantitative real time reverse transcription PCR

ChIP Chomatin Immunoprecipitation

GUS β -glucuronidase

MUG 4-Methylumbelliferyl b-D-glucuronide

BiFC Bimolecular Fluorescence

YFP Yellow Fluorescent Protein

ROS Reactive Oxygen Species

FAA Formaldehyde Alcohol Acetic acid

FM4-64FX (N-(3-triethylammoniumpropyl)-4-(6-(4-

Diethylamino) Phenyl Hexatrienyl Pyridinium

Dibromide)

TUNEL Terminal Deoxynucleotidyl Transferase dUTP

Nick End Labelling

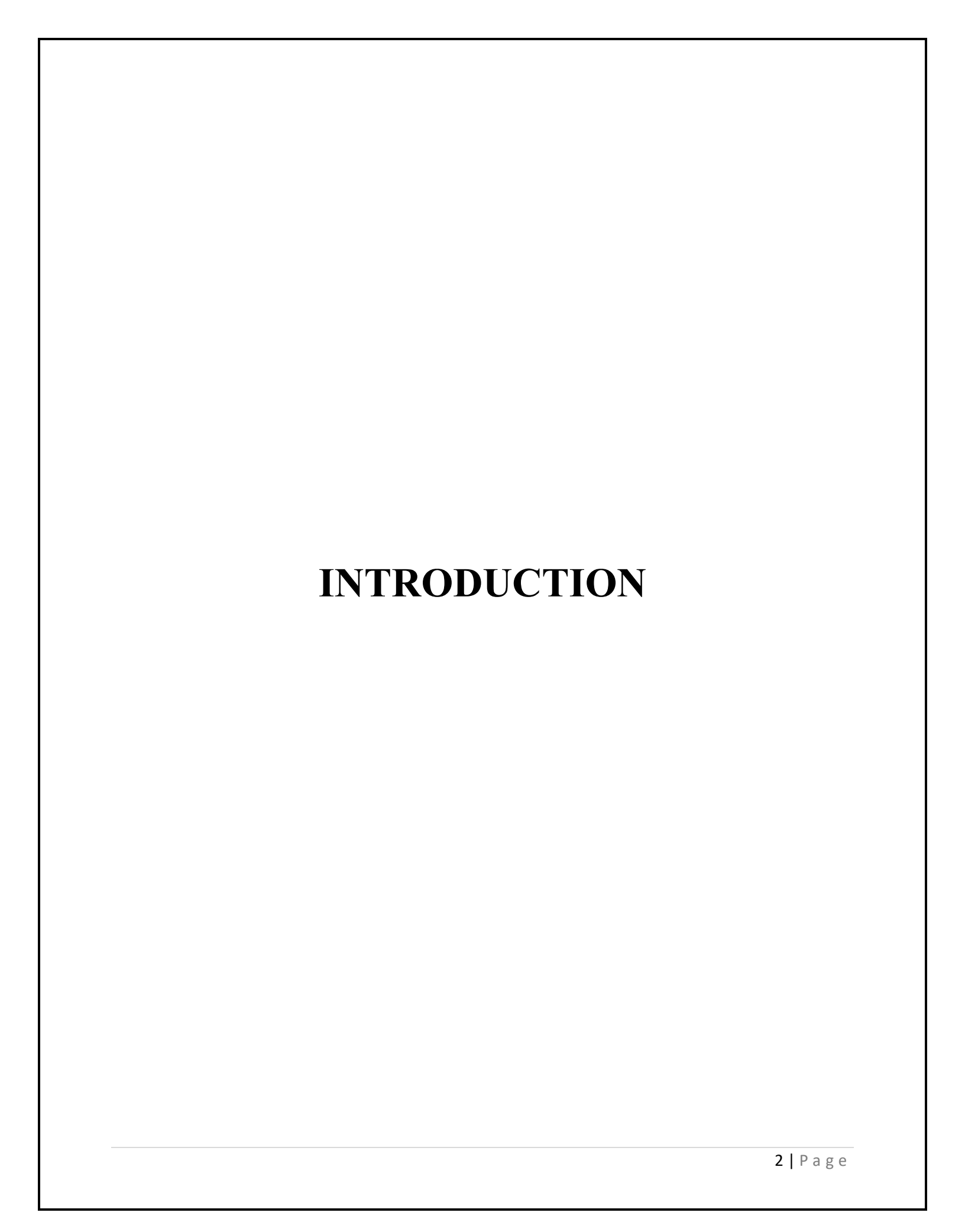
PGM Pollen Germination Media

TABLE OF CONTENTS

SL. NO.	SECTION	PAGE NO.
1.	ABSTRACT	1
2.	INTRODUCTION	2-53
3.	MATERIAL AND METHODS	54-92
4.	OBJECTIVES	93
5.	CHAPTER I:	94-128
	Study of tapetal function and degradation during pollen development in <i>athmgb15</i> and wild type.	;
6.	CHAPTER II:	129-150
	Study of pollen tube germination and growth in <i>athmgb15</i> and wild type	
7.	SUMMARY OF THE THESIS	151-153
8.	ANNEXURE	154-198
9.	WORK PRESENTED & LIST OF PUBLICATIONS	199

ABSTRACT

Male sterility is an outcome of improper coordination in the developmental processes in the male gametophytes of flowering plants. It has been shown that the temporal regulation of the function and degeneration via programmed cell death (PCD) of the somatic cell layer surrounding the developing pollen grains called tapetum, plays an important role in pollen development. This thesis attempts to the investigate the role of a nuclear architectural protein called the ARID-HMG protein 15, during the development of pollen grains. The comparative transcriptome analysis of different stages of anther development revealed differential regulation of gene clusters responsible for pollen maturation, PCD, actin binding and pollen germination in athmgb15 mutant compared to wildtype. As anther wax production is a function of tapetum necessary for pollen wall formation and pollen maturation, we estimated the anther wax content using GC-MS which revealed lower wax content in athmgb15. We demonstrated that AtHMGB15 shows an important regulatory role in controlling the expression of two pollen wall biosynthesis transcription factors namely, MYB21 and MYB24 using promoter assay. Semi thin section of anthers from different stages showed abnormal vacuolization in tapetal cells of athmgb15. TUNEL assay observations revealed prolonged PCD in AtHMGB15 loss of function mutant delayed anther dehiscence in simultaneously causing these mutants. Chromatin immunoprecipitation assay also indicated occupancy of AtHMGB15 in the promoters of PCD regulators and executer genes. Analysis of the bud transcriptome helped us identify the downregulation of actin-microfilament cluster in athmgb15. Since the distribution and arrangement of actin filaments in the pollen tube is critical for unidirectional growth, we visualised the f-actin in germinated pollen tubes of wild type and athmgb15 using rhodamine phalloidin. The observations indicated absence of f-actin polymers in the athmgb15 compared to the continuous f-actin observed in wild type pollen tubes. Our q-RTPCR data also showed downregulation of actin binding proteins like VLN2 and PRF4 in athmgb15. The study concludes with the interaction of AtHMGB15 and another nuclear protein ARP4 demonstrating their importance in the transcriptional regulation of pollen grain development.



AtHMGB15, an architectural protein

The variations in chromatin stability are dependent upon the interaction occurring int the hierarchical levels of chromatin organization namely, the intra-nucleosome, the internucleosome, and the non-histone architectural protein (Antosch et al., 2012; Mallik et al., 2020). There appears to be interplay between all these levels, such that one level can override another or act in a concerted manner (Antosch et al., 2012). The first level of stability in the nucleosome comes from the number and type of contacts exists between the core histones and the surrounding DNA, as well as protein-protein interactions within the core histone octamer (McBryant et al., 2006). The stability and organisation of the nucleosome is primarily dependent on the core histone variants, post-translational modifications that occur in the histones, and the linker histone binding to the DNA. (Bowman and Poirier, 2014). The arrangement of nucleosomes in an endwise manner in a linear chromatin array reveals the second level of organisation (McBryant et al., 2006). The interaction of the histone proteins in the nucleosome of a chromatin fibre with other adjacent chromatin fibres occurs through the amino terminal tails of the histone proteins (Erler et al., 2014). The intrinsic constraints by the chromatin interacting non-histone proteins is responsible for the third level of organisation in the chromatin architecture. (McBryant et al., 2006). These chromatin architectural proteins can, in some cases, circumvent the intrinsic constraints and impose their own topological effect, ensuing truly unique, self-assembling molecular complex that unquestionably impact the accessibility of the underlying DNA (McBryant et al., 2006).

The HMGs are the most abundant non histone proteins that is categorized into three classes based on the DNA binding domain namely, HMGA, HMGB and HMGN (Mallik et al., 2018). The HMGB family contains HMG-boxes, and the HMGN family contains nucleosome-binding domains (Mallik et al., 2018). The HMGA subfamily was grouped together because these proteins preferentially bind to the minor groove of AT-rich regions of DNA via several AT-hook motifs (Grasser, 2003). The AT-hook motif is a conserved DNA-binding motif commonly found in eukaryotes (Saha et al., 2023). HMGA proteins affect local chromatin structure in several ways, including bending, straightening, unwinding, and looping of substrate DNA, and they have been implicated in numerous DNA-based cellular processes (Saha et al., 2023).

AtHMGB15, is a plant exclusive unique architectural protein that belongs to the HMG-box superfamily protein having two DNA binding domains, one N-terminal ARID domain and a C-

terminal HMG-box domain (Mallik et al., 2020; Roy et al., 2016). AtHMGB15 is one of four members of the novel ARID-HMG group in Arabidopsis thaliana (Mallik et al., 2020; Roy et al., 2016). Biochemical analysis has shown that ARID-HMGs can bind to a variety of DNA topological structures majorly through the ARID domain whereas the HMG-box domain is involved in DNA bending and promoting transcription (Mallik et al., 2020; Roy et al., 2016). According to Mallik et al. the expression of AtHMGB15 transcript increases in wild type plants during early stages of cold stress in Arabidopsis seedlings (Mallik et al., 2020). Previous studies have shown that one of the members of ARID HMG, AtHMGB15, is highly expressed in flowers, mostly in the mature pollen (Xia et al., 2014). Xia et al. has shown the defective morphology of the mature pollen, although the percentage being 10% (Xia et al., 2014). Thus, AtHMGB15 plays a role not only in developmental stages of *Arabidopsis* but also during stress response. Moreover, the study has also indicated that the mutant pollen has retarded pollen tube growth (Xia et al., 2014). Since, HMG-box group of proteins are known to be involved in transcription regulation, we hypothesise that the mutation of AtHMGB15 can disrupt several signalling pathways that are directly linked to pollen maturation. Preliminary observation using homozygous athmgb15 knockout showed mutated pollen morphology with the following features: a) Most of the pollen from mutant plants were spherical in shape compared to elongated shape of wild type Arabidopsis pollen (Sachdev et al., 2024); b) the outermost exine wall of wild type pollen is ornamented which is completely defective in mutant plants (Sachdev et al., 2024). These observations show the importance of AtHMGB15 protein in pollen biology. The pollen grains or the male germline is indispensable to plants as carries the genetic information from one generation to another. Differentiation of the anther primordia into viable pollen grains requires developmental programmed cell death of the somatic tissue called tapetum, concerted with other cellular processes (Gómez et al., 2015). This programmed cell death is genetically coordinated in space and time to execute the death of various cell types within the anther that leads to its rupture and release of pollen grains (Varnier et al., 2005). The formation of viable pollen grains is heavily reliant on the nourishment it receives from the innermost anther wall lining the anther locule called tapetum (Chapman, 1987; Echlin, 1971b; El-Ghazaly, 1999). In the later stages of anther or pollen development, the tapetum undergoes PCD to release its contents stored from the secretory and biosynthetic phase into the anther locule (Hirano et al., 2008; Pacini, 2010, 2016; Parish and Li, 2010). Any form of precociousness or delay in PCD of the tapetal cells can have sever fertility defect in the plant (Lei and Liu, 2020; Yao et al., 2022; Zhang et al., 2006). Transcriptional variations in the expression of several transcriptional factors and executers controlling tapetal PCD have reported partial or complete male sterility in plants (Guo et al., 2022; Zhang et al., 2023a; Zheng et al., 2019). Therefore, the regulation of tapetal PCD has been established as an invaluable agronomic trait in the development of genetic male sterile lines in *Arabidopsis* as well as crop plants (Doll, 2023; Fábián et al., 2023; Hua et al., 2023; Jogam et al., 2024; Jung et al., 2005; Lavania et al., 2014; Wu et al., 2022).

An important factor governing transcriptional regulation in eukaryotes is overseen by architectural proteins (Lelli et al., 2012). Architectural proteins have been influencing DNA transactions by altering the flexibility of the chromatin structure (Gómez-Díaz and Corces, 2014). Based on their function, these proteins have been classified as wrappers, benders and bridgers (Gómez-Díaz and Corces, 2014; Mallik et al., 2018). The architectural proteins enable the stabilization and destabilization of the DNA structure and also helps in changing the accessibility of the DNA to the transcriptional machineries (Gómez-Díaz and Corces, 2014; Werner and Burley, 1997). In this thesis we have extensively, studied the role of AtHMGB15, an architectural protein in the regulation of genes responsible for tapetal function and degradation during pollen development.

Origin of tapetum in anther sac

The anther primordia arise from the floral meristem that differentiates into the male gametophytic body consisting of both reproductive and reproductive cells (Zhang and Yang, 2014). This demarcation in functional segregation is implemented by signals from the meiotic cells that suppress the germline cell fate in its adjacent cells (Strome and Updike, 2015). Specification of the anther primordia into specialized tissue begins with three multipotent cell layers called L1, L2, and L3, each layer further differentiates to perform their respective functions (Åstrand et al., 2021; Walbot and Egger, 2016a). The fate of the L1 layer is to form the epidermis and stomium of the anther tissue (Nagata and Abe, 2023; Walbot and Egger, 2016b). The L2 layer gives rise to two types of cells, the reproductive cells and the non-reproductive cells (Walbot and Egger, 2016a). The microspore mother cells, tapetal cells, middle layer, and endothecium are all L2-derived (Kelliher, 2013; van der Linde and Walbot,

2019; Walbot and Egger, 2016a; Zhang et al., 2021). The hypodermal cells in the L2 layer differentiate into the archesporial cells (AR) that finally form the sporogenous cells or pollen mother cells (Åstrand et al., 2021). These cells are few and have a dense cytoplasm with nuclei that can be easily viewed when viewed under a microscope (Åstrand et al., 2021). The remaining cells of L2 undergo periclinal division for the primary parietal cells (Gómez et al., 2015). From the primary parietal cells emerge the endothecium and the secondary parietal cells (Gómez et al., 2015). The secondary parietal cells give rise to the middle layer and tapetum after several periclinal and anticlinal divisions (Gómez et al., 2015). Finally, the differentiation of L3 gives rise to the surrounding tissue adjacent to the anther lobes and the vascular bundles (Åstrand et al., 2021; Gómez et al., 2015). Thus, the origin of tapetal cells is from a bipotent precursor which is influenced by varying oxygen conditions and several peptide signalling (Feng and Dickinson, 2010).

Table 1: List of genes and TFs involved in establishment of tapetum from the anther primordia.

Gene	Plant	Gene Description	Mutant Phenotype	References
PDF2	Arabidopsis thaliana	Encodes a homeodomain protein expressed in the LI layer of the vegetative, floral and inflorescence meristems.	The effect of the <i>pdf2</i> mutations on the floral development was largely different depending on T-DNA insertion locations.	(Kamata et al., 2013)
ATML1	Arabidopsis thaliana	Probable transcription factor involved in cell specification and pattern formation during embryogenesis. Functionally redundant to PDF2. Seems to promote cell differentiation.	Mutations in <i>ATML1</i> and its closest homologue, <i>PROTODE RMAL FACTOR2</i> (<i>PDF2</i>), caused the formation of leaves lacking an epidermis.	(Iida et al., 2023; Ogawa et al., 2015)
MSP1	Oryza sativa	The MSP1 gene encoded a Leu-rich repeat receptor—like protein kinase	The <i>msp1</i> mutation gave rise to an excessive number of both male and female sporocytes.	(Nonomura et al., 2003; Zhao et al., 2008)

TDL1	Arabidopsis thaliana	TPD1 encodes a small protein of 176 amino acids and is expressed mostly in developing microsporocytes in the anther.	tpd1, showed that functional interruption of TPD1 caused the precursors of tapetal cells to differentiate and develop into microsporocytes instead of tapetum. As a results, extra microsporocytes were formed and tapetum was absent in developing tpd1 anthers.	(Yang et al., 2003)
MAC1	Zea mays	MAC1 encodes a small protein with an N-terminal signal peptide and that it shares similarity with rice TDL1A and Arabido psis TPD1 genes	Loss-of-function <i>MAC1</i> gene increases the meiotically competent population and removes specification of somatic wall layers in anthers.	(Wang et al., 2012)
OCL4	Zea mays	Maize Outer cell layer 4 (OCL4) encodes an HD-ZIP IV transcription factor required for robust male fertility and 21-nt phasiRNA biogenesis.	The <i>ocl4</i> mutants were environment sensitive male sterile plants.	(Yadava et al., 2021)
ROXYI	Arabidopsis thaliana	ROXYI belongs to a subgroup of glutaredoxins that are specific for higher plants. ROXYI is predominantly expressed in tissues that give rise to new flower primordia, including petal precursor cells and petal primordia	Filamentous organs with stigmatic structures are formed in the second whorl of the <i>roxy1</i> mutant.	(Li et al., 2009; Xing et al., 2005)
ROXY2	Arabidopsis thaliana	Encodes a member of the CC-type glutaredoxin (ROXY) family that interacts	roxy1 roxy2 double mutants are sterile and do not produce pollen. As part of miR319-	(Xing and Zachgo, 2008)

		with the transcription factor TGA2 and suppress the promoter activity of ORA59. ROXY2, together with ROXY1, controls anther development.	TCPs- TGA9/TGA10/ROXY2 regulatory module controls cell fate specification in early anther development.	
TGA9	Arabidopsis thaliana	TGA9 belongs to the <i>Arabidopsis</i> TGACG motif-binding protein family (TGA), a subgroup of basic leucine-zipper transcription factors.	The <i>tga9tga10</i> double homozygous mutant is male sterile; anthers are reduced in size, dehiscence does not occur, and pollen grains are inviable	(Li et al., 2009; Murmu et al., 2010; Tao et al., 2023)
TGA10	Arabidopsis thaliana	TGA10 belongs to clade IV of the <i>Arabidopsis</i> TGACG motif-binding protein family (TGA), a subgroup of basic leucine-zipper transcription factors	The tga9tga10 double homozygous mutant is male sterile; anthers are reduced in size, dehiscence does not occur, and pollen grains are inviable	(Murmu et al., 2010; Tao et al., 2023)
MSCA1	Zea mays	The gene MSCA1 encodes a CC-type Glutaredoxins (GRXs).	In homozygous <i>msca1</i> mut ants of maize, stamen primordia are initiated normally and large hypodermal cells can be detected in developing anthers.	(Chaubal et al., 2003)
TGA1	Zea mays	Encodes for a basic leucin zipper transcription factors TGACG-BINDING FACTOR 1 (TGA1) protein	mutations in the maize gene teosinte glume architecture (tgal) is responsible for reduction in hardened structures, yielding free fruits that are easy to harvest.	(Preston et al., 2012)
MIL1	Oryza sativa	The genes encode a CC-type glutaredoxin	mil1 mutant anthers show defects in meiotic entry of the	(Hong et al., 2012; Yu and

		MICROSPORELESS1 (MIL1).	sporogenous cell progenies and differentiation of the surrounding somatic cell layers, resulting in locules filled with somatic cells instead of microspores.	Zhang, 2019)
SPL/NZZ	Arabidopsis thaliana	Encodes a presumed transcription factor that is needed for the initiation of both microand megagametogenesis. It is expressed in the sporogenous tissue of the anther and the ovule.	The <i>spl</i> mutant is ehibits abnormal differentiation of primary sporogenous cells into microsporocytes, and does form proper anther walls.	(Liu et al., 2009; Zhao et al., 2017)
MPK6	Arabidopsis thaliana	MPK6 encodes for a mitogen-activated protein kinase and it functions redundantly with MPK3.	The <i>mpk6</i> mutant is reported to have reduced fertility and smaller anthers compared to wild-type.	(Hord et al., 2008; Zhao et al., 2017)
BAMI	Arabidopsis thaliana	Encodes a CLAVATA1-related receptor kinase-like protein necessary for both shoot and flower meristem function. The BAM1 expression pattern supports both an early role in promoting somatic cell fates and a subsequent function in the pollen mother cells (PMCs).	Reduced shoot meristem size in bam1 mutant. Anthers of double mutants (bam1bam2) displayed abnormality from an early-stage and in later stages these mutants were without endothecium, middle, and tapetum layers.	(Hord et al., 2006)
BAM2	Arabidopsis thaliana	Belongs to the protein kinase superfamily. Ser/Thr protein kinase family. Very similar to BAM1, with more than 85% amino acid identity.	Anthers of double mutants (bam1bam2) had atypical early-stage growth and displayed absence of endothecium, middle	(Hord et al., 2006)

			layer and tapetum later on.	
EMS1	Arabidopsis thaliana	Encodes EMS1 (EXCESS MICROSPOROCYTES 1), a putative leucinerich repeat receptor protein kinase that regulates somatic and reproductive cell fates in anther.	ems1 is a male sterile mutant that generates extra meiocytes but lacks tapetal and middle cell layers.	(Canales et al., 2002; Cui et al., 2022; Huang et al., 2016)
SERK1	Arabidopsis thaliana	Plasma membrane LRR receptor-like serine threonine kinase that is expressed during embryogenesis in locules, with higher expression in the tapetal cell layer. SERK1 interacts with and transphosphorylates EMS1.	Neither the <i>serk1-1</i> nor <i>serk2-1</i> single mutant has a detectable phenotype, but anthers in the <i>serk1</i> serk2 double mutant show an identical phenotype to the <i>ems1</i> anther.	(Li et al., 2017)
SERK2	Arabidopsis thaliana	SERK2 is a plasma membrane LRR receptor-like serine threonine kinase. SERK1 and SERK2 receptor kinases function redundantly as an important control point for sporophytic development controlling male gametophyte production. The mRNA is cell-to-cell mobile.	Neither the <i>serk1-1</i> nor <i>serk2-1</i> single mutant has a detectable phenotype, but anthers in the <i>serk1</i> serk2 double mutant show an identical phenotype to the <i>ems1</i> anther.	(Chen et al., 2019; Li et al., 2017)
TPD1	Arabidopsis thaliana	Encodes a novel small protein similar to proteins of unknown function from other plant species. TPD1 is involved in cell specification during anther and pollen	Mutants lack tapetal cells and have an increased number of microsporocytes.	(Chen et al., 2019; Huang et al., 2016)

		development. It directly interacts with the LRR kinase EMS1 and that interaction results in phosphorylation of TPD1.		
RPK2	Arabidopsis thaliana	Encodes a receptor-like kinase RPK2 (also known as TOADSTOOL 2/TOAD2). The protein functions as a regulator of meristem maintenance.	Mutants are insensitive to synthetic CLV3 peptide. Mutations in the <i>RPK2</i> gene resulted in expansion of stem cells and increased number of floral organs, as seen in the other <i>clv</i> mutants.	(Hu et al., 2018)
UDTI	Oryza sativa	It is a bHLH transcription factor which is required for the differentiation of secondary parietal cells into mature tapetal cells.	The anther walls and meiocytes of the <i>udt1</i> mutants were normal during the early premeiosis stage, but their tapetal cells failed to differentiate and became vacuolated during the meiotic stage. The mutants failed to develop microspores, and middle layer degeneration was inhibited.	(Jung et al., 2005)
MS32	Zea mays	The maize gene <i>male</i> sterility32 (ms32) encodes a basic helix-loop-helix (bHLH) transcription factor, which functions as an important regulator of both division and differentiation during anther development.	The <i>ms32</i> mutant, tapetal precursor cells fail to differentiate, and, instead, undergo additional periclinal divisions to form extra layers of cells.	(Moon et al., 2013)
MS23	Zea mays	MS23 encodes for a bHLH transcription factor.	The <i>ms23</i> mutant showed the early signs of developmental	(Nan et al., 2022)

DCL5 Zea mays

cytologically visible in the tapetum.

defect, that were

Encodes a *Dicer-like* 5 (*Dcl5*) responsible for precise slicing in many monocots to generate diverse 24-nt phased, secondary small interfering RNAs (phasiRNAs)

dcl5 mutants have few (Teng et al., or no 24-nt phasiRNAs, 2020) develop short anthers with defective tapetal cells, and exhibit temperature-sensitive male fertility.

Preparation of tapetal cells for PCD

Once the tapetum is established in the anther, it performs several functions for the nourishment and maturation of the developing pollen grains before it endures complete elimination by the process of developmental programmed cell death (Pacini, 2016; Pacini et al., 1985). This section particularizes the detailed signaling and cytological changes in the tapetal cells prior to the end of its differentiation programme (Pacini et al., 1985). Studies have indicated that phytohormone cross-talks guide different aspects of plant development including cell differentiation and death (Hirano et al., 2008). Comprehensive research on complex crosstalk of plant hormones like auxin, gibberellic acid, jasmonic acid, brassinosteroids and ethylene have been reported during anther development (Hirano et al., 2008). Since hormones and hormonal crosstalk pleiotropically affect many aspects of plant development it is difficult to separate direct and indirect hormonal effects on cell death (Parish and Li, 2010; Van Durme and Nowack, 2016; Van Hautegem et al., 2015). Once hormone mediated signalling is charged, transcription of genes related to the process of differentiation are initiated (Yin et al., 2023). Previous studies have indicated the importance of the precise timing of this process for the formation of viable pollen grains in both model plants, Arabidopsis and rice. Loss of function of key transcription factors regulating the timing of PCD in tapetal cells have resulted in partial or complete male sterility (Wilson and Zhang, 2009). The Arabidopsis transcription factor MYB80 shows direct control over the transcription of the mitochondria-localised aspartic protease UNDEAD that acts as a repressor of tapetal PCD (Phan et al., 2011). The mitochondria release cytochrome C (Cyt C) into the cytoplasm to activate PCD in plant and animal system (Phan et al., 2011). The knockout mutants of MYB80 and UNDEAD exhibit early tapetal PCD

and subsequent male sterility (Phan et al., 2011). The plant homolog of the human anti-apoptotic protein Bax Inhibitor (BII) has been identified in Arabidopsis and rice (Sanchez et al., 2000). The expression of the AtBI1 gene under a tapetum-specific promoter demonstrated tapetal cells with large vacuoles that kept expanding and crushing the developing meiocytes (Sanchez et al., 2000; Watanabe and Lam, 2006). On the contrary in rice the bHLH TF ETERNAL TAPETUM1 has been identified as an activator of tapetal PCD by directly promoting the transcription of cell death inducing aspartic proteases AP25 and AP37 (Niu et al., 2013). Thus, both anti and pro apoptotic regulator of tapetal dPCD are transcriptionally controlled to ensure the exact timing of tapetal dPCD. Gibberellic acid (GA), has been identified as the phytohormone that primarily facilitates the onset of tapetal PCD (Qian et al., 2021). The GA-responsive MYB transcription factor or GAMYB regulates both tapetal development as well as tapetal PCD in rice while the two Arabidopsis GAMYB homologs are MYB33 and MYB65 (Millar and Gubler, 2005; Zhang et al., 2020). Recently, another GA regulated gene namely, RGA Target 1 (RGAT), has been identified in Arabidopsis that is predominantly encoded and expressed during stages 8-11 of pollen development (Qian et al., 2021). This gene is activated by RGA, a member of the DELLA family proteins that is repressed by GA (Qian et al., 2021). The overexpression and knockout mutants of this gene demonstrate partial male sterility by disturbing the timely occurrence of PCD and thereby pollen development (Qian et al., 2021). According to a study, Brassinosteroid (BR) is also an influential factor in controlling tapetal cell death (Yan et al., 2020). The important candidates of this signaling pathway act downstream of the EMS1-TPD1-SER1/2 complex (Chen et al., 2019). The transcription factors identified from the BR signaling pathway include BRI1 EMS Suppressor1 (BES1) family members like BES1, Brassinazole Resistant1 (BZR1), BES/BZR1 Homologuel (BEH1), BEH2, BEH3 and BEH4 (Kim et al., 2024). The mutants of these transcription factors have been reported to exhibit suppressed tetrad formation (Chen et al., 2019; Kim et al., 2024). Ethylene treatment for developing anthers led to pollen abortion and precocious degeneration of tapetum by the EIN2 EIN3/EIL1 signaling pathway (Zhu et al., 2022). Although studies on the effect of Jasmonic acid (JA) on tapetal PCD have not been reported yet the JA INSENSITIVE (JAI) gene is responsible for anther dehydration and pollen release (Dobritzsch et al., 2015; Schubert et al., 2019).

The findings collectively suggest that the differentiation of cell types that is preceded by a preparatory phase for the differentiation induced dPCD (Jiang et al., 2021; Van Durme and

Nowack, 2016). The transcriptional reprogramming has been proven to be crucial to acquire the proficiency to execute PCD as a fast response to both external and internal stimuli(Van Durme and Nowack, 2016). In order to achieve this quick reflex, plant dPCD is required to regulate the abundance of cell death and cell clearance effector molecules within the cell (Wang et al., 2021b). This is achieved by rendering then inactive either by sequestering them to isolated compartments such as vacuoles, endoplasmic reticulum or specialised vesicles or secreting inactive zymogens in the first place (Van Durme and Nowack, 2016). Upon perceiving the activation signal, these effector molecules are selectively released from their respective compartments to execute PCD while the remaining effectors are utilised post PCD for corpse clearance (Huysmans et al., 2017; Van Durme and Nowack, 2016).

Factors regulating tapetal PCD

Preparing a plant cell for the process of PCD marks its terminal stage in its differentiation programme that involves a gradual accumulation of mRNA and protein within the cell (Figure 1) (Van Durme and Nowack, 2016). The subsequent step following the establishment of the mRNA and protein pool within the cells is a tight regulation of the signal transduction to activate the PCD machinery upon perceiving the signal (Gadjev et al., 2008). Several secondary messengers and signal pathways have been identified that facilitates the finetuning of PCD and its activation.

Reactive oxygen species (ROS) are produced during the developmental process in a plant; however, higher concentrations of ROS can alter the antioxidant conditions within the cell consequently causing cell death (Gadjev et al., 2008). During developmental PCD, ROS generated in the form of H₂O₂ can act as a signalling molecule to regulate the rate of PCD occurring in the cell type (Gadjev et al., 2008; Gechev et al., 2010). In the event of anther development, ROS signatures oversee the spatiotemporal regulation of tapetal PCD (Zheng et al., 2019). A tissue specific NADPH oxidase namely, RESPIRATORY BURST OXIDASE HOMOLOGUE E (RBOHE) has been identified in *Arabidopsis* that vastly contributes to the H₂O₂ levels promoting tapetal cell death (Huang et al., 2019). The abundance or lack of this enzyme within the anther cells has been reported to disrupt the normal ROS concentration causing male sterility in the mutants (Huang et al., 2019). The two extension peroxidases PRX9 and PRX40, function as ROS-scavenging molecules in the tapetal cells to maintain the integrity of the tapetal cell wall (Jacobowitz et al., 2019). In rice, an ARGONAUTE (AGO) family

protein, OsAGO2 indirectly promotes anther development by epigenetically modifying the methylation state of the promoter region in a hexokinase (OsHXK) that is, in turn, responsible for ROS production to initiate tapetal PCD (Zheng et al., 2019). The MADS3 loss of function mutant in rice demonstrates premature tapetal PCD and differential regulation of the ROS homeostasis genes that are responsible for the characteristic variations in the ROS level (Hu et al., 2011). However, investigations on the mechanistic pathway related to cell death signalling upon ROS spikes in a cell have not been explored yet. The two organelles that are closely responsible for ROS production are mitochondria and chloroplasts, and have been reported to be targets of cellular degradation prior to vacuolar collapse during cell death (Corpas et al., 2015).

Following ROS signalling, calcium signatures have been identified to be crucial in developmental programmed cell death (Gilroy et al., 2014; Ren et al., 2021a). The calcium ion influx has been reported to cause H_2O_2 levels to rise, indicating ROS signalling to be downstream of Ca^{2+} signalling during programmed cell death (Gilroy et al., 2014). Studies on calcium signalling during tapetal cell death remains untouched and needs further research to elaborate the process.

As PCD is set into motion, a series of events follows within the cell subsequently, leading to an organised termination of the cells vital function. The autophagy observed in plant cells undergoing developmental PCD is analogous to the autophagic cell death in animals (van Doorn and Woltering, 2010). Autophagy is a conserved cellular mechanism in eukaryotes that involves the removal of damaged cellular components in case of an injury or remobilisation of nutrients in case of senescing cells (Minina et al., 2014). In OsATG7 loss of function mutants the tapetum is only partially removed after PCD and the mutants' exhibited defects in pollen maturation and subsequent pollen viability (Kurusu et al., 2014).

The remodelling of the cytoskeleton during programmed cell death has been as unexplored avenue (Ren et al., 2021b). The actin filament organisation observed in the embryonic suspensor cells of Norway spruce that is advancing for developmental PCD, was disrupted by the addition of actin depolymerising drugs that further inhibited their cell death (Ren et al., 2021b; Van Durme and Nowack, 2016). On the contrary, in an event of vacuolar collapse during PCD, actin filaments were first observed to be depolymerise and then aggregate that directly impacted the rate of advancement of PCD (Higaki et al., 2011). The loss of cellular integrity is highlighted

by the discharge of vacuolar contents into the cytoplasm after the tonoplast ruptures and this marks the final step of developmental PCD (Parish and Li, 2010). The vacuolar collapse not only releases the lytic enzymes, it also causes the pH in the cytoplasm to drop thus, providing optimal conditions for certain enzymes to function (Hara-Nishimura and Hatsugai, 2011). Recent studies have revealed that downstream cell death events could be inhibited by altering the cytosolic pH (Hara-Nishimura and Hatsugai, 2011). Thus, laying the foundation that vaculoar collapse is a function of cytoplasmic acidification rather than the intuitive notion that tonoplast rupture causes cytoplasmic acidification (Hara-Nishimura and Hatsugai, 2011).

Post PCD events

In animal system, the degrading apoptotic cells are fragmented into apoptotic bodies that are internalised for additional non cellular autonomous degradation (Taylor et al., 2008). Phagocytosis is signalled by molecules secreted on the surface of the apoptotic cells (Uribe-Querol and Rosales, 2020). Plant cells in contrast are non-motile and possess cell wall that limit their interaction to their neighbouring cells. This lays the basis for elimination of phagocytosis in plants cells, even though endocytosis remains conserved in both plant and animal systems (Dragwidge and Van Damme, 2020). Therefore, plants have their own clearing mechanism after PCD through a strictly regulated lytic enzyme utilisation throughout the event of PCD (Van Durme and Nowack, 2016). Cell clearance is initiate in the phase prior to tonoplast rupture through the action of several enzymes and autophagy (Van Doorn, 2011). However, the final completion of clearance of cellular debris happens via lytic enzymes in the terminal stages of developmental PCD (Van Durme and Nowack, 2016).

The autolysis of cell corpse occurs through the lytic enzymes that are accumulated as zymogens during the initial or preparatory phase of cells destined to undergo PCD (Van Durme and Nowack, 2016). Once the enzymes are released from their specialised compartments or have undergone maturation, many cellular components are supposedly rapidly degraded (Van Durme and Nowack, 2016). Analogous to animal PCD, the caspase-like endopeptidase activities has been explored in many forms of plant dPCD (Van Durme and Nowack, 2016). Interestingly, plant metacaspases were unaccountable for the typical caspase-like activities; instead, different caspase-like activities were credited to varied proteases like VACUOLAR PROCESSING ENZYMES (VPEs), a subunit of the proteasome, and other proteases such as phytaspases and saspases (Basak and Kundu, 2022). The MYB2 transcription factor is responsible for the direct

regulation of two key executers of tapetal PCD namely β-VACUOLAR PROCESSING ENZYME (βVPE) and CYSTEINE ENDOPEPTIDASE1 (CEP1) (Guo et al., 2022). βVPE is responsible for the maturation of CEP1, which is secreted as a proenzyme in precursor protease vesicles (Cheng et al., 2020). The temporal regulation of CEP1 expression is crucial for pollen wall formation and pollen fertility (Zhang et al., 2014). N-terminal acetylation of proteins is an important modification associated with eukaryotic genes (Feng J, 2022). Naa50 is a catalytic subunit of the N-terminal acetyltransferase NatE complex, that is expressed during stages 9-11 of pollen development in *Arabidopsis* anthers (Feng J, 2022). The loss of function of Naa50 leads to upregulation of *CEP1* causing accelerated tapetal cell death (Feng J, 2022).

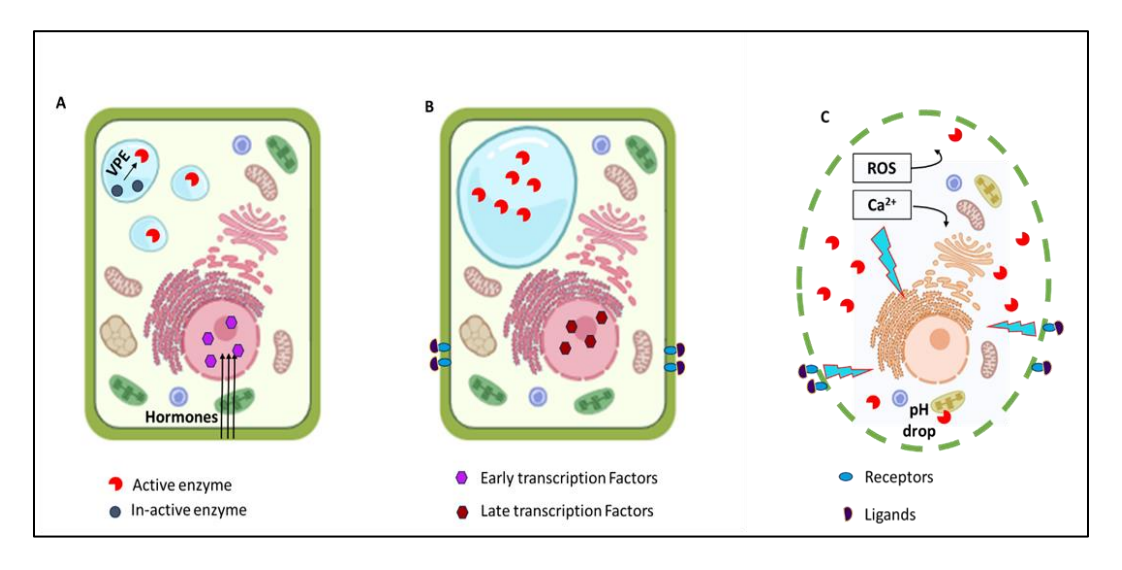


Figure 1: Schematic of the molecular mechanism central to different phases of differentiation-induced developmental programmed cell death (dPCD).

(A) An undifferentiated cell predestined to undergo dPCD. During the first phase a complex cross talk of hormone signalling prepares the cell for a transcriptional reprogramming (denoted by black arrows). This these cells lytic enzymes like proteases are stored as zymogens in vacuoles that require processing to become active. (B) In the second phase another set of transcription factors take over that regulate the conversion of zymogenes into active forms along with their accumulation in specialised compartments. In this phase several receptors are also primed with ligands signalling for the initiation of PCD. (C) The third phase is characterised by the activation of a signalling cascade due to sudden outburst of secondary messengers like Ca²⁺ and ROS. The pH of the cell also drops thus, promoting a suitable environment for the maturation of the remaining zymogens. The cell at this point exhibits loss of structural integrity because of the degradation of actin cytoskeleton and cell membrane from the action of the lytic enzymes. Post PCD, the cell debris are removed by autophagy or utilised by other cells for their own nourishment.

Secretory and Biosynthetic activity of the tapetum

The secretory activity in the tapetum is mediated by the COPII-coated vesicles that specifically are responsible for the anterograde transport from the endoplasmic reticulum to the Golgi 2016a). apparatus (Zhao al., In Arabidopsis, *GLYCEROL-3-PHOSPHATE* ACYLTRANSFERASE1 (AtGPAT1) and AtGPAT6 are involved in the preliminary steps of glycerolipid synthesis and mutation of these genes can lead to abnormal ER structure and reduced secretion from the tapetal cells (Li Xiao-Chuan, 2012; Zheng et al., 2003). The regulation of cation homeostasis during the secretory phase of the tapetum is mediated via a V P-type ATPase cation pump named MALE GAMETOGENESIS IMPAIRED ANTHERS (MGIA) (Shin, 2022). In Arabidopsis thaliana, SECRETORY31B (SEC31B) is a COPII protein that is driven by a tapetum-specific protein called A9 for the formation of viable protein (Zhao et al., 2016a). The transcription factor that has been identified to regulate the normal secretion of pollen wall material from the tapetum is MS1 (Yang et al., 2019). The secretion of an exoglucanse named A6 is dependent on an arabinogalactan β -(1,3)-galactosyltransferase that is encoded by a gene named UNEVEN PATTERN OF EXINE1 (UPEX1) (Diane L. Hird, 1993). The Arabidopsis loss of function mutant of HAPLESS13/AP-1µ (HAP13) exhibited compromised secretory function during pollen development (Gui-Min Yin a, 2024).

Within the tapetum occurs the synthesis of the exine constituents via the phenylpropanoid pathway (Battat et al., 2019; Geng et al., 2020; Li et al., 2015; Mir Derikvand et al., 2008). These constituents are released into the anther locule from anther stage 7 which corresponds to the tetrad stage of pollen development until the degeneration of the tapetum (Echlin, 1971a; Lallemand et al., 2013; Wang et al., 2018). In *Arabidopsis*, this pathway is exclusively operational in the tapetum and any mutation in this pathway leads to defective pollen wall formation and atypical anther dehiscence (Quilichini et al., 2015).

The intermediates from the phenylpropanoid pathway serve as resources for the biosynthesis of flavonoids, lignin, and hydroxycinnamoyl esters (Jing-Shi Xue 7, 2020). In *Arabidopsis*, this pathway begins with the transfer of phenylamine to cinnamic acid via PHENYLALANINE AMMONIA LYASE (PAL) that is converted to p-coumaric acid by CINNAMATE-4-HYDROXYLASE (C4H) and finally forming hydroxycinnamoyl-CoA using 4COUMARATE: COALIGASE (4CL) (Battat et al., 2019; Geng et al., 2020; Li et al., 2015; Mir Derikvand et al., 2008). The lignin-specific biosynthetic pathway utilizes hydroxycinnamoyl-CoA to form

hydroxycinnamyl aldehyde using CINNAMOYL COA REDUCTASE (CCR) and the aldehyde is further reduced to monolignol via CINNAMYL ALCOHOL DEHYDROGENASE (CAD). Studies have reported male sterility in *c4h* and *pal1 pal2 pal3 pal4*, *4cl1 4cl2 4cl3*, and *ccr1* mutants (Huang et al., 2010a). *PAL4* expression in the anther is controlled by stamen-specific transcription factors MYB99 and MYB21 (Battat et al., 2019). The expression of *PAL1*, *C4H*, *4CL3*, *CCR1*, *CAD4*, and *CAD5* genes was identified in *Arabidopsis* and detected in tapetum indicating their role in exine biosynthesis (Jing-Shi Xue 7, 2020).

Several genes are responsible for the biosynthesis of exine and pollen coat, although their connection with the phenylpropanoid pathway has not been explored yet. Some of the proteins that have been identified to be associated with the biosynthesis of sporopollenin in *Arabidopsis* thaliana are ACYL-COA SYNTHETASE (ACOS5), POLYKETIDE SYNTHASE A (PKSA), and PKSB, TETRAKETIDE α-PYRONE REDUCTASE 1 (TKPR1) and TKPR2 (Wang et al., 2018; Zhu, 2021). Two duplicate CYP704B1 homologous genes in Brassica napus namely, BnMs1 and BnMs2 are important for tapetal cell formation and its function in pollen exine formation (Yi et al., 2010). Studies indicate that the loss of function mutants of IMPERFECT EXINE FORMATION (IEF) exhibit male sterility and pollen abortion, deeming it an important candidate for pollen development and male fertility (Wang et al., 2021a). The ief mutants demonstrated undefined exine structure, unlike the wild-type pollen grains (Wang et al., 2021a). The mutation of another gene named TRANSPOSABLE ELEMENT SILENCING VIA AT-HOOK (TEK) leads to the absence of nexine in Arabidopsis thaliana (Lou et al., 2014). TEK encodes for an AT-HOOK nuclear-localized protein that is enriched in the tapetum, especially during the tetrad stage (Lou et al., 2014). The tek mutants have demonstrated disrupted intine deposition with unhindered sexine formation (Lou et al., 2014). The major glycine-rich family proteins that are involved in pollen coat formation are GRP14, 16, 17, 18, 19,20, and GRPoleosin (Lu et al., 2020). Apart from the GRPs a few calcosin-related family proteins namely AT1G23240 and AT1G23250 along with some lipase proteins namely EXL4, EXL5, and EXL6 have been identified (Lu et al., 2020). A study in rice, showed that SWOLLEN TAPETUM AND STERILITY 1 (STS1) gene is responsible for expression of an ER-localised protein with DUF726, and lipase activity (Yuan et al., 2022). STS1 promotes timely degeneration of tapetal cells and maintains anther lipid homeostasis (Yuan et al., 2022).

Trafficking of sporopollenin and other components of the tryphine coat

Once the cargo (sporopollenin and other elements of the typhine) is ready for shipment (trafficking), several transporter and transcription factors spring into action (Hyunju Choi, 2010). The export of metabolites from the tapetum to the anther locule takes place via ATPbinding cassette transporters that belong to the G-subfamily and are commonly called the ABCG transporters (Hyunju Choi, 2010; Zhao et al., 2016c). One of the most important transporters, responsible for the export of sporopollenin is ABCG26 (Quilichini et al., 2010). The NPF2.8 transporter facilitates the transport of flavonol sophorosides into the anther locule. The export of steryl glycosides is mediated by proteins encoded by ABCG9 and ABCG31 genes (Grunewald S, 2020;). In Arabidopsis, the tapetum-expressed lipid transfer proteins called ARABIDOPSIS THALIANA ANTHER7 (ARA7/A7) and A9 are synthesized to transport fatty acid components in specialized storage organelles called tapetosomes and elaioplasts (Huang et al., 2013). The wide range of metabolites produced in the ER-derived tapetosomes include alkane and triacylglycerol- rich oil droplets (Hsieh and Huang, 2007). These tapetosomes appear as electron-dense structures that are attached to the ER when viewed under a transmission electron microscope (Hsieh and Huang, 2007). Oleosins and elaioplasts are among the other organelles in the tapetum that maintain oil bodies and other steryl ester, free polar lipids, and plastid lipid-associated proteins (Hsieh and Huang, 2004, 2007). These organelles increase in size and number as the tapetal cells reach the later stages of pollen development (Hsieh and Huang, 2007).

For the expulsion of tapetal cell contents into the anther locule the tapetal cells also undergo exocytosis (Goodman et al., 2021; Hsieh and Huang, 2004). The tapetum exclusively synthesizes the seed plant-specific type III lipid transfer proteins (LTPs) via the Trans-Golgi Network, for expelling the tapetal contents into the anther locule (Goodman et al., 2021). These LTPs may or may not be associated with sporopollenin during the process (Goodman et al., 2021). The elaioplasts and tapetosomes discharged onto the surface of the maturing pollen grains serve their unique function to protect and make the pollen viable until pollination and pollen tube germination (Toshiya Suzuki, 2013). For instance, the steryl esters provide a waterproof surface for the pollen grains, however, after pollination when the pollen grains undergo rehydration, for pollen tube germination, the amphipathic oleosins make it feasible (Wei Zhao, 2023).

The tapetum is also responsible for the regulation of genes encoding several transporters, this is aided by several transcription factors that are localized to the tapetum. For instance, the expression of an R2R3 MYB gene, AtMYB103 is strictly detected only in the tapetum (Higginson et al., 2003). In Arabidopsis thaliana the MALE STERILITY 2 (MS2) protein is synthesized in the tapetum immediately after the release of tetrads and the ms2 mutants are characterized by very thin pollen walls that are sensitive to acetolysis treatment (Mark G.M. Aarts, 2003). The CDM1 gene regulates the callose metabolism to promote the formation of pollen exine (Lu et al., 2014). The Arabidopsis, ADP-RIBOSYLATION FACTOR-A1s (ArfA1s) are expressed especially during the tapetum mediated event of pollen development and all the six ArfA1s play a role in the post Golgi trafficking routes either to the plasma membrane or vacuoles (Zhu et al., 2021b). Thus, the ability of the tapetal cells to drastically change from biosynthetic to secretory activities to accommodate the demands of the developing meiocytes indicates a fine-tuned spatiotemporal regulation of their endomembrane secretory system and plasma membrane composition. The list of genes and transcription factors playing a role in the biosynthetic activity, signalling, and degradation of the tapetum has been listed in table 2 below.

Table 2: List of genes/TFs associated with the biosynthetic and signaling activities of the tapetum

Gene	Plant	Gene Description	Mutant Phenotype	References
PAL4	Arabidopsis thaliana	Encodes phenylalanine ammonia-lyase (PAL; EC 4.3.1.5) catalyzes the first step in phenylpropanoid metabolism.	The pal1pal2pal3pal4 quadruple knockout mutants exhibit stunted growth and are sterile.	(Huang et al., 2010b; Xue et al., 2020)
С4Н	Arabidopsis thaliana	Encodes a cinnamate-4-hydroxylase.	The loss of function mutants demonstrates phenotypes like dwarfism, male sterility, and the development of swellings at branch junctions.	(Schilmiller et al., 2009)

4CL3	Arabidopsis thaliana, Oryza sativa	Encodes an isoform of 4-coumarate: CoA ligase (4CL), which is required in the last step of the phenylpropanoid pathway.	The 4CL-suppressed transgenics of rice also displayed decreased panicle fertility, which may be attributed to abnormal anther development as a result of disrupted lignin synthesis.	(Gui et al., 2011)
CCR1	Arabidopsis thaliana	Encodes Cinnamoyl-CoA reductase 1 the main CCR isoform reported in the constitutive lignification	Mutants displayed dwarf phenotype and a delayed senescence	(Mir Derikvand et al., 2008)
CAD4	Arabidopsis thaliana	Encodes a catalytically active cinnamyl alcohol dehydrogenase which uses p-coumaryl aldehyde as a preferred substrate.	No knockout mutant phenotype characterisation has been reported till now.	(Xue et al., 2020)
CAD5	Arabidopsis thaliana	Encodes a catalytically active cinnamyl alcohol dehydrogenase that uses p-coumaryl aldehyde as a preferred substrate.	No knockout mutant phenotype characterisation has been reported till now.	(Xue et al., 2020)
PAL1	Arabidopsis thaliana	Encodes PAL1, a phenylalanine ammonialyase.	The <i>pal1pal2pal3pal4</i> quadruple knockout mutants exhibit stunted growth and are sterile.	(Xue et al., 2020)
ACOS5	Arabidopsis thaliana	Encodes an acyl-CoA synthetase, that has in vitro activity towards medium- to long-chain fatty acids and their hydroxylated derivatives.	Null mutants were lacking pollen grains at anther maturity and were completely male sterile.	(de Azevedo Souza et al., 2009)
PKSA	Arabidopsis thaliana	Encodes a chalcone and stilbene synthase family protein	Abnormal exine patterning. Pollen has a more extensively	(Kim SungSoo et al., 2010)

covered surface with broader muri and

			smaller lacunae. Reduced accumulation of flavonoid precursors and flavonoids in developing anthers.	
PKSB	Arabidopsis thaliana	Chalcone and stilbene synthase family protein	Abnormal exine patterning. Pollen lacks the characteristic reticulate structure. Reduced accumulation of flavonoid precursors and flavonoids in developing anthers.	(Kim SungSoo et al., 2010)
TKPR1	Arabidopsis thaliana	Encodes tetraketide α-pyrone reductase 1.	tkpr1 mutant in Arabidopsis makes completely sterile pollen grains with severely damaged exine.	(Zhu et al., 2021a)
TKPR2	Arabidopsis thaliana	Encodes tetraketide α-pyrone reductase 2.	the <i>tkpr2</i> mutant produces fertile pollen with only mildly impaired exine.	(Zhu et al., 2021a)
BnMs1	Brassica napus	Encodes a member of the cytochrome P450 family and functions redundantly with BnMs2.	The developing anther demonstrated of S45A severely compromised pollen-wall formation, that was lacking sporopollenin or exine.	(Yi et al., 2010)
BnMs2	Brassica napus	The gene encodes a protein member of the cytochrome P450 family and functions redundantly with BnMs1.	The developing anther showed that pollen-wall formation in the S45A mutant was severely compromised, with a lack of sporopollenin or exine.	(Yi et al., 2010)

IEF	Arabidopsis thaliana	Encodes a protein similar to fatty acid reductases.	ief mutants exhibit severe male sterility and pollen abortion	(Wang et al., 2021a)
TEK	Arabidopsis thaliana	TEK encodes an AT- hook nuclear localized family protein highly expressed in tapetum during the tetrad stage	Absence of nexine in <i>tek</i> disrupts the deposition of intine without affecting sexine formation.	(Lou et al., 2014)
At1G23240	Arabidopsis thaliana	Encodes a potential EF- hand Ca ²⁺ -binding protein also known as caleosin-related family protein associated with lipid droplet and endoplasmic reticulum	Single mutant phenotype has not been reported until now.	(Lu et al., 2020)
At1G23250	Arabidopsis thaliana	Caleosin-related family protein associated with lipid droplet and endoplasmic reticulum.	Single mutant phenotype has not been reported until now.	(Lu et al., 2020)
EXL4	Arabidopsis thaliana	Encodes a member of Lipase proteins that is involved in lipid metabolism and pollen wall formation.	ex14-1 shows a reduced rate of pollen hydration.	(Updegraff et al., 2009)
STS1	Oryza sativa	STS1 encodes an endoplasmic reticulum (ER)-localized protein that contains domain of unknown function (DUF) 726 and exhibits lipase activity.	Mutation of STS1 gene causes delayed tapetum degradation and aborted pollen wall formation	(Yuan et al., 2022)
ABCG26	Oryza sativa	OsABCG26 encodes an ATP binding cassette transporter G26.	osabcg26 mutant plant displayed defects in tapetal cells, Ubisch bodies, pollen exine, anther cuticle.	(Chang et al., 2016; Quilichini et al., 2014)
MYB103	Oryza sativa	Encodes a member of the R2R3 MYB gene family.	osmyb103 mutants exhibited delayed tapetum degradation	(Lei et al., 2022)

	UCT	

				25 D a a a
UPEX1	Arabidopsis thaliana	<i>UPEX1</i> encodes for an arabinogalactan b-(1,3)-	Extremely thin pollen exine layer. Nexine,	(Wang et al., 2022)
A6	Arabidopsis thaliana	Encodes the Anther- specific protein 6, a member of the callase complex that affects callose wall degradation.	Mutants exhibited tapetal ablation and male sterility.	(Hird et al., 1993)
MS1	Arabidopsis thaliana	MS1 encodes a nuclear protein with Leu zipper—like and PHD-finger motifs.	The <i>ms1</i> mutants exhibited absence of pollen wall.	(Ito et al., 2007; Yang et al., 2019)
SEC31B	Arabidopsis thaliana	Encodes a COPII protein SECRETORY 31B.	The atsec31b mutant demonstrated severe pollen and seed abortion. The pollen exine formation in the mutant is disrupted significantly.	(Zhao et al., 2016b)
AtGPAT6	Arabidopsis thaliana	Encodes a member Glycerol-3-phosphate acyltransferase family protein.	gpat6, caused a massive reduction in seed production.	(Li et al., 2012)
AtGPAT1	Arabidopsis thaliana	Encodes a membrane- bound glycerol-3- phosphate acyltransferase.	Disruption of the <i>AtGPAT1</i> gene causes an arrest in pollen development. The mutation perturbed degeneration of the tapetum, which is associated with altered endoplasmic reticulum profiles and reduced secretion.	(Zheng et al., 2003)
MS2	Glycine max	MS2 encodes a bHLH transcriptional factor, and both the gene and protein express exclusively in the anther.	Male sterile line with a highest record for seed set.	(Fang et al., 2023)
			and defective mature pollen.	

		galactosyltransferase involved in the formation of pollen exine.	bacula, and tectum is present. Many mature pollen grains are withered and aggregated, but fertility is normal.	
HAP13	Arabidopsis thaliana	Encodes for HAPLESS13/AP-1μ, a component of the Adaptor Protein 1 (AP-1) complex.	The <i>hap13</i> mutant shows a reduction in pollen sac number. It is also defective in tapetal secretion and programmed cell death, resulting in male sterility.	(Yin et al., 2024)
MYB33	Arabidopsis thaliana, Solanum lycopersicum	Encodes a R2R3-MYB protein family. Contains a binding site for miRNA159 and may be spatially regulated by this microRNA.	Silencing of <i>SlMYB33</i> leads to delayed flowering, aberrant pollen viability, and poor fertility in tomato.	(Millar et al., 2019; Zhang et al., 2020)
MYB65	Arabidopsis thaliana	Member of the R2R3-MYB gene family.	Double mutants with MYB33 are male sterile, showing defects in pollen development and anther development.	(Millar and Gubler, 2005)
RGAT	Arabidopsis thaliana	RGAT1 encodes an unknown protein of 117 amino acids that does not contain any known domain and has no homologous genes in Arabidopsis.	Loss of <i>RGAT1</i> function induced the premature degeneration of tapetal cells with defective ER-derived tapetosomes, while <i>RGAT1</i> overexpre ssion delayed tapetum degeneration.	(Qian et al., 2021)
BES1	Arabidopsis thaliana	Encodes a Brassinosteroid signaling positive regulator family protein	bes1 single mutants do not display characteristic brassinosteroid phenotype. Anthers of a	(Chen et al., 2019; Kim et al., 2024)

		BRI1-EMS- SUPPRESSOR 1	quintuple mutant, bes1-1 bzr1-1 beh1-1 beh3-1 beh4-1 (qui-1), show an incompletely developed tapetum-like cell layer, which losses normal tapetum cell identity.	
BZR1	Arabidopsis thaliana	Encodes a Brassinosteroid signaling positive regulator (BZR1) family protein	Bzr1 single mutant do not display characteristic brassinosteroid phenotype. Anthers of a quintuple mutant, bes1-1 bzr1-1 beh1-1 beh3-1 beh4-1 (qui-1), show an incompletely developed tapetum-like cell layer, which losses normal tapetum cell identity.	(Chen et al., 2019; Kim et al., 2024)
ВЕН1	Arabidopsis thaliana	Encodes for BES1/BZR1 homolog 1.	Anthers of a quintuple mutant, bes1-1 bzr1-1 beh1-1 beh3-1 beh4-1 (qui-1), show an incompletely developed tapetum-like cell layer, which losses normal tapetum cell identity.	(Kim et al., 2024)
ВЕН3	Arabidopsis thaliana	Encodes a BES1/BZR1 homolog 3	Anthers of a quintuple mutant, bes1-1 bzr1-1 beh1-1 beh3-1 beh4-1 (qui-1), show an incompletely developed tapetum-like cell layer, which losses normal tapetum cell identity.	(Kim et al., 2024)
BEH4	Arabidopsis thaliana	Encodes a BES1/BZR1 homolog 4	Anthers of a quintuple mutant, bes1-1 bzr1-1 beh1-1 beh3-1 beh4-1 (qui-1), show an incompletely developed tapetum-like cell layer, which losses normal tapetum cell identity.	(Kim et al., 2024)

ATG7	Oryza sativa	Encodes for AUTOPHAGY RELATED GENE 7.	The mutant showed complete sporophytic male sterility, failed to accumulate lipidic and starch components in pollen grains at the flowering stage, showed reduced pollen germination activity, and had limited anther dehiscence.	(Kurusu et al., 2014; Sera et al., 2019)
PRX9	Arabidopsis thaliana	Encodes for a class III peroxidase-encoding protein, PEROXIDASE 9	The prx9 prx40 double mutants exhibit distinctive tapetum swelling and enlarged developing pollen grains, ultimately leading to microspore degeneration and male sterility.	(Jacobowit z et al., 2019)
PRX40	Arabidopsis thaliana	Encodes for a class III peroxidase-encoding protein, PEROXIDASE40	The prx9 prx40 double mutants exhibit distinctive tapetum swelling and enlarged developing pollen grains, ultimately leading to microspore degeneration and male sterility.	(Jacobowit z et al., 2019)
OsAGO2	Oryza sativa	Encodes protein of the ARGONAUTE (AGO) family.	The knocked down <i>OsAGO2</i> expressi on led to the early initiation of tapetal PCD	(Zheng et al., 2019)
OsHXK	Oryza sativa	Encodes for Hexokinase 1	Overexpression of <i>OsHXK1</i> also resulted in the overaccumulation of ROS, premature initiation of PCD, and pollen abortion. The knockdown	(Zheng et al., 2019)

			of <i>OsHXK1</i> restored pollen fertility in <i>OsAGO2</i> knockdown plants.	
DTC1	Oryza sativa	Encodes Defective Tapetum Cell Death 1 (DTC1), that controls this degeneration by modulating the dynamics of ROS.	Mutants defective in DTC1 exhibit phenotypes of an enlarged tapetum and middle layer with delayed degeneration, causing male sterility.	(Yi et al., 2016)
βVPE	Arabidopsis thaliana	Encodes for a Vacuolar processing enzyme (VPE)	βvpe mutants exhibited delayed vacuolar degradation and decreased pollen fertility.	(Cheng Z, 2020 Mar 25)
CEP1	Arabidopsis thaliana	Encodes a papain-like cysteine protease	cep1 mutants exhibited aborted tapetal PCD and decreased pollen fertility with abnormal pollen exine.	(Zhang et al., 2014)
AtHMGB15	Arabidopsis thaliana	Encodes for an ARID- HMG DNA binding protein	Knockout mutants <i>athmgb15</i> exhibit prolonged PCD of tapetal cells.	(Biswas, 2024)
Naa50	Arabidopsis thaliana	Encodes for N-terminal acetyltransferase Naa50	The lack of Naa50 resulted in collapsed and sterile pollen in Arabidopsis.	(Feng et al., 2022)
MYB108	Solanum melongena	Encodes for a R2R3-MYB transcription factor	Overexpression of <i>SmMYB108</i> in tobacco caused anther dehiscence.	(Hu R, 2023 Jul 11)
MYB80	Arabidopsis thaliana	MYB80 encodes a MYB transcription factor that is essential for tapetal and pollen development.	The <i>myb80</i> mutant exhibits signs of premature tapetal degeneration in anthers, which becomes more pronounced at later stages, where an	(Higginson et al., 2003; Phan et al., 2011)

			increase in tapetal vacuolation occurs.	
Al	Arabidopsis thaliana, Oryza sativa	A1 is an aspartic protease encoded by <i>UNDEAD</i>	The knockdown of <i>UNDEAD</i> causes premature tapetal PCD	(Niu et al., 2013)
BII	Arabidopsis thaliana	Encodes BI-1, a homolog of mammalian Bax inhibitor 1	Bax-induced cell death can be downregulated by ectopically expressing AtBI in planta.	(Kawanabe et al., 2006)
DYT1	Arabidopsis thaliana	Encodes for DYSFUNCTIONAL TAPETUM 1	dyt1 mutant exhibits increased vacuolation and dysfunction of the tapetum.	(Cui et al., 2016; Zhang et al., 2006)
TCP15	Solanum lycopersicum	Encodes a transcription factor TEOSINTE BRANCHED1- CYCLOIDEA-PCF15	sltcp15 knockout showed significant decreases in pollen viability, fruit yield, and fruit seed number	(Xu et al., 2024)
AMS	Arabidopsis thaliana	ABORTED MICROSPORE encodes a basic helix-loop-helix (bHLH) factor	ams mutants were sterile.	(Lou et al., 2018; Nan et al., 2022; Xiong et al., 2016)
CYP7032A	Arabidopsis thaliana	Encodes for a cytochrome P450 family protein	CYP703A2 knockout lines showed impaired pollen development and a partial male-sterile phenotype.	(Morant M, 2007;; Xiong et al., 2016)
<i>MYB99</i>	Arabidopsis thaliana	Encodes a putative transcription factor MYB99	myb99 mutants have shorter siliques and reduced viable pollens	(Battat et al., 2019)
<i>MYB32</i>	Arabidopsis thaliana	Encodes a member of the R2R3 transcription	Mutation in <i>MYB32</i> exhibited	(Verma, 2019)

MYB4	Arabidopsis thaliana	Encodes a R2R3 MYB transcription factor MYB4 which is a negative regulator of phenylpropanoid pathway.	MYB4 insertion mutant also showed aberrant pollen grains, that were partially or completely devoid of cellular content.	(Verma, 2019)
SIHB8	Solanum lycopersicum	SIHB8 encodes a HD-Zip III family transcription factor.	SIHB8 knockout using CRISPR/Cas9 increased pollen activity, resulting in early fruit setting, whereas overexpression displayed opposite phenotypes.	(Wu et al., 2022)

The extended journey of the pollen grain after landing on the stigma

In order to ensure the delivery of the non-motile male gamete from the pollen grain to the ovule after pollination, pollen tube germination and its uninterrupted growth are the most crucial facets of a viable pollen grain. The contents of the tapetal cells discharged onto the surface of the maturing pollen grains serves their unique function to protect and make the pollen viable until pollination and pollen tube germination. The amphipathic oleosins containing steryl esters provide a waterproof surface for the pollen grains until pollination and later undergo rehydration, for pollen tube germination (Hsieh and Huang, 2007). However, the tip growth of the pollen tube is an extreme form of polarized cell growth that occurs exclusively from a single site. The pollen tube growth unlike plant cell wall expansion, grows specifically at the tip by exocytosis of pectins (Hayashi and Palmgren, 2021).

Pollen tube growth is extremely rapid, with a growth rate of up to 1 cm/h (Bedinger et al., 1994). The growth results from the dynamic formation of actin cables along which secretory vesicles move to provide new material to the tip of the pollen tube (Wen et al., 2016). Changes in H⁺ and Ca²⁺ concentrations control actin dynamics (Takeshita et al., 2017). In case of a polarized growth observed in pollen tubes, the directionality of cytoplasmic streaming is crucial. (Zhang et al., 2023b). The arrangement of the actin filaments within the tube directs this cytoplasmic streaming where the distribution of actin filaments at the cortex region have their barbed end facing towards the tip, while actin filaments at the inner region of the tube have barbed ends facing away from the tip (Figure 2). This ensures that organelle trafficking to the apex is

INTRODUCTION

prevented thus, facilitating their reverse movement toward the core (Jiang et al., 2017). Actin filament formation is regulated by a numerous of proteins that bind to actin. Actin regulatory proteins like formins, villins, fimbrins, LIMS, and profilins function in different stages of actin polymerization or depolymersation (Campellone and Welch, 2010). These regulatory proteins work at the nucleation stage of actin polymerization, capping of the barbed end of actin filament, severing and bundling of the filaments (Campellone and Welch, 2010).

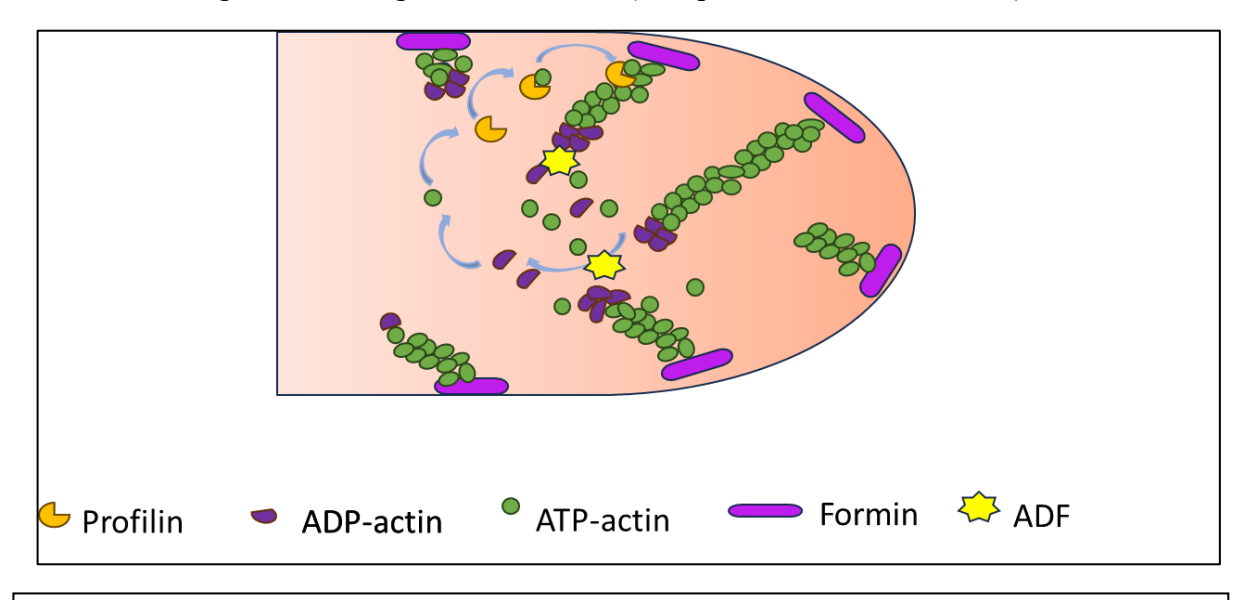


Figure 2: Schematic of actin filament polymerisation and depolymerisation in a pollen tube.

Formins initiate the dimerization and trimerization of actin monomers in the process of actin polymerisation, thus formins can be considered as cellular nucleators in the event of f-actin formation. The process begins with anchoring of a subset of plant formins (referred to as Group I formins) to the plasma membrane through their N-terminal transmembrane domain (Lan et al., 2018). In the growth domain of *Arabidopsis* pollen tubes, the Group I actin-nucleating formins FH3 and in particular, FH5 direct the formation of actin assemblies (Breitsprecher and Goode, 2013; Lan et al., 2018; Ye et al., 2009). Plant villins, belong to the villin/gelsolin/fragmin superfamily these proteins contain multiple 15 kDa gelsolin/severin domains in their peptide structure (Qu et al., 2013). Apart from the six gelsolin domains, villins have a head domain at the C-terminal that provides an additional microfilament binding site (Huang et al., 2015; Qu et al., 2013). This superfamily can manipulate microfilaments in multiple ways, including capping, severing, promoting nucleation, and bundling, some of which

are influenced by Ca²⁺ (Huang et al., 2015). Fimbrins are extensively studied actin-bundling proteins that are crucial for numerous actin-based processes across different species. Five fimbrin-like genes, FIM1-FIM5, are present in the Arabidopsis genome (Staiger and Hussey, 2004). Previous studies on AtFIM5 have been instrumental in advancing our understanding in the role AtFIM5 plays during pollen tube growth (Su et al., 2012; Wu et al., 2010; Zhang et al., 2016). AtFIM5 is present in the shank-oriented actin filaments of pollen tubes that gets concentrated in the apical region during pollen tube growth (Wu et al., 2010; Zhang et al., 2016). As a result the *atfim5* mutant show inhibited growth of pollen tube because of the disorganised actin filament in the apical and shank region of the pollen tube (Zhang et al., 2016). Profilin are multifaceted actin binding regulatory protein that interacts in a 1:1 stoichiometry with actin monomers (Liu et al., 2015). Studies have shown that the binding of Profilin to G-actin and localization of this actin-profilin complex to growing barbed end of actin, thus promoting actin polymerization (Liu et al., 2021; Pollard, 2016). Plant LIM proteins that are named after initials of containing proteins Lin11, Isl-1, and Mec-3, respectively play an active role in bundling of the f-actins in the pollen tubes (Ye et al., 2013). According to a recent study, the *PLIM2a* mutation resulted in short and swollen *Arabidopsis* pollen tube with defective actin bundles (Ye et al., 2013). There is a partially redundant function between PLIM2a and PLIM2b in the shank actin bundle organization during Arabidopsis pollen tube growth, as PLIM2b could rescue for the defective shank actin bundles in PLIM2a mutation pollen tubes (Ye et al., 2013). Profilin, is another actin filament binding protein that has been proposed to promote actin depolymerization by attaching themselves to actin monomers and sequestering them depending upon the Ca²⁺ concentration of the cell (Pollard, 2016). Finally, actin-depolymerizing factor (ADF) is a small molecular weight actin binding protein that regulates actin turnover in the cell (Inada, 2017). ADF preferentially binds to ADP-G actin and inhibit ADP- to ATP- nucleotide exchange.

This thesis attempts to identify the aberration during the development of the male gametes in *Arabidopsis* upon the mutation of *AtHMGB15*. The protein AtHMGB15 has been shown to interact closely with two pollen specific transcription factors AGL66 and AGL104 during pollen tube germination, and their respective knockout mutants have also been reported to exhibit male sterility (Xia et al., 2014). Studies until now have not explored the exact mechanism by which the mutants are projecting defective pollen grains. In this work, we have

INTRODUCTION

shown that AtHMGB15 also tweaks the expression of genes necessary for programmed cell death of tapetal cells, that is crucial during the formation of viable pollen grains with the signature exine ornamentation. Although the exact role of actin dynamics in vacuole organization and vesicle transport during post-tapetal degradation is not known, understanding these dynamics could lead to increased understanding of the PCD process during the development of pollen grains. We also studied the effects of disturbed pollen developmental process in the pollen tube germination stage of *athmgb15* pollen grains since our study revealed that AtHMGB15 also regulates the transcription of actin-related genes. The thesis begins by identifying the enriched gene clusters during different stages of anther development in *athmgb15* compared to wildtype followed by characterizing the tapetum degradation pattern in the AtHMGB15 loss of function mutant and the wild type anthers. The thesis also briefly elucidates the role of AtHMGB15 in the transcriptional network operational during the biosynthetic activity of the tapetal cells. Finally, it concludes with a comparative study of pollen grain development in another partially male sterile mutant, *arp4* and a discussion on how nuclear architectural proteins regulates pollen development and germination.

REFERENCES:

- 1. Antosch, M., Mortensen, S. A., and Grasser, K. D. (2012). Plant proteins containing high mobility group box DNA-binding domains modulate different nuclear processes. *Plant physiology* **159**, 875-883.
- 2. Åstrand, J., Knight, C., Robson, J., Talle, B., and Wilson, Z. A. (2021). Evolution and diversity of the angiosperm anther: trends in function and development. *Plant reproduction* **34**, 307-319.
- 3. Basak, S., and Kundu, P. (2022). Plant metacaspases: Decoding their dynamics in development and disease. *Plant Physiology and Biochemistry* **180**, 50-63.
- 4. Battat, M., Eitan, A., Rogachev, I., Hanhineva, K., Fernie, A., Tohge, T., Beekwilder, J., and Aharoni, A. (2019). A MYB triad controls primary and phenylpropanoid metabolites for pollen coat patterning. *Plant Physiology* **180**, 87-108.
- 5. Bedinger, P. A., Hardeman, K. J., and Loukides, C. A. (1994). Travelling in style: the cell biology of pollen. *Trends in cell biology* **4**, 132-138.
- 6. Biswas, R., Chaudhuri, S. (2024). AtHMGB15 regulates tapetal apoptosis in pollen development and actin dynamics during pollen germination in arabidopsis. . *Plant Reproduction*.
- 7. Bowman, G. D., and Poirier, M. G. (2014). Post-translational modifications of histones that influence nucleosome dynamics. *Chemical reviews* **115**, 2274-2295.
- 8. Breitsprecher, D., and Goode, B. L. (2013). Formins at a glance. *Journal of cell science* **126**, 1-7.
- 9. Campellone, K. G., and Welch, M. D. (2010). A nucleator arms race: cellular control of actin assembly. *Nature reviews Molecular cell biology* **11**, 237-251.
- 10. Canales, C., Bhatt, A. M., Scott, R., and Dickinson, H. (2002). EXS, a putative LRR receptor kinase, regulates male germline cell number and tapetal identity and promotes seed development in Arabidopsis. *Current biology* 12, 1718-1727.
- 11. Chang, Z., Chen, Z., Yan, W., Xie, G., Lu, J., Wang, N., Lu, Q., Yao, N., Yang, G., and Xia, J. (2016). An ABC transporter, OsABCG26, is required for anther cuticle and pollen exine formation and pollen-pistil interactions in rice. *Plant Science* **253**, 21-30.
- 12. Chapman, G. (1987). The tapetum. *In* "International review of cytology", Vol. 107, pp. 111-125. Elsevier.
- 13. Chaubal, R., Anderson, J. R., Trimnell, M. R., Fox, T. W., Albertsen, M. C., and Bedinger, P. (2003). The transformation of anthers in the mscal mutant of maize. *Planta* **216**, 778-788.

- 14. Chen, W., Lv, M., Wang, Y., Wang, P.-A., Cui, Y., Li, M., Wang, R., Gou, X., and Li, J. (2019). BES1 is activated by EMS1-TPD1-SERK1/2-mediated signaling to control tapetum development in Arabidopsis thaliana. *Nature Communications* **10**, 4164.
- 15. Cheng, Z., Guo, X., Zhang, J., Liu, Y., Wang, B., Li, H., and Lu, H. (2020). βVPE is involved in tapetal degradation and pollen development by activating proprotease maturation in Arabidopsis thaliana. *Journal of Experimental Botany* **71**, 1943-1955.
- 16. Cheng Z, G. X., Zhang J, Liu Y, Wang B, Li H, Lu H. βVPE is involved in tapetal degradation and pollen development by activating proprotease maturation in Arabidopsis thaliana. J Exp Bot. 2020 Mar 25;71(6):1943-1955. doi: 10.1093/jxb/erz560. PMID: 31858 (2020 Mar 25). βVPE is involved in tapetal degradation and pollen development by activating proprotease maturation in Arabidopsis thaliana. . J Exp Bot. 71(6):1943-1955.
- 17. Corpas, F. J., Gupta, D. K., and Palma, J. M. (2015). Production sites of reactive oxygen species (ROS) in organelles from plant cells. *Reactive oxygen species and oxidative damage in plants under stress*, 1-22.
- 18. Cui, J., You, C., Zhu, E., Huang, Q., Ma, H., and Chang, F. (2016). Feedback regulation of DYT1 by interactions with downstream bHLH factors promotes DYT1 nuclear localization and anther development. *The Plant Cell* **28**, 1078-1093.
- 19. Cui, Y., Lu, X., and Gou, X. (2022). Receptor-like protein kinases in plant reproduction: Current understanding and future perspectives. *Plant Communications* 3.
- 20. de Azevedo Souza, C., Kim, S. S., Koch, S., Kienow, L., Schneider, K., McKim, S. M., Haughn, G. W., Kombrink, E., and Douglas, C. J. (2009). A novel fatty acyl-CoA synthetase is required for pollen development and sporopollenin biosynthesis in Arabidopsis. *The Plant Cell* 21, 507-525.
- 21. Diane L. Hird, D. W., Rachel Hodge, Sarah Smartt, Wyatt Paul, Rod Scott (1993). The anther-specific protein encoded by the Brassica napus and Arabidopsis thaliana A6 gene displays similarity to β-1,3-glucanases. *The Plant Journal* **Volume4**, .
- 22. Dobritzsch, S., Weyhe, M., Schubert, R., Dindas, J., Hause, G., Kopka, J., and Hause, B. (2015). Dissection of jasmonate functions in tomato stamen development by transcriptome and metabolome analyses. *BMC biology* **13**, 1-18.
- 23. Doll, N. M. (2023). Stop vitamins: Low levels of ascorbic acid regulate the transition from cell proliferation to differentiation in Arabidopsis tapetum. Oxford University Press US.

- 24. Dragwidge, J. M., and Van Damme, D. (2020). Visualising endocytosis in plants: past, present, and future. *Journal of microscopy* **280**, 104-110.
- 25. Echlin, P. (1971a). Production of sporopollenin by the tapetum. *In* "Sporopollenin", pp. 220-247. Elsevier.
- 26. Echlin, P. (1971b). The role of the tapetum during microsporogenesis of angiosperms. *In* "Pollen", pp. 41-61. Elsevier.
- 27. El-Ghazaly, G. (1999). Tapetum and orbicules (Ubisch bodies): development, morphology and role of pollen grains and tapetal orbicules in allergenicity. *In* "Fertilization in Higher Plants: Molecular and Cytological Aspects", pp. 157-173. Springer.
- 28. Erler, J., Zhang, R., Petridis, L., Cheng, X., Smith, J. C., and Langowski, J. (2014). The role of histone tails in the nucleosome: a computational study. *Biophysical journal* **107**, 2911-2922.
- 29. Fábián, A., Péntek, B. K., Soós, V., and Sági, L. (2023). Heat stress during male meiosis impairs cytoskeletal organization, spindle assembly and tapetum degeneration in wheat. *Frontiers in Plant Science* 14.
- 30. Fang, X., Feng, X., Sun, X., Yang, X., Li, Q., Yang, X., Xu, J., Zhou, M., Lin, C., and Sui, Y. (2023). Natural variation of MS2 confers male fertility and drives hybrid breeding in soybean. *Plant Biotechnology Journal* **21**, 2322-2332.
- 31. Feng, J., Qin, M., Yao, L., Li, Y., Han, R., and Ma, L. (2022). The N-terminal acetyltransferase Naa50 regulates tapetum degradation and pollen development in Arabidopsis. *Plant Science* **316**, 111180.
- 32. Feng J, Q. M., Yao L, Li Y, Han R, Ma L. (2022). The N-terminal acetyltransferase Naa50 regulates tapetum degradation and pollen development in Arabidopsis. . *Plant Sci.* .
- 33. Feng, X., and Dickinson, H. G. (2010). Tapetal cell fate, lineage and proliferation in the Arabidopsis anther. *Development* **137**, 2409-2416.
- 34. Gadjev, I., Stone, J. M., and Gechev, T. S. (2008). Programmed cell death in plants: new insights into redox regulation and the role of hydrogen peroxide. *International review of cell and molecular biology* **270**, 87-144.
- 35. Gechev, T., Petrov, V., and Minkov, I. (2010). Reactive oxygen species and programmed cell death. *In* "Reactive oxygen species and antioxidants in higher plants", pp. 81-94. CRC Press.
- 36. Geng, P., Zhang, S., Liu, J., Zhao, C., Wu, J., Cao, Y., Fu, C., Han, X., He, H., and Zhao, Q. (2020). MYB20, MYB42, MYB43, and MYB85 regulate phenylalanine and lignin biosynthesis during secondary cell wall formation. *Plant Physiology* **182**, 1272-1283.

- 37. Gilroy, S., Suzuki, N., Miller, G., Choi, W.-G., Toyota, M., Devireddy, A. R., and Mittler, R. (2014). A tidal wave of signals: calcium and ROS at the forefront of rapid systemic signaling. *Trends in plant science* **19**, 623-630.
- 38. Gómez-Díaz, E., and Corces, V. G. (2014). Architectural proteins: regulators of 3D genome organization in cell fate. *Trends in cell biology* **24**, 703-711.
- 39. Gómez, J. F., Talle, B., and Wilson, Z. A. (2015). Anther and pollen development: a conserved developmental pathway. *Journal of integrative plant biology* **57**, 876-891.
- 40. Goodman, K., Paez-Valencia, J., Pennington, J., Sonntag, A., Ding, X., Lee, H. N., Ahlquist, P. G., Molina, I., and Otegui, M. S. (2021). ESCRT components ISTL1 andLIP5 are required for tapetal function and pollen viability. *The Plant Cell* 33, 2850-2868.
- 41. Grasser, K. D. (2003). Chromatin-associated HMGA and HMGB proteins: versatile co-regulators of DNA-dependent processes. *Plant molecular biology* **53**, 281-295.
- 42. Grunewald S, M. S., Hause G, et al. (2020;). The Tapetal Major Facilitator NPF2.8 Is Required for Accumulation of Flavonol Glycosides on the Pollen Surface in Arabidopsis thaliana. . *Plant Cell.* **32(5):**, 1727-1748. .
- 43. Gui-Min Yin a, Y.-R. F. a., Jia-Gang Wang b 1, Yue Liu b, Xiaojiao Xiang b, Sha Li b, Yan Zhang (2024). Arabidopsis HAPLESS13/AP-1μ is critical for pollen sac formation and tapetal function. *Plant Sci.* Volume 341, .
- 44. Gui, J., Shen, J., and Li, L. (2011). Functional characterization of evolutionarily divergent 4-coumarate: coenzyme a ligases in rice. *Plant physiology* **157**, 574-586.
- 45. Guo, X., Li, L., Liu, X., Zhang, C., Yao, X., Xun, Z., Zhao, Z., Yan, W., Zou, Y., and Liu, D. (2022). MYB2 Is Important for Tapetal PCD and Pollen Development by Directly Activating Protease Expression in Arabidopsis. *International Journal of Molecular Sciences* 23, 3563.
- 46. Hara-Nishimura, I., and Hatsugai, N. (2011). The role of vacuole in plant cell death. *Cell Death & Differentiation* **18**, 1298-1304.
- 47. Hayashi, M., and Palmgren, M. (2021). The quest for the central players governing pollen tube growth and guidance. *Plant Physiology* **185**, 682-693.
- 48. Higaki, T., Kurusu, T., Hasezawa, S., and Kuchitsu, K. (2011). Dynamic intracellular reorganization of cytoskeletons and the vacuole in defense responses and hypersensitive cell death in plants. *Journal of plant research* **124**, 315-324.

- 49. Higginson, T., Li, S. F., and Parish, R. W. (2003). AtMYB103 regulates tapetum and trichome development in Arabidopsis thaliana. *The Plant Journal* **35**, 177-192.
- 50. Hirano, K., Aya, K., Hobo, T., Sakakibara, H., Kojima, M., Shim, R. A., Hasegawa, Y., Ueguchi-Tanaka, M., and Matsuoka, M. (2008). Comprehensive transcriptome analysis of phytohormone biosynthesis and signaling genes in microspore/pollen and tapetum of rice. *Plant and Cell Physiology* **49**, 1429-1450.
- 51. Hird, D. L., Worrall, D., Hodge, R., Smartt, S., Paul, W., and Scott, R. (1993). The anther-specific protein encoded by the Brassica napus and Arabidopsis thaliana A6 gene displays similarity to β-1, 3-glucanases. *The Plant Journal* **4**, 1023-1033.
- 52. Hong, L., Tang, D., Zhu, K., Wang, K., Li, M., and Cheng, Z. (2012). Somatic and reproductive cell development in rice anther is regulated by a putative glutaredoxin. *The Plant Cell* **24**, 577-588.
- 53. Hord, C. L., Chen, C., DeYoung, B. J., Clark, S. E., and Ma, H. (2006). The BAM1/BAM2 receptor-like kinases are important regulators of Arabidopsis early anther development. *The Plant Cell* **18**, 1667-1680.
- 54. Hord, C. L., Sun, Y.-J., Pillitteri, L. J., Torii, K. U., Wang, H., Zhang, S., and Ma, H. (2008). Regulation of Arabidopsis early anther development by the mitogen-activated protein kinases, MPK3 and MPK6, and the ERECTA and related receptor-like kinases. *Molecular plant* 1, 645-658.
- 55. Hsieh, K., and Huang, A. H. (2004). Endoplasmic reticulum, oleosins, and oils in seeds and tapetum cells. *Plant Physiology* **136**, 3427-3434.
- 56. Hsieh, K., and Huang, A. H. (2007). Tapetosomes in Brassica tapetum accumulate endoplasmic reticulum–derived flavonoids and alkanes for delivery to the pollen surface. *The Plant Cell* **19**, 582-596.
- 57. Hu, C., Zhu, Y., Cui, Y., Cheng, K., Liang, W., Wei, Z., Zhu, M., Yin, H., Zeng, L., and Xiao, Y. (2018). A group of receptor kinases are essential for CLAVATA signalling to maintain stem cell homeostasis. *Nature plants* **4**, 205-211.
- 58. Hu, L., Liang, W., Yin, C., Cui, X., Zong, J., Wang, X., Hu, J., and Zhang, D. (2011). Rice MADS3 regulates ROS homeostasis during late anther development. *The Plant Cell* **23**, 515-533.
- 59. Hu R, W. J., Yang H, Wei D, Tang Q, Yang Y, Tian S, Wang Z. (2023 Jul 11). Comparative transcriptome analysis reveals the involvement of an MYB transcriptional activator, SmMYB108, in anther dehiscence in eggplant. . *Front Plant Sci.* 14:1164467.

- 60. Hua, M., Yin, W., Fernández Gómez, J., Tidy, A., Xing, G., Zong, J., Shi, S., and Wilson, Z. A. (2023). Barley TAPETAL DEVELOPMENT and FUNCTION1 (HvTDF1) gene reveals conserved and unique roles in controlling anther tapetum development in dicot and monocot plants. *New Phytologist* **240**, 173-190.
- 61. Huang, J., Gu, M., Lai, Z., Fan, B., Shi, K., Zhou, Y.-H., Yu, J.-Q., and Chen, Z. (2010a). Functional Analysis of the Arabidopsis PAL Gene Family in Plant Growth, Development, and Response to Environmental Stress *Plant Physiology* **153**, 1526-1538.
- 62. Huang, J., Gu, M., Lai, Z., Fan, B., Shi, K., Zhou, Y.-H., Yu, J.-Q., and Chen, Z. (2010b). Functional analysis of the Arabidopsis PAL gene family in plant growth, development, and response to environmental stress. *Plant physiology* **153**, 1526-1538.
- 63. Huang, J., Zhang, T., Linstroth, L., Tillman, Z., Otegui, M. S., Owen, H. A., and Zhao, D. (2016). Control of anther cell differentiation by the small protein ligand TPD1 and its receptor EMS1 in Arabidopsis. *PLoS Genetics* **12**, e1006147.
- 64. Huang, M.-D., Chen, T.-L. L., and Huang, A. H. C. (2013). Abundant Type III Lipid Transfer Proteins in Arabidopsis Tapetum Are Secreted to the Locule and Become a Constituent of the Pollen Exine *Plant Physiology* **163**, 1218-1229.
- 65. Huang, S., Qu, X., and Zhang, R. (2015). Plant villins: versatile actin regulatory proteins. *Journal of integrative plant biology* **57**, 40-49.
- 66. Huang, Y., Cao, H., Yang, L., Chen, C., Shabala, L., Xiong, M., Niu, M., Liu, J., Zheng, Z., and Zhou, L. (2019). Tissue-specific respiratory burst oxidase homolog-dependent H2O2 signaling to the plasma membrane H+-ATPase confers potassium uptake and salinity tolerance in Cucurbitaceae. *Journal of Experimental Botany* 70, 5879-5893.
- 67. Huysmans, M., Coll, N. S., and Nowack, M. K. (2017). Dying two deaths—programmed cell death regulation in development and disease. *Current opinion in plant biology* **35**, 37-44.
- 68. Hyunju Choi, J.-Y. J., Setbyoul Choi, Jae-Ung Hwang, Yu-Young Kim, Mi Chung Suh, Youngsook Lee (2010). An ABCG/WBC-type ABC transporter is essential for transport of sporopollenin precursors for exine formation in developing pollen. *The Plant Journal*.
- 69. Iida, H., Mähönen, A. P., Jürgens, G., and Takada, S. (2023). Epidermal injury-induced derepression of key regulator ATML1 in newly exposed cells elicits epidermis regeneration. *Nature Communications* **14**, 1031.

- 70. Inada, N. (2017). Plant actin depolymerizing factor: actin microfilament disassembly and more. Journal of plant research 130, 227-238.
- 71. Ito, T., Nagata, N., Yoshiba, Y., Ohme-Takagi, M., Ma, H., and Shinozaki, K. (2007). Arabidopsis MALE STERILITY1 encodes a PHD-type transcription factor and regulates pollen and tapetum development. *The Plant Cell* **19**, 3549-3562.
- 72. Jacobowitz, J. R., Doyle, W. C., and Weng, J.-K. (2019). PRX9 and PRX40 are extensin peroxidases essential for maintaining tapetum and microspore cell wall integrity during Arabidopsis anther development. *The Plant Cell* **31**, 848-861.
- 73. Jiang, C., Wang, J., Leng, H.-N., Wang, X., Liu, Y., Lu, H., Lu, M.-Z., and Zhang, J. (2021). Transcriptional regulation and signaling of developmental programmed cell death in plants. *Frontiers in Plant Science* **12**, 702928.
- 74. Jiang, Y., Zhang, M., and Huang, S. (2017). Analysis of actin-based intracellular trafficking in pollen tubes. *Plant Protein Secretion: Methods and Protocols*, 125-136.
- 75. Jing-Shi Xue 7, B. Z., HuaDong Zhan 7, Yong-Lin Lv, Xin-Lei Jia, TianHua Wang, Nai-Ying Yang, Yu-Xia Lou, Zai-Bao Zhang, Wen-Jing Hu, Jinshan Gui, Jianguo Cao, Ping Xu, Yihua Zhou, Jin-Feng Hu, Laigeng Li, Zhong-Nan Yang (2020). Phenylpropanoid Derivatives Are Essential Components of Sporopollenin in Vascular Plants.
- 76. Jogam, P., Savitikadi, P., Sandhya, D., Ellendula, R., Peddaboina, V., Allini, V. R., and Abbagani, S. (2024). Tapetum-specific expression of cysteine protease induces male sterility in tomato. *Plant Gene* **38**, 100454.
- 77. Jung, K.-H., Han, M.-J., Lee, Y.-S., Kim, Y.-W., Hwang, I., Kim, M.-J., Kim, Y.-K., Nahm, B. H., and An, G. (2005). Rice Undeveloped Tapetum1 is a major regulator of early tapetum development. *The Plant Cell* 17, 2705-2722.
- 78. Kamata, N., Sugihara, A., Komeda, Y., and Takahashi, T. (2013). Allele-specific effects of PDF2 on floral morphology in Arabidopsis thaliana. *Plant signaling & behavior* **8**, e27417.
- 79. Kawanabe, T., Ariizumi, T., Kawai-Yamada, M., Uchimiya, H., and Toriyama, K. (2006). Abolition of the tapetum suicide program ruins microsporogenesis. *Plant and Cell Physiology* **47**, 784-787.
- 80. Kelliher, T. J. (2013). "Germinal and somatic cell fate acquisition in early maize anther development: morphogenetic mechanisms underlying pre-meiotic differentiation," Stanford University.

- 81. Kim, S. H., Lee, S. H., Park, T. K., Tian, Y., Yu, K., Lee, B. h., Bai, M. Y., Cho, S. J., and Kim, T. W. (2024). Comparative analysis of BZR1/BES1 family transcription factors in Arabidopsis. *The Plant Journal* 117, 747-765.
- 82. Kim SungSoo, K. S., Grienenberger, E., Lallemand, B., Colpitts, C., Kim SunYoung, K. S., Souza, C. d. A., Geoffroy, P., Heintz, D., Krahn, D., and Kaiser, M. (2010). LAP6/POLYKETIDE SYNTHASE A and LAP5/POLYKETIDE SYNTHASE B encode hydroxyalkyl-pyrone synthases required for pollen development and sporopollenin biosynthesis in Arabidopsis thaliana.
- 83. Kurusu, T., Koyano, T., Hanamata, S., Kubo, T., Noguchi, Y., Yagi, C., Nagata, N., Yamamoto, T., Ohnishi, T., and Okazaki, Y. (2014). OsATG7 is required for autophagy-dependent lipid metabolism in rice postmeiotic anther development. *Autophagy* **10**, 878-888.
- 84. Lallemand, B., Erhardt, M., Heitz, T., and Legrand, M. (2013). Sporopollenin biosynthetic enzymes interact and constitute a metabolon localized to the endoplasmic reticulum of tapetum cells. *Plant physiology* **162**, 616-625.
- 85. Lan, Y., Liu, X., Fu, Y., and Huang, S. (2018). Arabidopsis class I formins control membrane-originated actin polymerization at pollen tube tips. *PLoS Genetics* **14**, e1007789.
- 86. Lavania, U. C., Basu, S., Kushwaha, J. S., and Lavania, S. (2014). Seasonal temperature variations influence tapetum mitosis patterns associated with reproductive fitness. *Genome* **57**, 517-521.
- 87. Lei, T., Zhang, L., Feng, P., Liu, Y., Yin, W., Shang, L., He, G., and Wang, N. (2022). OsMYB103 is essential for tapetum degradation in rice. *Theoretical and Applied Genetics*, 1-17.
- 88. Lei, X., and Liu, B. (2020). Tapetum-dependent male meiosis progression in plants: increasing evidence emerges. *Frontiers in Plant Science* **10**, 1667.
- 89. Lelli, K. M., Slattery, M., and Mann, R. S. (2012). Disentangling the many layers of eukaryotic transcriptional regulation. *Annual review of genetics* **46**, 43-68.
- 90. Li, S., Lauri, A., Ziemann, M., Busch, A., Bhave, M., and Zachgo, S. (2009). Nuclear activity of ROXY1, a glutaredoxin interacting with TGA factors, is required for petal development in Arabidopsis thaliana. *The Plant Cell* **21**, 429-441.
- 91. Li, X.-C., Zhu, J., Yang, J., Zhang, G.-R., Xing, W.-F., Zhang, S., and Yang, Z.-N. (2012). Glycerol-3-phosphate acyltransferase 6 (GPAT6) is important for tapetum development in Arabidopsis and plays multiple roles in plant fertility. *Molecular Plant* 5, 131-142.

- 92. Li Xiao-Chuan, Z. J., Yang Jun, Zhang Guo-Rui, Xing Wei-Feng, Zhang Sen, Yang Zhong-Nan (2012). Glycerol-3-Phosphate Acyltransferase 6 (GPAT6) Is Important for Tapetum Development in Arabidopsis and Plays Multiple Roles in Plant Fertility. *Molecular Plant* **Volume 5**,
- 93. Li, Y., Kim, J. I., Pysh, L., and Chapple, C. (2015). Four isoforms of Arabidopsis 4-coumarate: CoA ligase have overlapping yet distinct roles in phenylpropanoid metabolism. *Plant physiology* **169**, 2409-2421.
- 94. Li, Z., Wang, Y., Huang, J., Ahsan, N., Biener, G., Paprocki, J., Thelen, J. J., Raicu, V., and Zhao, D. (2017). Two SERK receptor-like kinases interact with EMS1 to control anther cell fate determination. *Plant Physiology* **173**, 326-337.
- 95. Liu, C., Zhang, Y., and Ren, H. (2021). Profilin promotes formin-mediated actin filament assembly and vesicle transport during polarity formation in pollen. *The Plant Cell* **33**, 1252-1267.
- 96. Liu, X., Huang, J., Parameswaran, S., Ito, T., Seubert, B., Auer, M., Rymaszewski, A., Jia, G., Owen, H. A., and Zhao, D. (2009). The SPOROCYTELESS/NOZZLE gene is involved in controlling stamen identity in Arabidopsis. *Plant Physiology* **151**, 1401-1411.
- 97. Liu, X., Qu, X., Jiang, Y., Chang, M., Zhang, R., Wu, Y., Fu, Y., and Huang, S. (2015). Profilin regulates apical actin polymerization to control polarized pollen tube growth. *Molecular Plant* **8**, 1694-1709.
- 98. Lou, Y., Xu, X.-F., Zhu, J., Gu, J.-N., Blackmore, S., and Yang, Z.-N. (2014). The tapetal AHL family protein TEK determines nexine formation in the pollen wall. *Nature Communications* **5**, 3855.
- 99. Lou, Y., Zhou, H. S., Han, Y., Zeng, Q. Y., Zhu, J., and Yang, Z. N. (2018). Positive regulation of AMS by TDF1 and the formation of a TDF1–AMS complex are required for anther development in Arabidopsis thaliana. *New Phytologist* **217**, 378-391.
- 100. Lu, J.-Y., Xiong, S.-X., Yin, W., Teng, X.-D., Lou, Y., Zhu, J., Zhang, C., Gu, J.-N., Wilson, Z. A., and Yang, Z.-N. (2020). MS1, a direct target of MS188, regulates the expression of key sporophytic pollen coat protein genes in Arabidopsis. *Journal of Experimental Botany* **71**, 4877-4889.
- 101. Lu, P., Chai, M., Yang, J., Ning, G., Wang, G., and Ma, H. (2014). The Arabidopsis CALLOSE DEFECTIVE MICROSPORE1 Gene Is Required for Male Fertility through Regulating Callose Metabolism during Microsporogenesis *Plant Physiology* 164, 1893-1904.
- 102. Mallik, R., Kundu, A., and Chaudhuri, S. (2018). High mobility group proteins: the multifaceted regulators of chromatin dynamics. *The Nucleus* **61**, 213-226.
- 103. Mallik, R., Prasad, P., Kundu, A., Sachdev, S., Biswas, R., Dutta, A., Roy, A., Mukhopadhyay, J., Bag, S. K., and Chaudhuri, S. (2020). Identification of genome-wide targets and DNA recognition

- sequence of the Arabidopsis HMG-box protein AtHMGB15 during cold stress response. *Biochimica et Biophysica Acta (BBA)-Gene Regulatory Mechanisms* **1863**, 194644.
- 104. Mark G.M. Aarts, R. H., Kriton Kalantidis, Dion Florack, Zoe A. Wilson, Bernard J. Mulligan, Willem J. Stiekema, Rod Scott, Andy Pereira (2003). The Arabidopsis MALE STERILITY 2 protein shares similarity with reductases in elongation/condensation complexes. *The Plant Journal*.
- 105. McBryant, S. J., Adams, V. H., and Hansen, J. C. (2006). Chromatin architectural proteins. *Chromosome Research* **14**, 39-51.
- 106. Millar, A. A., and Gubler, F. (2005). The Arabidopsis GAMYB-like genes, MYB33 and MYB65, are microRNA-regulated genes that redundantly facilitate anther development. *The Plant Cell* **17**, 705-721.
- 107. Millar, A. A., Lohe, A., and Wong, G. (2019). Biology and function of miR159 in plants. *Plants* **8**, 255.
- 108. Minina, E. A., Smertenko, A. P., and Bozhkov, P. V. (2014). Vacuolar cell death in plants: metacaspase releases the brakes on autophagy. *Autophagy* **10**, 928-929.
- 109. Mir Derikvand, M., Sierra, J. B., Ruel, K., Pollet, B., Do, C.-T., Thévenin, J., Buffard, D., Jouanin, L., and Lapierre, C. (2008). Redirection of the phenylpropanoid pathway to feruloyl malate in Arabidopsis mutants deficient for cinnamoyl-CoA reductase 1. *Planta* 227, 943-956.
- 110. Moon, J., Skibbe, D., Timofejeva, L., Wang, C. J. R., Kelliher, T., Kremling, K., Walbot, V., and Cande, W. Z. (2013). Regulation of cell divisions and differentiation by MALE STERILITY 32 is required for anther development in maize. *The Plant Journal* 76, 592-602.
- 111. Morant M, J. K., Schaller H, et al. (2007;). CYP703 is an ancient cytochrome P450 in land plants catalyzing in-chain hydroxylation of lauric acid to provide building blocks for sporopollenin synthesis in pollen. . *Plant Cell.* **19(5):1473-1487.** .
- 112. Murmu, J., Bush, M. J., DeLong, C., Li, S., Xu, M., Khan, M., Malcolmson, C., Fobert, P. R., Zachgo, S., and Hepworth, S. R. (2010). Arabidopsis basic leucine-zipper transcription factors TGA9 and TGA10 interact with floral glutaredoxins ROXY1 and ROXY2 and are redundantly required for anther development. *Plant Physiology* **154**, 1492-1504.
- 113. Nagata, K., and Abe, M. (2023). A conserved mechanism determines the activity of two pivotal transcription factors that control epidermal cell differentiation in Arabidopsis thaliana. *Journal of Plant Research* **136**, 349-358.

- 114. Nan, G.-L., Teng, C., Fernandes, J., O'Connor, L., Meyers, B. C., and Walbot, V. (2022). A cascade of bHLH-regulated pathways programs maize anther development. *The Plant Cell* **34**, 1207-1225.
- 115. Niu, N., Liang, W., Yang, X., Jin, W., Wilson, Z. A., Hu, J., and Zhang, D. (2013). EAT1 promotes tapetal cell death by regulating aspartic proteases during male reproductive development in rice. *Nature communications* **4**, 1445.
- 116. Nonomura, K.-I., Miyoshi, K., Eiguchi, M., Suzuki, T., Miyao, A., Hirochika, H., and Kurata, N. (2003). The MSP1 gene is necessary to restrict the number of cells entering into male and female sporogenesis and to initiate anther wall formation in rice. *The Plant Cell* **15**, 1728-1739.
- 117. Ogawa, E., Yamada, Y., Sezaki, N., Kosaka, S., Kondo, H., Kamata, N., Abe, M., Komeda, Y., and Takahashi, T. (2015). ATML1 and PDF2 play a redundant and essential role in Arabidopsis embryo development. *Plant and Cell Physiology* **56**, 1183-1192.
- 118. Pacini, E. (2010). Relationships between tapetum, loculus, and pollen during development. *International Journal of Plant Sciences* **171**, 1-11.
- 119. Pacini, E. (2016). 11 Tapetum and microspore function. *Microspores Evolution and Ontogeny:* Evolution and Ontogeny, 213.
- 120. Pacini, E., Franchi, G., and Hesse, M. (1985). The tapetum: its form, function, and possible phylogeny in Embryophyta. *Plant Systematics and Evolution* **149**, 155-185.
- 121. Parish, R. W., and Li, S. F. (2010). Death of a tapetum: a programme of developmental altruism. *Plant Science* **178**, 73-89.
- 122. Phan, H. A., Iacuone, S., Li, S. F., and Parish, R. W. (2011). The MYB80 transcription factor is required for pollen development and the regulation of tapetal programmed cell death in Arabidopsis thaliana. *The Plant Cell* **23**, 2209-2224.
- 123. Pollard, T. D. (2016). Actin and actin-binding proteins. *Cold Spring Harbor perspectives in biology* **8**, a018226.
- 124. Preston, J. C., Wang, H., Kursel, L., Doebley, J., and Kellogg, E. A. (2012). The role of teosinte glume architecture (tga1) in coordinated regulation and evolution of grass glumes and inflorescence axes. *New Phytologist* **193**, 204-215.
- 125. Qian, Q., Yang, Y., Zhang, W., Hu, Y., Li, Y., Yu, H., and Hou, X. (2021). A novel Arabidopsis gene RGAT1 is required for GA-mediated tapetum and pollen development. *New Phytologist* **231**, 137-151.

- 126. Qu, X., Zhang, H., Xie, Y., Wang, J., Chen, N., and Huang, S. (2013). Arabidopsis villins promote actin turnover at pollen tube tips and facilitate the construction of actin collars. *The Plant Cell* **25**, 1803-1817.
- 127. Quilichini, T. D., Friedmann, M. C., Samuels, A. L., and Douglas, C. J. (2010). ATP-binding cassette transporter G26 is required for male fertility and pollen exine formation in Arabidopsis. *Plant Physiology* **154**, 678-690.
- 128. Quilichini, T. D., Grienenberger, E., and Douglas, C. J. (2015). The biosynthesis, composition and assembly of the outer pollen wall: A tough case to crack. *Phytochemistry* **113**, 170-182.
- 129. Quilichini, T. D., Samuels, A. L., and Douglas, C. J. (2014). ABCG26-mediated polyketide trafficking and hydroxycinnamoyl spermidines contribute to pollen wall exine formation in Arabidopsis. *The Plant Cell* **26**, 4483-4498.
- 130. Ren, H., Zhao, X., Li, W., Hussain, J., Qi, G., and Liu, S. (2021a). Calcium signaling in plant programmed cell death. *Cells* **10**, 1089.
- 131. Ren, W., Zhao, W., Cao, L., and Huang, J. (2021b). Involvement of the actin machinery in programmed cell death. *Frontiers in Cell and Developmental Biology* **8**, 634849.
- 132. Roy, A., Dutta, A., Roy, D., Ganguly, P., Ghosh, R., Kar, R. K., Bhunia, A., Mukhobadhyay, J., and Chaudhuri, S. (2016). Deciphering the role of the AT-rich interaction domain and the HMG-box domain of ARID-HMG proteins of Arabidopsis thaliana. *Plant molecular biology* **92**, 371-388.
- 133. Sachdev, S., Biswas, R., Roy, A., Nandi, A., Roy, V., Basu, S., and Chaudhuri, S. (2024). The Arabidopsis ARID-HMG DNA-BINDING PROTEIN 15 modulates JA signaling by regulating MYC2 during pollen development. *Plant Physiology*.
- 134. Saha, D., Hailu, S., Hada, A., Lee, J., Luo, J., Ranish, J. A., Lin, Y.-c., Feola, K., Persinger, J., and Jain, A. (2023). The AT-hook is an evolutionarily conserved auto-regulatory domain of SWI/SNF required for cell lineage priming. *Nature communications* **14**, 4682.
- 135. Sanchez, P., de Torres Zabala, M., and Grant, M. (2000). AtBI-1, a plant homologue of Bax inhibitor-1, suppresses Bax-induced cell death in yeast and is rapidly upregulated during wounding and pathogen challenge. *The Plant Journal* **21**, 393-399.
- 136. Schilmiller, A. L., Stout, J., Weng, J. K., Humphreys, J., Ruegger, M. O., and Chapple, C. (2009). Mutations in the cinnamate 4-hydroxylase gene impact metabolism, growth and development in Arabidopsis. *The Plant Journal* **60**, 771-782.

- 137. Schubert, R., Grunewald, S., von Sivers, L., and Hause, B. (2019). Effects of jasmonate on ethylene function during the development of tomato stamens. *Plants* **8**, 277.
- 138. Sera, Y., Hanamata, S., Sakamoto, S., Ono, S., Kaneko, K., Mitsui, Y., Koyano, T., Fujita, N., Sasou, A., and Masumura, T. (2019). Essential roles of autophagy in metabolic regulation in endosperm development during rice seed maturation. *Scientific reports* **9**, 18544.
- 139. Shin, R. (2022). Chapter 24 Regulation of cation transports and cation homeostasis in higher plants. *Cation Transporters in Plants*, Pages 437-453.
- 140. Staiger, C. J., and Hussey, P. J. (2004). Actin and actin-modulating proteins. *The Plant Cytoskeleton in Cell Differentiation and Development. Blackwell Scientific Publications, Oxford*, 32-80.
- 141. Strome, S., and Updike, D. (2015). Specifying and protecting germ cell fate. *Nature reviews Molecular cell biology* **16**, 406-416.
- 142. Su, H., Zhu, J., Cai, C., Pei, W., Wang, J., Dong, H., and Ren, H. (2012). FIMBRIN1 is involved in lily pollen tube growth by stabilizing the actin fringe. *The Plant Cell* **24**, 4539-4554.
- 143. Takeshita, N., Evangelinos, M., Zhou, L., Serizawa, T., Somera-Fajardo, R. A., Lu, L., Takaya, N., Nienhaus, G. U., and Fischer, R. (2017). Pulses of Ca2+ coordinate actin assembly and exocytosis for stepwise cell extension. *Proceedings of the National Academy of Sciences* **114**, 5701-5706.
- 144. Tao, J., Pan, Z., Kong, W., Mo, B., Chen, X., and Yu, Y. (2023). miR319-TCPs-TGA9/TGA10/ROXY2 regulatory module controls cell fate specification in early anther development in Arabidopsis. *Science China Life Sciences*, 1-4.
- 145. Taylor, R. C., Cullen, S. P., and Martin, S. J. (2008). Apoptosis: controlled demolition at the cellular level. *Nature reviews Molecular cell biology* **9**, 231-241.
- 146. Teng, C., Zhang, H., Hammond, R., Huang, K., Meyers, B. C., and Walbot, V. (2020). Dicer-like 5 deficiency confers temperature-sensitive male sterility in maize. *Nature communications* **11**, 2912.
- 147. Toshiya Suzuki, S. T., Chie Koizuka, Kanta Yamamoto, Jun Imamura, Kenzo Nakamura, Sumie Ishiguro (2013). Development and disintegration of tapetum-specific lipid-accumulating organelles, elaioplasts and tapetosomes, in Arabidopsis thaliana and Brassica napus. *Plant Science* **207**, 25-36.
- 148. Updegraff, E. P., Zhao, F., and Preuss, D. (2009). The extracellular lipase EXL4 is required for efficient hydration of Arabidopsis pollen. *Sexual plant reproduction* **22**, 197-204.
- 149. Uribe-Querol, E., and Rosales, C. (2020). Phagocytosis: our current understanding of a universal biological process. *Frontiers in immunology* **11**, 1066.

- 150. van der Linde, K., and Walbot, V. (2019). Pre-meiotic anther development. *Current topics in developmental biology* **131**, 239-256.
- 151. Van Doorn, W. G. (2011). Classes of programmed cell death in plants, compared to those in animals. *Journal of experimental botany* **62**, 4749-4761.
- 152. van Doorn, W. G., and Woltering, E. J. (2010). What about the role of autophagy in PCD? *Trends in Plant Science* **15**, 361-362.
- 153. Van Durme, M., and Nowack, M. K. (2016). Mechanisms of developmentally controlled cell death in plants. *Current opinion in plant biology* **29**, 29-37.
- 154. Van Hautegem, T., Waters, A. J., Goodrich, J., and Nowack, M. K. (2015). Only in dying, life: programmed cell death during plant development. *Trends in plant science* **20**, 102-113.
- 155. Varnier, A.-L., Mazeyrat-Gourbeyre, F., Sangwan, R. S., and Clément, C. (2005). Programmed cell death progressively models the development of anther sporophytic tissues from the tapetum and is triggered in pollen grains during maturation. *Journal of Structural Biology* **152**, 118-128.
- 156. Verma, N. (2019). Transcriptional regulation of anther development in Arabidopsis. *Gene* **689**, 202-209.
- 157. Walbot, V., and Egger, R. L. (2016a). Pre-meiotic anther development: cell fate specification and differentiation. *Annual Review of Plant Biology* **67**, 365-395.
- 158. Walbot, V., and Egger, R. L. (2016b). Pre-meiotic anther development: cell fate specification and differentiation. *Annual Review of Plant Biology* **67**, 365-395.
- 159. Wang, C.-J. R., Nan, G.-L., Kelliher, T., Timofejeva, L., Vernoud, V., Golubovskaya, I. N., Harper, L., Egger, R., Walbot, V., and Cande, W. Z. (2012). Maize multiple archesporial cells 1 (mac1), an ortholog of rice TDL1A, modulates cell proliferation and identity in early anther development. *Development* 139, 2594-2603.
- 160. Wang, K., Guo, Z.-L., Zhou, W.-T., Zhang, C., Zhang, Z.-Y., Lou, Y., Xiong, S.-X., Yao, X.-z., Fan, J.-J., and Zhu, J. (2018). The regulation of sporopollenin biosynthesis genes for rapid pollen wall formation. *Plant physiology* **178**, 283-294.
- 161. Wang, K., Zhao, X., Pang, C., Zhou, S., Qian, X., Tang, N., Yang, N., Xu, P., Xu, X., and Gao, J. (2021a). IMPERFECTIVE EXINE FORMATION (IEF) is required for exine formation and male fertility in Arabidopsis. *Plant Molecular Biology* **105**, 625-635.

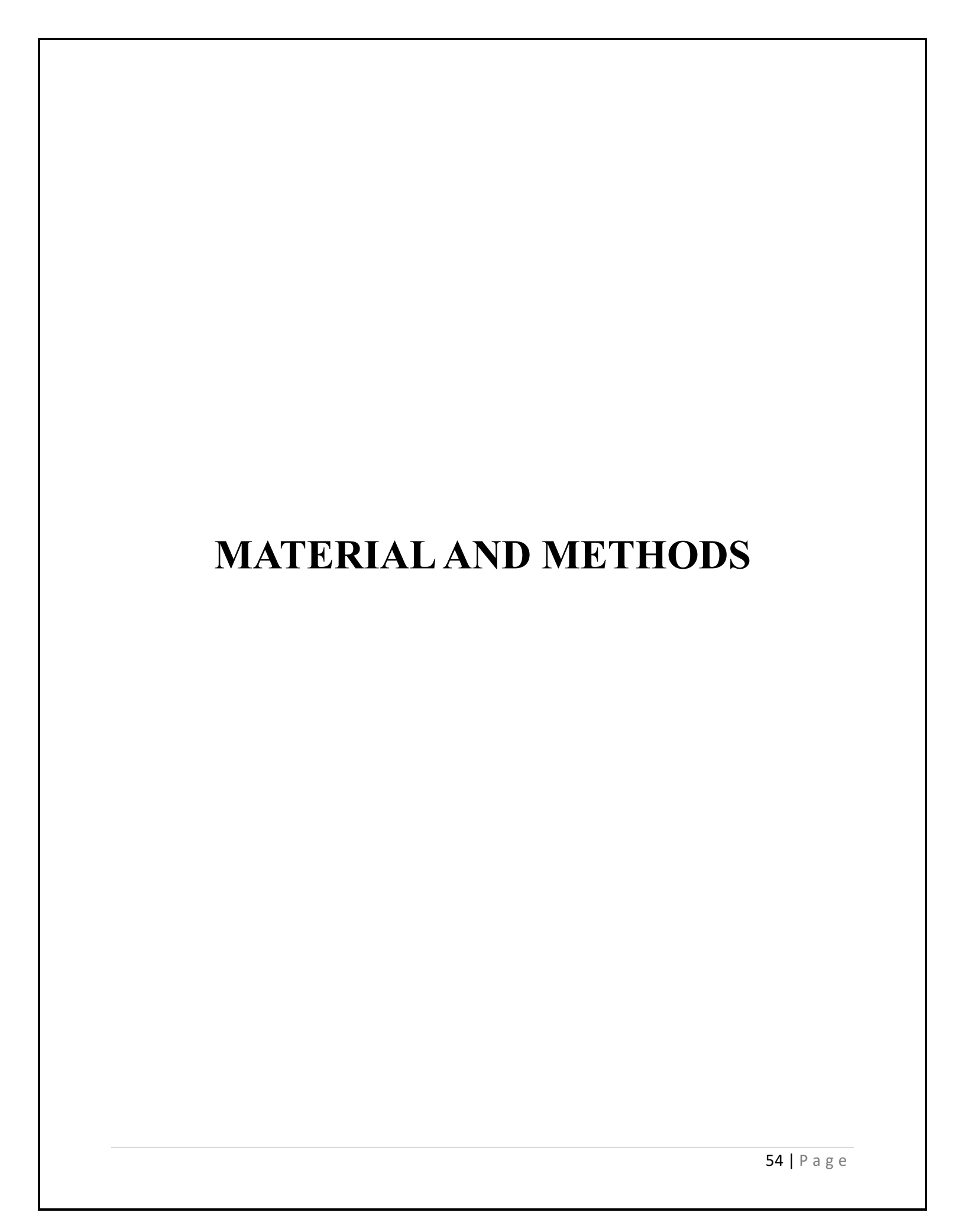
- Wang, K. Q., Yu, Y. H., Jia, X. L., Zhou, S. D., Zhang, F., Zhao, X., Zhai, M. Y., Gong, Y., Lu, J. Y., and Guo, Y. (2022). Delayed callose degradation restores the fertility of multiple P/TGMS lines in Arabidopsis. *Journal of Integrative Plant Biology* 64, 717-730.
- 163. Wang, Y., Ye, H., Bai, J., and Ren, F. (2021b). The regulatory framework of developmentally programmed cell death in floral organs: A review. *Plant Physiology and Biochemistry* **158**, 103-112.
- 164. Watanabe, N., and Lam, E. (2006). Arabidopsis Bax inhibitor-1 functions as an attenuator of biotic and abiotic types of cell death. *The plant journal* **45**, 884-894.
- 165. Wei Zhao, Q. H., Yuchen Qi, Suowei Wu, Xiangyuan Wan (2023). Structural and molecular basis of pollen germination. *Plant Physiology and Biochemistry* **203**.
- 166. Wen, P. J., Grenklo, S., Arpino, G., Tan, X., Liao, H.-S., Heureaux, J., Peng, S.-Y., Chiang, H.-C., Hamid, E., and Zhao, W.-D. (2016). Actin dynamics provides membrane tension to merge fusing vesicles into the plasma membrane. *Nature communications* 7, 12604.
- 167. Werner, M. H., and Burley, S. K. (1997). Architectural transcription factors: proteins that-remodel DNA. *Cell* **88**, 733-736.
- 168. Wilson, Z. A., and Zhang, D.-B. (2009). From Arabidopsis to rice: pathways in pollen development. *Journal of experimental botany* **60**, 1479-1492.
- 169. Wu, C., Yang, Y., Su, D., Yu, C., Xian, Z., Pan, Z., Guan, H., Hu, G., Chen, D., and Li, Z. (2022). The SlHB8 acts as a negative regulator in tapetum development and pollen wall formation in tomato. *Horticulture research* **9**, uhac185.
- 170. Wu, Y., Yan, J., Zhang, R., Qu, X., Ren, S., Chen, N., and Huang, S. (2010). Arabidopsis FIMBRIN5, an actin bundling factor, is required for pollen germination and pollen tube growth. *The Plant Cell* **22**, 3745-3763.
- 171. Xia, C., Wang, Y. J., Liang, Y., Niu, Q. K., Tan, X. Y., Chu, L. C., Chen, L. Q., Zhang, X. Q., and Ye, D. (2014). The ARID-HMG DNA-binding protein At HMGB 15 is required for pollen tube growth in Arabidopsis thaliana. *The Plant Journal* **79**, 741-756.
- 172. Xing, S., Rosso, M. G., and Zachgo, S. (2005). ROXY1, a member of the plant glutaredoxin family, is required for petal development in Arabidopsis thaliana.
- 173. Xing, S., and Zachgo, S. (2008). ROXY1 and ROXY2, two Arabidopsis glutaredoxin genes, are required for anther development. *The Plant Journal* **53**, 790-801.

- 174. Xiong, S. X., Lu, J. Y., Lou, Y., Teng, X. D., Gu, J. N., Zhang, C., Shi, Q. S., Yang, Z. N., and Zhu, J. (2016). The transcription factors MS 188 and AMS form a complex to activate the expression of CYP 703A2 for sporopollenin biosynthesis in Arabidopsis thaliana. *The Plant Journal* 88, 936-946.
- 175. Xu, R., Chong, L., and Zhu, Y. (2024). Mediator kinase subunit CDK8 phosphorylates transcription factor TCP15 during tomato pollen development. *Plant Physiology*, kiae079.
- 176. Xue, J.-S., Zhang, B., Zhan, H., Lv, Y.-L., Jia, X.-L., Wang, T., Yang, N.-Y., Lou, Y.-X., Zhang, Z.-B., and Hu, W.-J. (2020). Phenylpropanoid derivatives are essential components of sporopollenin in vascular plants. *Molecular plant* 13, 1644-1653.
- 177. Yadava, P., Tamim, S., Zhang, H., Teng, C., Zhou, X., Meyers, B. C., and Walbot, V. (2021). Transgenerational conditioned male fertility of HD-ZIP IV transcription factor mutant ocl4: impact on 21-nt phasiRNA accumulation in pre-meiotic maize anthers. *Plant Reproduction* **34**, 117-129.
- 178. Yan, M. Y., Xie, D. L., Cao, J. J., Xia, X. J., Shi, K., Zhou, Y. H., Zhou, J., Foyer, C. H., and Yu, J. Q. (2020). Brassinosteroid-mediated reactive oxygen species are essential for tapetum degradation and pollen fertility in tomato. *The Plant Journal* **102**, 931-947.
- 179. Yang, S.-L., Xie, L.-F., Mao, H.-Z., Puah, C. S., Yang, W.-C., Jiang, L., Sundaresan, V., and Ye, D. (2003). Tapetum determinant1 is required for cell specialization in the Arabidopsis anther. *The Plant Cell* **15**, 2792-2804.
- 180. Yang, Z., Liu, L., Sun, L., Yu, P., Zhang, P., Abbas, A., Xiang, X., Wu, W., Zhang, Y., and Cao, L. (2019). OsMS1 functions as a transcriptional activator to regulate programmed tapetum development and pollen exine formation in rice. *Plant molecular biology* **99**, 175-191.
- 181. Yao, X., Hu, W., and Yang, Z.-N. (2022). The contributions of sporophytic tapetum to pollen formation. *Seed Biology* **1**, 1-13.
- 182. Ye, J., Zheng, Y., Yan, A., Chen, N., Wang, Z., Huang, S., and Yang, Z. (2009). Arabidopsis formin3 directs the formation of actin cables and polarized growth in pollen tubes. *The Plant Cell* **21**, 3868-3884.
- 183. Ye, J., Zhou, L., and Xu, M. (2013). Arabidopsis LIM proteins PLIM2a and PLIM2b regulate actin configuration during pollen tube growth. *Biologia plantarum* **57**, 433-441.
- 184. Yi, B., Zeng, F., Lei, S., Chen, Y., Yao, X., Zhu, Y., Wen, J., Shen, J., Ma, C., and Tu, J. (2010). Two duplicate CYP704B1-homologous genes BnMs1 and BnMs2 are required for pollen exine formation and tapetal development in Brassica napus. *The Plant Journal* **63**, 925-938.

- 185. Yi, J., Moon, S., Lee, Y.-S., Zhu, L., Liang, W., Zhang, D., Jung, K.-H., and An, G. (2016). Defective tapetum cell death 1 (DTC1) regulates ROS levels by binding to metallothionein during tapetum degeneration. *Plant physiology* **170**, 1611-1623.
- 186. Yin, G.-M., Fang, Y.-R., Wang, J.-G., Liu, Y., Xiang, X., Li, S., and Zhang, Y. (2024). Arabidopsis HAPLESS13/AP-1µ is critical for pollen sac formation and tapetal function. *Plant Science*, 111998.
- 187. Yin, L., Zander, M., Huang, S.-s. C., Xie, M., Song, L., Guzmán, J. P. S., Hann, E., Shanbhag, B. K., Ng, S., and Jain, S. (2023). Transcription factor dynamics in cross-regulation of plant hormone signaling pathways. *bioRxiv*.
- 188. Yu, J., and Zhang, D. (2019). Molecular control of redox homoeostasis in specifying the cell identity of tapetal and microsporocyte cells in rice. *Rice* **12**, 42.
- 189. Yuan, G., Zou, T., He, Z., Xiao, Q., Li, G., Liu, S., Xiong, P., Chen, H., Peng, K., and Zhang, X. (2022). SWOLLEN TAPETUM AND STERILITY 1 is required for tapetum degeneration and pollen wall formation in rice. *Plant Physiology* **190**, 352-370.
- 190. Zhang, D., Liu, D., Lv, X., Wang, Y., Xun, Z., Liu, Z., Li, F., and Lu, H. (2014). The cysteine protease CEP1, a key executor involved in tapetal programmed cell death, regulates pollen development in Arabidopsis. *The Plant Cell* **26**, 2939-2961.
- 191. Zhang, D., and Yang, L. (2014). Specification of tapetum and microsporocyte cells within the anther. *Current opinion in plant biology* **17**, 49-55.
- 192. Zhang, J., Zhang, L., Liang, D., Yang, Y., Geng, B., Jing, P., Qu, Y., and Huang, J. (2023a). ROS accumulation-induced tapetal PCD timing changes leads to microspore abortion in cotton CMS lines. *BMC Plant Biology* **23**, 1-13.
- 193. Zhang, M., Zhang, R., Qu, X., and Huang, S. (2016). Arabidopsis FIM5 decorates apical actin filaments and regulates their organization in the pollen tube. *Journal of experimental botany* **67**, 3407-3417.
- 194. Zhang, R., Xu, Y., Yi, R., Shen, J., and Huang, S. (2023b). Actin Cytoskeleton in the Control of Vesicle Transport, Cytoplasmic Organization and Pollen Tube Tip Growth. *Plant Physiology*, kiad203.
- 195. Zhang, W., Sun, Y., Timofejeva, L., Chen, C., Grossniklaus, U., and Ma, H. (2006). Regulation of Arabidopsis tapetum development and function by DYSFUNCTIONAL TAPETUM1 (DYT1) encoding a putative bHLH transcription factor.

- 196. Zhang, X., He, Y., Li, L., Liu, H., and Hong, G. (2021). Involvement of the R2R3-MYB transcription factor MYB21 and its homologs in regulating flavonol accumulation in Arabidopsis stamen. *Journal of experimental botany* **72**, 4319-4332.
- 197. Zhang, Y., Zhang, B., Yang, T., Zhang, J., Liu, B., Zhan, X., and Liang, Y. (2020). The GAMYB-like gene SIMYB33 mediates flowering and pollen development in tomato. *Horticulture research* 7.
- 198. Zhao, B., Shi, H., Wang, W., Liu, X., Gao, H., Wang, X., Zhang, Y., Yang, M., Li, R., and Guo, Y. (2016a). Secretory COPII Protein SEC31B Is Required for Pollen Wall Development *Plant Physiology* **172**, 1625-1642.
- 199. Zhao, B., Shi, H., Wang, W., Liu, X., Gao, H., Wang, X., Zhang, Y., Yang, M., Li, R., and Guo, Y. (2016b). Secretory COPII protein SEC31B is required for pollen wall development. *Plant Physiology* **172**, 1625-1642.
- 200. Zhao, F., Zheng, Y.-F., Zeng, T., Sun, R., Yang, J.-Y., Li, Y., Ren, D.-T., Ma, H., Xu, Z.-H., and Bai, S.-N. (2017). Phosphorylation of SPOROCYTELESS/NOZZLE by the MPK3/6 kinase is required for anther development. *Plant Physiology* 173, 2265-2277.
- 201. Zhao, G., Shi, J., Liang, W., and Zhang, D. (2016c). ATP binding cassette G transporters and plant male reproduction. *Plant signaling & behavior* 11, e1136764.
- 202. Zhao, X., De Palma, J., Oane, R., Gamuyao, R., Luo, M., Chaudhury, A., Hervé, P., Xue, Q., and Bennett, J. (2008). OsTDL1A binds to the LRR domain of rice receptor kinase MSP1, and is required to limit sporocyte numbers. *The Plant Journal* 54, 375-387.
- 203. Zheng, S., Li, J., Ma, L., Wang, H., Zhou, H., Ni, E., Jiang, D., Liu, Z., and Zhuang, C. (2019). OsAGO2 controls ROS production and the initiation of tapetal PCD by epigenetically regulating OsHXK1 expression in rice anthers. *Proceedings of the National Academy of Sciences* **116**, 7549-7558.
- 204. Zheng, Z., Xia, Q., Dauk, M., Shen, W., Selvaraj, G., and Zou, J. (2003). Arabidopsis AtGPAT1, a member of the membrane-bound glycerol-3-phosphate acyltransferase gene family, is essential for tapetum differentiation and male fertility. *The Plant Cell* **15**, 1872-1887.
- 205. Zhu, B.-S., Zhu, Y.-X., Zhang, Y.-F., Zhong, X., Pan, K.-Y., Jiang, Y., Wen, C.-K., Yang, Z.-N., and Yao, X. (2022). Ethylene activates the EIN2-EIN3/EIL1 signaling pathway in tapetum and disturbs anther development in Arabidopsis. *Cells* **11**, 3177.
- 206. Zhu, L., Zhang, T., and Teeri, T. H. (2021a). Tetraketide α-pyrone reductases in sporopollenin synthesis pathway in Gerbera hybrida: diversification of the minor function. *Horticulture research* 8.

- 207. Zhu, L., Zhang, T. & Teeri, T.H. (2021). Tetraketide α-pyrone reductases in sporopollenin synthesis pathway in Gerbera hybrida: diversification of the minor function. *Horticulture Research*.
- 208. Zhu, R. M., Li, M., Li, S. W., Liang, X., Li, S., and Zhang, Y. (2021b). Arabidopsis ADP-RIBOSYLATION FACTOR-A1s mediate tapetum-controlled pollen development. *The Plant Journal* **108**, 268-280.



1) Plant material and growth conditions:

Arabidopsis thaliana ecotype Columbia (Col-0) seeds, after cold (4°C) treatment, were germinated under 16hr light (~150±10 μmol m-2 s -1) and 8hrs dark at 22°C on MS Agar plates. T-DNA insertion lines of *Arabidopsis* ecotype Col-0 lines at AtHMGB15 locus were procured from GABI-Kat collection (351D08). The T-DNA insertion was screened by the presence of sulfadiazine (Sulr) resistance.

A. Media preparation and seed plating

Murashige & Skoog media preparation:

- a. For 1 litre of MS media 1 sachet of MS media (Himedia PT010) was dissolved in 800 mL of milipore water.
- b. 0.44 gm of CaCl₂ was added.
- c. pH was adjusted to 5.6-5.8 using 4N KOH solution.
- d. 0.8% (w/v) agar was added to the media.
- e. Volume was adjusted to 1 litre.
- f. The media was autoclaved in 15 psi at 121°C for 15 mins.
- g. The media was allowed to cool and ~25mL was poured per tissue culture plate in laminar air flow.

Sterilisation and plating of seeds:

Reagents required for seed sterilisation:

Reagents	Stock concentration 100%		
70% Ethanol	35mL	Volume made upto	
		50mL with autoclaved	
50% Bleach	25mL	Millipore water. Filter	
		sterilized in laminar air	
0.05% TritonX-100	25mL	flow. Stored at 4°C.	

- a. In a sterile laminar airflow, Arabidopsis seeds were suspended in 200 μ L of 70% ethanol and vortexed mildly for 5minutes.
- b. The solution was removed, and seeds were repeatedly washed with 600 μL of filter sterilized water for 5 minutes with occasional vortexing.

- c. The seeds were then soaked in 600 µL of 50% bleach solution (sodium hypochlorite) for not more than 5minutes followed by thoroughly rinsing in water as in step b.
- d. The seeds were then treated with $600 \,\mu\text{L}$ of 0.05% TritonX-100 solution for 10 minutes and subsequently rinsed with water for 10 times with repeated vortexing.
- e. The seeds were suspended in sterile water and ~20-25 seeds were carefully placed on MS agar plates.
- B. The 2 weeks old seedlings were then transferred to the soilrite. After 4 weeks from transfer when the first bolts started appearing in both wild type and *athmgb15*, buds from this stage were harvested for study.

2) Transgenic screening and confirmation

Transgenic seeds of ARP4 knockout mutants were procured from ABRC namely CS876625. The individual lines were heterozygous in nature and needed screening before proceeding with further studies. In order to confirm their zygosity, 20 seeds from CS876625 were first plated in MS media. After 2 weeks they were transferred to individual soil pots that was labelled. When the plants were 4 weeks old, a leaf was harvested from each plant to isolate the genomic DNA and test its zygosity using specific primers.

In order to confirm the T-DNA insertion within the gDNA of the mutants, gene specific and T-DNA Left Border primers were used. The primers and their sequence are as follows:

Primer	Sequence
SAIL LB-1	TAGCATCTGAATTTCATAACCAATCTCGATACAC
ARP4 forward	CACC GAATTC TCA ACA CTC GAA AAT CTA TGG AGC
ARP4 reverse	CCATGG GGC TGC AGC GAA CGA CAA G

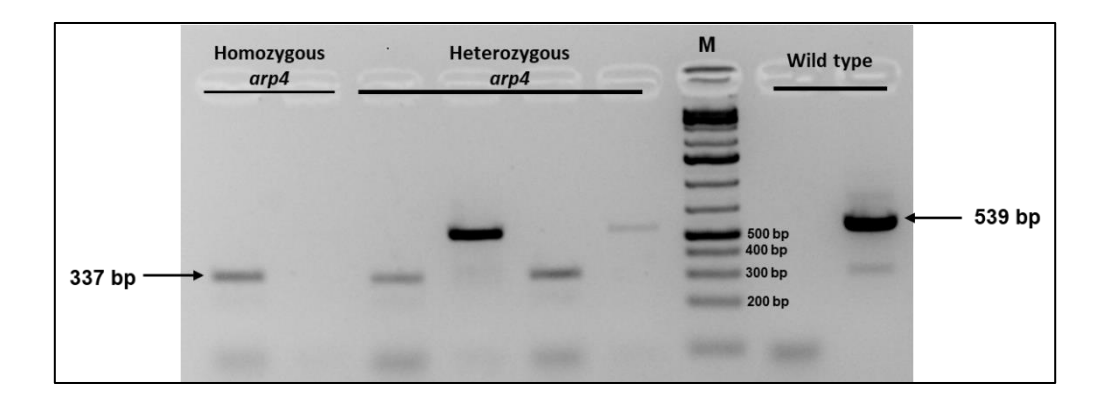


Fig. M1: Screening of homozygous and heterozygous lines of *arp4* using PCR amplification. The 337bp amplicon was obtained using the SAIL LB1 and ARP4 forward primers. The 539bp amplicon was obtained from ARP4 forward and AR4 reverse primers

3) Genomic DNA isolation

DNA isolation was carried out using the Plant DNAzol Reagent (Invitrogen) as follows:

- a. Crush plant sample (100 mg) in liquid nitrogen till a homozygous powder was obtained.
- b. To it 300 μL of Plant DNAzol reagent (containing RNase A 0.1 mg/mL) was added and mixed by inverting the tubes several times for 5 minutes.
- c. To it 300 μ L of chloroform was added and mixed vigorously for 5 minutes at room temperature.
- d. This was then centrifuged at 12000g for 10 minutes after which the aqueous phase was collected in a fresh centrifuge tube.
- e. To precipitate the DNA from the aqueous phase 225 μ L of 100% ethanol was added and the tube was inverted few times to mix and then allowed to rest in room temperature for 5 minutes.
- f. This was then centrifuged at 5000g for 4 minutes at room temperature. The supernatant was discarded and the pellet was further processed.
- g. To was the DNA pellet, an ethanol DNAzol wash solution was prepared using 1 volume of Plant DNAzol with 0.75 volume of 100% ethanol. 0.3 mL of this Plant DNAzol-ethanol was solution was added to the pellet followed by vortexing.
- h. After 5 minutes rest at room temperature, the sample was centrifuged at 5000g for 4 minutes.
- i. The DNAzol wash solution was removed and the pellet was rigorously washed with 0.3 mL of 75% ethanol followed by centrifugation at 5000g for 4 minutes.

- j. The excess ethanol was removed by decanting and the DNA pellet was air dried.
- k. The DNA was then dissolved in 30 μ L of TE buffer and quantified using a nanodrop spectrophometer.

4) RNA isolation

RNA was isolated from buds of stages 8-11 of anther development by TRIzol method.

The following materials were required before beginning RNA isolation:

- a. TRIzol reagent
- b. Liquid nitogen
- c. DEPC water: 0.1% DEPC (Sigma) in water, stirred for ~3hours in dark and double autoclaved.
- d. Mortar and pestle overnight treated with unautoclaved water and baked in 200°C for 6 hours.
- e. 75% 70% ethanol made from autoclaved DEPC water.
- f. DNase I (Fermentas), 10X DNase I buffer.

Method:

- a. 200 mg tissue was homogenized using liquid nitrogen to the fine powder ad suspended in 1 mL of TRIzol (Invitrogen) reagent per 100 mg of tissue. the homogenate was kept at room temperature for 10 minutes.
- b. The homogenate was centrifuges at 12000g for 10 minutes at 4°C and the supernatant was transferred to a new autoclave tube. To the supernatant, 200 μL of chloroform per 1 mL of TRIzol reagent reagent was added, mixed gently and centrifuges at 12000g for 15 minutes.
- c. The supernatant (aqueous phase) was taken and total RNA was precipitated by adding 0.5 mL of isopropyl alcohol per 1 mL of TRIzol reagent. The samples were centrifuged at 12000g for 10 minutes at 4°C.
- d. The RNA pellet was washed by 75% ethanol (prepared in DEPC water). The RNA pellet was air dried, was dissolved in 50 μL RNase free water and subjected to DNase I treatment.

e. DNase I treatment:

To avoid any DNA contamination, the RNA isolated using TRIzol reagent was treated with DNase I (thermoscientific) for 2 hours at 37°C. The DNase I digestion was set up as follows:

Reagent	Volume
RNA	50 μL
10X DNase I buffer with MgCl ₂	10 μL
DNase 1 (1U/μL)	4 μL
RNase free water	Volume made up to 200 μL

- f. The above reaction was extracted with trizol:chloroform. An equal volume of TRIzol (100 μ L) and chloroform (100 μ L) was added and mixed properly, followed by centrifugation at 12000 rpm for 10minutes at 4°C.
- g. The upper aqueous phase ($\sim 200~\mu L$) was taken into a fresh microcentrifuge tube and to it 100% ethanol (3X of the volume), 3M Na-acetate pH: 5.2 (0.1X of sample volume) were added, mixed properly and incubated to precipitate the RNA from the sample either at -20°C overnight or at -80°C for at least 1 hour. The samples were the centrifuges at 13000 rpm for 30minutes to 4°C to pellet the DNA.
- h. The supernatant was then carefully removed, and the RNA pellet was washed with 75% ethanol (1 mL) and centrifuged at 13000rpm for 10 minutes at 4°C.
- i. Following centrifugation, the supernatant was discarded, and the RNA pellet was air dried and dissolved in 30 μ L of RNase free water. The concentration of the RNA samples was determined by using a nanodrop spectrophotometer and quality was checked by denaturing MOPS-formaldehyde agarose gel electrophoresis.

Denaturing MOPS-Formaldehyde gel electrophoresis

Preparation of 10X MOPS Buffer (1 litre):

Reagents	Final concentration	Quantity
3-[N-Morpholino] propane	200 mM	41.8 gm of MOPS
sulphonic acid (MOPS)		
Sodium Acetate. 3H ₂ O	20 mM	2.72 gm of Sodium acetate
EDTA	10 mM	20 mL from 0.5M stock of pH:8

The pH of the buffer was adjusted to 7 with 10 N NaOH. The solution was filtered with a 0.2μ filter syringe to a new autoclaved container.

Composition of the 5X RNA loading dye:

Reagent	Volume
Saturated aqueous Bromophenol Blue solution	3.2 μL
600 mM EDTA	1.6 μL
37% (12.3 M) Formaldehyde	1.5 μL
100% Glycerol	0.4 μL
Formamide	616.8 μL
10X MOPS buffer	0.8 μL
RNase free water	376 μL

MOPS-formaldehyde gel:

- a. 1.5 gm of agarose was added to 10 mL of 10X MOPS buffer and 72 mL of autoclaved DEPC treated water.
- b. The mixture was heated to dissolve the agarose completely.
- c. After cooling it to ~65°C, 18 mL of formaldehyde was added, and the gel was immediately poured in the gel casting tray and kept at room temperature for until the gel solidified.
- d. The gel was equilibrated by running in 1X MOPS running buffer in a gel running tank for 30 minutes at 80V before use.
- e. Into each 10 μ L sample, 3 μ L of ethidium bromide (1 mg/mL) was added and the samples were incubated at 65°C for 15 minutes in dry heat block, snap chilled on ice for 5 minutes. 6 μ L of 5X RNA loading dye was added to each sample and run on the denaturing MOPS gel.
- f. The samples were electrophoresed in 1X MOPS at 80V for 2 hours.
- g. The quality of RA was ensured by high quality 18S and 28S band of RNA, total RNA was quantified by Nanodrop Spectrophotometer.

5) cDNA synthesis from RNA

To obtain the first strand cDNA, reverse transcription was performed using 5 μg of RNA and oligo dT $_{(18)}$ primer. The reaction is carried out in two steps:

For step 1:

a. A reaction mix A was prepared as follows:

Components	Quantity
Total RNA	5 μg
Oligo dT (18) primer (0.5 μg/μL)	1 μL
RNase free water	Volume made up to 13 μL

b. The mix is incubated at 65°C for 5 minutes in a thermal cycler and quickly snap chilled on ice for 2 minutes.

For step 2:

a. Another reaction mix B was prepared as follows:

Component	Volume
5X first strand buffer	4 μL
dNTO mixture (10mM of each dNTP made in RNase free	2 μL
water)	
Reverse transcriptase enzyme (200 U/ µL, RivertAid,	1 μL
Fermentas)	

- b. The contents of mix B were added to mix A and the 20 μ L total reaction mix was incubated at 42°C for 1 hour.
- c. The reaction ws then terminated by heating at 70°C for 15minutes.

6) q-RTPCR:

Real time PCR assay was performed for validating the expression of the genes that were significantly altered in the *athmgb15* mutant. cDNA preparation and real time PCR analysis were performed using 3 µg of total RNA, Revertaid RT and oligo(dT)₁₈ primers. Synthesized cDNA was diluted 1/4th times and used as template. Real time PCR was carried out in 20ul reaction volume containing 1X buffer with SYBR Green (Applied Biosystems) and 0.25 µM gene specific primers using ABI 7500 Fast. Primers used for real time are

listed in table 1. α EF1 was used as internal control and a threshold of 0.1 was set manually to obtain a threshold cycle (C_T) value for each gene.

Real time PCR data was analysed as previously mentioned (Livak and Schmittgen, 2001), where C_T values for gene of interest ($C_{T.GOI}$) were normalized to the C_T values of $\alpha EF1$ ($C_{T.\alpha EF1}$) for each sample [$\delta CT=(C_{T.GOI})$ - ($C_{T\alpha EF1}$)]. Relative transcript level for each gene was calculated with respect to $\alpha EF1$ transcript level (the % relative expression to $\alpha EF1$) using $2^{-\delta CT}$ value and plotted in the graph. Three biological replicates were used for the study.

7) Chromatin Immunoprecipitation (ChIP) Assay:

Nuclei isolation was performed from wild type *Arabidopsis thaliana* buds using plant nuclei isolation kit (Sigma CELLYTPN 1) according to the manufacturer's protocol.

The following	1 00	. 1	C .1	•
The tollowing	huttore w	vara radiiirad	tor the	avnariment.
THE TOHOWINE	Duncis v	vere reduired	TOI THE	CADCITITION.

Solution	Composition	
250 mM PMSF	0.44 gm in 10 mL of Isopropanol	
Nuclear Lysis Buffer	50 mM Tris-Cl (pH 8), 10 mM EDTA, 1% SDS, 1 mM	
	PMSF	
ChIP dilution Buffer	16.7 mM Tris-Cl (pH 8), 1.2 mM EDTA, 167 mM NaCl,	
	1.1% TritonX-100	
Low Salt Wash Buffer	150 mM NaCl, 0.1% SDS, 1% TritonX-100, 2mM	
	EDTA, 20mM Tris-Cl (pH 8)	
High Salt Buffer	500 mM NaCl. 0.1% SDS, 1% TritonX-100, 2 mM	
	EDTA, 20 mM Tris-Cl (pH 8)	
LiCl Wash Buffer	0.25 M LiCl, 1% NP-40, 1% Sodium deoxycholate, 1	
	mM EDTA, 10 mM Tris-Cl (pH 8)	
TE	1 mM EDTA, 10 mM Tris-Cl (pH 8)	
Elution Buffer	1% SDS, 100 mM NaHCO ₃	

All steps were done at 2-8°C using pre cooled buffers and rotors.

A. Cell Lysis

a. 1X Nuclear Isolation Buffer (NIB) was prepared from the 4X NIB with deionized water. To the 1X NIB, 1 mM DTT was added just before the extraction procedure.

- b. The buds were crushed to a fine powder using liquid nitrogen in autoclaved mortar using a pestle. The powder was transferred to new falcon (15 mL) containing 3 mL of 1X NIB with 1 mM DTT. The mixture was mixed gently without any vortexing.
- c. The slurry was the passed through an autoclaved filter mesh 100. The filtrate was collected in a fresh 15 mL falcon.
- d. This tube was then spun at 1260g for 10 minutes at 4°C.
- e. The supernatant was discarded by inverting the tube and the pellet was resuspended in 500 μ L of 1X NIBA (1X NIB + 1 mM DTT + 1 mM PMSF).
- f. For cell membrane lysis, 10% TritonX-100 was added to a final concentration of 0.3%.

B. Isolation of Nuclei

- a. Semi pure preparation of nuclei.
 - The lysate from the previous step was layered gently on top of $800 \,\mu\text{L}$ of 1.5M sucrose in a $1.5 \,\text{mL}$ centrifuge tube.
- b. Centrifuge at 12000g for 10 minutes at 4°C.
- c. The upper green phase and sucrose cushion was discarded by inverting the tube and without disturbing the nuclei pellet.
- d. The pellet was washed twice with 750 μ L of NIBA buffer and then resuspending the pellet in 300 μ L of Nuclei Storage Buffer (provided with the kit). The sample was then kept in ice and resuspended very carefully with a cut tip on the opposite end of the pellet.

C. Crosslinking

- a. $8.1~\mu L$ of 37% formaldehyde was added to 300 μL of the lysate and kept on a rocker at room temperature for 15 minutes.
- b. To quench the extra formaldehyde from the suspension 22.5 μ L of 2M glycine was added and kept on the rocker for 10 minutes.
- c. The tubes were then spun at 13000 rpm for 5 minutes at 4°C. the supernatant was discarded and the pellet was dissolved in 600 μ L of freshly prepared Nuclear Lysis Buffer very carefully.

D. Sonication and checking for shearing

a. $50 \,\mu\text{L}$ of the suspension was kept aside and labelled as "unsonicated" sample.

- b. The rest of the suspension was sonicated at 40Hz at 0.4 duty cycle for 7, 10 seconds' pulse.
- c. After sonication 50 μ L of the sonicated cell lysate was taken in a fresh centrifuge tube and labelled as "sonicated" sample.
- d. To both the sonicated and unsonicated cell lysates, $10~\mu L$ of 5M NaCl was added and boiled at 65°C for 15 minutes in a water bath to reverse crossling the DNA and proteins.
- e. To the reverse crosslinked product $60~\mu L$ of phenol chloroform isoamyl mix was added and mixed.
- f. This was then centrifuged at 13000 rpm for 5minutes at room temperature.
- g. The aqueous phase was collected and 50% glycerol was added. The samples were then run in a 1.2% agarose gel.
- E. Dilution of nuclear lysate by freshly prepared ChIP dilution buffer
 - a. The 500 μL of the nuclear lysate after sonication was then spun at 13000 rpm for
 5minutes in cold and the supernatant was collected in fresh tube (2 mL).
 - b. The nuclear lysate was then diluted 4 times so that the final dilution was 1:4
 - c. This diluted nuclear lysate was then dived into two eppendorfs (1.5 mL), keeping 1/10th of the lysate labelled as "input" before proceeding to immunoprecipitation.

F. Immunoprecipitation

10 μ L of the AtHMGb15 antibody (4.6 mg/mL) was added to each tube (1 mL) and rotated in 4°C for overnight.

G. Bead Adding

To the nuclear and antibody suspension, $30~\mu L$ of Magna Beads was added and left on a cyclo-rotor for 3 hours at $4^{\circ}C$.

H. Washing of the Magna Beads

- a. The tubes were placed on a magnetic rack and the supernatant was discarded.
- b. 1 mL of low salt wash buffer was added. The tubes were rotated for 5 minutes and the supernatant was discarded.
- c. This was followed by high salt wash buffer, LiCl wash buffer and two washes of TE.

- d. After the TE washes, 250 μL of elution buffer, pre warmed in a water bath at 65°C was added to the beads and vortexed. The beads with Elution buffer (EB) were then incubated at 65°C for 15 minutes followed by a gentle vortexing and centrifugation at 13000 rpm for 30 seconds.
- e. The tubes were then placed on the Magna Grip rack and the supernatant was collected in a fresh centrifuge tube and labelled as IP. The above step d was repeated twice.
- f. The previously labelled input sample's volume was also made upto 500 μL using EB.

I. Reverse Crosslinking

To both the input and IP tubes 20 μL of 5M NaCl was added and kept in water bath at 65° for overnight.

J. DNA precipitation and cleanup

- a. The tubes were pluse spun to bring down the solution from the lid
- b. A cocktail of EDTA, Tris-Cl and proteinase K was prepared and added to each tube:

Reagent	Volume
0.5 M EDTA, pH 8	10 μL
1 M Tris-Cl, pH6.5	20 μL
Proteinase K	2 μL

- c. This reaction was incubated at 45°C for 2-3 hours before proceeding to phenol-chloroform.
- d. To the reaction $550~\mu L$ of Phenol Chloroform Isoamyl mix was added and invert mixed. This was then centrifuges at 13000rpm for 15 minutes at room temperature.
- e. The top aqueous layer was collected in a fresh centrifuge tube, to it $1/10^{th}$ volume of 3M Na-acetate (pH 5.2), 3 volumes of 100% ethanol and 3 μ L of glycogen (20 mg/mL) was added to each tube and kept in -20°C for overnight.

K. Solubilization of the precipitated DNA

- a. The tubes were then centrifuges at 13000 rpm for 15 minutes at 4°C.
- b. The supernatant was discarded by decanting and the pellet was washed with 70% ethanol (1 mL), centrifuged at 13000 rpm for 15 minutes at room temperature.

- c. The supernatant was discarded and the DNA pellet was air dried.
- d. The pellet was then dissolved in 30 μ L of TE and kept in 4°C for overnight, before proceeding to q-RTPCR.

ChIP-qPCR

To validate our findings from the previously published ChIP-chip data (Mallik et al., 2020), ChIP-qRTPCR was carried out. The immunoprecipitated (IP) DNA were normalized with respect to input and the fold change was calculated against a negative control region (p>0.05 with very low normalized signal ratio) using $2^{-\Delta\Delta}$ method. Three independent replicates of wild type buds were used for q-RTPCR experiments, where each replicate contained more than ≥ 500 flower buds of stages 8-11 of anther development. The significance of the results was analysed by student's t-test (* denotes p ≤ 0.05). the primers used for the ChIP analysis are listed in **Annexure 1**.

8) Agrobacterium-mediated transient assay and fluorometric GUS assay (Promoter assay):

- a) Agrobacterium tumefaciens strain EHA105 harbouring the proMYB21:pKGWFS7, pro MYB24:pKGWFS7 and the empty vector (pKGWFS7) plasmid constructs were grown overnight at 28°C in LB with rifampicin (50 μg/ml) and Spectinomycin (100 μg/ml).
- b) Overnight cultures of the transformed *Agrobacterium* were spun at 5000 rpm for 10mins at room temperature.
- c) The pellet was washed with 5 ml of infiltration buffer twice before resuspending in 2ml of the infiltration buffer.

Gus Infiltration Buffer Composition:

Reagent	Stock concentration	Working concentration
MgCl ₂	1 M	10 mM
MES (pH 5.6)	1 M	10 mM
Acetosyringone	0.5 M	100 μΜ
Water	Volume made upto 100 mL	

- d) The O.D. was measured and adjusted to 0.8.
- e) The co-infiltration mixes were prepared in 1:1 ratio and incubated in 28°C for 3hours before infiltering in 6 weeks old tobacco leaves (*Nicotiana tabacum*).
- f) The tissue was harvested after 48hrs and 72hrs. The harvested tissue was then homogenized using liquid Nitrogen, to which 500ul of Gus Extraction buffer was added.

Gus Extraction Buffer (GEB) Composition:

Reagent	Working concentration	Stock concentration
NaHPO ₄ (pH:7)	50mM	1M
β-mercaptoethanol	10mM	14.4M
Na ₂ EDTA	10mM	0.5M
Sarcosyl	0.1%	30%
TritonX-100	0.1%	10%
H ₂ O		

- g) The suspension was then spun at 13000rpm for 15mins at 4°C for 15mins.
- h) The supernatant was collected and kept in ice.
- i) To estimate the fluorescence from MU, 1 mM GUS extraction buffer was added to 50 μ l of the protein extract and incubated at 37°C for 60 minutes.
- i) The reaction was stopped by adding 100ul of 0.2M Na₂CO₃.
- k) Fluorometric analysis was measured 455nm emission and 365nm excitation.

MU standard curve:

100mM MU (β-umbelliferone) was prepared in DMSO. For which 17.62 mg of MU was dissolved in 1 ml of DMSO.

Where, $100 \text{ mM} => 100 \text{ nmoles/}\mu\text{L} \text{ or } 10^5 \text{ picomoles/}\mu\text{L}.$

We prepared 1 mL of this stock that contained approximately 10^8 picomoles of MU. Two standard curves were prepared, one in the μM range and the other in nM range.

BSA standard curve:

The BSA standard curve was prepared using Bradford reagent using the standard protocol.

9) Bimolecular fluorescence complement (BiFC) assay

Bimolecular fluorescence complement (BiFC) assay is widely adopted to determine the physical interaction of two proteins *in vivo*. The full length CDS of AtHMGB15 was cloned into pEarlyGate101 to obtain C-terminus YFP fusion protein previously by Dr. Adrita Roy. The full length CDS of ARP4 was cloned into the BiFC vector pSITE-nEYFP-C1 (CD3-1648). For transient study, Bi-molecular fluorescence complementation assay was performed in onion epidermal cells.

A. Cloning the gene of interest into pENTR-D-TOPO vector Generation of blunt end PCR product.

a. The ARP4 CDS was amplified using a thermostable, proofreading DNA polymerase and the PCR primers that include the 4 base pair sequence (CACC) necessary for directional cloning on the 5'end of the forward primer to produce blunt end PCR product. For PCR, following components were added to a 50μL reaction volume:

Reagent	Volume
2X PCR Buffer for KOD FX Neo	25 μ1
2 mM dNTPs	10 μ1
KOD FX Neo (1 U/μl)	1 μ1
Forward primer (10µM)	1.5 μ1
Reverse Primer (10µM)	1.5 μ1
Nuclease free water	6 μl
Template (WT bud cDNA)	5 μ1

PCR cycle for amplification:

Temperature	Time
94°C	2mins
94°C	10 secs
67°C	30 secs
68°C	2 mins
68°C	7 mins
4°C	α

Primers used for cloning in pSITE-nEYFP-C1 (CD3-1648)

Primer name	Sequence
ARP4 AD forward with Sal1:	CACC GTC GAC ATG TAC GGC GGA GAT GAA
	GTG TCA GC
ARP4 AD reverse with Pst1:	CTG CAG TTA AGG GCA TTT TCT CTG AAT GTA
	GG

b. The PCR product was run on a 1% gel and subsequently extracted from the gel using a gel extraction kit (Qiagen).

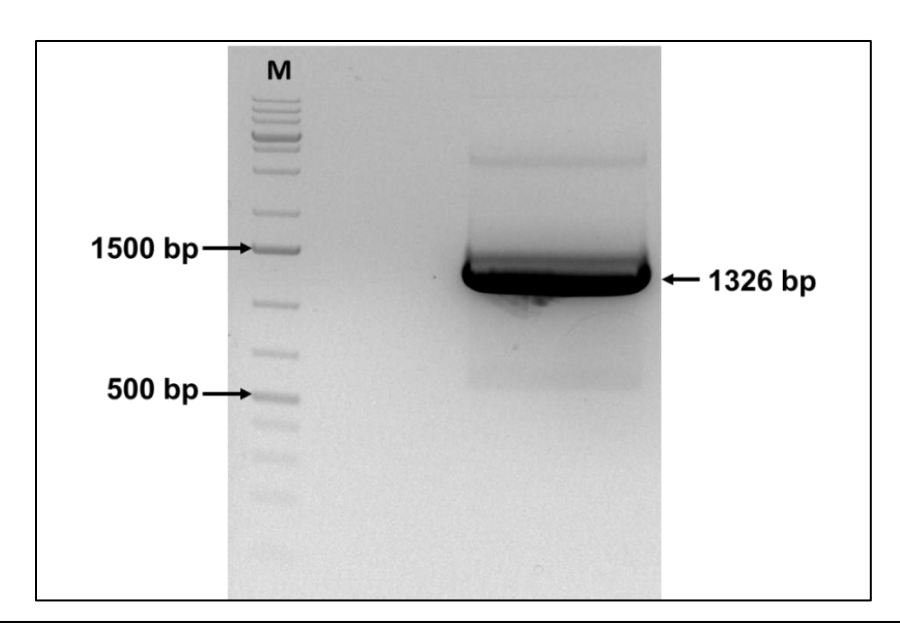


Fig M2: The fragment (1326 bp) represents the PCR product obtained using ARP4 CDS primers from *Arabidopsis* genomic DNA. The lane labelled M represents marker.

B. TOPO cloning reaction using pENTR/D-TOPO cloning kit (Invitrogen)

Reagent	Volume
Purified PCR product	0.5 μ1
Salt solution	1 μ1
TOPO-vector	1 μ1
Nuclease free water	2.5 μ1

The reaction was kept in room temperature for 30minutes before transforming competent DH5 α cells.

C. Competent cell preparation

Prior to transformation DH5 α competent cells were prepared. The composition of solutions required for competent cell preparation are as follows:

Reagent	Composition
Solution I	80mM MgCl ₂ , 20mM CaCl ₂
Solution II	0.1M CaCl ₂ , 15% glycerol
LB media (1ltr)	5gm Yeast Extract, 10gm Tryptone, 10gm NaCl, pH adjusted
	to 7.5 with 1N NaOH. For solid media 1.5% wt/vol agar was
	added.

The solutions and media were autoclaved and cooled prior to use. The procedure of competent cell preparation is as follows:

- a. A colony of *Escherichia coli* DH5α was grown in 10mL of LB medium at 37°C overnight with shaking.
- b. 1mL of the overnight culture was then inoculated in 300mL of LB medium in a 1litre conical flask and grown at 37°C with shaking till the optical density reached at 600nm reached 0.6 (~2-3hrs).
- c. The cell suspension was then cooled on ice for ~1hour with occasional swirling of the conical flask.
- d. The cell suspension was then decanted into six 50mL falcon tubes and centrifuged at 5000rpm for 15minutes.
- e. The supernatant was completely removed and the bacterial pellet was resuspended in 30 mL of ice-cold solution I and mixed by gently vortexing.
- f. The cells were combined into two tubes and centrifuged at 5000rpm for 15minutes.
- g. After centrifugation, the supernatant was completely removed and the pellet was resuspended in 30mL of ice-cold solution II and incubated on ice for 20 minutes.
- h. The cell suspension was again centrifuged at 5000rpm for 15minutes and the supernatant was discarded completely.
- i. Finally, the bacterial pellet was gently resuspended in $3\,\text{mL}$ of solution II into one tube and distributed as $100\,\mu\text{L}$ aliquotes of competent cells to pre chilled microcentrifuge tubes, frozen in liquid nitrogen and stored at $-80\,^{\circ}\text{C}$.
- D. Transformation of the circularized pENTR/D-TOPO vectors

The transformation was carried out as follows:

- a. DH5 α competent cells were thawed on ice and to it vector was added and mixed gently.
- b. The tubes were then incubated on ice for 30 minutes followed by heat shock at 42°C for exactly 90 seconds.
- c. The tubes were immediately transferred to ice for 5minutes and then 1mL of LB broth (without any antibiotics) was added. The cells were allowed to revive for 1 hour at 37°C under shaking condition.
- d. The cells were plated on LB plates supplemented with the antibiotic Kanamycin (50 μ g/ml). the plates were then incubated overnight in inverted position at 37°C.

j. The positive clones were confirmed by restriction digestion and were sequenced before LR clonase reaction.

E. Plasmid isolation

Isolation was performed by alkaline lysis method from the transformed bacterial colonies as follows:

Reagent	Composition
Solution I	50mM glucose, 25mM Tris-Cl (pH: 8), 1 mM EDTA (pH: 8).
	Solution I is autoclaved and can be stored at 4°C. To an aliquot of
	Solution I, RNase A is added to a final concentration of 100 µg/mL
	before use.
Solution II	0.2 N NaOH, 1% (w/v) SDS. Solution II is freshly prepared and
	used at room temperature.
Solution III	3M potassium acetate pH adjusted to 5.5 with glacial acetic acid.
	Solution III is autoclaved and can be stored at 4°C.

- a. An overnight culture was given from at least 5 colonies in LB medium containing antibiotic Kanamycin (50 μg/mL final concentration).
- b. The overnight bacterial culture was pelleted by centrifugation at 5000rpm for 5mins.
- c. The bacterial pellet was resuspended in 200 μ L of Solution I containing RNase A, lysed with the addition of 400 μ L of Solution II (2-3 minutes incubation at room temperature) with occasional inverting the tubes and neutralization by 300 μ L of Solution III with proper mixing and incubated on ice for 15 minutes.
- d. The samples were centrifuges at 13000rpm for 10minutes. The supernatant was transferred to a fresh microcentrifuge tube avoiding any whitish precipitate and precipitated with 0.7 volumes ($\sim 630 \mu L$) of isopropanol.
- e. The samples were centrifuged at 13000rpm for 10minutes and the DNA pellet was washed with 70% EtOH (1mL), dried and resuspended in 20 μL water.

F. Restriction digestion for clone confirmation

The isolated plasmid DNA was then digested using the two restriction sites present in the insert (double digestion).

Reagents	Volume
Plasmid (~ 5ug)	5 μl
10X reaction buffer O	2 μ1
Pst1	2 μ1
Sal1	1 μ1
Nuclease free water	10 μ1

The above 20 µl reaction was kept in water bath for 2hrs at 37 °C.

After incubation $5\mu L$ of 6X gel loading dye was added and a 1% agarose gel was run. The solutions required for gel electrophoresis are as follows:

Reagent	Composition
50X TAE (1 liter)	Tris-base (242 gm), glacial acetic acid (57.1mL), 0.5 M
	EDTA- pH:8 (100mL). the volume was made upto 1 litre with
	water. Sterilized by autoclaving and stored at 4°C. Working
	stock is generally 1X TAE made in water.
EtBr (1mL)	10 g EtBr was dissolved in 1 mL of water.

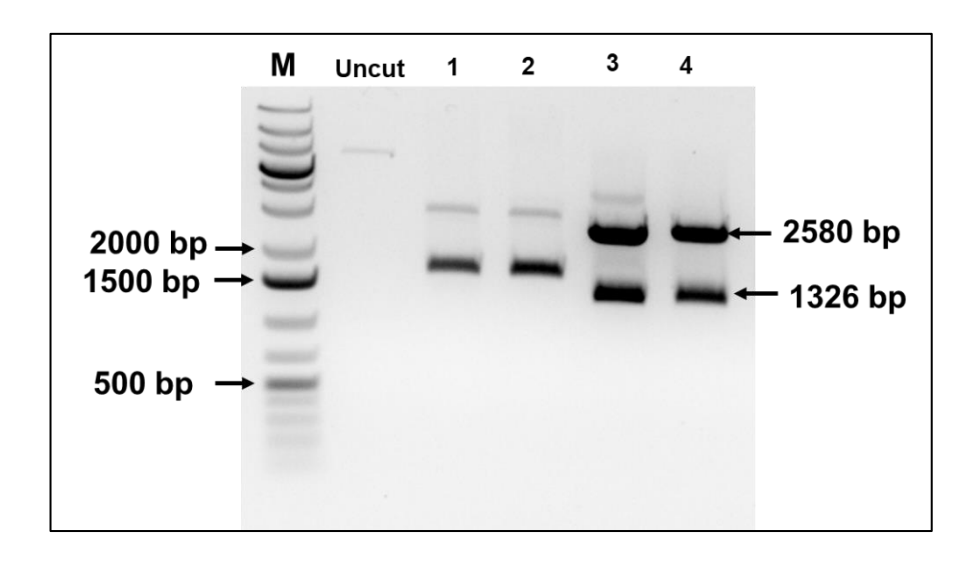


Fig M3: Section of positive clones after digesting the isolated plasmids with Pst1 and Sal1. Two fragments were obtained an insert of 1326bp and a backbone fragment of 2580bp. The un-digested vector can be seen at the top of the lane labelled uncut. Lanes 1-4 represents the restriction digestion profile of the plasmids isolated from four colonies obtained after kanamycin selection. M represents marker.

G. Sequencing of the plasmid DNA for clone confirmation

The clones confirmed by restriction digestion were further sequenced using the Big Dye Terminator Automated Sequencer (Applied Biosystems). The following sequencing reaction was setup:

Reagent	Volume
Ready reaction mix	1
5X buffer	2
Plasmid (100-150 ng)	1
Primer (GSP F/R) (10 ug)	1
Nuclease free water	10

PCR program:

Temperature	time	cycle
96°C	2mins	1
96°C	30 secs	
55°C	15 secs	25cycles
60°C	4mins	
4°C	α	

The sequencing products were purified as follows:

- a. $10\mu L$ of nuclease free water was added to the above PCR product to make the final volume $20\mu L$ and the samples were transferred to a 0.5mL microcentrifuge tube.
- b. 1μL of 125mM EDTA and 2μL of 3M Na-Acetate (pH 5.2) was added to the sample and mixed properly.
- c. To the sample $50 \,\mu\text{L}$ of 100% EtOH was added and kept under dark at room temperature for 20minutes.
- d. The samples were then centrifuged at 13000 rpm for 30mins and washed with 200 μ L of 70% EtOH at 13000rpm for 5minutes.
- e. The DNA pellet was air dried and dissolved in 12 µL of Hi Di Formamide.
- f. The samples were then heated at 95°C for 5minutes; snap chilled on ice for 5minutes and 10 μ L was loaded into the automated sequencer machine for sequencing.
- g. The sequence for the clones were analysed using the software CHOMAS and the clone that matched best with the insert i.e. the one where the sequence was in frame with for protein synthesis were selected for further procedure.

H. Mlu I digestion

Once the clones were confirmed by both restriction digestion and sequencing, the plasmid DNA were subjected to Mlu I digestion. Mlu I digestion eliminates a portion of the vector that contains the kanr cassette (smaller fragment) thereby enabling further selection of clones in destination vector that harbors the kanr cassette. Also, linearizing the entry clone increases the efficiency of cloning by upto 2-fold. Mlu I digestion was setup as follows:

Components	Volume
10X Buffer R	5 μL
Mlu I (10U/ μL)	1 μL
Plasmid (117 μg/mL)	10 μL
water	Volume made up to $50 \mu L$

After Mlu I digestion, the restriction digested product was run on a 1% agarose gel and the larger DNA fragment containing the gene of interest was eluted from the gel-by-gel extraction kit (Qiagen). The concentration of the eluted DNA was determined using a nanodrop spectrophotometer. The concentration of the digested product was $29 \,\mu g/mL$.

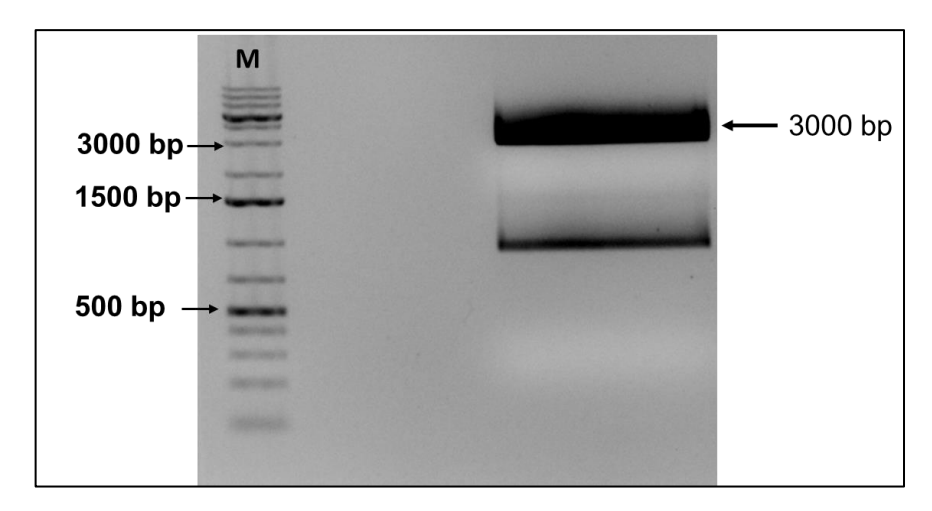


Fig M4: Gel profile of MluI digested ENTRY vector containing ARP4 CDS. The 3000bp fragment was eluted. The lane M represents marker.

- I. Cloning gene of interest into destination vector CD3-1648
 - a. LR reaction transfers the gene of interest from a Gateway entry clone pENTR/D-TOPO to a destination vector CD3-1648 by LR clonase reaction. The reaction was setup using the LR cloning kit (Invitrogen) as follows:

Reagent	Volume
Entry clone (50-150ng) [gene of interest in	5 μL
pENTR/D-TOPO that was Mlu I digested]	
Destination vector CD3-1648 (300ng)	1 μL
Sterile TE buffer	3 μL
LR Clonase II Enzyme	1 μL

- b. The above reaction was mixed properly and incubated at 25°C for 1hour.
- c. The reaction was terminated by addition of 1 μ L of Proteinase K (10mg/mL) to the samples at 37° for 10minutes.
- d. 6 μL of the LR clonase reaction mix was used to transform *Escherichia coli* DH5α cells by the usual transformation protocol as described previously.
- e. The positive clones were confirmed by restriction digestion using Pst 1 and Sal 1 enzymes. The restriction digested product was run on a 1% agarose gel.

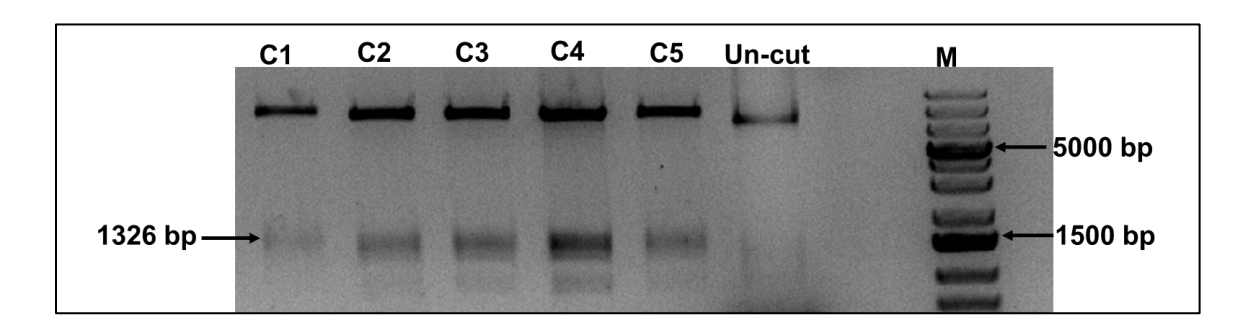


Fig M5: Gel profile of plasmid isolated from transformed colonies digested with Pst1 and Sal1. The 1326bp fragment confirmed the ARP4 CDS in the CD3-1648 destination vector. C1-C5 represent plasmid from colonies obtained after spectinomycin selection. The undigested profile of the recombinant vector (ARP4 CDS:CD3-1648) is present in the lane labelled Un-cut. M represents marker.

J. Agrobacterium competent cell preparation

- a. A single colony of Agrobacterium (EHA105) was picked from a freshly streaked plate and inoculated into 10mL of Rifampicine (50 μg/mL) in a culture tube.
- b. The tube was kept at 28°C for 48 hrs.
- c. From the culture 1mL was added to 50ml of fresh LB+Rifampicin, and incubated at 28°C till the O.D. reached 0.8-1.
- d. The 0.8 O.D. culture was centrifuges in an oakridge tube tube at 8000rpm for 10mins at 4°C to pellet the cells.
- e. The pellet was washed with 5mL of fresh LB and 100 μ L aliquots were made while keeping on ice.
- f. The aliquots were stored at -80°C.

K. Transformation of the CD3-1648 clone into Agrobacterium

- a. Agrobacterium competent cell vials were thawed on ice.
- b. To the thawed cells $0.5-1 \mu g$ of plasmid was added.
- c. The tubes were tapped to mix the contents and kept at 4°C for 30mins
- d. The tubes were then kept in liquid nitrogen for 5mins
- e. The tubes were then quickly transferred to a water bath maintained at 37°C for 5mins.
- f. 1mL of LB was added to the tubes and incubated at 28°C for 24hrs.
- g. The tubes were centrifuged at 5000rpm for 5minutes.
- h. The supernatant was discarded leaving 100 μL, in which the pellet was dissolved.
- i. The cells were plated on LB plates containing Rifampicin (50 $\mu g/mL$) and Spectinomycin (100 $\mu g/mL$).
- j. The plates were incubated at 28° for 48 hours.

L. Clone confirmation by colony PCR

Once colonies were observed on the plates after transformation, a colony PCR was performed to confirm the positive clones.

a. The colonies on the transformed plate were picked one at a time and streaked into another LB (Rifampicin + Spectinomycin) plate that had a checker board assigning each colony a number. The plate was incubated at 28°C for 48hours.

- b. The same loop after streaking the plate was used to inoculate 2mL LB containing Rifampicin and Spectinomycin for each colony respectively. The tubes were numbered according to the number on the replica plate.
- c. The culture was grown at 28°C overnight.
- d. From the grown culture 1 μL was taken in a PCR tube and diluted 100-fold with water.
- e. $5 \mu L$ from the diluted culture was used to serve as template for subsequent PCR reaction. Primers used for the PCR are listed in Annexure 1.

The PCR reaction was setup as per the table below:

Reagents	Volume
Reaction buffer (10X)	3 μL
dNTPs (10mM)	1 μL
MgCl ₂ (25 mM)	0.6 μL
Forward primer (10 μM)	0.5 μL
Reverse primer (10 μM)	0.5 μL
DNA Polymerase (5U/uL, Abcam)	0.5 μL
Template (diluted culture)	5 μL
Nuclease free water	Volume made upto 30 μL

The PCR program used was as follows:

Temperature	Time	Cycles
95°C	5mins	1
95°C	30 secs	35
53°C	30 secs	
72°C	50 secs	
72°C	7 mins	1
4°C	α	

g. The samples were visualized on a 1.5% agarose gel and positive clones were selected.

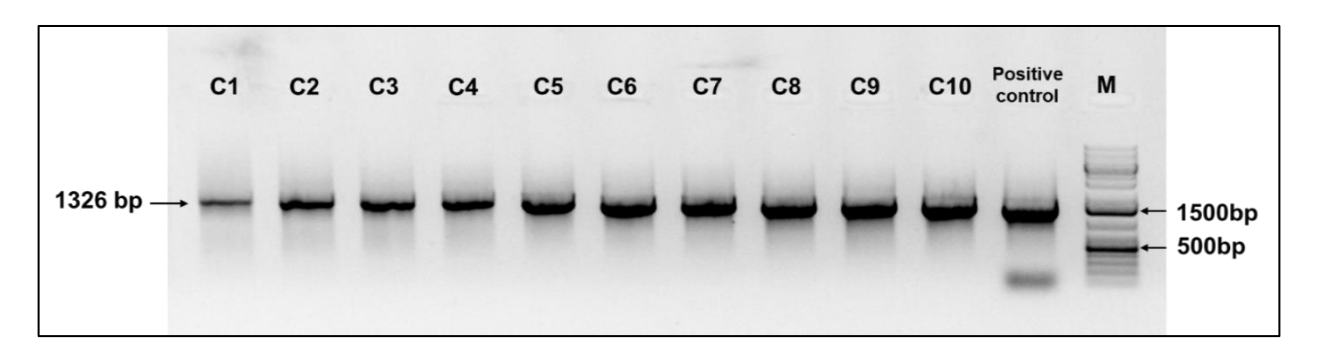


Fig M6: Colony PCR of transformed *Agrobacterium* using ARP4 CDS forward and ARP4 CDS reverse primers. The 1326bp amplicon confirmed the positively transformed Agrobacterium colonies. C1-C10 represent colonies from Rifampicin and Spectinomycin selection. The confirmed vector was used as template for the positive control setup and the PCR product was run in the lane labelled Positive control. M represents marker.

M. Agrobacterium-mediated-transformation of onion epidermal cells

The transient method to validate the protein-protein interaction of the two proteins AtHMGB15 and ARP4 was carried out as follows:

- a. The overnight *Agrobacterium* cultures of CD3 1651-AtHMGB15 and CD3 1648-ARP4 clones were pelleted at 5000rpm for 15mins at room temperature.
- b. The pellet was washed twice using the infiltration buffer.Infiltration buffer composition:

Reagent	Stock concentration	Working concentration
MgCl ₂	1 M	10 mM
MES (pH 5.6)	1 M	10 mM
Acetosyringone	0.5 M	100 μΜ
Water	Volume made upto 100 mL	

- c. The pellet was resuspended in 5ml of infiltration buffer after which the o.D. was measured using a spectrophotometer.
- d. The O.D. was adjusted to 0.8 using the buffer for following culture combinations before infiltration:
 - CD3 1648-ARP4 + CD3 1651
 - CD3 1651-AtHMGB15 + CD3 1648
 - CD3 1651- AtHMGB15 + CD3 1648- ARP4
- e. Once the combination cultures were prepared, they were kept in the incubator shaker at 28°C for 3hours.
- f. A 2 mL syringe was used to infilter the onion epidermal layer with the constructs.

- g. The infiltered onions were kept in dark for 48hrs at 28 °C
- h. After incubation, the onion peels were carefully taken out and washed in 1X PBS and placed on a cleaned glass slide.
- i. A coverslip was positioned on the onion peel and the extra water oozing out was carefully wiped and sealed.
- j. The samples were then visualised under a confocal microscope at an excitation wavelength of 514 nm and emission at 530-600 nm.

10) Estimation of anther wax content using Gas Chromatography Mass Spectrometry

Wax estimation from anther tissue was performed according to the protocol described by Razeq et al. with modifications (Goodman et al., 2021; Razeq et al., 2021).

- a) Approximately 50 anthers were isolated from wild type and *athmgb15* flowers corresponding to stage 12 of anther development and frozen in liquid nitrogen until further use.
- b) Anthers from WT and athmgb15 mutant were placed in individual glass test tubes and immersed in 5 mL of Chloroform and vortexed for 1 minute.
- c) The extract was then transferred to a fresh round bottom glass tube and the chloroform was evaporated by heating it in a rotary water bath.
- d) The contents of the tube were then redissolved in a mixture of hexane and chloroform (4:1) and passed through a solid-phase extraction (SPE) cartridge (SepPak Vac 3cc, 500mg Waters) that was pre conditioned by passing 4ml of hexane previously.
- e) The three standards used to measure are:
 - i. 1-pentadecanol (15:0-OH) for estimating anther sterols and fatty alcohols
 - ii. Heptadecanoic acid (17:0-coumarates) for quantifying alkyl coumarates and monoacylglycerols
 - iii. Tetracosane (24-0- alkane) for quantifying alkanes in the anther
- f) The fraction was evaporated in a laminar air flow and analysed as TMS ether and ester derivatives.
- g) After resuspending each derivatized sample in 200 μL hexane, it was filter sterilized and the sample were transferred to GC vials and analysed by a GC-MS on a TRACE 1300 Thermoscientific GC with a Thermoscientific ISQ single quadrupole MS detector.

- h) The process and programme used to analyse the anther extract in the GC-MS was:
 - i. A spitless injection was used with a TG-5MS capillary coloumn (30 m * 0.25 mm id, and $0.10 \mu m$ film thickness) and a helium flow set at $1.0 \mu m$ min.
 - ii. Temperature settings were as follows: inlet 330°C, detector 300°C, oven temperature set at 150°C for 3 minutes and then increased to 300°C at a rate of 4°C/min, with a final hold at 300°C for 5 minutes.

Wax components were identified by their relative retention time and characteristic mass spectra.

11) ROS estimation in bud and flower tissue

- a. 100 mg of tissue was homogenized and to it 1 mL of 100 mM TrisCl (pH: 7.2) was added.
- b. The slurry was then centrifuged in cold at 12000 g for 20 minutes.
- c. The supernatant was collected and the following reactions were prepared:

Sample	Volume of	Volume of Tris	DCFDA (1 mM stock)
	Supernatant	Cl (pH 7.2)	
Experimental	40 μL	360 μL	4 μL
sample			
Blank	-	400 μL	4 μL
sample			

- d. Observations were made using a fluorimeter (Varioskan) by exciting the reaction at 504 nm and measuring emission at 525 nm.
- e. total protein estimation was done using Bradford assay.

12) Histological sectioning of Arabidopsis buds of different developmental stages

- a. Entire flower inflorescence of different developmental stages was collected and placed in FAA fixative. Making sure that the volume of FAA is three times that of the tissue.
- b. The eppendorfs with the tissue was kept in vacuum for 15 mins. After that the vacuum was slowly released and the tissue would sink to the bottom of the tubes. A second application of vacuum improved the fixation.
- c. The fixative was changed and the tissue was incubated in the fresh fixative for overnight.

- d. The tissue was dehydrated using an alcohol gradient
 - i. 50% ethanol
 - ii. 60% ethanol
 - iii. 70% ethanol
 - iv. 80% ethanol
 - v. 90% ethanol
 - vi. 100% ethanol

Subsequently dehydrating it twice in 100% ethanol for 1hr. To the dehydrated tissue 0.1% Eosine Y was added and kept for overnight incubation in cold.

- e. Washing away of the excess stain and clearing of the tissue was done using different Histochoice and ethanol gradient.
 - i. 250ul Histochoice + 750 ul Ethanol
 - ii. 500 ul Histochoice + 500 ul Ethanol
 - iii. 750 ul Histochoice + 250 ul ethanol
 - iv. 1000 ul Histochoice. This step was repeated twice.
- f. After the second Histochoice step, fresh Histochoice was added and to it 500ul of melted paraplast was added and incubated at 60°C.
- g. The paraplast was changed every 12hrs for 6times before proceeding to mould preparation.
- h. A hot plate was set at 45°C and the mold was placed on the hot plate. Liquid paraplast was added to the mold and the tissue was placed carefully using needles and forceps. Note: be careful not to puncture the tissue and keep distance between the tissues
- i. The mold was removed from the hot plate and placed on a cooler surface to let the sample solidify, then the plastic holder was placed on the sample where the melted paraplast was poured.
- j. The waterbath was set to 40°C and the 3um sections were allowed to float on the waterbath to flatten them out.

- k. After 5-10mins the sections were transferred onto a clean glass slide with the help of a brush and labelled accordingly.
- 1. This was then kept in 37°C to remove the water and fix the samples to the glass slide.
- m. The glass slide with the sample was then immersed in Histochoice twice, for 5mins each followed by rehydration in ethanol gradient from 100% to 0%, for 30 secs in each grade.

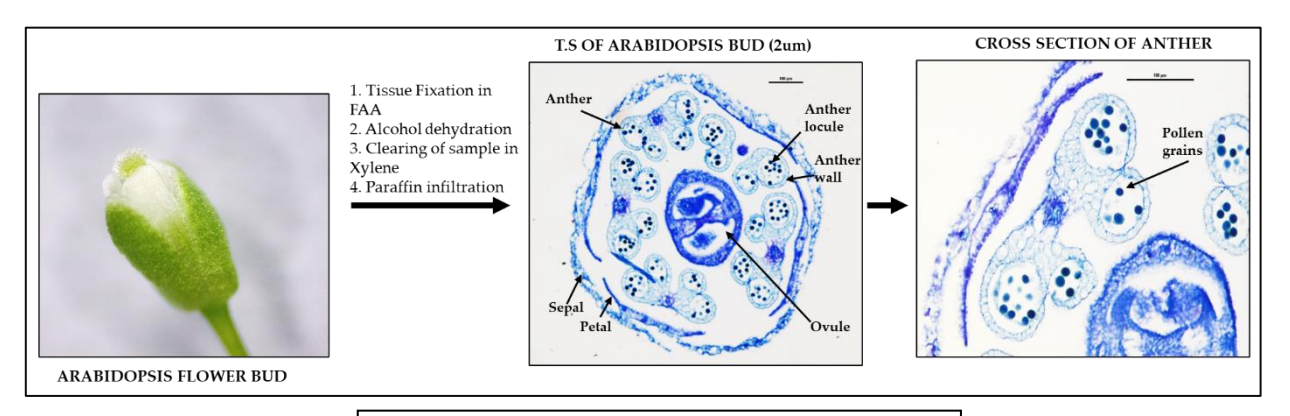


Fig. M7: Outline of the microscopy study

12.1 Vacuole staining of tapetal cells using FM4-64FX

- a. The slide with semi thin anther sections from step 2.1 l was placed in a 4% formaldehyde (1X PBS) and kept in 60° for 20mins.
- b. After which it was washed in 1X PBS for 5mins
- c. The paraplast from the samples were removed by immersing in Histochoice for 5mins followed by rehydration in alcohol gradient as mentioned in step 2.1 m.
- d. The sample was then washed in 0.85% NaCl for 5mins followed by a PBS wash for 5mins at room temperature.
- e. The sample was fixed by immersing the slide in 4% methanol free formaldehyde solution (in 1X PBS) for 15mins at room temperature.
- f. the samples were then washed in 1X PBS, twice for 5mins each in room temperature.

- g. The samples were then stained with 1 μ M of FM4-64FX (100 mM stock prepared in DMSO) for 15 minutes at room temperature.
- h. The excess stain was washed off with 1X PBS.
- i. Visualization was done at 514nm wavelength excitation and >580nm emission.

12.2 Terminal deoxynucleotidyl transferase dUTP nick end labeling (TUNEL) assay

Buds from different developmental stages were fixed by submerging them in a FAA (Formaldehyde: acetic acid: ethanol) fixative overnight at 4°C. The buds were then treated with xylene before being embedded in paraffin wax. The 5-um paraffin sections of the treated buds were then assessed with a TUNEL apoptosis detection kit (DeadEnd Fluorometric TUNEL system; Promega) according to the manufacturer's instructions as follows:

- a. The samples from step 2.1 l were then immersed in 4% methanol free formaldehyde solution in 1X PBS buffer for 15mins at room temperature.
- b. The slides were then washed by immersing them in appreciated volume of 1X PBS and incubating at 70°C for 10mins.
- c. For paraplast removal and rehydration: the samples were washed in histochoice, twice for 5mins each followed by passing it through an alcohol gradient from 100% -> 0% for 30secs in each grade.
- d. The fixed tissue was then washed in 0.85% NaCl for 5mins at room temperature followed by a PBS wash for 5mins
- e. The tissue in the slide was then fixed by immersing the slides in 4%methanol free formaldehyde solution in PBS for 15mins at room temperature followed by two PBS washes for 5mins at room temperature.
- f. The slides were then laid on a flat surface and the excess liquid was removed from the tissue. A 20ug/ml proteinase K solution was prepared in 1X PBS and 100ul of this solution was added to each sample. The slides were incubated for 20mins at room temperature before washing them off with 1X PBS.

- g. After proteinase K treatment, the samples were fixed in 4% methanol free formaldehyde for 5mins followed by a PBS wash in room temperature. For the positive control sample, the following steps were followed:
 - 100 μl of DnaseI buffer was added to the fixed cells and incubated at room temperature for 5mins.
 - ii) The extra liquid was removed by tilting the slide and 100ul of DNaseI buffer containing 5-10 units of DNaseI was added to the fixed tissue and incubated for 5minutes at room temperature.
 - iii) The samples were washed extensively for 3-4times in deionized water in a coplin jar dedicated for the control.
 - iv) The positive control was processes separately.
- h. The excess liquid was removed from the slides and covered with $100\mu l$ of equilibration buffer for 10mins at room temperature.
- i. While the cells were equilibrating, the rTdT incubation buffer was prepared according to the table:

Buffer Component	Component volume/slide
Equilibration buffer	45 μl
Nucleotide mix	5 μ1
rTdT enzyme	1 μ1

- j. For the negative control: A control incubation buffer was prepared without rTdT enzyme by combining 45ul of equilibration buffer, 5ul of nucleotide mix and 1ul of sterile water.
- k. The excess equilibration buffer was blotted off with a tissue paper and the 50ul of the rTdT incubation buffer was added to the sample and covered with the plastic coverslips to ensure even distribution of the reagent.
- 1. The slides were then placed in a humidification chamber previously laid with wet paper towels and kept in 37°C for 1hr to allow the tailing reaction to occur. The

humidification chamber was covered with aluminum fold to protect the reaction from direct sunlight.

- m. To stop the reaction, first the coverslips were removed then the slides were immersed in a coplin jar containing 2X SSC for 15mins.
- n. The samples were then washed in PBS for 5mins in room temperature. This step was repeated thrice to remove unincorporated fluorescein-12-dUTP.
- o. The samples were then stained with 1 μ g/ml propidium iodide for 15mins at room temperature in dark.
- p. The excess stain was removed by washing the slides three times in PBS for 5mins at room temperature.
- q. The excess water was drained and a drop of 50% glycerol was affed on the sample before visualization under a fluorescence microscope. The excitation wavelength of Fluorescein 12 dUTP is 496nm and emission at 515nm. The excitation wavelength of PI is 540 nm and emission at 640 nm.

The samples were photographed using a Leica STELLARIS confocal laser scanning microscope.

12.3Toluidine blue staining of semi thin anther sections

- a. Samples were prepared as mention in section 2.1. followed by staining of the samples using 0.5% toluidine blue O solution.
- b. The sample was incubated with the stain for 1minute and then washed with water.
- c. The samples were mounted on DPX, covered with a coverslip and dried to be finally observed under a light microscope.

13) Pollen grain isolation

- a) Proximately 200 mg of full bloomed flowers of both wild type and *athmgb15* mutant were collected in a 2 mL centrifuge tube.
- b) The flowers were then air dried by keeping the tubes open in the greenhouse or laminar airflow for 30 minutes.

c) To the flowers 1 mL of freshly prepared pollen germination media was added and vortexed vigorously for 10-15 minutes.

Reagent	Stock	Working concentration
Tris MES (pH 5.8)	200 mM	5 mM
CaCl ₂	1 M	10 mM
Boric acid	100 mM	1.5 mM
MgSO ₄	1 M	0.8 mM
KC1	500 mM	1 mM
Sucrose	20 %	5 %
PEG 4000	30 %	15 %

- d) The sample in the tube was centrifuged at 3000 rpm for 15 minutes.
- e) The pollen grains were deposited at the bottom of the tube (appear as a pale-yellow pellet).
- f) The flowers suspended in the solution were carefully removed using a small spatula by scooping them out and placed in another tube for a second round of vortexing and centrifugation.
- g) To the pollen pellet was then resuspended in 250 μL of fresh PGM.

13.1Pollen germination assay

- h) 50 μL of the isolated pollen was applied on a clean grooved glass slide and a coverslip (22 mm * 50 mm) was placed gently on the pollen suspension.
- i) This slide was then kept in the *Arabidopsis* growth chamber
- j) Observations were made under a light microscope (Nikon Ni Eclipse) with a high-resolution camera mounted on the top.
- k) The pollen grains were observed after every 30 minutes for 4 hours and images were collected for every time point to determine the germination pattern and growth of the pollen grains and pollen tubes, respectively.

13.2 Differential staining of pollen grains using FDA and PI

- a) The pollen grains were isolated using method 13.
- b) Double staining with fluorescein diacetate (FDA) and propidium iodide (PI) was performed using the method of Chang et al. (2014). To 100 μL of pollen grain suspension, 2 μL of the dye mix (0.5 μg/mL FDA and 10 μg/mL of PI) was added and incubated for 5 minutes.
- c) 50 µL of the stained pollen grains were viewed under a fluorescence microscope (Nikon ECLIPSE Ni). The excitation wavelength used to observe PI was 535 nm, the exposure

duration was 100 ms, and the gain was 1x. The excitation wavelength for fluorescein diacetate was 488 nm, the exposure duration was 200 ms, and the gain was 1.5x. The red fluorescence was from PI-stained pollen grains and the green fluorescence was from the FDA-stained pollen grains.

14) Actin visualization and quantification.

The protocol for visualisation and quantification of the spatial organization of actin using fluorescent phalloidin-staining in fixed *Arabidopsis* pollen grains and pollen tubes has been followed as described by Qu et al. with a few modifications (Qu et al., 2020).

A. Materials

- a. 12 cm x 12 cm square Petri dish
- b. 9 cm x 9 cm glass Petri dish
- c. Microscope slide
- d. Parafilm
- e. Glass bottom dish
- B. Plant materials: *Arabidopsis thaliana* (Col-0) The plants were grown in culture room under 16 h-light/8 h-dark photoperiod at 22 °C. Those plants with best flower production were chosen for the study. These plants had over 5 siliques on the main inflorescence stem, and older plant with few flower buds were avoided.

C. Chemical reagents

- a. Calcium chloride
- b. Calcium nitrate
- c. Magnesium sulfate
- d. Boric acid
- e. Sucrose
- f. Low melting point agarose
- g. Potassium hydroxide
- h. LatrunculinB (LatB)
- i. Dimethyl sulfoxide (DMSO)
- j. 3-Maleimidobenzoic acid N-hydroxysuccinimide ester (MBS)
- k. Sodium chloride
- 1. Nonidet P-40 (NP-40) (IGEPAL CA-630)

m. Alexa Fluor 488 phalloidin

Pollen germination medium

- 1 mM CaCl₂, 1 mM Ca (NO₃)₂, 1 mM MgSO₄, 0.01% H₃BO₃ (wt/vol), 18% (wt/vol) sucrose.
- Adjust pH to 6.85-7.0 with KOH For solid PGM, add 0.8% agarose
- > Stock solution 100 mM MBS (in DMSO)
- > 5 mM LatB (in DMSO)
- > 6.6 μM Alexa Fluor 488 phalloidin (in methanol)

The aliquotes were made and stored in -20 °C freezer to avoid repeated freeze-thaw cycles

Tris Buffered Saline (TBS)

- 50 mM Tris (diluted from 1 M stock, pH 7.4)
- 200 mM NaCl
- 400 mM Sucrose

D. Procedure:

Preparation of Arabidopsis pollen germination medium

- a. 100 mL of the liquid PGM was prepared (pH at 6.85-7.0)
- b. To 30 mL of this liquid PGM, 0.8% LMP agarose was added to prepare solid PGM.
- c. This was melted in a microwave, and evenly spread the medium into two or three glass Petri dishes.
- d. The PGM could be used within 3 days provided it was kept under 4 °C. As old PGM dramatically reduces the germination rate.
- e. It was made sure that the cooling surface for placing the Petri dishes was kept horizontal.
- f. The solid PGM were cut into 1 cm x 1 cm pieces and placed onto pieces of parafilm, on a clean microscope slide.
- g. The microscope slide was then kept at 28°C with a moist tissue paper to maintain humidity.

Pollen collection and pollen germination

- a. Arabidopsis flowers were harvested from 9:30 am to 12:00 am in clean labelled 2 mL centrifuge tubes and left them for drying at room temperature for not more than 1 h.
- b. The open flowers were gently dipped onto the medium to spread the pollen. (For the observation of pollen grains, collect pollen grains from over 20 Arabidopsis flowers in order to get a higher density. For the observation of pollen tubes, collect pollen grains from 10 fresh *Arabidopsis* flowers will be enough).
- c. The pollen were allowed to germinate by incubating them in the solid PGM blocks at 28 °C for 2 h.

Actin staining with phalloidin conjugated to fluorescent dye

- a. The chemicals listed above were dissolved in solvent according to the product specification and store as stock solution.
- b. To treat pollen cells with LatB, LatB was diluteted into liquid PGM to certain concentrations (10 nM). After incubation with LatB for 30 min, pollen cells were subjected to fixation with MBS.
- c. The pollen grains were fixed with 300 μ M MBS for 1 h at 28 °C. (100 μ l of MBS-PGM was added to each slice.)
- d. The MBS-PGM was removed and allowed to penetrate the pollen cells by incubating them in 0.05% NP-40, 150 μ M MBS in PGM for 10 min.
- e. The samples were washed with TBS + 0.05% NP40 for three times. (100 μ l TBS + 0.05% NP40 was kept on samples for 10 min each time.)
- f. The samples were stained with 200 nM Alexa Fluor 488 phalloidin in TBS over night at 4 $^{\circ}$ C in humid square Petri dish. 30 μ l phalloidin buffer was enough for each slice.
- g. The samples were then washed with TBS once before observation.

Visualization of actin filaments with laser scanning confocal microscope

a. The solid PGM pieces were mounted to glass bottom dish to image with Leica confocal microscope (Stellaris) equipped with a 100x objective.

The samples were excited with 488 nm laser and emission light was collected at 505-605 nm wavelength. The pollen tubes were zoomed by 2x, image optical slice at 1 µm step size. (Note: For image quantification, acquisition parameters must be identical in all images).

15) Transcriptome

15.1 RNA Isolation by Kit

The RNA was extracted from bud tissue corresponding to stages 8-11 of anther development using RNA Sure plant kit (Genetix).

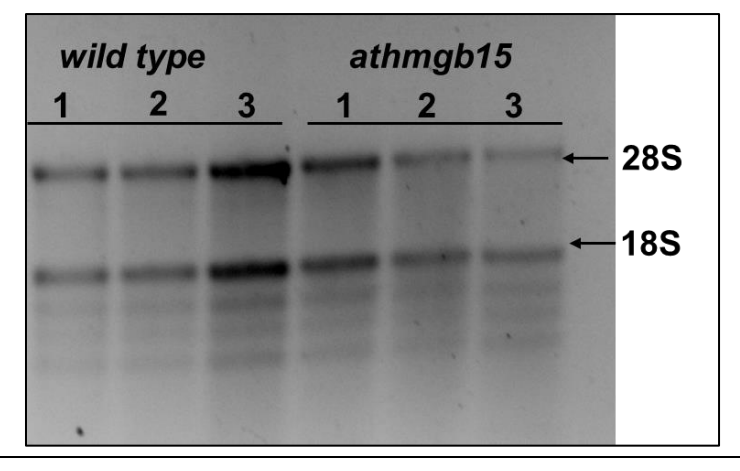


Fig. M8: RNA profile of the transcriptome samples

Sample name	Qubit ng/μL	QC status	Volume (µL)
Wild type_1	35.4	PASS	12
Wild type_2	62.4	PASS	12
Wild type_3	39	PASS	12
athmgb15_1	15.1	PASS	12
athmgb15_2	35.1	PASS	12
athmgb15_3	60.2	PASS	12

15.2 Data Processing

NEBNext® Ultra II Directional RNA library Prep Kit was used to prepare high quality libraries, according to manufacturer's protocols and paired end sequencing reads of read length 151bp was generated with Ilumina HiSeq-X sequencing platform. Raw reads were checked individually by using FASTQC. Quality control and per-processing of FASTQ files are essential to providing clean data for downstream analysis. Fastp, an ultra-fast FASTQ pre-processor with useful quality control and data-filtering features was used. It performs quality control, adapter trimming, quality filtering, per-read quality pruning and

many other operations with a single scan of the FASTQ data. This tool is developed in C++ and has multi-threading support. A cutoff of 30 was set for the quality phred score and only high-quality reads were retained. High quality reads were aligned against NCBI Reference of *Arabidopsis thaliana* (assembly TAIR10.1) by using ultra-fast, splice-ware aligner Hisat2. To understand the alignment quality, we checked several parameters including mapping percentage of reads. Details of mapping read percentage per sample given billow. Mapped reads were further considered for transcript assembly and quantification of transcript abundance by using stringtie. Transcript count, obtain from each sample were further used for analysis of differential expression of transcripts between alternate conditions by using DESeq2. A p-value cutoff of 0.05 and less was used to identify the significantly expressed transcripts. Genes with absolute values of fold change (FC) > 2 were considered to be differentially expressed. An FC > 2 was considered as significant upregulation, while FC < -2 was considered as significant downregulation.

16) Bioinformatics analysis:

Gene ontology (GO) term enrichment and KEGG pathway analysis of the transcriptomes were done using DAVID database v2021. The Venn diagrams were prepared using Venny 2.1. PlantPAN 3.0 was used to analyse the promoters of *MYB21*, and *MYB24* genes. STRING database was used for identifying the protein-protein interactors of AtHMGB15. Heatmaps were prepared using MeV 4.9.0. Statistical analysis was done using GraphPad Prism.

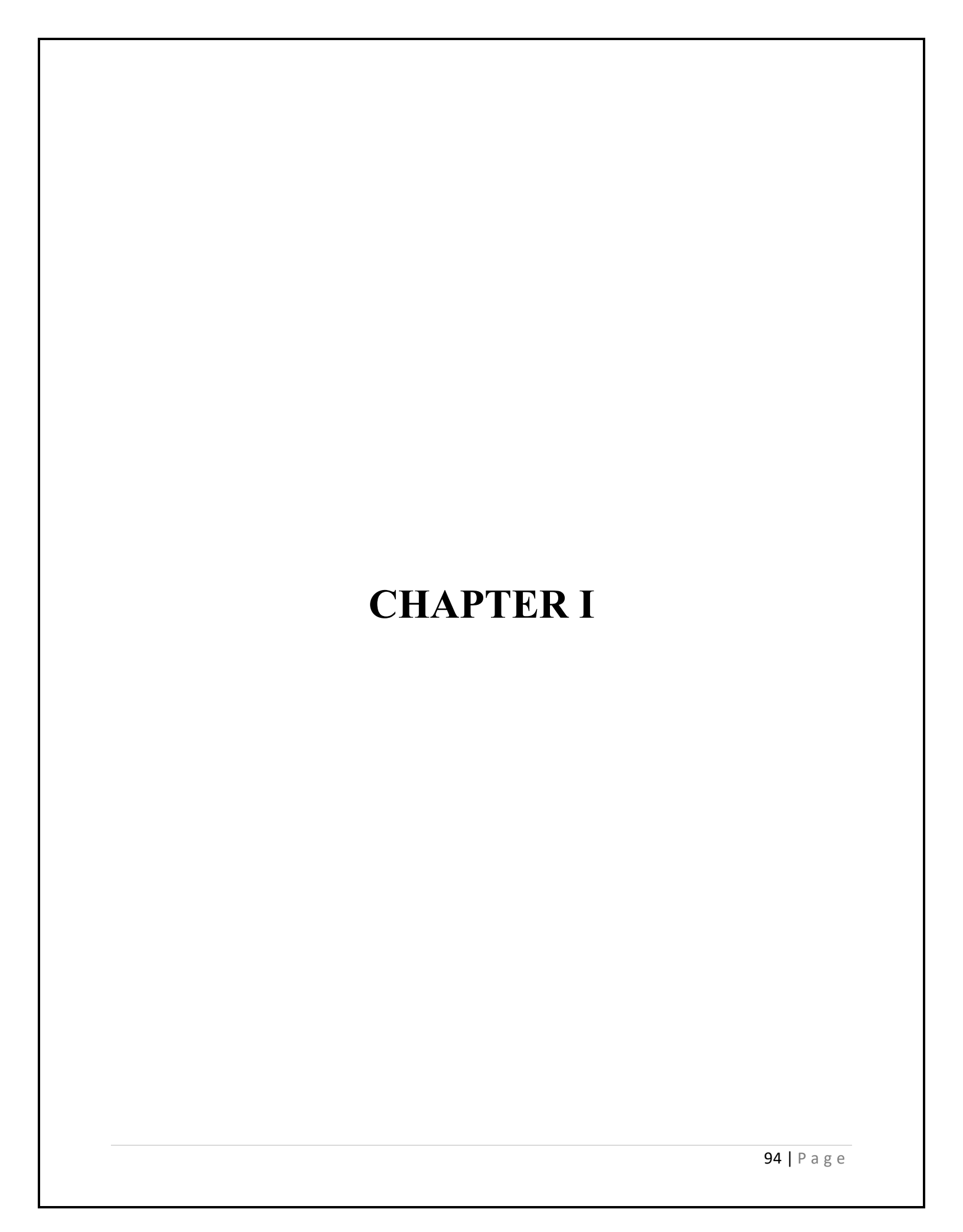
MATERIAL AND METHODS: REFERENCES

REFERENCES:

- 1. Goodman, K., Paez-Valencia, J., Pennington, J., Sonntag, A., Ding, X., Lee, H. N., Ahlquist, P. G., Molina, I., and Otegui, M. S. (2021). ESCRT components ISTL1 and LIP5 are required for tapetal function and pollen viability. *The Plant Cell* 33, 2850-2868.
- 2. Livak, K. J., and Schmittgen, T. D. (2001). Analysis of relative gene expression data using real-time quantitative PCR and the $2-\Delta\Delta$ CT method. *methods* **25**, 402-408.
- 3. Mallik, R., Prasad, P., Kundu, A., Sachdev, S., Biswas, R., Dutta, A., Roy, A., Mukhopadhyay, J., Bag, S. K., and Chaudhuri, S. (2020). Identification of genome-wide targets and DNA recognition sequence of the Arabidopsis HMG-box protein AtHMGB15 during cold stress response. *Biochimica et Biophysica Acta (BBA)-Gene Regulatory Mechanisms* 1863, 194644.
- 4. Qu, X., Wang, Q., Wang, H., and Huang, S. (2020). Visualization of actin organization and quantification in fixed Arabidopsis pollen grains and tubes. *Bio-protocol* **10**, e3509-e3509.
- 5. Razeq, F. M., Kosma, D. K., França, D., Rowland, O., and Molina, I. (2021). Extracellular lipids of Camelina sativa: Characterization of cutin and suberin reveals typical polyester monomers and unusual dicarboxylic fatty acids. *Phytochemistry* **184**, 112665.

OBJECTIVES

- 1. Determination of PCD in the developmental stages of athmgb15 and wildtype pollen.
- 2. Study the expression profile of the curated developmental PCD (dPCD) genes in wild type and *athmgb15* mutant.
- 3. Investigating the role of AtHMGB15 in PCD during pollen development.
- 4. Comparative study of pollen development in *athmgb15* and another PCD defective mutant



A defective pollen wall morphology is indicative of an abnormal developmental process during pollen grain formation (Quilichini et al., 2015). Studies have confirmed that normal development of the tapetum is indispensable for the maturation of the pollen grain prior to dehiscence (Kawanabe et al., 2006; Wei and Ma, 2023; Yao et al., 2022). Disruption in the process of tapetum development results in variations in the expression of a large range of genes involved in male reproduction (Kawanabe et al., 2006; Pacini, 2016; Parish and Li, 2010; Quilichini et al., 2014). Genetic screens have identified several genes that are expressed during different developmental stages of tapetum and disrupting them have resulted in male sterility (Parish and Li, 2010; Wei and Ma, 2023; Yao et al., 2022). Many transcription factors regulating the biosynthetic and degradational pathway in the tapetum have been identified and organized into a transcriptional network (Verma, 2019; Yang et al., 2019). Expanding this network has been hindered due to lack of data from the transient (4 days life span) of the tapetum in *Arabidopsis* (Goodman et al., 2021).

In order to investigate the developmental process of pollen development in *athmgb15*, we undertook a comparative transcriptome corresponding to two different stages of pollen grain development. The first transcriptome (previously done) is from stage 13 and the other transcriptome is performed from stages 8-11 of pollen grain development. The two stages signify a tapetum lacking stage and a tapetum active stage in wild type *Arabidopsis*. The transcriptome data was explored and tested for phenotypes in wild type and *athmgb15* mutant. Finally, DNA protein interaction studies were employed to determine the regulation of AtHMGB15 during tapetal cell death and tapetal cell function.

Analysis of the sequenced and filtered transcriptome of athmgb15 flower

Analysis of an existing transcriptome between *athmgb15* and wild type flowers corresponding to stage 13 of anther development was performed from three individual biological replicates of *athmgb15* and wild type flowers that was pooled into one for sequencing.

Sample	Total no. of reads	Aligned reads	Percentage aligned
athmgb15_1	32,104,392	31,109,155.8	96.9
Wild type_1	36,597,635	35,316,717.8	96.5

Significance of the Differentially Expressed Genes (DEGs) was determined by the Fold Change (FC) value, genes with FC were greater than zero along with P value threshold of 0.05 were considered up-regulated whereas less than zero were down-regulated significant expression (**Fig** 1.1). These genes were further categorized on the basis of their statistical significance (which can be either "yes" or "no", depending on FDR (False discovery rate 0.05) after Benjamin-Hochberg correction for multiple-testing) for their significant expression. The analysis revealed that 1674 genes were significantly expressed in the *athmgb15* flower tissue. The exercise of the statistical parameters narrowed-down the differentially expressed genes to 757 upregulated genes and 905 downregulated genes.

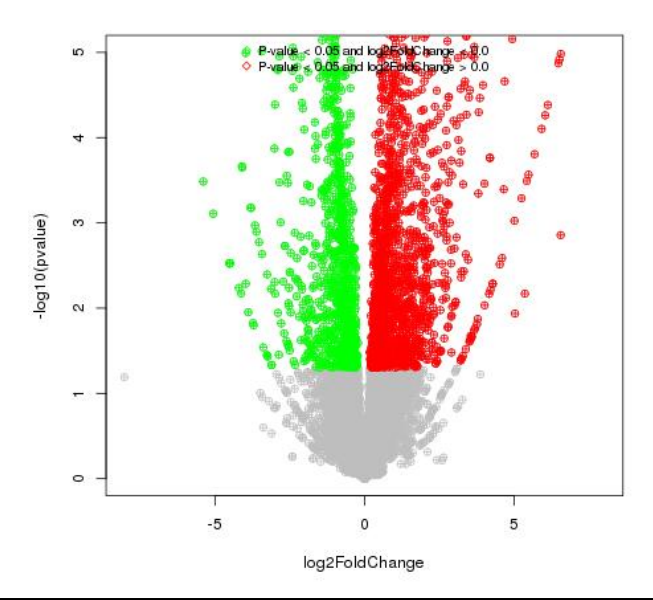


Fig. 1.1: Volcano plot depicting the genes categorised at upregulated (red), and downregulated (green) regulated in *athmgb15* in comparison to wild type flowers (stage 13 of pollen development) based on their $\log 10$ (p value < 0.05). The grey dots represent statistically not significant genes.

Functional annotation clustering of the significant differentially regulated genes in stages 13 of anther development in *athmgb15*

Study of the DEGs from the existing comparative transcriptome was done using an online available software, DAVID v6.2 database (**Fig 1.2**). The gene ontology study unfolded the enrichment of several terms in category of biological processes, like negative regulation of programmed cell death (GO:0043069), programmed cell death (GO:0012501), pollen tube growth (GO: 0009860), and pollen tube germination (GO:0009846). The enriched terms under molecular function category

included calcium ion binding (GO:0005509), calmodulin binding (GO:0005516), and calcium dependent protein serine/threonine activity (GO:0009931). The enrichment of terms in the cellular compartments category were pollen tube (GO:0090406), pollen tube tip (GO:0090404), pollen coat (GO:0070505), secretory vesicle (GO:0099503) and vacuole (GO:0005773). KEGG pathway analysis revealed that genes belonging to the phenylpropanoid pathway (PATH: ko00940), endocytosis (PATH: ko04144) and plant hormone signal transduction (PATH: ko04075) were significantly differentially regulated in the flower transcriptome corresponding to stage 13 of pollen grain development.

Analysis of the sequenced and filtered transcriptome of athmgb15 bud

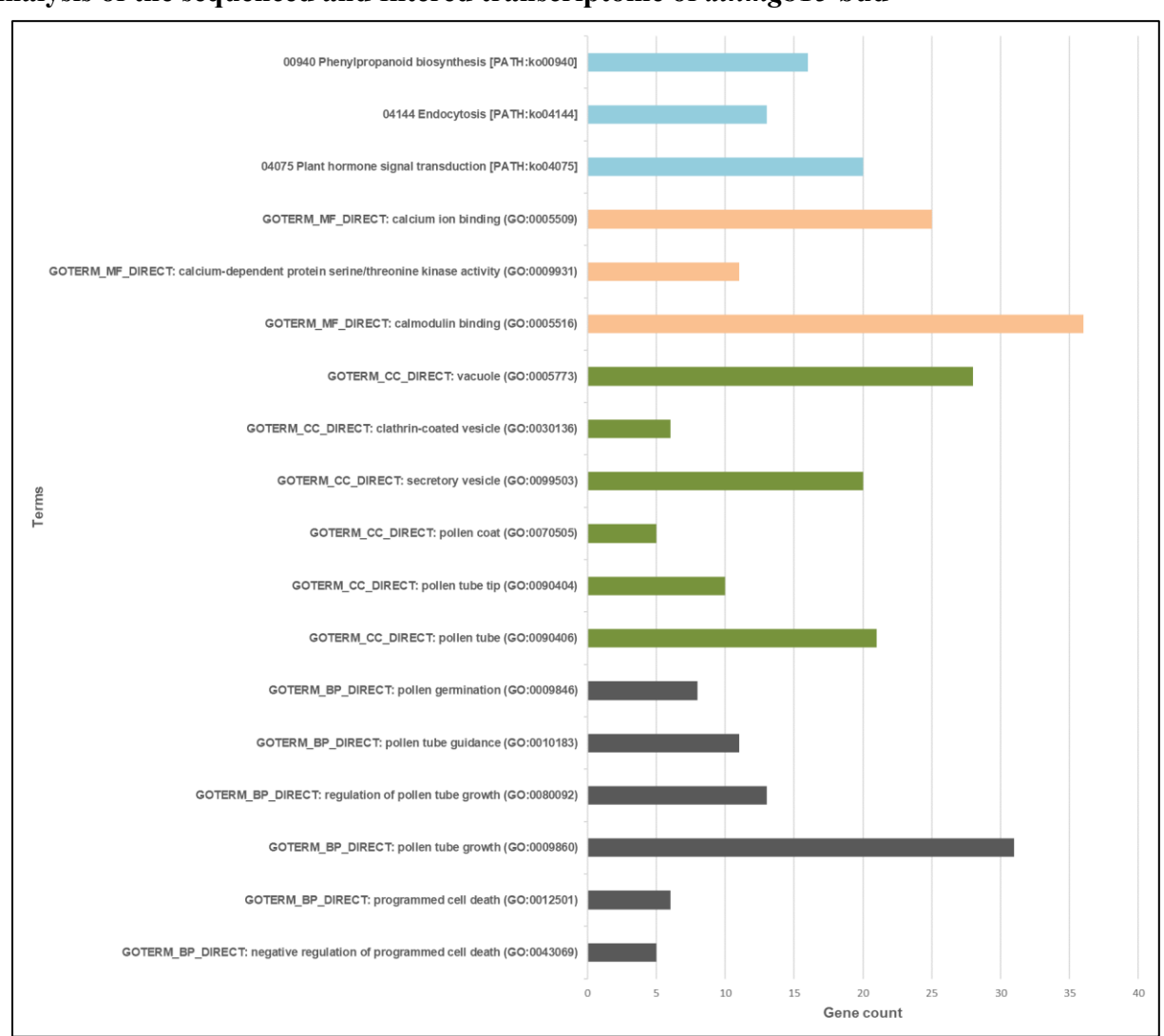


Fig. 1.2: Graphical representation of the enriched GO and KEGG pathway terms in the flower transcriptome.

A comparative transcriptome was employed in order to identify the genes regulated by AtHMGB15 (AT1G04880) in the bud stage, corresponding to anther development stages 8-11. Analysis of the transcriptome was done to determine the fold change in the expression of genes that were differentially regulated in *athmgb15* mutant compared to wild type buds. Stages 8-11 of anther development have been identified to exhibit tapetum degradation in *Arabidopsis*. Buds of these stages for *athmgb15* and wild type Arabidopsis were collected for RNA isolation that was reverse transcribed for cDNA preparation and then used for Illumina library preparation and sequencing. The table below states that over 99% reads could be aligned to the Arabidopsis reference CDS database that covered most of the *Arabidopsis* reference genome.

Sample	Total reads	Aligned Reads	Percentage aligned
athmgb15_1	19644638	19475694.11	99.14%
athmgb15_2	22823643	22615947.85	99.09%
athmgb15_3	30535776	30361722.08	99.43%
Wild type_1	26838009	26660878.14	99.34%
Wild type_2	32789986	32573572.09	99.34%
Wild type_3	26113935	25928526.06	99.29%

A p-value cutoff of ≤ 0.05 was used to identify the significantly expressed transcripts and a log2 fold change cut off ($\geq +2$) for upregulated transcripts and (≤ -2) for downregulated transcripts was used. According to these criteria, 2226 genes were significantly expressed in the bud stage. Out of these genes, 434 genes were significantly downregulated, 616 genes were upregulated and 1176 genes were neutrally regulated in *athmgb15* mutant (**Fig 1.3**).

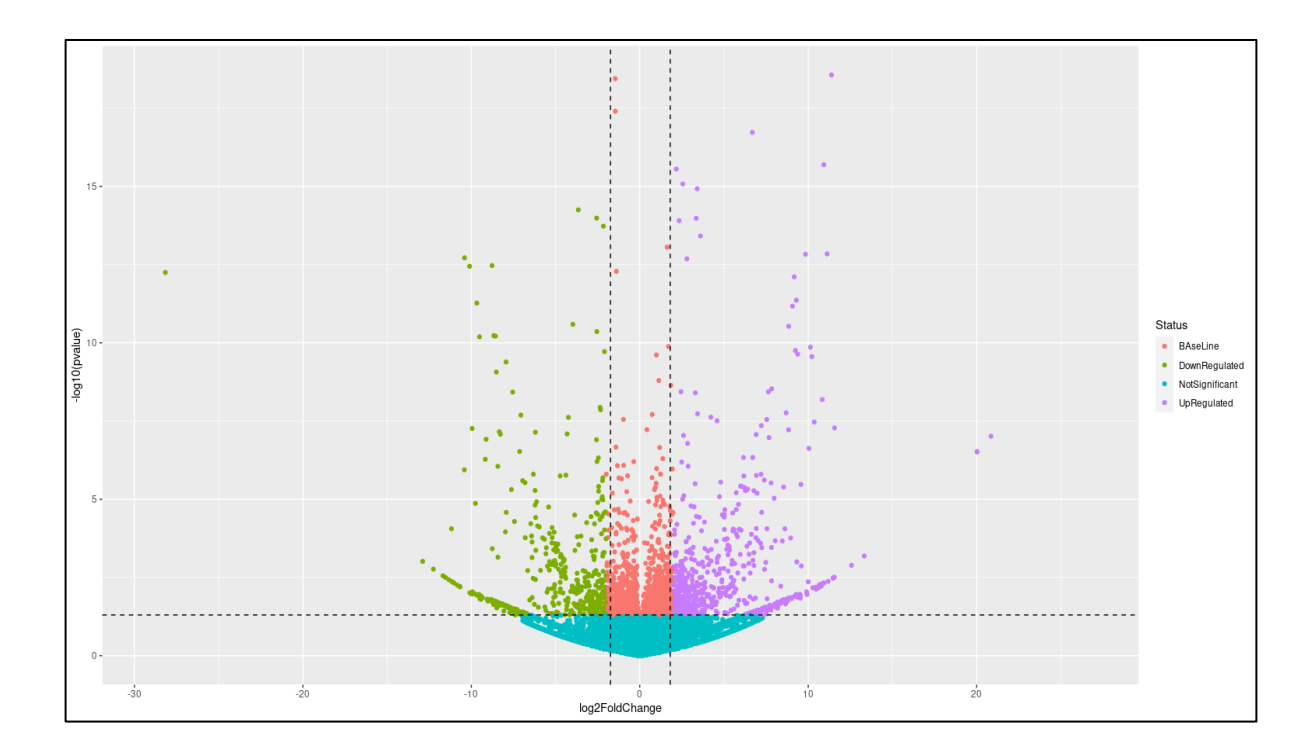


Fig. 1.3: Volcano plot depicting the genes categorised at upregulated, downregulated and neutrally regulated in *athmgb15* in comparison to wild type based on their log10 (p-value < 0.05)

Functional annotation clustering of the significant differentially regulated genes in stages 8-11 of anther development in *athmgb15*

In order to understand the consequences of AtHMGB15 loss of function mutation on the biological processes, molecular functions and cellular components during pollen developmental stages, we performed gene ontology (GO) clustering and KEGG pathway analysis of the significant differentially regulated genes using the DAVID web platform (Dennis et al., 2003) (Fig 1.4). The GO terms enriched under biological processes (BP) included negative regulation of programmed cell death (GO:0043069), programmed cell death (GO:0012501), vesicle transport along actin filament (GO:0030050), actin filament organisation (GO:0007015), pollen maturation (GO:0010152), and wax biosynthesis processes (GO:0010025). The cellular components (CC) that were involved in the GO term analysis of the transcriptome consisted of inner mitochondrial membrane (GO:0005743), myosin complex (GO:0016459), actin cytoskeleton (GO:0015629), and plant type vacuole (GO:0000325). Lastly, the GO terms that were highlighted under molecular functions (MF) were protein binding (GO:0005515), actin binding (GO:0003779), microfilament

motor activity (GO:0000146), motor activity (GO: 0003774), and calmodulin binding (GO:0005516).

The KEGG pathway analysis of the significant DEGs showed enrichment of different metabolic pathways that included sulphur metabolism (ath00920), pyruvate metabolism (ath00620), carbon metabolism (ath01200), biosynthesis of secondary metabolites (ath01120) and biosynthesis of amino acids (ath01230).

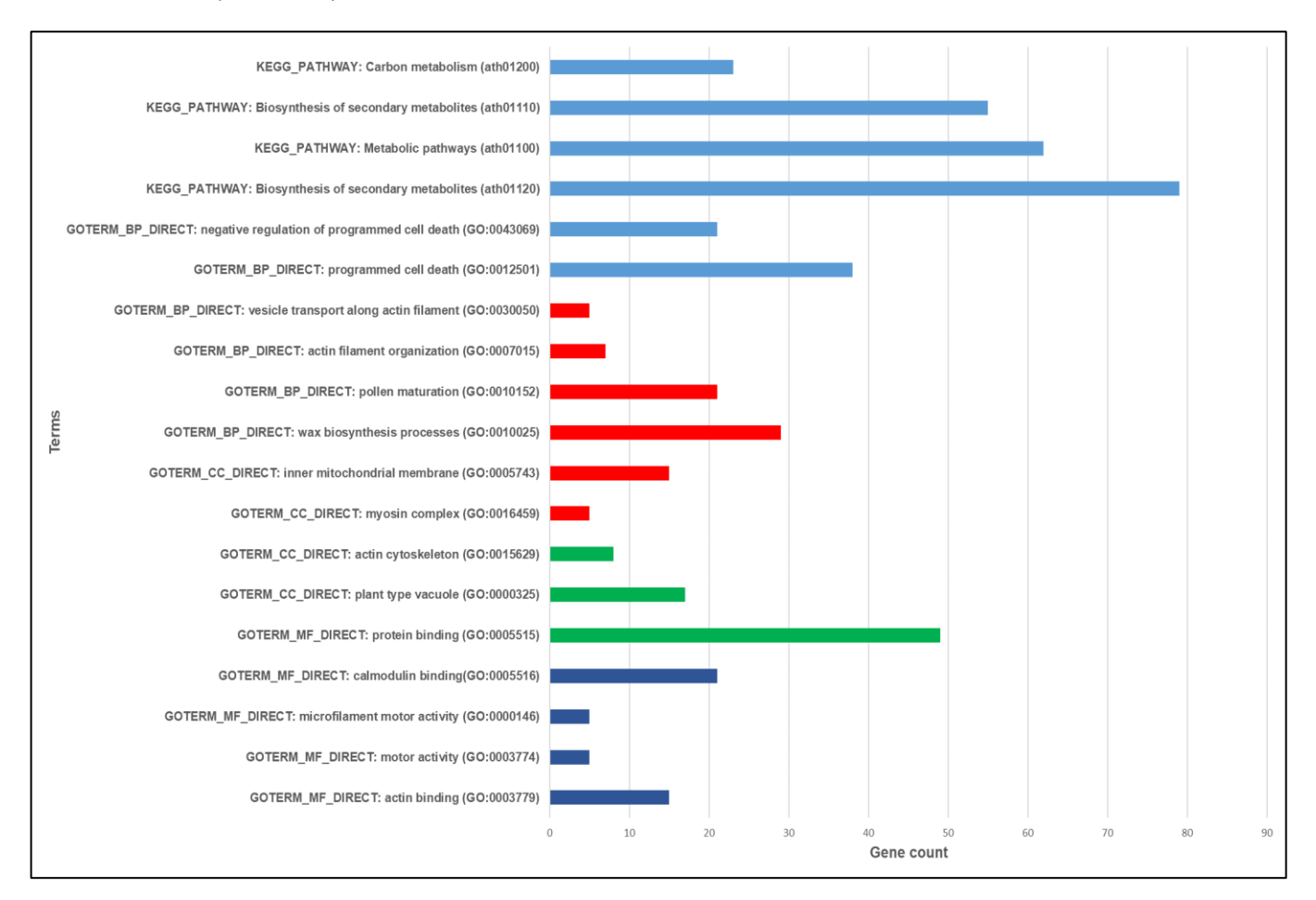


Fig. 1.4: Graphical representation of the enriched GO and KEGG pathway terms in the bud transcriptome.

Validation of athmgb15 bud transcriptome using q-RTPCR

q-RTPCR was performed to validate the bud (stages 8-11 of anther development) transcriptome. Several genes corresponding to actin -myosin cluster, cell division, tapetal cell specific transcription factors, sporopollenin biosynthesis pathway and its trafficking were shortlisted for

the validation of the transcriptome (**Fig 1.5**). The expression of actin binding protein genes like *PRF4 (AT4G29340)*, *VLN2 (AT2G41740)*, and *villin like 1 (AT2G29890)* is downregulated while that of *ADF4 (AT3G44540)* is upregulated in *athmgb15*. Amongst the myosin gene cluster, the expression of myosin *XID (AT2G33240)* and myosin *XIF (AT2G31900)* were downregulated while that of myosin *XIJ (AT3G58160)* was upregulated in both the transcriptome and q-RTPCR data. Recently identified tapetum specific transcription factors *LBD2 (AT1G06280)* and *MYB124 (AT1G14350)* were also differentially regulated in the *athmgb15* mutant. The expression of antiapoptotic transcription factors *Bax Inhibitor 1 (AT5G47120)* and *B11 family protein (AT4G02690)* were upregulated during stages 8-11 of anther development in *athmgb15*. The expression of a sporopollenin biosynthesis gene *RUPTURED POLLEN GRAIN1 (RPG1)* was downregulated several folds along with the expression of a sporopllenin transporter *ABCG31*.

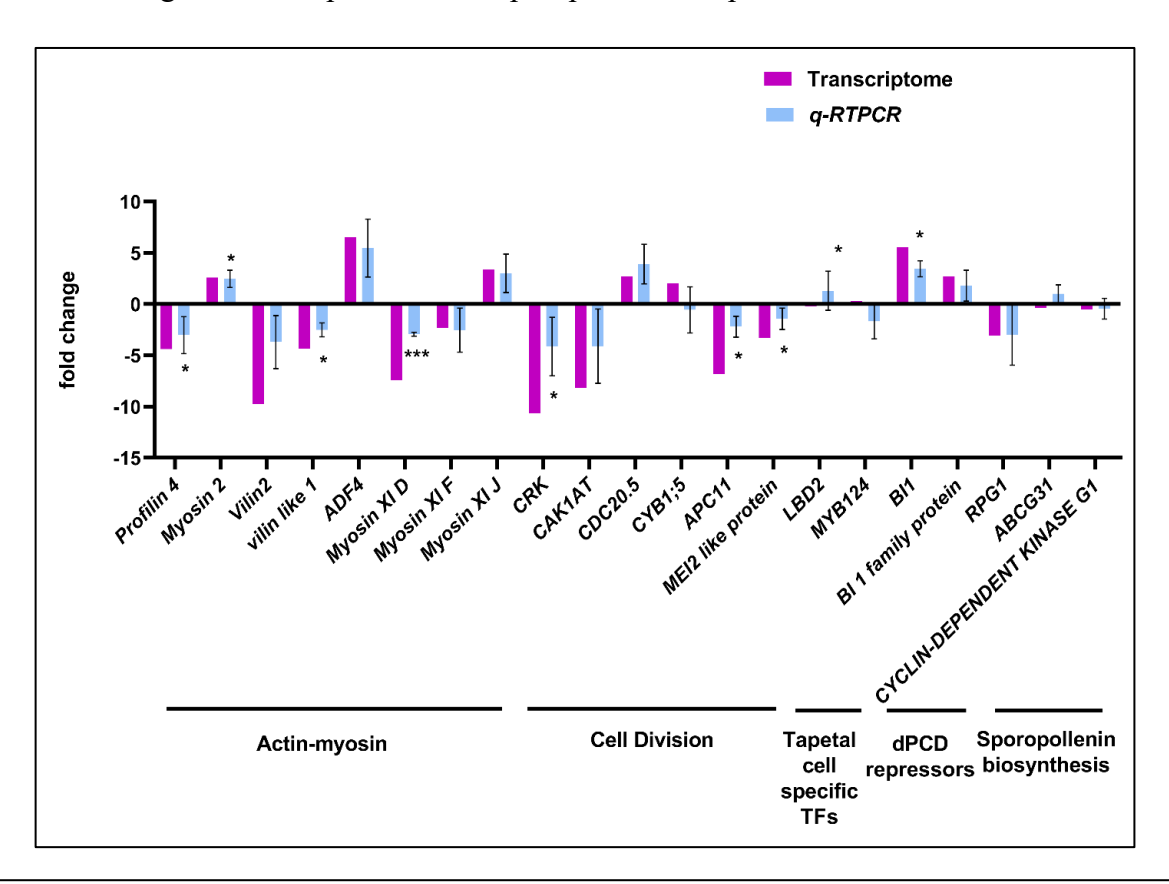


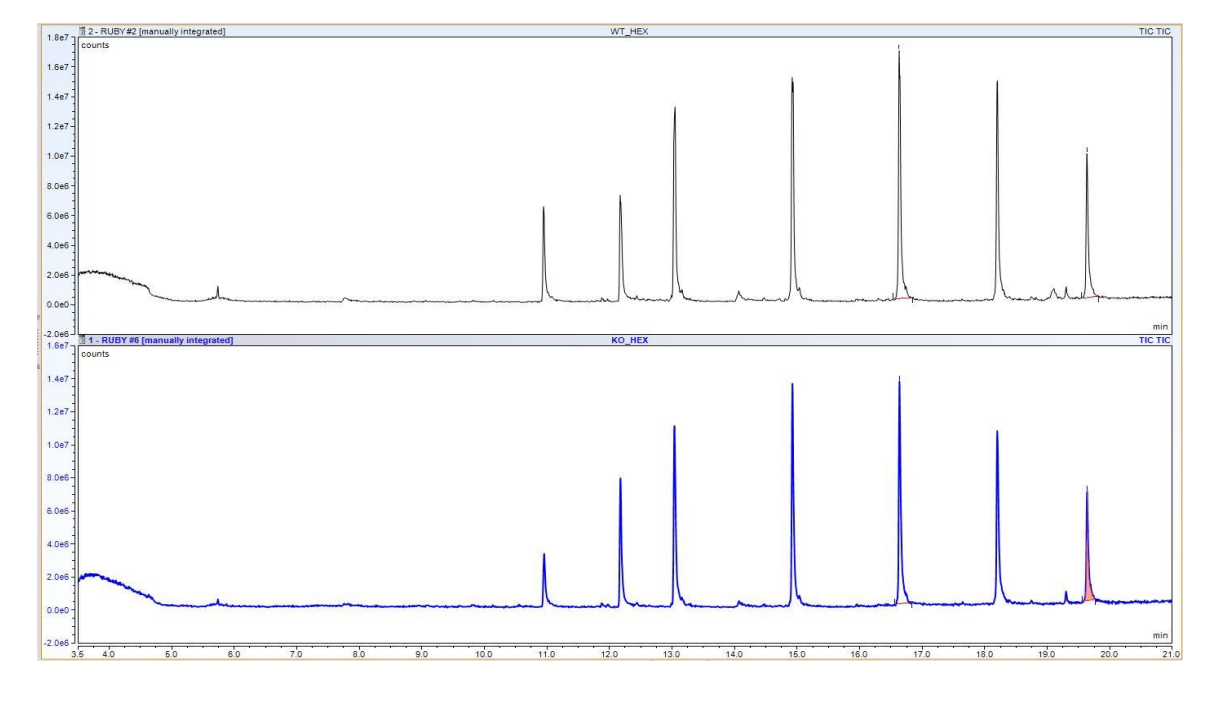
Fig. 1.5: Graphical representation of relative fold change values (log2) in transcriptome and the q-RTPCR validation for athmgb15 with respect to wild type buds from three biological replicates. The statistical analysis was performed using GraphPad Prism and two tailed students' t-test was done to determine the statistical significance of the q-RTPCR experiment. The significance to the genes' expression was assigned if the p-value < 0.05. *, and *** indicates p-value < 0.05 and 0.0005, respectively.

Estimation of anther wax content

The enrichment of phenylpropanoid pathway in the KEGG pathway analysis of the flower transcriptome indicated a differential regulation of the sporopollenin biosynthesis genes. The tryphine or pollen coat synthesis is an orchestrated cascade of events involving coordination from both sporophytic (anther walls) and gametophytic tissue (developing meiocytes). The outer layer or exine of the pollen wall is composed of sporopollenin that is responsible for the signature morphological patterns displayed by the pollen grains. Sporopollenin is considered to be the most complex and durable plant extracellular matrices (Lallemand et al., 2013). Fourier transform infrared and NMR data combined with research on exine mutants suggest that sporopollenin is composed of complex biopolymers derived mainly from long-chain fatty acids and phenolics such as p-coumaric acid (Battat et al., 2019). The phenolic monomers form ester and ether linkages to in-chain hydroxy lauric acids making sporopollenin similar to cutin, suberin, and lignin polymers (Goodman et al., 2021). During stages 7-9 of anther development, the tapetum synthesize steryl esters, waxes, flavonoids, and proteins that fill the cavities and crevices of the exine forming the pollen coat (Goodman et al., 2021). Flavonoids and alkanes are stored in a tapetum-specific organelle called the tapetosome which is derived from the endoplasmic reticulum (ER), whereas steryl esters accumulate in modified plastids called elaioplasts (Goodman et al., 2021). Finally, the cellular contents of the tapetum are trafficked and released in the anther locule via exocytosis and PCD of the tapetal cells.

Thus, the defect observed in the pollen wall morphology from previous studies (Xia et al., 2014) and enrichment of phenylpropanoid pathway genes in *athmgb15* inspired us to estimate the wax content of stage 8-11 anthers from *athmgb15* mutant and wild type using gas chromatography coupled with mass spectrometry (GC-MS). The experiment was performed twice with 50 anthers in each biological replicate for both *athmgb15* and wildtype. The results obtained indicated that the fold change in the abundance of the sterol, fatty acid and alkane group was 0.5-fold, 2.9-fold and 3.6-fold less respectively in the *athmgb15* compared to wild type anthers (**Fig 1.6**). The fold change for wild type was taken as 1. These results show that all major wax components were altered and that the accumulation of some alkane, sterols and free fatty acid components was lower in the *athmgb15* anthers than it should be as observed in wild type.







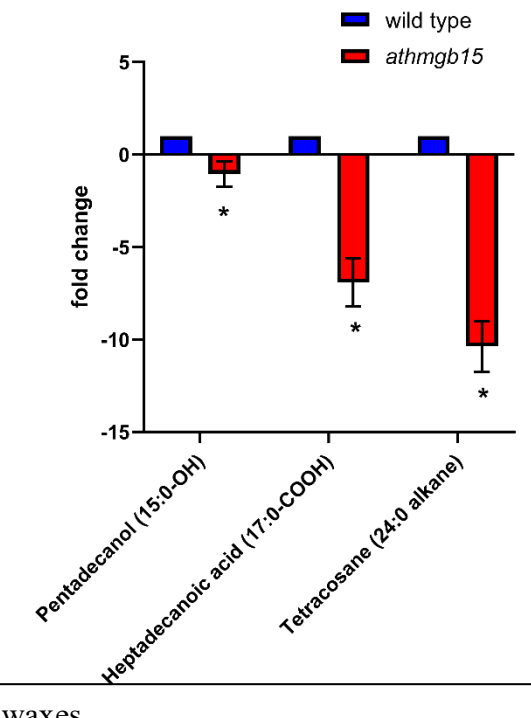


Fig 1.6: Analysis of anther waxes

- (A) Screenshot of abundance peaks observed for the individual anther wax components at their respective retention time, detected in GC-MS
- **(B)** Values are means of fold change observed from two biological replicates consisting of 50 anthers in each replicate and the error bars represents \pm SD. Statistical analysis was performed with GraphPad Prism using two-way ANOVA. Results were designated significant when the p< 0.05 (* p<0.05)

Downregulation of PCD executors in stages 8-11 of athmgb15 anthers

The enrichment of programmed cell death genes and negative regulation of programmed cell death in both flower and bud transcriptome analyses encouraged us to observe the expression pattern of the crucial genes enriched in these clusters. We investigated the expression profile of tapetum-specific transcription factors, PCD executers, PCD repressors and RBOHD gene. The heatmap clearly indicates that the expression of the PCD executers namely, CEP1, MC9, BFN1, α-VPE, and RNS3 are downregulated in the athmgb15 buds (stages 8-11 of anther development) (Fig 1.7). The expression of these genes neutrally regulated or upregulated in the later stage (stage 13) of pollen development. The expression of anti-apoptotic genes or negative regulators of PCD like Bax Inhibitor1 and BI1 family protein genes were downregulated in the early stages while upregulated in the later stages of anther development in athmgb15.

An evolutionarily conserved signal for initiation of PCD has been attributed to ROS surge. Previous studies have also shown that production of reactive oxygen species is an indication of PCD activation even in tapetal cells (Zhang et al., 2023). We therefore analyzed the transcriptome to determine the expression pattern of ROS specific genes in *athmgb15*, results showed that the down regulation of *RESPIRATORY BURST OXIDASE HOMOLOGUE D (RBOHD*) in the later of anther development.

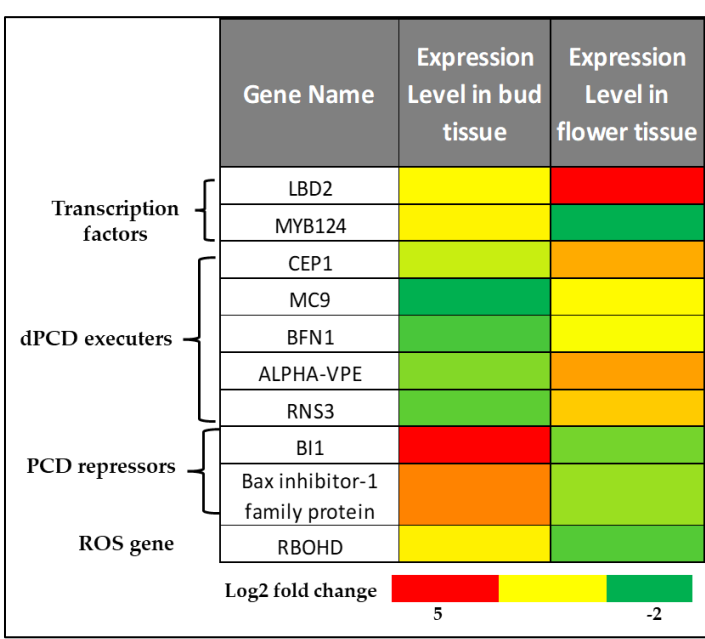


Fig 1.7: Heatmap of differentially regulated genes related to developmental PCD corresponding to different stages of pollen development in *athmgb15*

Occupancy of AtHMGB15 in the promoter of *BI1* an anti-apoptotic transcription factor and *CEP1*, *RNS3*, *MC9* genes in stages 8-11 of wild type anthers

To explore the probability of a potential interaction between AtHMGB15 and the upstream regions of the anti-apoptotic transcription factor *BI1*, and PCD executer genes *CEP1*, *RNS3*, and *MC9* we performed a chromatin immunoprecipitation (ChIP) assay from wild type buds corresponding to stage 8-11 of anther development, using the custom-made (thermo scientific) affinity-purified anti-AtHMGB15 antibody. The immunoprecipitated DNA was subjected to q-RTPCR. The antibody used for ChIP analysis was previously validated in the whole genome ChIP-on-chip study (Mallik et al., 2020). The ChIP data were normalized with At1g01310, showing no AtHMGB15 occupancy according to the previous study (Mallik et al., 2020). The primers were designed from *in silico* analysis of promoter/upstream region of *BI1*, *CEP1*, *RNS3*, and *MC9* that contain AtHMGB15 binding site A(A/C)--ATA---(A/T)(A/T) (Mallik et al., 2020). The q-PCR analysis showed AtHMGB15 occupancy at the promoter/upstream region of *BI1*, *CEP1*, *RNS3* and *MC9* compared to the occupancy observed in *At1G01310* promoter. The graph clearly demonstrates a 2-fold increase in occupancy compared to the negative control (**Fig 1.8**).

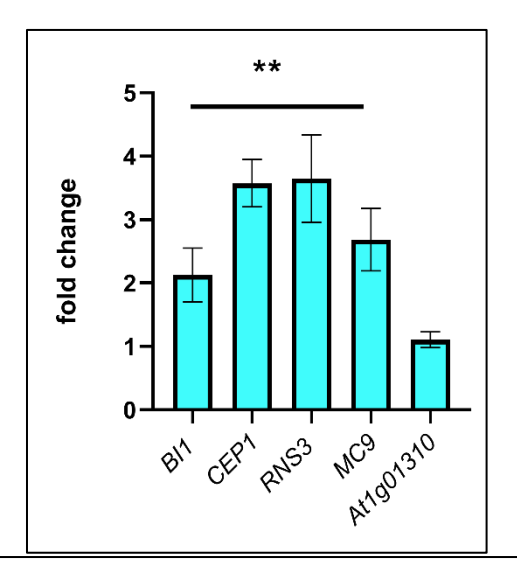


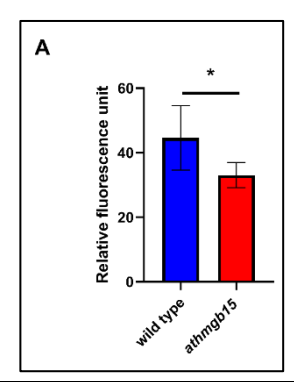
Fig 1.8: Occupancy of AtHMGB15 in promoter or upstream region of *BI1*, *CEP1*, *RNS3 MC9* and *At1g01310*.

The graph represents fold change in the enrichment of genes from the chromatin immunoprecipitation assay performed using anti-AtHMGB15 antibody. Statistical tests were performed with GraphPad Prism, using one sample t-test. The error bars represent \pm SD. Results were assigned significance when p < 0.05 (** p<0.005, n=3).

Lowered ROS content in wildtype and athmgb15 buds and flowers

Reactive oxygen species exert a strong effect on PCD during the development of tapetum cells (Ye et al., 2021). Studies have reported that excessive accumulation of ROS can trigger PCD and play potential roles in inducing PCD (Ye et al., 2021). ROS burst occurs during the early stages of PCD, whereas during the termination of PCD, ROS production decreases to a low level (Ye et al., 2021). Maintaining high ROS concentrations can lead to abnormalities in PCD, which in turn causes tapetal dysfunction and pollen abortion (Ye et al., 2021). It was therefore important for us to investigate the total ROS content in the flower buds corresponding to stage 10 of anther development in *athmgb15* and wildtype.

The graph displays a 11% lower content of reactive oxygen species in *athmgb15* during stage 10 of pollen development. (Fig 1.9). The lowered ROS content in the *athmgb15* mutants could be a probable implication of the neutrally regulated or downregulated expression of ROS producing genes in *athmgb15*. The lowered production of ROS also predicts that the *athmgb15* mutants lack the required amount of ROS to synchronize PCD in the tapetal cells, thus causing a lag in PCD signaling in *athmgb15* mutant that has been investigated earlier. However, the more than 50% difference in ROS content of wild type and *athmgb15* flowers infers a constitutive defect in the regulation of ROS production genes in *athmgb15*.



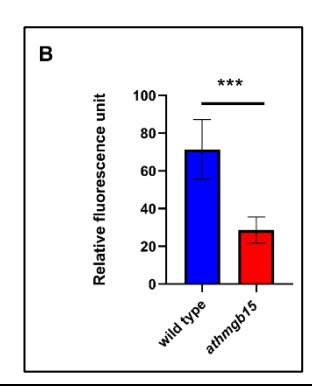


Fig 1.9: Estimation of total ROS content in buds and flower tissue of wild type and *athmgb15* using DCFH-DA

Values represent the mean relative fluorescence unit obtained for the total ROS content in 5 biological replicates, each containing 100 mg (A) bud tissue (corresponding to stages 8-11) and (B) flower tissue of *athmgb15* and wild type. The error bars represent \pm SD. The statistical analysis was performed in GraphPad Prism, using unpaired 2-tailed students' t-test and significance was assigned when p value < 0.05 (*, and *** for p value < 0.05 and p-value < 0.005, respectively)

Prolonged PCD in the tapetal cells of athmgb15

To corroborate our findings from transcriptome studies and biochemical analyses of anther wax content and ROS levels in *athmgb15* we performed the terminal deoxynucleotidyl transferase-mediated dUTP nick-end labelling (TUNEL) assay to determine the progression of PCD in the tapetal cells of *athmgb15* and wild type. We observed TUNEL positive signal for fragmentation of tapetal cell DNA at stage 10 in both *athmgb15* and wildtype anther. No TUNEL positive signals were observed by stage 12 or later for wildtype anther indicating complete degeneration of tapetal cells. However, the strong TUNEL positive signal was observed in stage 12 of *athmgb15*, indicating that tapetal nuclei degeneration was not completed (Fig 1.10). TUNEL assay study confirmed that the onset of tapetal cell degeneration is in the *athmgb15* and wild type was on time, but its termination was prolonged in case of the mutant.

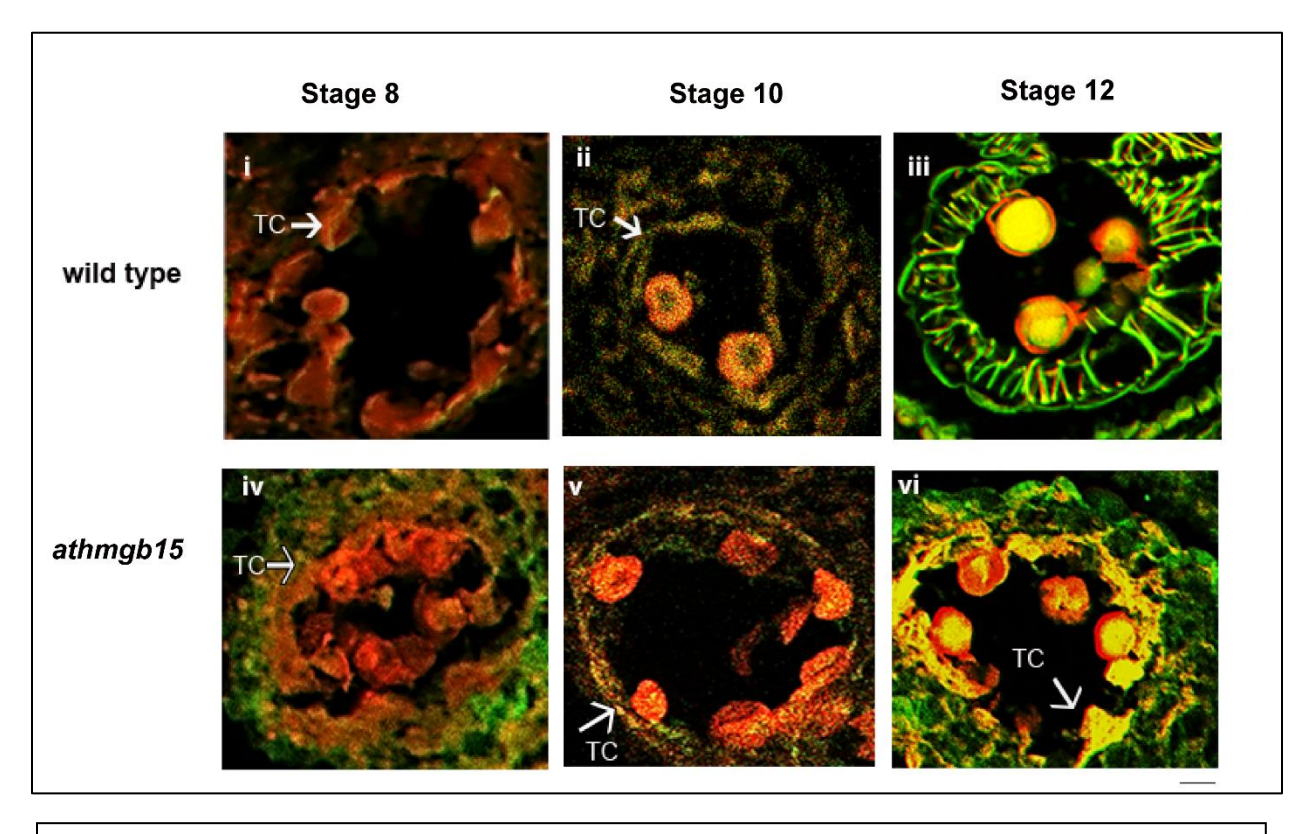


Fig 1.10: Progression of tapetal PCD was monitored using TUNEL Assay in wildtype and *athmgb15-4* anther from stages 8, 10 and 12.

(i-iii) TUNEL positive signal (yellow) from wildtype anther, TUNEL positive signal (yellow) from *athmgb15-4* anther (iv-vi). The scalebar represents 10µm.

We then investigated the expression of key PCD genes that are have been previously established to play a vital role in tapetum degradation. *CEP1* and *RNS3* have been previously shown to be highly expressed during tapetal-PCD (Buono et al., 2019; Zhang et al., 2014). The role of *MC9* and *BFN1* however, has not been shown in tapetal PCD (Buono et al., 2019). Our bud transcriptome identified downregulation of these genes namely *CEP11*, *MC9*, *RNS3* and α -*VPE* in *athmgb15*. q-RTPCR results also validated our transcriptome (**Fig 1.11**). We also observed upregulation of *Bax inhibitor B11* expression in *athmgb15* mutant. BI proteins are known as anti-PCD proteins that inhibit ROS-mediated cell death in plants (Ishikawa et al., 2011).

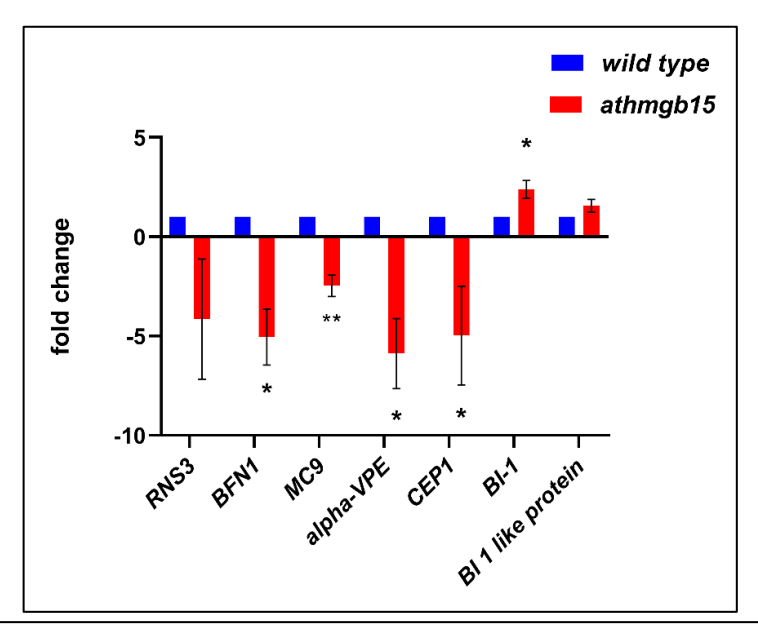


Fig 1.11: q-RTPCR of PCD genes in wild type and athmgb15-4.

The values represent the mean fold change in the expression of the genes and the error bars represent the \pm SD (n=3). Statistical analysis was performed using GraphPad Prism and a paired 2-tailed students t-test was done to determine the significance of the fold change for each gene. Significance was assigned based on the p-value < 0.05 (*, ** represent p<0.05 and p<0.005 respectively)

Abnormal vacuolation in athmgb15 tapetal cells

The vacuoles in the tapetum supply tetrad wall-degrading enzymes before their secretion into the anther locules (Wu and Yang, 2005). Abnormal vacuolization in the tapetum during the tetrad stage causes abnormal tapetal PCD and results in male sterility (Wan et al., 2010). The vacuole processing enzymes (VPEs) transcends into the vacuoles for isolation and storage by autophagy to later induce programmed cell death (Teper-Bamnolker et al., 2021).

To visualize the vacuoles in the anthers of wild type and *athmgb15* we stained the semi-thin sections (5μm) of anthers from stages 5, 7,11 and 12 of wildtype and *athmgb15* with FM4-64FX. The result indicates abnormal vacuolation in *athmgb15* compared to the wild type with a lesser number of vacuoles in tapetum cell cytoplasm (**Fig 1.12**). Wild type *Arabidopsis* tapetal cells have enlarged vacuoles compared to *athmgb15*. With the advancement of anther development in *athmgb15*, there were fewer enlarged vacuoles in the tapetum cell cytoplasm than observed in the wild type.

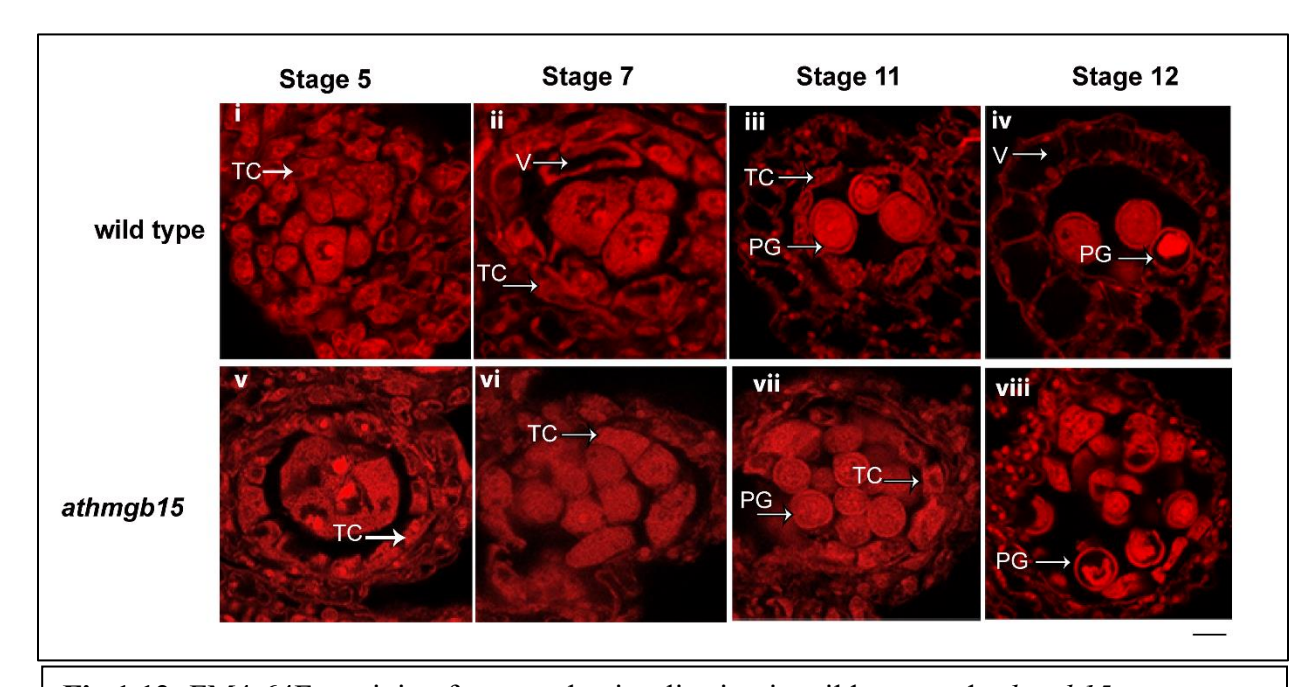


Fig 1.12: FM4-64Fx staining for vacuole visualisation in wild type and *athmgb15* tapetum Anther sections from stages 5, 7, 11 and 12 were stained with FM4-64FX. V is vacuoles, E is endothecium, PG is pollen grains and T is tapetum. (i-iv) represents stage 5,7, 11& 12 of wild type, (v-viii) represents stages 5, 7, 11 & 12 of *athmgb15*. The scalebar represents 10μm.

Delayed anther dehiscence

Inorder to study the dehiscence timing of *athmgb15* with respect to wildtype we made microscopic observations of semi-thin anther sections. Stage 11 of anther development in wild type *Arabidopsis* is identified by the binucleation of microspores and expansion of the endothecium (Gómez et al., 2015; Marchant and Walbot, 2022; Sanders et al., 1999). The septum is still present, the tapetal layer has almost fully degraded, and the pollen grains begin to acquire their characteristic elliptical shape. This continues until stage 12, at which point the microspores contain a vegetative nucleus

as well as two generative nuclei. The pollen grains at this stage are largely starch—filled and the tapetum is fully degraded in the wild type *Arabidopsis*. In the *athmgb15* mutant, however, the stage 11 anther exhibited a perceptible increase in size along its major axis even though developmental progress marking the onset of the next stage is not observed. The pollen grains had not yet acquired their final shape, unlike the wild type. This is consistent with the observational evidence of prolonged tapetal PCD. Due to a retardation in the execution phase of PCD, the rate of availability of exine constituents becomes a limiting factor in *athmgb15*. By the end of stage 14 of anther development, the septum of the wild type *Arabidopsis* exhibits complete disintegration, and dehiscence of the anther is also observed. In case of *athmgb15*, however, the septum is still intact in stage 14 (Fig 1.13) and no signs of anther dehiscence are detected, indicating an abnormally delayed anther dehiscence in the mutant. Collectively, these data suggested that prolonged tapetal degeneration and incomplete pollen development in *athmgb15* can lead to delayed dehiscence of the mutant anthers.

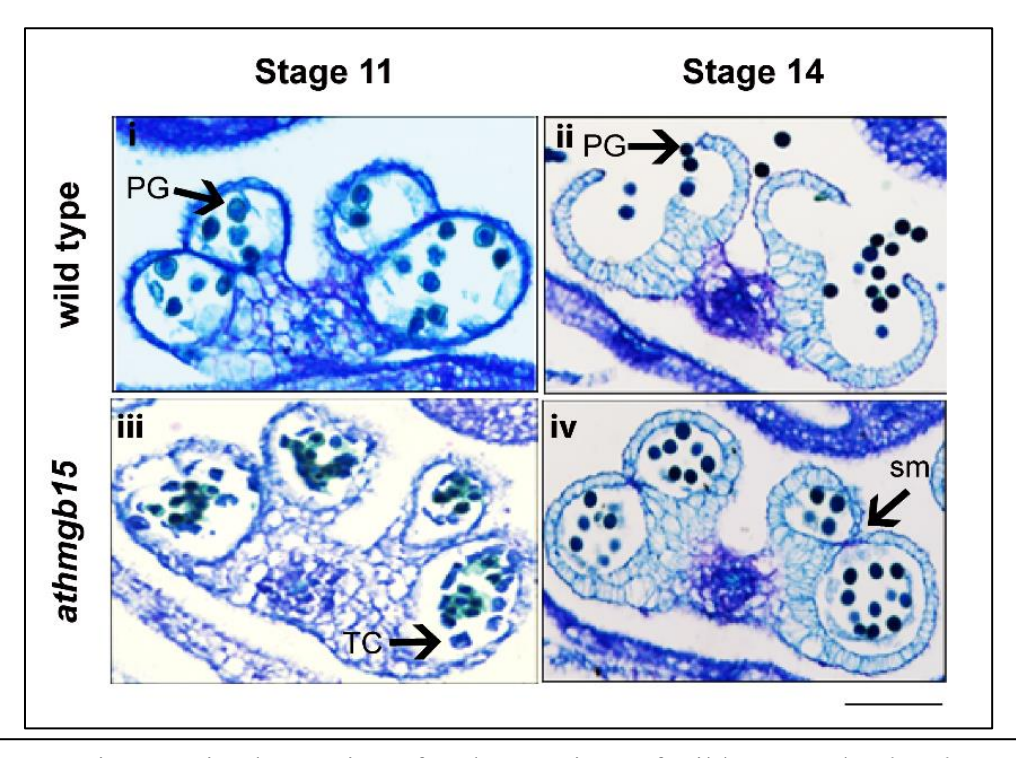


Fig 1.13: Microscopic observation of anther sections of wild type and *athmgb15 Arabidopsis* anthers during development monitored using light microscopy. Transverse sections of WT and *athmgb15* buds were stained with 1% toluidine blue and observed under white light. (i & ii) represents the stages of wild type anther development; (iii & iv) represents the stages of pollen development in *athmgb15* mutant. The scalebar represents 50μm

Comparative pollen viability

The presence of a regular pollen coat serves as a chemical and physical interface between the pollen grain and its environment. It determines the viability of the pollen grains by serving as a critical barrier for protection against UV (ultraviolet) radiation, enabling insect-mediated pollination, and promoting pollen hydration at the stigma. It is the amphipathic deposition from the tapetum on pollen grains during its maturation facilitates the rehydration of pollen grain for pollen tube germination and subsequent transfer of the non-motile male gametes to the ovule (Wei and Ma, 2023).

Since our mutant demonstrated a defective pollen wall biosynthesis pathway and pollen wall morphology from the start, it was important for us to determine the implications of these abnormalities on its pollen viability. We therefore differentially stained the viable (live) and non-viable pollen grains using FDA and PI respectively (Fig 1.14 A). As FDA is permeable to the cell membrane and can stain live cells, PI is impermeable and can stain DNA only when the cell integrity is compromised (Chang et al., 2014). Upon counting the red and green pollen grains in wild type and *athmgb15* separately, we could report a higher percentage of non-viable pollens (55%, $p \le 0.005$) in *athmgb15* plants compared to wild-type (30%, $p \le 0.05$ in mutant plants (Fig 1.14 B).

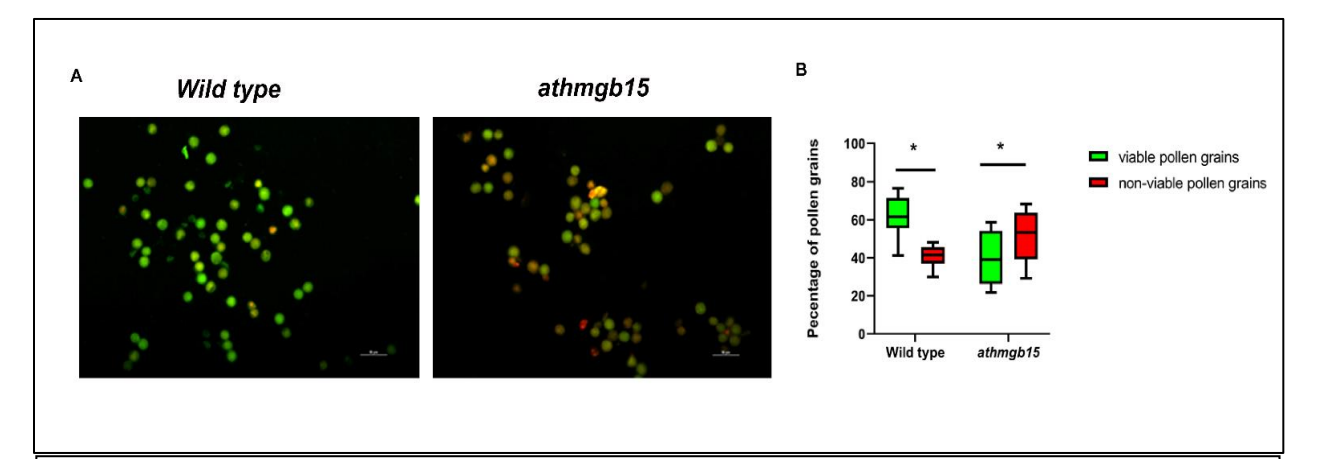


Fig. 1.13: (A) Microscope image of FDA-PI-stained pollen grains of *athmgb15-4* and wildtype. Scale bar represents 50 μ m.

(B) Box plot representation of pollen viability between wildtype and *athmgb15*. Whiskers represent mean \pm SD (n=12). The significance was analysed by paired two-tailed Student's ttest. Asterisks represent significant differences as indicated, * p-value <0.05. The centre line of the box denotes the median. Box limits denote the upper quartile (Q1) and the lower quartile (Q3). The whiskers extend to the maximum and minimum data values.

Interaction of AtHMGB15 with the MYB24-MYB21 complex to regulate phenylpropanoid synthesis for pollen coat patterning.

Since the tapetal cells serves as the centre for the biosynthesis of sporopollenin that forms the key constituent of the pollen wall material (Echlin, 1971; Wang et al., 2018). The lowered wax content was an indication to analyse the expression and regulation of the phenylpropanoid pathway components (Jing-Shi Xue 7, 2020; Xiong et al., 2016). According to previous studies, the production of sporopollenin in the tapetal cells is directly influenced by changing the flux of the phenylpropanoid pathway that is tightly regulated by a MYB triad namely MYB21-MYB24-MYB99 (Battat et al., 2019). The transcriptome analysis of *athmgb15* flowers corresponding to stage 13 of anther development revealed the down-regulation of the key transcription factors of *MYB21*, and *MYB24*. The expression of CCR1 (At1G15950), a gene of the phenylpropanoid pathway was significantly upregulated by 1.4 log 2-fold in *athmgb15* mutant. Although the expression of CYP73A5 or C4H (At2G30490) is not significantly differentially regulated. The gene regulatory network analysis of AtHMGB15 and the components of the phenylpropanoid pathway using STRING database search clearly indicated the presence of network (Fig 1.15). The search suggested that AtHMGB15 interacts with the transcription factor MYC2 via MED25 to regulate MYB21 and MYB24.

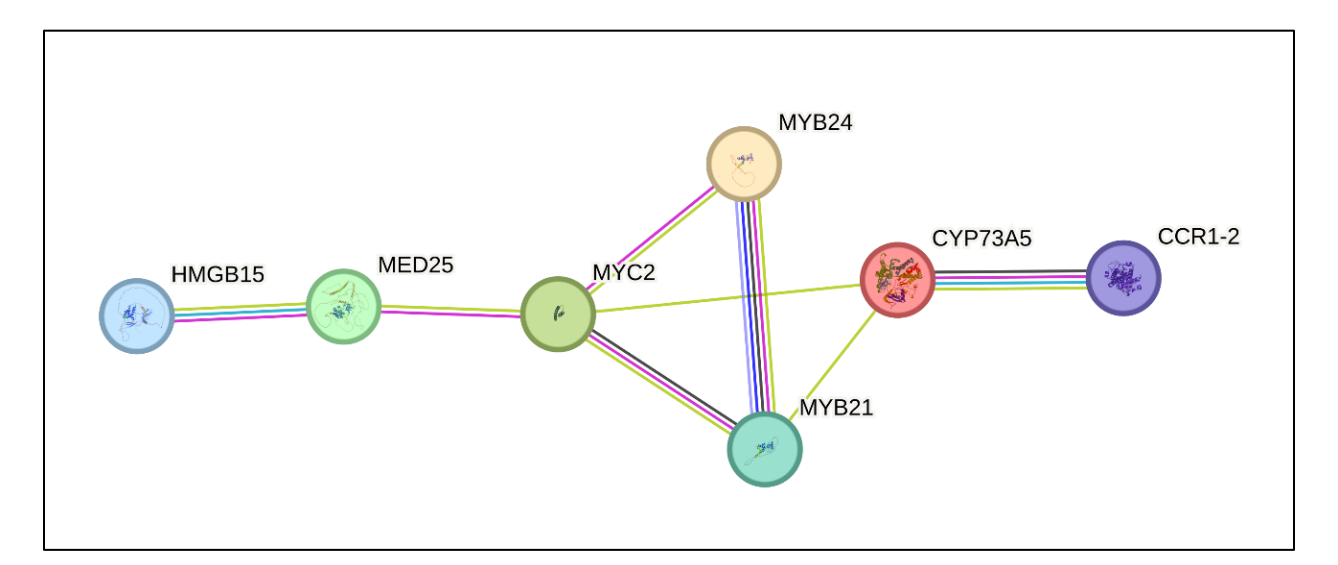


Fig 1.15: Existing network of proteins from STRING database

To investigate the regulatory role of AtHMGB15 as a transcription activator in the expression of these genes, an *in-silico* analysis of promoter/upstream region of *MYB21*, and *MYB24* was performed using Plant Pan v3.0 software (**Fig 1.16**). Results obtained from the database indicated the AtHMGB15 binding site A(A/C)--ATA---(A/T)(A/T) in the promoter region of *MYB24*, and *MYB21* (Mallik et al., 2020). Previous ChIP-on-chip data also supported the presence of AtHMGB15 binding site at the *MYB24* locus, further suggesting its role in regulating the transcription of these genes (Mallik et al., 2020).

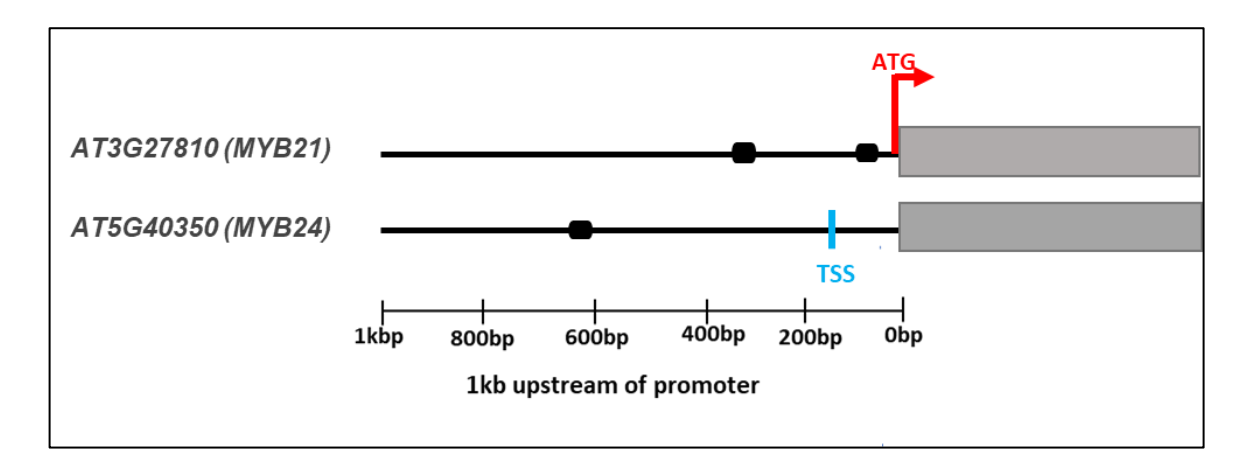


Fig 1.16: Gene-wise occupancy of ATHMGB15 protein.

Predicted ARID4 binding sites in the MYB24 and MYB21 genes within 1kb upstream regions from ATG. The blue line denotes the transcription start site and the red bent arrow indicates the translation start site of the genes. The black boxes represent the ATHMGB15 binding motif A(A/C)--ATA---(A/T)(A/T).

The occupancy of AtHMGB15 at the promoter/upstream region of *MYB24* and *MYB21* encouraged us to investigate to perform a promoter assay. We therefore, investigated the promoter activity of *MYB21* and *MYB24* in the presence of AtHMGB15. For this, a promoter assay was performed using ~2Kb promoter/upstream region of *MYB24* and *MYB21* previously cloned in a promoterless vector pKGWFS7 to generate pMYB24::24 and pMYB21::GUS individual reporter constructs. The constructs were infiltrated into tobacco plants to examine the promoter activity (pMYB24 and pMYB21) by measuring GUS activity in the absence and presence of AtHMGB15. Results from **Fig 1.17**, indicates that GUS activity of MYB24 and MYB21 promoters significantly increased in presence of AtHMGB15 protein. The GUS activity was represented as nanomoles of 4-MU

produced per mg of protein and the total data was obtained from 20 sets of biological repeats (n=15). Statistical significance in GUS activity after 48 hours incubation was tested using. Standard deviation was calculated and represented as error bars using GraphPad Prism.

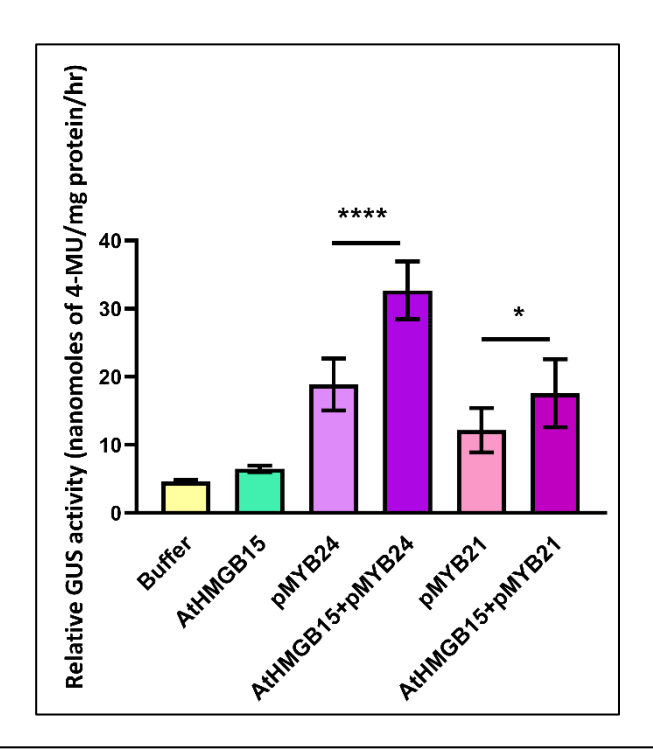


Fig 1.17: Leaves of 6 week old Tobacco plants (*Nicotiana tabacum*) were co-infiltrated with *A. tumefaciens* containing AtHMGB15 effector with proMYB24::pKGWFS7 or proMYB21::pKGWFS7. Quantification of GUS activity was measured 48hrs of infiltration. Values were normalized against fluorescence from only infiltration buffer. The relative GUS activity is expressed as nanomoles of 4 -MU per mg of total protein with standard error of mean bars (n=15). Statistical analysis was done using two-way analysis of variance (ANOVA) with p-value < 0.05 (*, *** represents p-value < 0.05 and *** p-value < 0.005, respectively).

Defective stamen morphology in athmgb15

A vital phenotype regulated by the MYB TFs, MYB21 and MYB24 is elongation of stamen during flower development (Wang et al., 2023). Since, AtHMGB15 regulates the expression of *MYB21* and *MYB24* we investigated the stamen morphology of *athmgb15* and compared it to wildtype *Arabidopsis* flower.

Our observation suggests that around 30% of *athmgb15-4* flowers have shorter stamen filaments compared to wild-type (Fig 1.18). This may be one of the reasons for poor fertilization and low

seed yield in *athmgb15* mutants. Collectively, these findings suggest that AtHMGB15 regulates the transcription of R2R3-MYB transcription factors during flower development, thereby regulating the elongation of stamens.

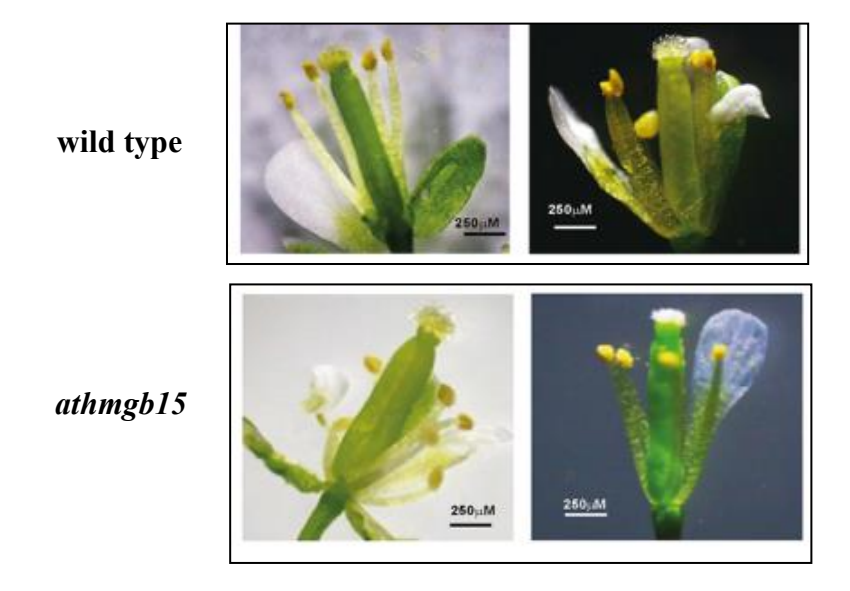
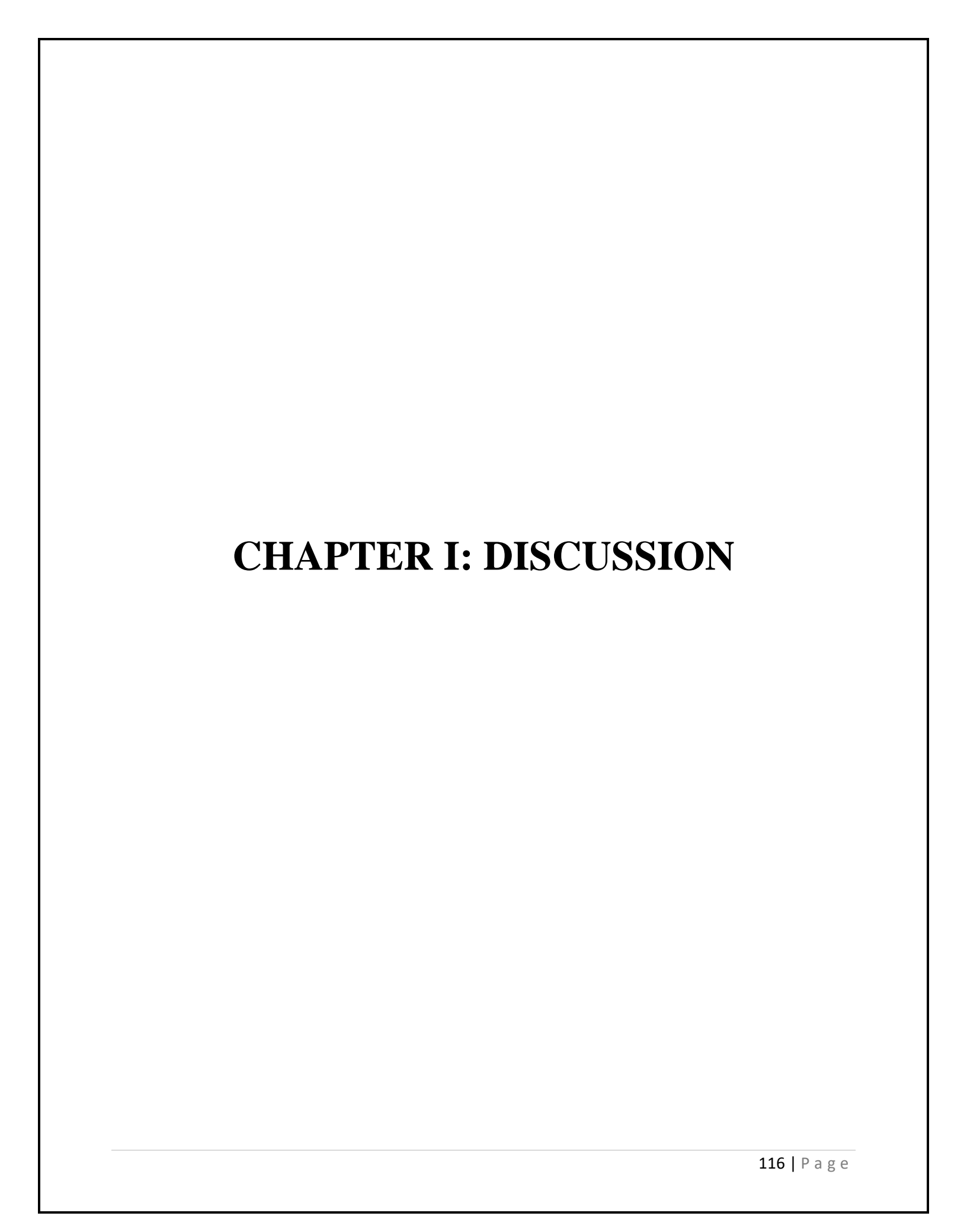


Fig. 1.18: Stamen morphology of wild type and athmgb15 flowers



The role of tapetum in pollen viability remains limited owing to the unavailability of data on tapetum specifically. Studies from the two transcriptomes provides the preliminary cues to test and validate tapetum development and function during pollen grain development in *athmgb15* and wild type. Analysis of the expression profiles of the individual transcriptomes reveal a number of genes that are differentially regulated during the two stages. Although the stages represented here correspond to a tapetum free stage (flower transcriptome) and a tapetum active stage (bud transcriptome). The expression of genes extant in other floral tissue have not been overlooked. However, the focus of the study remains on the expression of genes specifically attributed to tapetal cells that have been identified from previous literature survey.

AtHMGB15 mutation disrupts the spatiotemporal expression of PCD genes during pollen grain development

The analysis of the genes responsible for the timely occurrence of programmed cell death of tapetal cells was undertaken in both stage 13 and stage 8-11 transcriptome. The study revealed that the expression of PCD executers like CEP1, RNS3, BFN1 and MC9 were upregulated in stage 13 transcriptome while the expression of these genes was downregulated in the stage 8-11 transcriptome. However, the expression of the anti-apoptotic plant homolog AtB11 and its family protein is downregulated in the stage 13 transcriptome and upregulated several folds in stage 8-11 transcriptome. This phenomenon was indicative of the fact that AtHMGB15 interacted with the PCD regulator AtB11 to regulate the expression of PCD executers. The hypothesis was conclusively proved from the chromatin immunoprecipitation assay results which showed a 2-fold enrichment in the AtB11 gene compared to the negative control (At1G01310). The occupancy of AtHMGB15 in CEP1, MC9 and RNS3 promoter region also indicates a regulatory role of AtHMGB15 in the execution of tapetal degradation. Previous studies have demonstrated that mutants expressing AtB11 under a tapetum specific promoter did not undergo tapetal PCD and subsequent abortion of the pollen grains (Ishikawa et al., 2011; Watanabe and Lam, 2006).

One of the well-established cues for PCD is a surge in ROS levels (Pacini, 2016; Zhang et al., 2023). During differentiation induced programmed cell death (PCD), ROS production occurs when the turnover of cell contents is required (Zhang et al., 2023). As observed in case of tapetal PCD where the cell content of tapetal cells is utilized by the developing meiocytes (Yu and Zhang, 2019; Zhang et al., 2023). However, in case of xylem formation also a case of differentiation induced

programmed cell death, there is no requirement of ROS generation as the cell material here needs to be cleared out to form hollow channels for water conduction (Bollhöner et al., 2012; Cheng et al., 2019). The significant difference in total ROS content of athmgb15 buds and flowers compared to wild type is a crucial indication for a defective PCD signaling. The spatiotemporal regulation and occurrence of tapetal PCD is extremely crucial for the stage specific development of the microspores. Any defect as in delay or precociousness results in pollen abortion. Tapetal PCD initiates at stage 10 of pollen development and is complete by stage 11 (Jiang et al., 2021; Varnier et al., 2005). The progression of PCD observed in athmgb15 anthers clearly depicts its continuation into stage 12 of anther development thus, inferring that it is prolonged in the mutant compared to wild type. The execution of PCD is controlled by several proteases and nucleases that have been recently identified. Studies have shown that cysteine proteases CEP1 is a key executor of tapetal PCD that participate directly in tetrad cell wall hydrolysis in *Arabidopsis* (Zhang et al., 2014). cep1 mutants have aborted PCD leading to the formation of pollens with abnormal exine. The defective pollens have a low fertility rate (Zhang et al., 2014). Interestingly, the q-RTPCR data also confirmed the downregulation of the PCD executor genes like CEP1, RNS3, BFN1 and αVPE in stages 8-11 of anther development for athmgb15.

AtHMGB15 regulates the expression of actin binding proteins and pollen viability

The results from *athmgb15* and wild type bud (stages 8-11 of pollen grain development) transcriptome study displayed a significant number of genes from the actin filament binding cluster to be differentially regulated and enriched in the GO analysis. Although no investigations have been reported on the role of actin during the development of tapetum or pollen grain formation. Our approach to study actin dynamics in tapetum involved observing the change in vacuole size, as the stages of pollen grain development advanced. FM4-64FX staining studies demonstrated smaller vacuoles in the *athmgb15* tapetal cells prior to tetrad separation compared to wild type. The presence of enlarged vacuoles in the wild type tapetal cells before the tetrad separation indicate the characteristic conditions for viable pollen formation (Wu and Yang, 2005). As the tetrads progresses towards separation the secretory activity of the tapetum surges and it is preceded by enlargement of vacuoles in the tapetal cells (Koyano et al., 2014; Wan et al., 2010).

Proteomic analysis has established that the vacuoles in the tapetal cells function as storehouse of cell wall degrading enzymes like β -1,3-glucanases, polygalacturonases, and endocellulases that

actively participate in the degradation of the callose wall keeping the tetrads (Wan et al., 2010). The drastic reduction in the volume of the vacuoles during the tetrad separation stage indicate that the enzymes are releases from the tapetal vacuoles into the anther locule (Koyano et al., 2014; Wan et al., 2010; Wu and Yang, 2005). In the case of *athmgb15* mutant, we have observed delayed enlargement of vacuoles of the tapetal layer. In wildtype anther, the tapetal layers have enlarged vacuoles at stage 7 and by stage 12, the tapetal layer is completely degraded and PCD has extended to outer layers of anther lobes. Since vacuole enlargement is followed by the rupture of the tonoplast to release the enzymes, a pre requisite for the tapetal degradation to proceed (Teper-Bamnolker et al., 2021; Yamada et al., 2020), our observation suggested that degradation of the tapetum is compromised in the AtHMGB15 loss of function mutant.

During tapetal PCD vacuole plays another important role as it acts as a storehouse for the vacuolar processing enzymes (VPE) (Teper-Bamnolker et al., 2021; Yamada et al., 2020). VPE are endopeptidase that stays in inactive proprotein precursors and undergoes self-catalysis to attain a mature form under acidic condition (Cheng et al., 2020; Cheng et al., 2019). Previous studies have shown that β -VPE is involved in tapetal degradation (Cheng et al., 2020). Pro- β VPE transformed to mature form during the early stage of vacuole acidification and mature β VPE was released into cytoplasm during late stage 8, post vacuole rupture (Cheng et al., 2020). Mature β VPE participate in the activation of cysteine proteases like CEP1, RD19A and RD19C (Cheng et al., 2020). Deletion of β VPE function causes abnormal pollen development and failure of tapetal degeneration due to loss of active cysteine proteases (Cheng et al., 2020). Thus, vacuole acidification and rupture are prerequisites for the release of mature VPE for the activation of cysteine protease for tapetal degradation (Cheng et al., 2020; Cheng et al., 2019).

Dehiscence of the anther is observed during stage 14 of pollen development in wildtype (Goldberg et al., 1993; Sanders et al., 1999). This is associated with the disintegration of the septum, breakage along the stomium and release of pollen (Sanders et al., 1999). However, in *athmgb15* mutants, no signs of anther dehiscence are detected at stage 14. There may be multiple reasons for the delayed dehiscence of *athmgb15* anther. First, the pollen development process of *athmgb15* is not completed due to delayed tapetal PCD in these mutants. Second, we may speculate that the same PCD components that are responsible for tapetal degradation may be involved in the PCD of

septum and stomium. It has been shown in *Lilium* that PCD of tapetal tissue after completion extend to outer anther tissue and stomium region (Wilson et al., 2011).

A direct consequence of prolonged tapetal PCD and delayed dehiscence was observed in the viability of the pollen grains of *athmgb15*. The differential staining of viable and non-viable pollen grains using FDA and PI stain, respectively, demonstrated a significantly lower number of viable pollen grains in *athmgb15* compared to wild type.

AtHMGB15 interacts with MYB transcription factors MYB21 and MYB24 to regulate the biosynthetic activity of the tapetal cells

Several genes have been predicted to encode enzymes involved in lipid synthesis necessary for anther cuticle and/or pollen exine in *Arabidopsis*. The CYP704B2 belongs to the evolutionarily conserved P450 subfamily protein that is preferentially expressed in tapetal cells (Yi et al., 2010). The protein catalyzes the hydroxylation of palmitic acid and unsaturated C18 fatty acid (Yi et al., 2010). The *cyp704B2* mutants display under developed anther epidermal cuticle and aborted pollen grains with defective exine (Yi et al., 2010). The precursors of exine or pollen wall is mainly composed of sporopollenin that is synthesized through the phenylpropanoid pathway functioning in the tapetum (Jing-Shi Xue 7, 2020). Perturbation in this pathway leads to defective pollen wall formation and even atypical anther dehiscence (Battat et al., 2019; Jing-Shi Xue 7, 2020). The deposition and ornamentation of the exine on pollen grains is subjected to the availability of sporopollenin production via the phenylpropanoid pathway (Battat et al., 2019; Jing-Shi Xue 7, 2020). Several intermediates produced from this pathway, serve as substrate for lignin and flavonoid biosynthesis (Jing-Shi Xue 7, 2020).

Transcription factors like MYBs control a large number of genes in stamen development (Higginson et al., 2003; Huang et al., 2017; Wang et al., 2023; Yang et al., 2007; Zhang et al., 2021). Recently, a MYB triad comprising of MYB21-MYB24-MY99 was identified to control the phenylpropanoid pathway in *Arabidopsis* (Battat et al., 2019). MYB21 negatively regulates the expression of *MYB99* which in turn activates the promoter of *MYB24*(Battat et al., 2019). MYB21 and MYB24 co-activate the promoters of one another (Battat et al., 2019; Cheng et al., 2009; Huang et al., 2017; Wang et al., 2023). A notable decrease in the transcript level of the phenylpropanoid metabolic gene *PHENYLAMINE AMMONIALYASE4* (*PAL4*) was observed in all the mutant genotypes (*myb21*, *myb24* and *myb99*) (Battat et al., 2019). According to our flower

transcriptome the expression of MYB21 and MYB24 were significantly downregulated in athmgb15 and KEGG pathway analysis showed an enrichment of genes in the phenylpropanoid pathway. Since our mutant exhibited loss of normal exine structure and ornamentation we first investigated the interaction of AtHMGB15 with MYB21 and MYB24 using in silico approach. The results indicated an indirect interaction between AtHMGB15 and the MYB TFs mediated through a master regulator MYC2. Our subsequent study from promoter analysis using PlantPAN3.0 we inferred the occupancy of AtHMGB15 in the promoter region of MYB21 and MYB24. These finding were validated using the GUS reporter assay and the graphical representation of the experimental results clearly showed a significant increase in GUS activity under MYB21 and MYB24 promoters in presence of AtHMGB15.

The biosynthesis of specialized metabolites in plants relies on an uninterrupted supply of the precursor molecule that can meet the production demands (Echlin, 1971; Jing-Shi Xue 7, 2020; Lallemand et al., 2013; Wang et al., 2018; Zhu, 2021). Therefore, transcriptional regulation of specialized metabolites is likely to be associated with the activation of primary, precursor pathways (Echlin, 1971; Xiong et al., 2016). Since all phenylpropanoids are ultimately derived from Phenylamine, it is crucial to maintain the metabolic flux in order to secure precursor supply and availability of this amino acid (Jing-Shi Xue 7, 2020). The key enzymes that catalyse phenylamine to hydroxy cinniamyl alcohol (lignin) during stages 7-11 of pollen development are in the following order PHENYLALANINE AMMONIA LYASE (PAL) (Huang et al., 2010), CINNAMATE-4-HYDROXYLASE (C4H) (Schilmiller et al., 2009), 4COUMARATE: COALIGASE (4CL) (Li et al., 2015), CINNAMOYL COA REDUCTASE (CCR) (Mir Derikvand et al., 2008) and CINNAMYL ALCOHOL DEHYDROGENASE (CAD) (Sibout et al., 2005). The up regulation of 4CL8 (At5G38120) and CCR1 (At1G15950) in stage 13 of athmgb15 indicates a delay in tapetum biosynthetic activity. The gas chromatography report indicates a significant shortage in the abundance of the all-major wax components like alkane, sterols and free fatty acid in the athmgb15 anthers than wild type. We also observed impairment in filament length in athmgb15 mutants compared to the filament length observed in wild type from our filament length study.

Thus, the chapter conclusively shows the importance of AtHMGB15 in the temporal regulation of genes responsible for tapetal function and its programmed cell death which is a vital step in the

formation of viable pollen grains. Although, it is not known that actin dynamics plays an important role in vacuole organization this can be another avenue to understand PCD process during differentiation of microspore mother cells into matured pollen grains.

REFERENCES:

- 1. Battat, M., Eitan, A., Rogachev, I., Hanhineva, K., Fernie, A., Tohge, T., Beekwilder, J., and Aharoni, A. (2019). A MYB triad controls primary and phenylpropanoid metabolites for pollen coat patterning. *Plant Physiology* **180**, 87-108.
- 2. Bollhöner, B., Prestele, J., and Tuominen, H. (2012). Xylem cell death: emerging understanding of regulation and function. *Journal of experimental botany* **63**, 1081-1094.
- 3. Buono, R. A., Hudecek, R., and Nowack, M. K. (2019). Plant proteases during developmental programmed cell death. *Journal of Experimental Botany* **70**, 2097-2112.
- 4. Chang, F., Zhang, Z., Jin, Y., and Ma, H. (2014). Cell biological analyses of anther morphogenesis and pollen viability in Arabidopsis and rice. *Flower development: Methods and protocols*, 203-216.
- 5. Cheng, H., Song, S., Xiao, L., Soo, H. M., Cheng, Z., Xie, D., and Peng, J. (2009). Gibberellin acts through jasmonate to control the expression of MYB21, MYB24, and MYB57 to promote stamen filament growth in Arabidopsis. *PLoS genetics* 5, e1000440.
- 6. Cheng, Z., Guo, X., Zhang, J., Liu, Y., Wang, B., Li, H., and Lu, H. (2020). βVPE is involved in tapetal degradation and pollen development by activating proprotease maturation in Arabidopsis thaliana. *Journal of experimental botany* **71**, 1943-1955.
- 7. Cheng, Z., Zhang, J., Yin, B., Liu, Y., Wang, B., Li, H., and Lu, H. (2019). γVPE plays an important role in programmed cell death for xylem fiber cells by activating protease CEP1 maturation in Arabidopsis thaliana. *International journal of biological macromolecules* 137, 703-711.
- 8. Dennis, G., Sherman, B. T., Hosack, D. A., Yang, J., Gao, W., Lane, H. C., and Lempicki, R. A. (2003). DAVID: database for annotation, visualization, and integrated discovery. *Genome biology* **4**, 1-11.
- 9. Echlin, P. (1971). Production of sporopollenin by the tapetum. *In* "Sporopollenin", pp. 220-247. Elsevier.
- 10. Goldberg, R. B., Beals, T. P., and Sanders, P. M. (1993). Anther development: basic principles and practical applications. *The Plant Cell* **5**, 1217.
- 11. Gómez, J. F., Talle, B., and Wilson, Z. A. (2015). Anther and pollen development: a conserved developmental pathway. *Journal of integrative plant biology* **57**, 876-891.

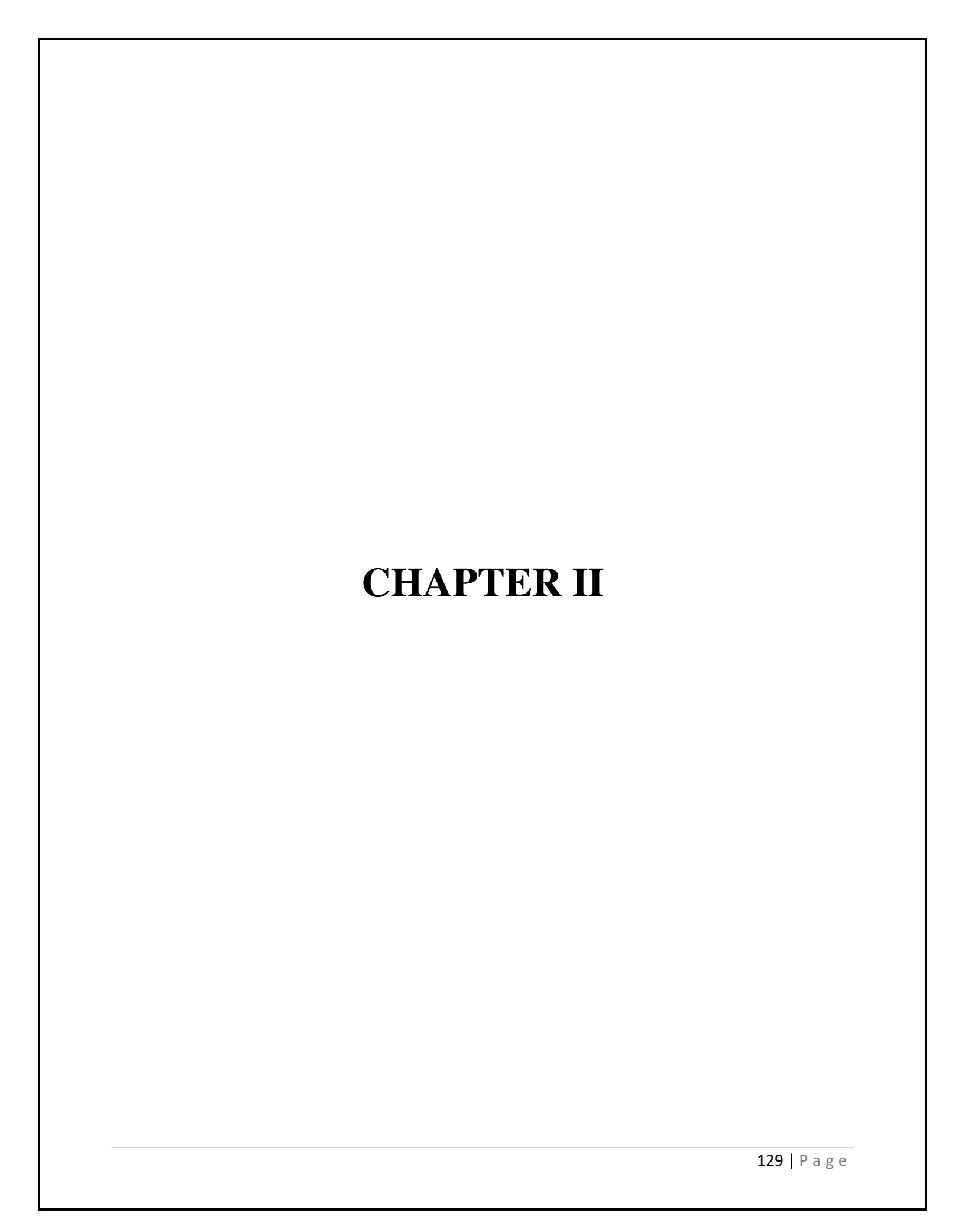
- 12. Goodman, K., Paez-Valencia, J., Pennington, J., Sonntag, A., Ding, X., Lee, H. N., Ahlquist, P. G., Molina, I., and Otegui, M. S. (2021). ESCRT components ISTL1 and LIP5 are required for tapetal function and pollen viability. *The Plant Cell* 33, 2850-2868.
- 13. Higginson, T., Li, S. F., and Parish, R. W. (2003). AtMYB103 regulates tapetum and trichome development in Arabidopsis thaliana. *The Plant Journal* **35**, 177-192.
- 14. Huang, H., Gao, H., Liu, B., Qi, T., Tong, J., Xiao, L., Xie, D., and Song, S. (2017). Arabidopsis MYB24 regulates jasmonate-mediated stamen development. *Frontiers in Plant Science* **8**, 1525.
- 15. Huang, J., Gu, M., Lai, Z., Fan, B., Shi, K., Zhou, Y.-H., Yu, J.-Q., and Chen, Z. (2010). Functional Analysis of the Arabidopsis PAL Gene Family in Plant Growth, Development, and Response to Environmental Stress *Plant Physiology* **153**, 1526-1538.
- 16. Ishikawa, T., Watanabe, N., Nagano, M., Kawai-Yamada, M., and Lam, E. (2011). Bax inhibitor-1: a highly conserved endoplasmic reticulum-resident cell death suppressor. *Cell Death & Differentiation* **18**, 1271-1278.
- 17. Jiang, C., Wang, J., Leng, H.-N., Wang, X., Liu, Y., Lu, H., Lu, M.-Z., and Zhang, J. (2021). Transcriptional regulation and signaling of developmental programmed cell death in plants. *Frontiers in Plant Science* **12**, 702928.
- 18. Jing-Shi Xue 7, B. Z., HuaDong Zhan 7, Yong-Lin Lv, Xin-Lei Jia, TianHua Wang, Nai-Ying Yang, Yu-Xia Lou, Zai-Bao Zhang, Wen-Jing Hu, Jinshan Gui, Jianguo Cao, Ping Xu, Yihua Zhou, Jin-Feng Hu, Laigeng Li, Zhong-Nan Yang (2020). Phenylpropanoid Derivatives Are Essential Components of Sporopollenin in Vascular Plants.
- 19. Kawanabe, T., Ariizumi, T., Kawai-Yamada, M., Uchimiya, H., and Toriyama, K. (2006). Abolition of the tapetum suicide program ruins microsporogenesis. *Plant and Cell Physiology* **47**, 784-787.
- 20. Koyano, T., Kurusu, T., Hanamata, S., and Kuchitsu, K. (2014). Regulation of vacuole-mediated programmed cell death during innate immunity and reproductive development in plants. *In* "Sexual reproduction in animals and plants", pp. 431-440. Springer Japan.
- 21. Lallemand, B., Erhardt, M., Heitz, T., and Legrand, M. (2013). Sporopollenin biosynthetic enzymes interact and constitute a metabolon localized to the endoplasmic reticulum of tapetum cells. *Plant physiology* **162**, 616-625.

- 22. Li, Y., Kim, J. I., Pysh, L., and Chapple, C. (2015). Four isoforms of Arabidopsis 4-coumarate: CoA ligase have overlapping yet distinct roles in phenylpropanoid metabolism. *Plant physiology* **169**, 2409-2421.
- 23. Mallik, R., Prasad, P., Kundu, A., Sachdev, S., Biswas, R., Dutta, A., Roy, A., Mukhopadhyay, J., Bag, S. K., and Chaudhuri, S. (2020). Identification of genome-wide targets and DNA recognition sequence of the Arabidopsis HMG-box protein AtHMGB15 during cold stress response. *Biochimica et Biophysica Acta (BBA)-Gene Regulatory Mechanisms* **1863**, 194644.
- 24. Marchant, D. B., and Walbot, V. (2022). Anther development—The long road to making pollen. *The Plant Cell* **34**, 4677-4695.
- 25. Mir Derikvand, M., Sierra, J. B., Ruel, K., Pollet, B., Do, C.-T., Thévenin, J., Buffard, D., Jouanin, L., and Lapierre, C. (2008). Redirection of the phenylpropanoid pathway to feruloyl malate in Arabidopsis mutants deficient for cinnamoyl-CoA reductase 1. *Planta* 227, 943-956.
- 26. Pacini, E. (2016). 11 Tapetum and microspore function. *Microspores Evolution and Ontogeny: Evolution and Ontogeny*, 213.
- 27. Parish, R. W., and Li, S. F. (2010). Death of a tapetum: a programme of developmental altruism. *Plant Science* **178**, 73-89.
- 28. Quilichini, T. D., Douglas, C. J., and Samuels, A. L. (2014). New views of tapetum ultrastructure and pollen exine development in Arabidopsis thaliana. *Annals of botany* **114**, 1189-1201.
- 29. Quilichini, T. D., Grienenberger, E., and Douglas, C. J. (2015). The biosynthesis, composition and assembly of the outer pollen wall: A tough case to crack. *Phytochemistry* **113**, 170-182.
- 30. Sanders, P. M., Bui, A. Q., Weterings, K., McIntire, K., Hsu, Y.-C., Lee, P. Y., Truong, M. T., Beals, T., and Goldberg, R. (1999). Anther developmental defects in Arabidopsis thaliana male-sterile mutants. *Sexual plant reproduction* **11**, 297-322.
- 31. Schilmiller, A. L., Stout, J., Weng, J. K., Humphreys, J., Ruegger, M. O., and Chapple, C. (2009). Mutations in the cinnamate 4-hydroxylase gene impact metabolism, growth and development in Arabidopsis. *The Plant Journal* **60**, 771-782.

- 32. Sibout, R., Eudes, A., Mouille, G., Pollet, B., Lapierre, C., Jouanin, L., and Séguin, A. (2005). CINNAMYL ALCOHOL DEHYDROGENASE-C and-D are the primary genes involved in lignin biosynthesis in the floral stem of Arabidopsis. *The Plant Cell* 17, 2059-2076.
- 33. Teper-Bamnolker, P., Danieli, R., Peled-Zehavi, H., Belausov, E., Abu-Abied, M., Avin-Wittenberg, T., Sadot, E., and Eshel, D. (2021). Vacuolar processing enzyme translocates to the vacuole through the autophagy pathway to induce programmed cell death. *Autophagy* 17, 3109-3123.
- 34. Varnier, A.-L., Mazeyrat-Gourbeyre, F., Sangwan, R. S., and Clément, C. (2005). Programmed cell death progressively models the development of anther sporophytic tissues from the tapetum and is triggered in pollen grains during maturation. *Journal of Structural Biology* **152**, 118-128.
- 35. Verma, N. (2019). Transcriptional regulation of anther development in Arabidopsis. *Gene* **689**, 202-209.
- 36. Wan, L., Xia, X., Hong, D., Li, J., and Yang, G. (2010). Abnormal vacuolization of the tapetum during the tetrad stage is associated with male sterility in the recessive genic male sterile Brassica napus L. Line 9012A. *Journal of Plant Biology* **53**, 121-133.
- 37. Wang, K., Guo, Z.-L., Zhou, W.-T., Zhang, C., Zhang, Z.-Y., Lou, Y., Xiong, S.-X., Yao, X.-z., Fan, J.-J., and Zhu, J. (2018). The regulation of sporopollenin biosynthesis genes for rapid pollen wall formation. *Plant physiology* **178**, 283-294.
- 38. Wang, Y., Zhou, H., He, Y., Shen, X., Lin, S., and Huang, L. (2023). MYB transcription factors and their roles in the male reproductive development of flowering plants. *Plant Science* **335**, 111811.
- 39. Watanabe, N., and Lam, E. (2006). Arabidopsis Bax inhibitor-1 functions as an attenuator of biotic and abiotic types of cell death. *The plant journal* **45**, 884-894.
- 40. Wei, S., and Ma, L. (2023). Comprehensive Insight into Tapetum-Mediated Pollen Development in Arabidopsis thaliana. *Cells* **12**, 247.
- 41. Wilson, Z. A., Song, J., Taylor, B., and Yang, C. (2011). The final split: the regulation of anther dehiscence. *Journal of experimental botany* **62**, 1633-1649.

- 42. Wu, H., and Yang, M. (2005). Reduction in vacuolar volume in the tapetal cells coincides with conclusion of the tetrad stage in Arabidopsis thaliana. *Sexual Plant Reproduction* **18**, 173-178.
- 43. Xia, C., Wang, Y. J., Liang, Y., Niu, Q. K., Tan, X. Y., Chu, L. C., Chen, L. Q., Zhang, X. Q., and Ye, D. (2014). The ARID-HMG DNA-binding protein A t HMGB 15 is required for pollen tube growth in Arabidopsis thaliana. *The Plant Journal* **79**, 741-756.
- 44. Xiong, S. X., Lu, J. Y., Lou, Y., Teng, X. D., Gu, J. N., Zhang, C., Shi, Q. S., Yang, Z. N., and Zhu, J. (2016). The transcription factors MS 188 and AMS form a complex to activate the expression of CYP 703A2 for sporopollenin biosynthesis in Arabidopsis thaliana. *The Plant Journal* 88, 936-946.
- 45. Yamada, K., Basak, A. K., Goto-Yamada, S., Tarnawska-Glatt, K., and Hara-Nishimura, I. (2020). Vacuolar processing enzymes in the plant life cycle. *New Phytologist* **226**, 21-31.
- 46. Yang, C., Xu, Z., Song, J., Conner, K., Vizcay Barrena, G., and Wilson, Z. A. (2007). Arabidopsis MYB26/MALE STERILE35 regulates secondary thickening in the endothecium and is essential for anther dehiscence. *The Plant Cell* **19**, 534-548.
- 47. Yang, Z., Liu, L., Sun, L., Yu, P., Zhang, P., Abbas, A., Xiang, X., Wu, W., Zhang, Y., and Cao, L. (2019). OsMS1 functions as a transcriptional activator to regulate programmed tapetum development and pollen exine formation in rice. *Plant molecular biology* **99**, 175-191.
- 48. Yao, X., Hu, W., and Yang, Z.-N. (2022). The contributions of sporophytic tapetum to pollen formation. *Seed Biology* **1**, 1-13.
- 49. Ye, C., Zheng, S., Jiang, D., Lu, J., Huang, Z., Liu, Z., Zhou, H., Zhuang, C., and Li, J. (2021). Initiation and execution of programmed cell death and regulation of reactive oxygen species in plants. *International Journal of Molecular Sciences* 22, 12942.
- 50. Yi, B., Zeng, F., Lei, S., Chen, Y., Yao, X., Zhu, Y., Wen, J., Shen, J., Ma, C., and Tu, J. (2010). Two duplicate CYP704B1-homologous genes BnMs1 and BnMs2 are required for pollen exine formation and tapetal development in Brassica napus. *The Plant Journal* **63**, 925-938.
- 51. Yu, J., and Zhang, D. (2019). Molecular control of redox homoeostasis in specifying the cell identity of tapetal and microsporocyte cells in rice. *Rice* **12**, 1-9.

- 52. Zhang, D., Liu, D., Lv, X., Wang, Y., Xun, Z., Liu, Z., Li, F., and Lu, H. (2014). The cysteine protease CEP1, a key executor involved in tapetal programmed cell death, regulates pollen development in Arabidopsis. *The Plant Cell* **26**, 2939-2961.
- 53. Zhang, J., Zhang, L., Liang, D., Yang, Y., Geng, B., Jing, P., Qu, Y., and Huang, J. (2023). ROS accumulation-induced tapetal PCD timing changes leads to microspore abortion in cotton CMS lines. *BMC Plant Biology* **23**, 1-13.
- 54. Zhang, X., He, Y., Li, L., Liu, H., and Hong, G. (2021). Involvement of the R2R3-MYB transcription factor MYB21 and its homologs in regulating flavonol accumulation in Arabidopsis stamen. *Journal of experimental botany* **72**, 4319-4332.
- 55. Zhu, L., Zhang, T. & Teeri, T.H. (2021). Tetraketide α-pyrone reductases in sporopollenin synthesis pathway in Gerbera hybrida: diversification of the minor function. *Horticulture Research*.



The implications of an abnormal pollen grain development can be observed during its pollen tube germination stage. After the pollen grain is released from the anther, its purpose is to transfer the two non-motile male gametes to the ovule and this is achieved through the pollen tube (Bedinger et al., 1994). The pollen tube germinates once the pollen grain has landed on the stigma. Pollen tube growth is a rapid process with a growth rate of 1 cm/h (Bedinger, 1992). This growth is achieved by the concerted efforts of the actin-myosin machinery that provide a constant supply of secretory vesicles to the tip of the tube (Duan and Tominaga, 2018). The arrangement of the actin filaments within the pollen tube provides a directionality to the cytoplasmic streaming in the growing pollen tube (Jiang et al., 2017). In this chapter we explore the post development abnormalities in *athmgb15* pollen grains and identify the underlying cause of it.

Retarded pollen tube germination in athmgb15 mutants

To investigate the implications of a defective developmental process in the *athmgb15* mutant we performed an *in vitro* pollen germination assay (refer to material methods for composition and protocol) with *athmgb15* and wild type pollen grains. We observed the germination status of the pollen grains after every 1 hour for both the wild type and the mutant.

After incubating the pollen grains in the pollen germination media (PGM) for 4 hours, we observed germination in 30-40% of the pollen grains in *athmgb15-4* compared to 80% germination observed in wild type pollen grains (**Fig 2.1**).

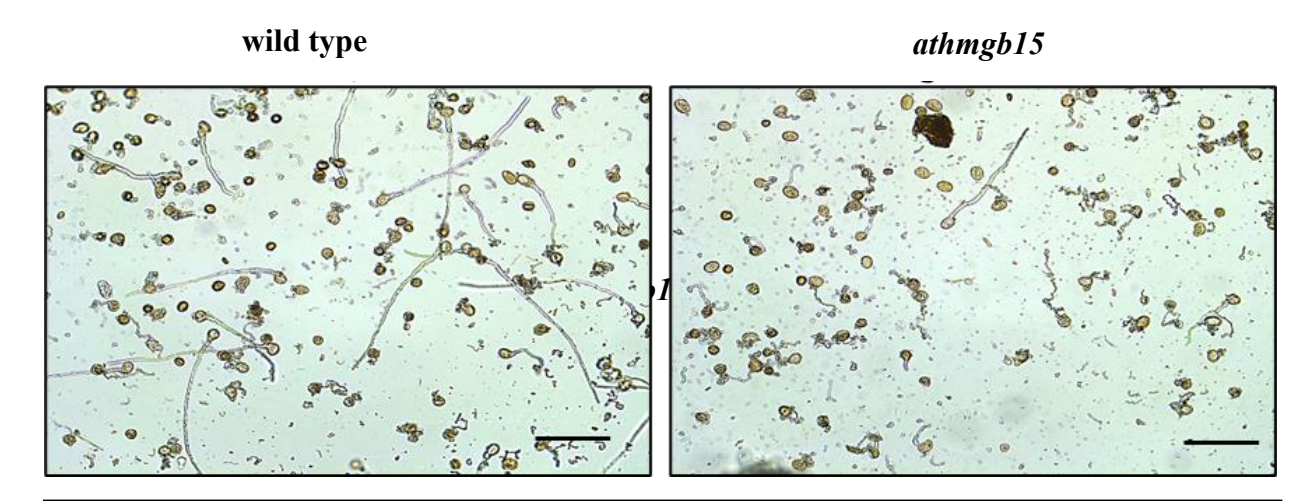


Fig 2.1: In vitro pollen tube germination assay of wild type and athmgb15 mutant after 4 h. The scalebar represents 100 μ m

Enrichment of actin binding gene cluster in *athmgb15* mutants during early and late stages of pollen development

A previous study on AtHMGB15 loss of function mutant had reported a list of differentially regulated genes in *athmgb15* pollen grain and was available in the NCBI database (Xia et al., 2014). We performed a comparative analysis of the microarray data from *athmgb15* pollen grains (stage 14) with our transcriptome from stages 8-11 of anther development to get an overview of the common genes differentially regulated during the two phases of pollen grain development (post meiotic phase and mature dehisced phase) (Marchant and Walbot, 2022). The Venn diagram represents the overlapping genes between the two transcriptomes (pollen and bud of *athmgb15*). A total of 76 genes were identified from the Venn diagram that was differentially regulated in both bud (stages 8-11) and pollen (stage 14) of *athmgb15* mutants (**Fig 2.2 A**) (**Annexure Table 6**). To gain further insights into the gene functions that were perturbed in both the phases of pollen grain development of *athmgb15*, we performed a functional annotation clustering of the overlapping genes using DAVID v 6.2 reported that the most enriched cluster was that of actin binding with an enrichment score of 3.03 (**Fig 2.2 B**).

The differential regulation of the actin binding genes enriched in *athmgb15* bud transcriptome were identified and represented in a heatmap (Fig 2.2C). The validation of the differentially expressed genes was done using q-RTPCR and the expression of *PRF4*, *VLN2* and *villin like 1* gene was downregulated while the expression of *ACTIN DEPOLYMERISING FACTOR 4 (ADF4)* was found to be upregulated (Fig 2.2D). The proteins of the above-mentioned genes are responsible for binding to the actin filament and change the polymerisation rate of the filament formation. A significant change in the expression of transcripts for these genes predicts defective actin filament organisation in the mutant.

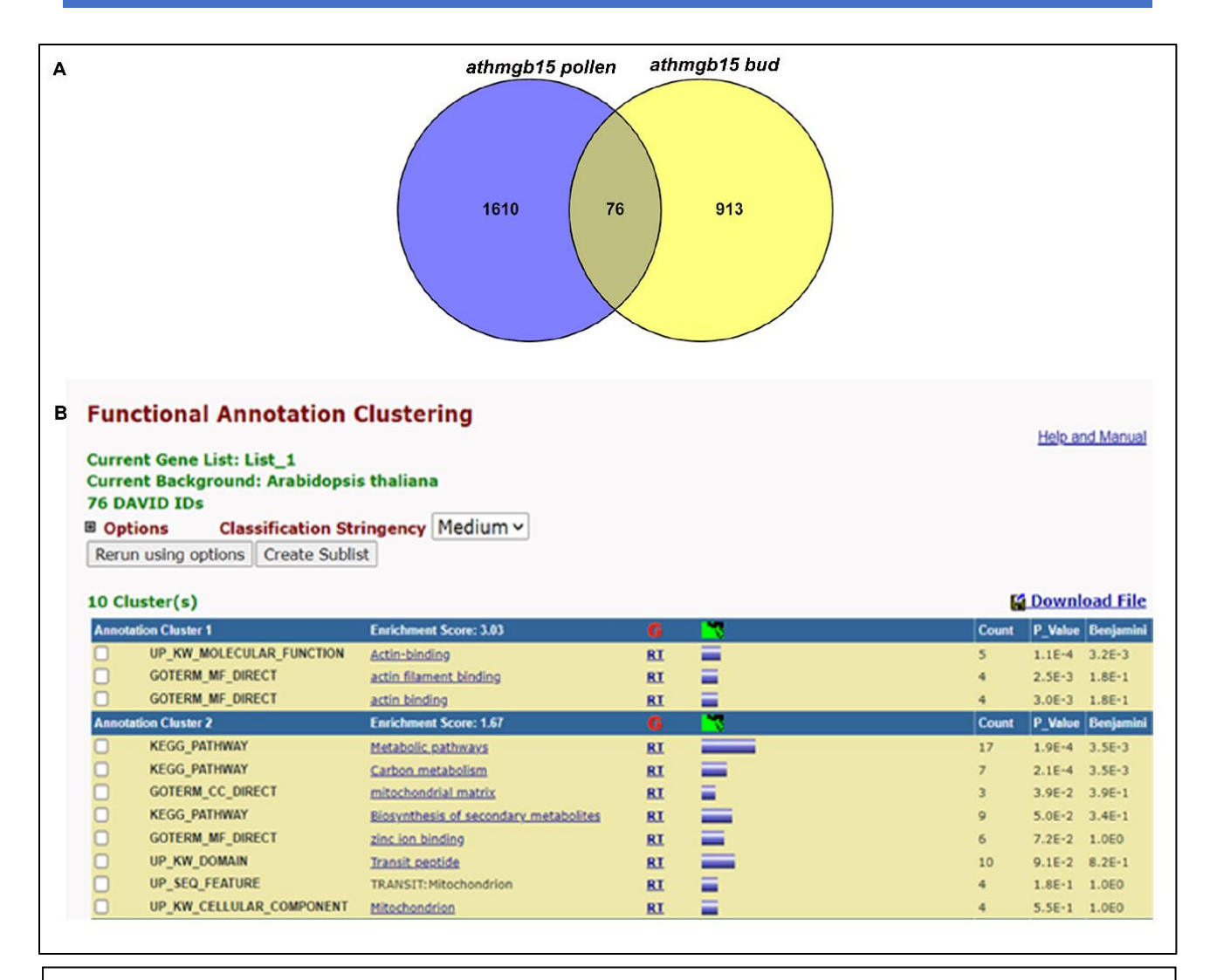


Fig 2.2: (A) Venn diagram representing the overlapping genes in the pollen microarray and the bud transcriptome of *athmgb15*

(B) Screenshot of the functional annotation clustering results obtained from analyzing the overlapping genes.

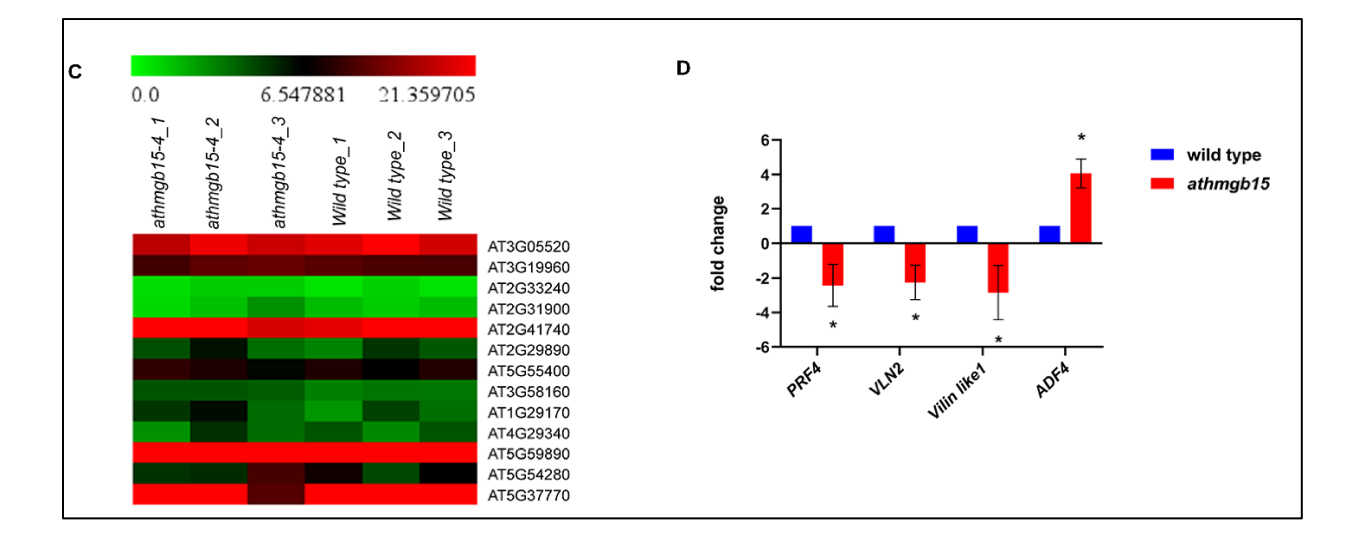


Fig 2.2 (C) Heatmap of the FPKM values of genes from biological processes corresponding to actin binding & organization in *athmgb15* and wildtype buds (stages 8-11). The data set is a representation of the significant (p<0.05) differentially expressed genes from three biological replicates.

(D) Graphical representation of the expression profile from q-RTPCR of the actin binding genes in wild type and *athmgb15* buds (stage 8-11). The values represent the mean fold change in the expression of the genes and the error bars represent the \pm SD (n=3). Statistical analysis was performed using GraphPad Prism and a paired 2-tailed students t-test was done to determine the significance of the fold change for each gene. Significance was assigned based on the p-value < 0.05 (*represent p<0.05)

Visualization and quantification of F-actin arrangement in germinated pollen tubes

The preliminary findings from our transcriptome analysis indicating a defective actin filament formation in *athmgb15* mutants, we decided to visualise the actin filaments in the germinated pollen tubes of the mutant and wild type. It is known that the fluorescent dye phalloidin preferentially binds to f-actin in the pollen tube of *Arabidopsis* (Qu et al., 2020). We used the technique given by Qu et al. in to visualize and quantitate the difference in actin distribution of germinating pollen tubes in anthers of wild type and *athmgb15* mutant (Qu et al., 2020). The image (Fig 2.4A) clearly shows the filamentous appearance of f-actin in wild type compared to the fragmented specks of rhodamine phalloidin observed in the pollen tubes of *athmgb15*. Also, the fluorescence intensity of rhodamine phalloidin was observed to be concentrated towards the apex in wild type, indicating a high concentration of f-actin at the pollen tube apex. The intensity of

fluorescence was found to be more concentrated in the subapical (or shank) region of the pollen tube in *athmgb15* with negligible apical concentration. This represents a spatially defective f-actin distribution and organisation in *athmgb15* mutant during pollen tube germination.

Since the genes that were differentially regulated the mutant belonged primarily to the f-actin polymerising cluster, we also decided to observe the effects of a widely known actin polymerisation inhibitor Latrunculin B on the f-actin organisation in the germinated pollen tubes. Latrunculin B is an actin polymerization inhibitor, that has been used to disrupt actin organization in different tissue from several organisms, and its mechanism of action is also well understood (Chen et al., 2007). We investigated the action of 10 nM Latrunculin B in germinated pollen tubes of *athmgb15-4* and wild type. Upon 10 nM treatment of Latrunculin B the mean fluorescent intensity dropped significantly in both wild type and *athmgb15-4* (Fig 2.4B). The mean intensity observed from the maximum projected slices was recorded for quantifying the f-actin present in the pollen tubes. The graphical representation of the mean intensity quantified from control and Latrunculin B treated samples shows that post treatment, the wild type exhibited a 50% reduction in available f-actin content while the *athmgb15* mutant showed an intensity decrease by 75% (Fig 2.4C). This indicates that the rate of polymerization and depolymerization of f-actin in the germinating pollen tubes of *athmgb15* is severely affected by the knockout of *AtHMGB15* gene.

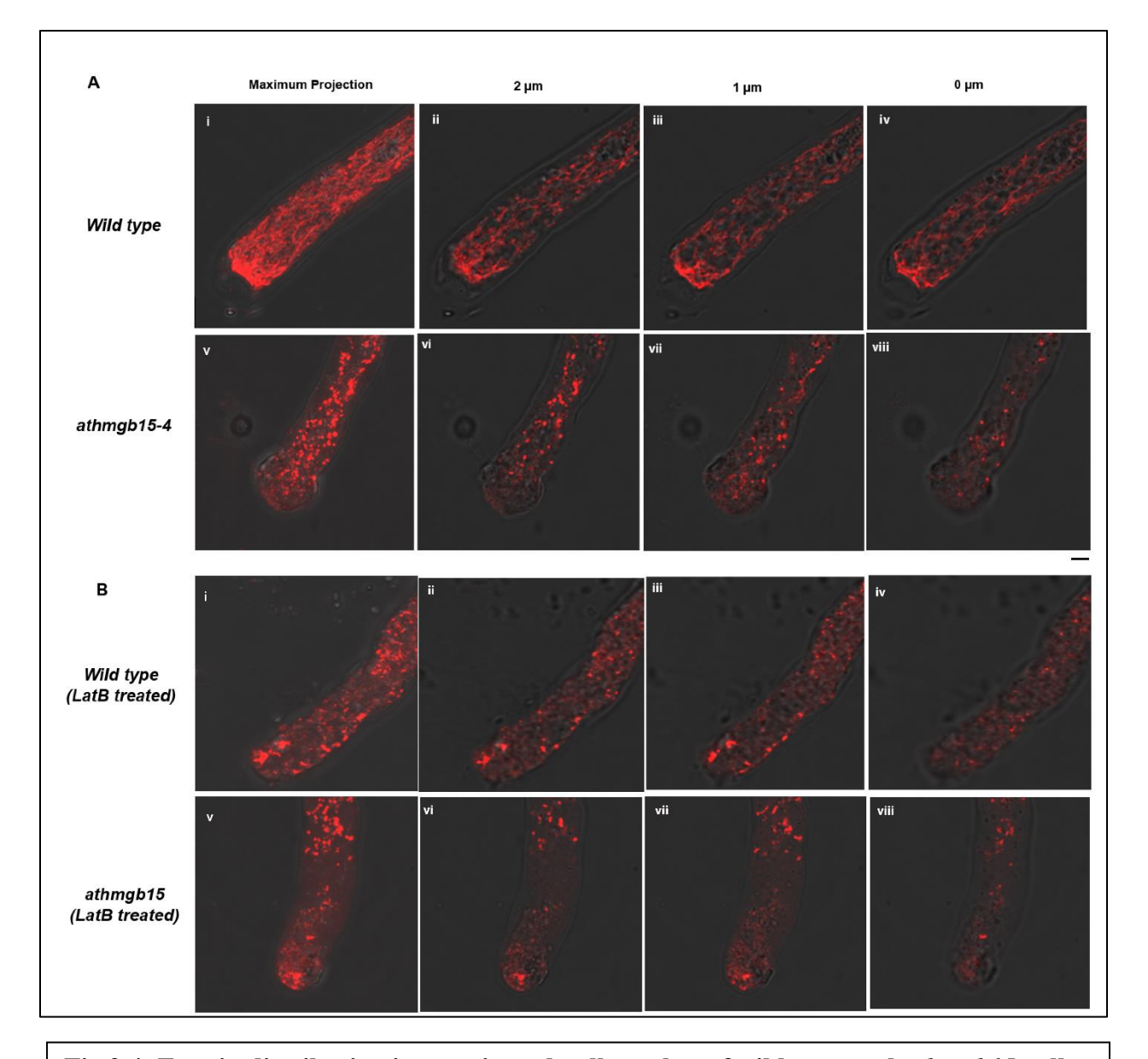


Fig 2.4: F-actin distribution in germinated pollen tubes of wild-type and *athmgb15* pollen grains.

- (A) Optical Z-slice (1 μ m) images of an elongating pollen tube of wild type (i-iv) and *athmgb15* (v-viii). The F-actin distribution in germinating pollen tube was stained using rhodamine phalloidin, and the maximum intensity projected pollen tubes are shown in (i&v). The scale bar represents 5 μ m.
- **(B)** Optical Z-slice (1 μm) images of a pollen tube of wild type (i-iv) and *athmgb15* (v-vi) treated with 10nM LatB. F-actin was distributed in germinating pollen tube germination LatB treatment was stained using rhodamine phalloidin, and the maximum intensity projected pollen tubes are shown in (i&v). The scale bar represents 5 μm.

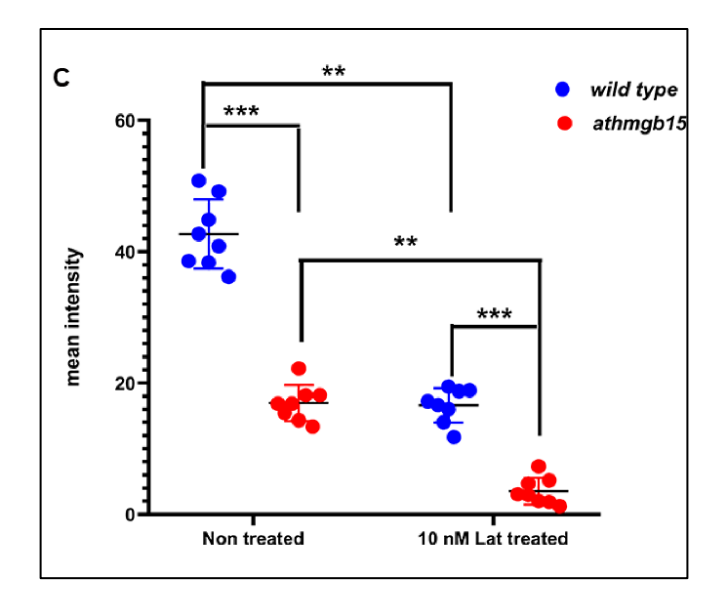


Fig. 2.4(C) Graphical representation of the rhodamine-phalloidin fluorescence intensity in control and LatB-treated pollen tubes of wildtype and *athmgb15*. The bars represent the means \pm (n=8) and significance was calculated using Student's t test. ** denotes p<0.005 and *** denotes p<0.0005.

AtHMGB15 interacts with ARP4 to regulate the expression of actin related genes during pollen development

AtHMGB15 is a transcription co-activator and functions along with other proteins to regulate their expression. In order to identify the candidate proteins interacting directly or indirectly with AtHMGB15 to specifically regulate the expression of actin gene cluster, a single protein search was performed using the STRING database. The results retrieved from the database displayed a network of 10 nodes interacting with AtHMGB15 (Fig 2.5). Based on literature survey on every protein in the network, we identified the nuclear Actin Related Proteins (ARPs) that are a part of the chromatin–remodeling complexes regulating plant development processes. Amongst these ARPs, ARP4 is a component of the ATP-dependent chromatin remodeling complexes such as NuA4 HAT complex along with SWI/SNF, INO80 and SWR1 that interacts AtHMGB15 (Kandasamy et al., 2005). Previous study has shown that *arp4* mutants which have moderate reduction in ARP4 protein in *Arabidopsis*, are partially male sterile with small immature anther containing small number of mature pollen grains (Kandasamy et al., 2005). Thus, serving as our

first evidence towards finding the probable interactor of AtHMGB15 in the regulation of actin binding genes during the male gametophytic development.

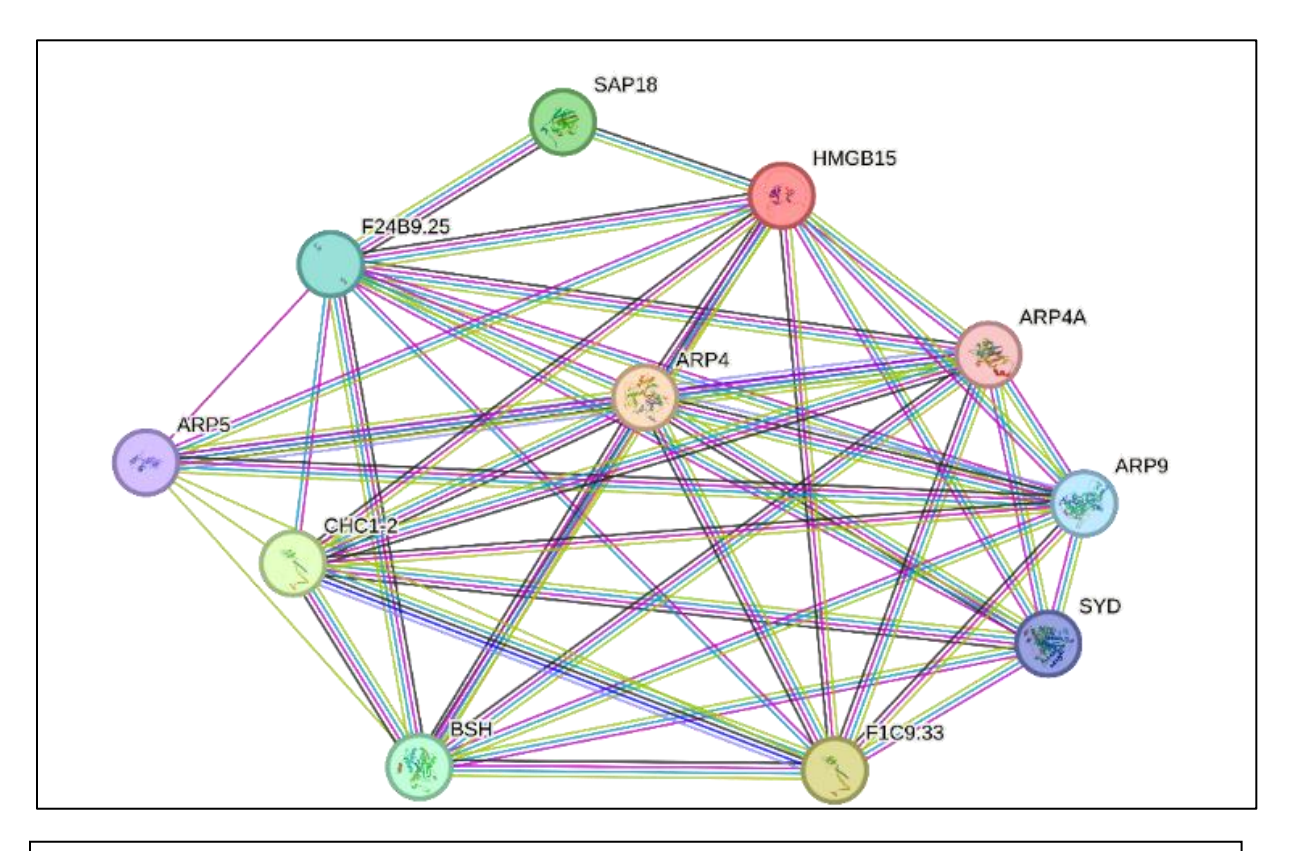


Fig. 2.5: Protein-Protein interaction network of AtHMGB15 reported in STRING database

We performed a biofluorescence complementation assay by cloning the CDS of AtHMGB15 in the C- terminal of a YFP vector and cloned the CDS of ARP4 in the N-terminal of a YFP vector and co-infiltered the two constructs in an onion epidermis. The results of the experiment showed a clear interaction between AtHMGB15 and ARP4 and their localization to the nucleus and plasma membrane of the onion epidermal cells. The onion epidermal cells did not show any EYFP fluorescence for both AtHMGB15-cYFP: pSITE-nYFP and ARP4-nYFP: pSITE-cYFP combinations. The study thus, confirmed that AtHMGB15 interact with ARP4 (**Fig 2.6**).

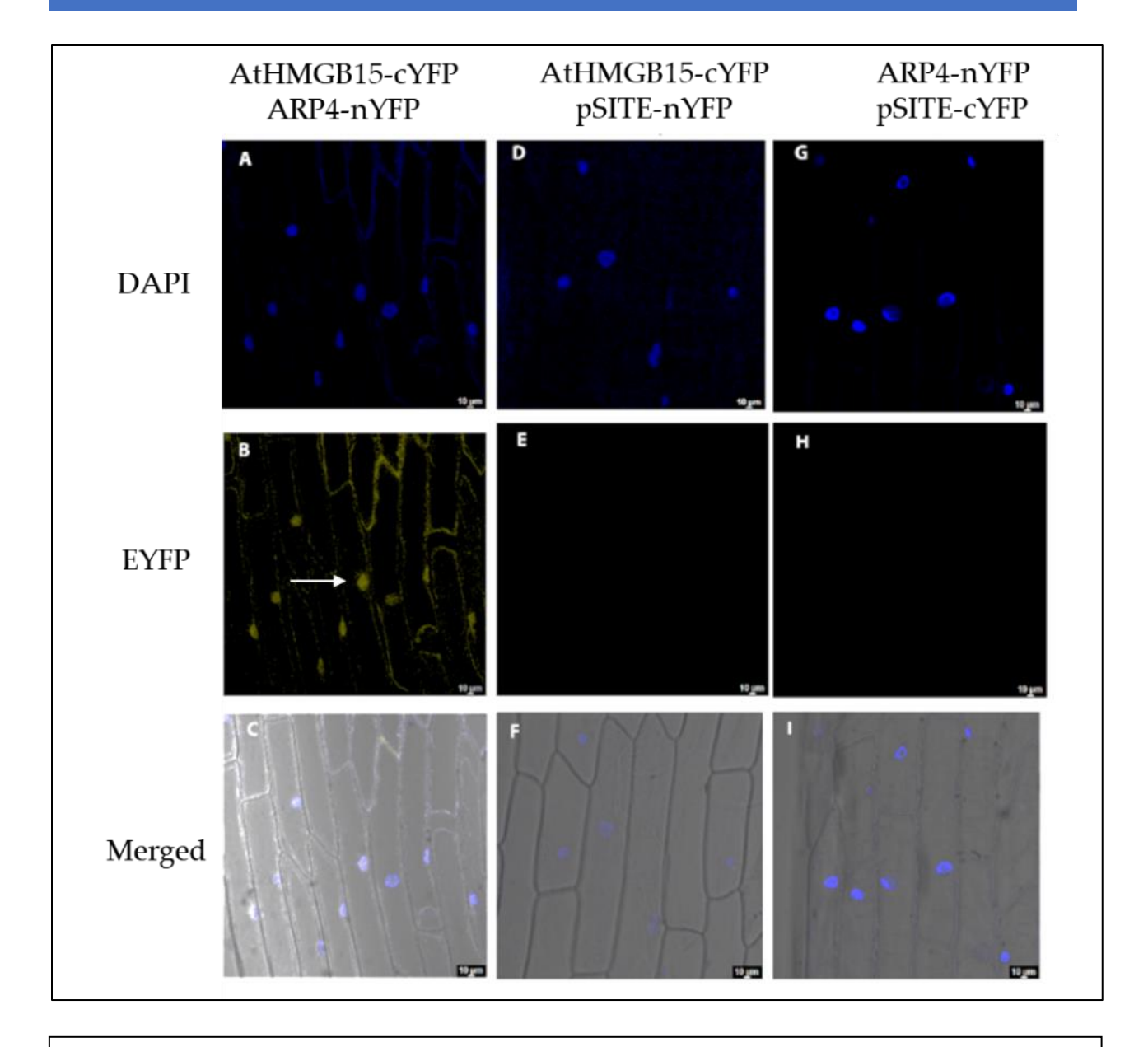


Fig 2.6: ATHMGB15 interacts with ARP4 Bimolecular fluorescence complementation assay showed that AtHMGB15 interacted with ARP4 in onion epidermis AtHMGB15-cYFP +pSITE-nYFP-C1 and ARP4-nYFP +pSITE-cYFP-N1 was used as control. Scale bar=10 μ m.

Differentially regulated genes in athmgb15 and arp4 mutants

The set of differentially regulated genes for each mutant has an overlap of 50 genes, (**Fig 2.7**) and list of genes are provided in **Annexure Table 7.** In this set, 32 genes are known to have a binding site for AtHMGB15, as per ChIP chip data reported in previous literature and the gene list is provided (**Annexure Table 8**). Upon functional annotation using DAVID v6.2, the most enriched gene ontology terms are those responsible for processes like sequestering of actin monomers and regulation of pollen tube growth. The specific genes involved in these processes are *Profilin 4 (PRF4)*, and Lorelei-Like-GPI Anchored protein 3 (LLG3). PRF4 is a low molecular weight protein which binds to actin monomers, and is responsible for the regulation of the actin cytoskeleton (Bubb et al., 2003; Liu et al., 2015). During pollen development, PRF4 promotes formin-mediated actin filament assembly and vesicle transport during the polarity formation stage (Breitsprecher and Goode, 2013; Bubb et al., 2003; Lan et al., 2018; Liu et al., 2015). LLG3 is a positive regulator of biosynthetic processes responsible for reactive oxygen species (ROS) formation, and regulates pollen tube growth by acting as chaperones and coreceptors for ANXUR/BUPS Receptor Kinases in *Arabidopsis* (Feng et al., 2019).

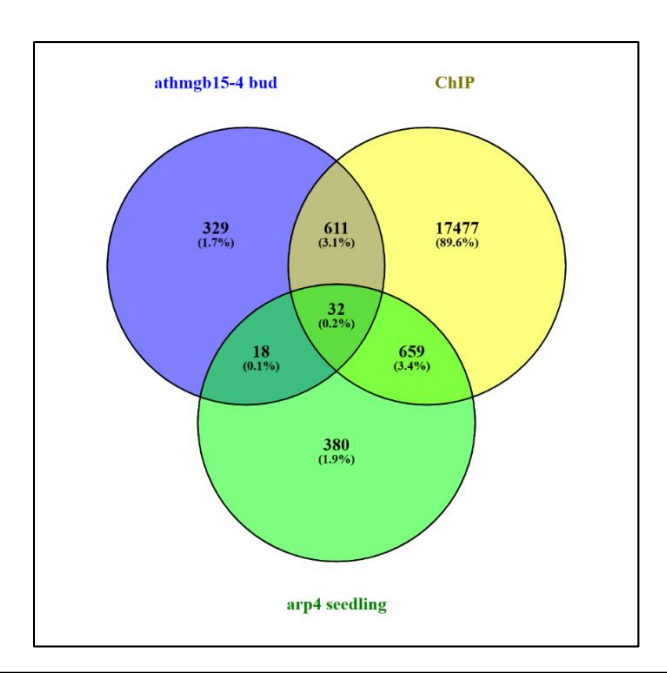


Fig. 2.7: Venn diagram of the differentially regulated genes in *athmgb15* bud transcriptome and *arp4* Nie et al., 2021) containing the AtHMGB15 binding site (ChIP-chip data (Mallik et al., 2020))

Expression profiling of PCD and actin binding proteins gene clusters using q-RTPCR

The advancement of PCD in tapetal cells is directly proportional to the abundance of PCD executers in the cell. The expression of *CEP1*, *MC9* and *RNS3*, the commonly known developmental PCD executers is significantly downregulated in both *athmgb15* and *arp4* (Fig 2.8). However, the expression of anti-apoptotic proteins might influence the rate of progression of cell death. The *BI1* and *BI1 family protein* transcripts are upregulated in *athmgb15* whereas they are downregulated in *arp4*.

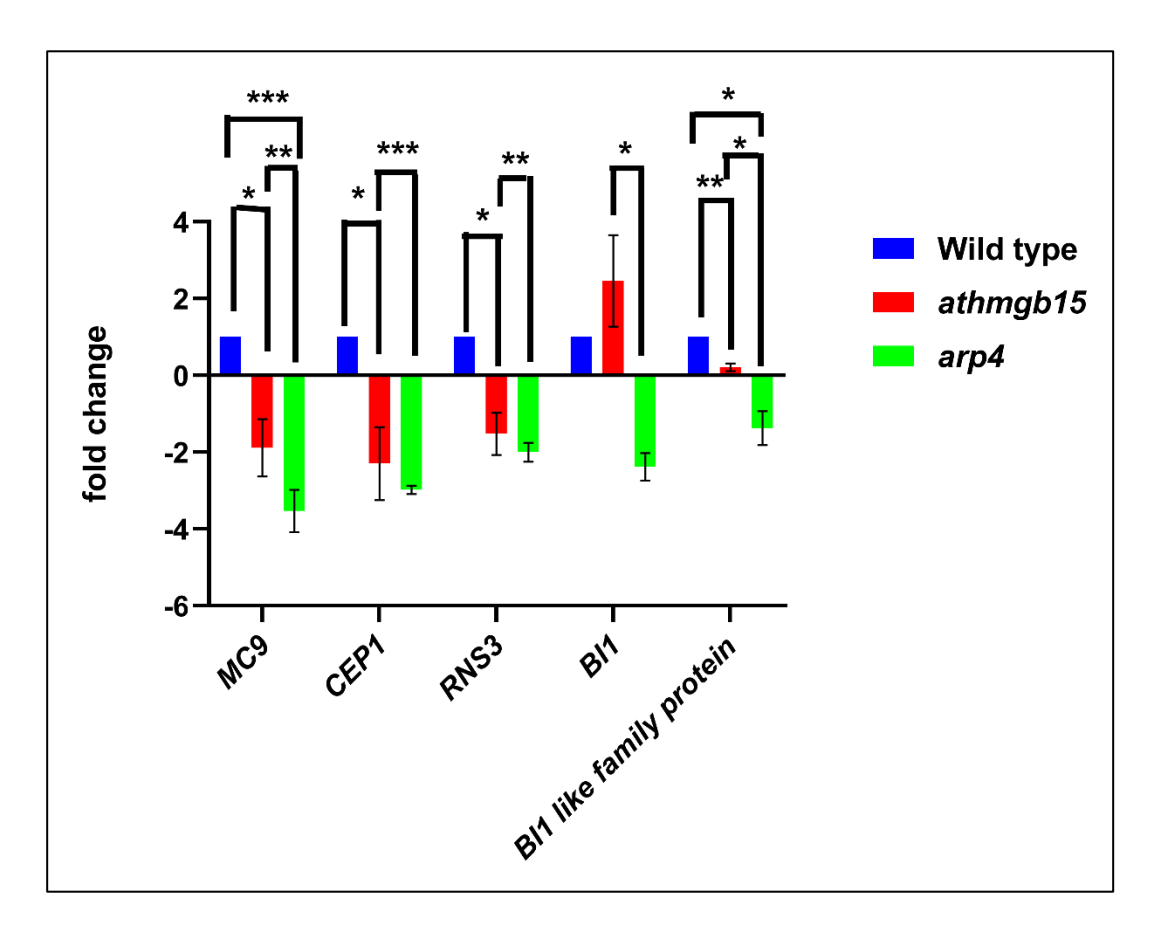


Fig 2.8: q-RTPCR of dPCD genes in wild type, athmgb15-4 and arp4. The bars represent the mean \pm SD (n=3). Statistical test was performed using two tailed Student t-test and the significance was assigned to genes when p-value <0.05. *, ** and *** indicates p-value < 0.05, p-value < 0.005, p-value < 0.005 respectively. The lines indicate the significance of fold change between the genotypes.

CHAPTER II: RESULTS

The polymerization processes of f-actin in germinating pollen tubes of *Arabidopsis* are controlled by Profilins and Villins (Liu et al., 2015; Qu et al., 2013). The transcriptome analysis was validated via q-RTPCR of the relevant genes, and it was found that in both the *athmgb15* and *arp4* mutants (Fig 2.9), *Profilin 4* (*PRF4*) and *Vilin 2* (*VLN2*), exhibited significant downregulation. On the other hand, the depolymerization cycle of f-actin is controlled by Actin Depolymerization Factors (Jiang et al., 2022), and our q-RTPCR validation reveals a differential regulation of *Actin Depolymerization Factor 4* (*ADF4*) in both *athmgb15* and *arp4* mutants. However, the *athmgb15* mutant exhibits an upregulated *ADF4* transcript compared to the downregulation observed in the *arp4*.

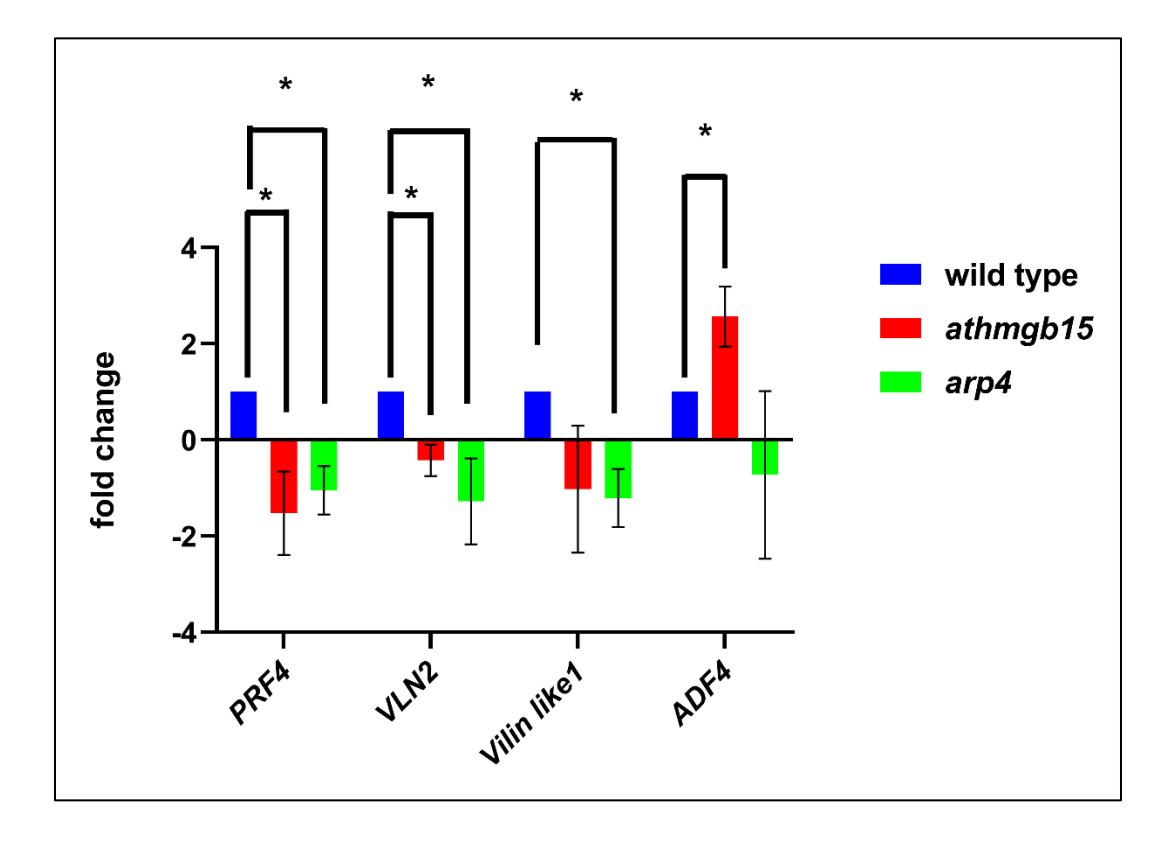


Fig 2.9: q-RTPCR of genes expressing actin binding proteins in wild type, *athmgb15-4* and *arp4*. The bars represent the mean \pm SD(n=3). Statistical test was performed using two tailed Student t-test and the significance was assigned to genes when p-value <0.05. * Indicates p<0.05. The lines indicate the significance of fold change between the genotypes.

Prolonged tapetal PCD in arp4 mutants

The indication of partial male sterility phenotypes in *arp4* mutants encouraged us to investigate the trajectory of tapetal PCD in this mutant. TUNEL assay results showed that PCD of the tapetal cells in *arp4* is prolonged compared to wildtype however it is not as drastic as observed in *athmgb15*. The tapetum in stage 10 is prominent and the green spots observed in stage 12 of *arp4* indicates the residues of tapetal cells undergoing PCD (Fig 2.10).

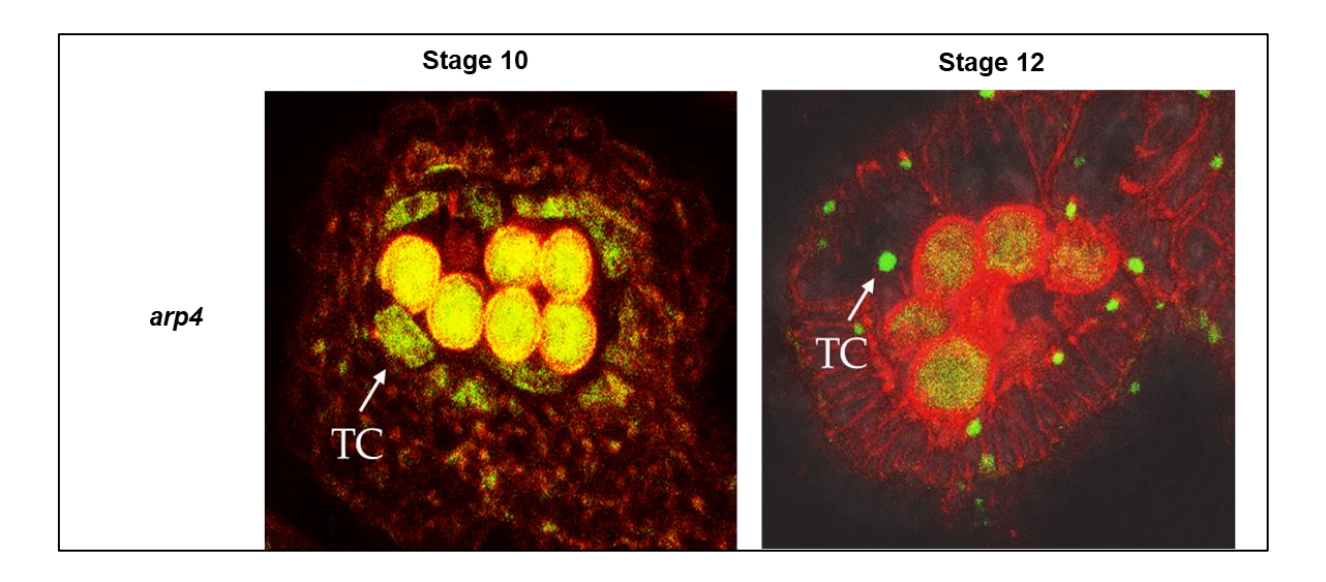


Fig. 2.10: TUNEL assay of stages 10 and 12 in arp4 mutant

Quantification and visualisation of actin distribution in germinating pollen tubes of arp4

The germinated pollen tubes of *arp4* mutant exhibited fragmented actin and the localization of fluorescence from rhodamine phalloidin was restricted to spots throughout the pollen tube (**Fig 2.11 A**). The mutant did not show any presence of continuous actin filaments as earlier observed in wild type pollen tubes. The spots increased in number and appeared duller compared to the spots in the control pollen tubes (**Fig 2.11B**). The intensity of the fluorescence dropped by nearly 50% after 10 nM LatB treatment (**Fig 2.11C**).

CHAPTER II: RESULTS

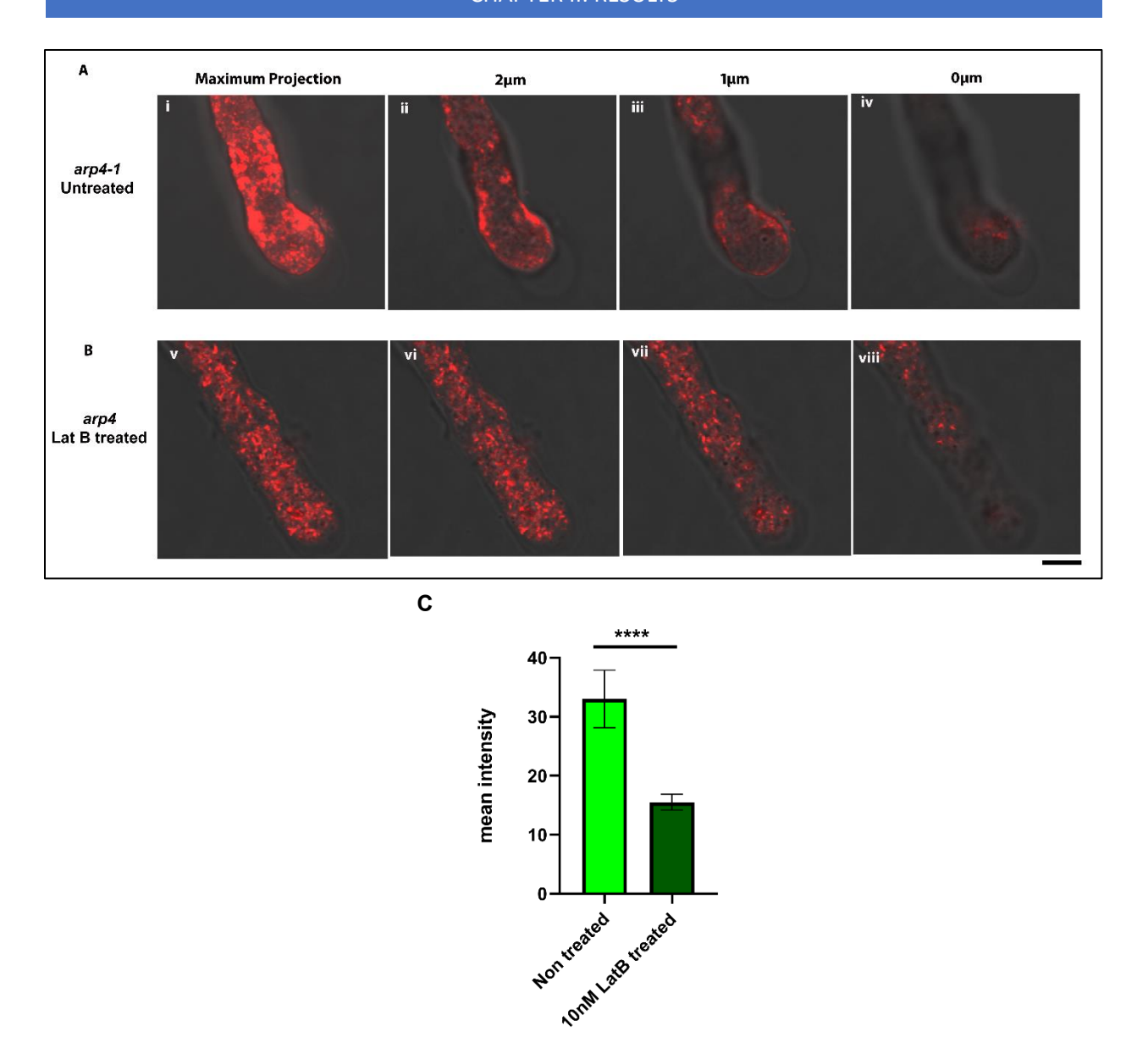
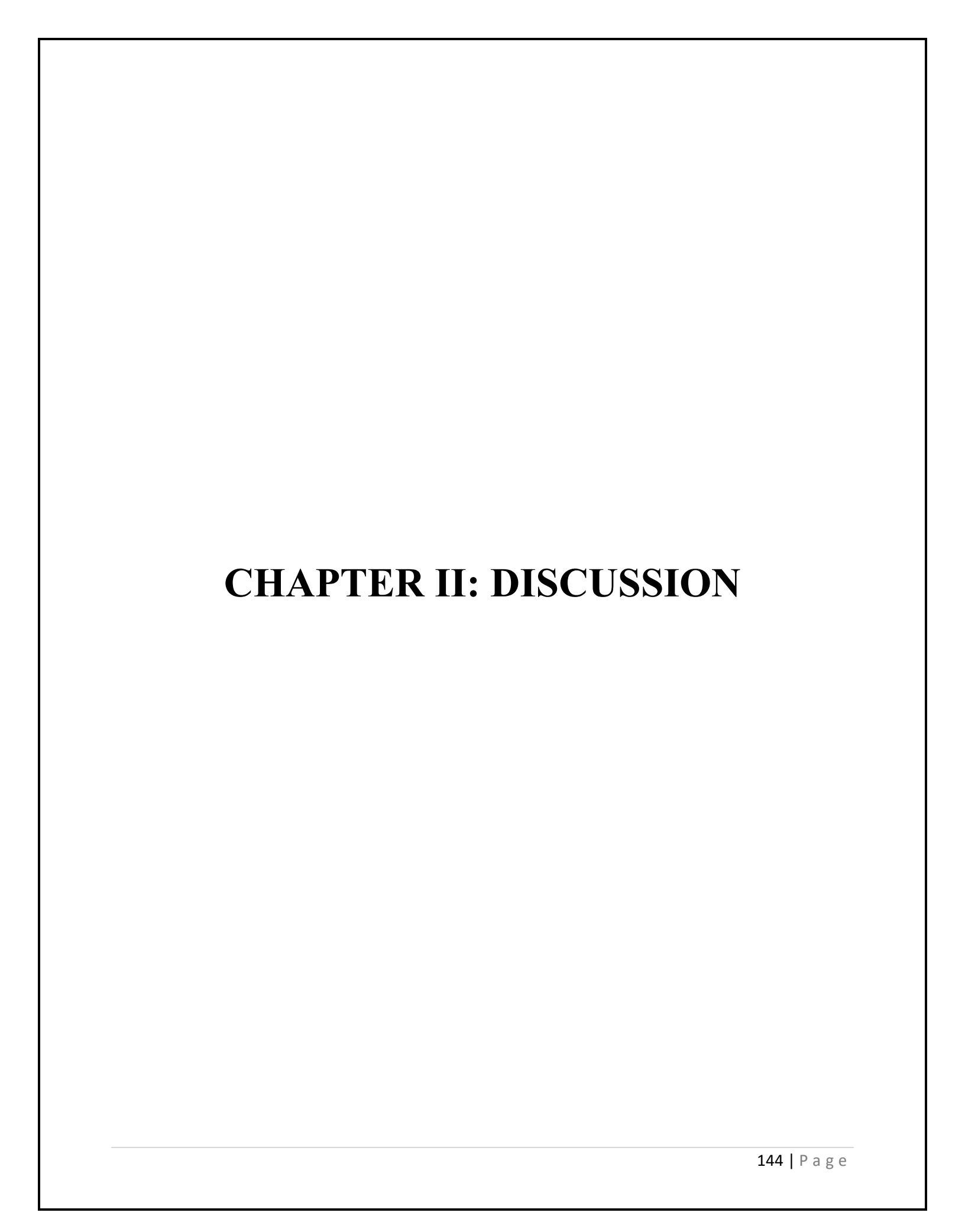


Figure 2.11: f-actin distribution observed in germinated pollen tube using rhodamine phalloidin of *Arabidopsis arp4*.

- (A) Optical Z-slice images of a pollen tube, with $1\mu m$ z-step-size. (i-iv) represents the pollen tubes of arp4.
- **(B)** Optical Z-slice images of a pollen tube, with 1 μ m z-step-size. (v-vi) represents the pollen tubes of arp4 after 10 nM LatB treatment. The scalebar represents 5μ m.
- (C) Graphical representation of Rhodamine phalloidin fluorescence intensity in control and LatB treated pollen tubes of arp4. n = 10, **** P < 0.0005 by Student's t-test.



CHAPTER II: DISCUSSION

Extensive studies on abnormal pollen tube germination and growth have been illustrated in completely or partially male sterile lines in plants (Farinati et al., 2023). However, investigations during the development stages of these mutants demonstrating defective pollen tube germination and growth rate have remained unreported. The inability of 60% population of *athmgb15* mutants to germinate poses serious threat to the fertility of the mutant. This chapter attempts to bridge the gap in study on abnormalities during pollen development and defects in pollen tube germination.

AtHMGB15 loss of function mutants exhibit defective actin dynamics during pollen tube germination & growth

Identification of the actin binding gene cluster from our transcriptome analysis paved the way to test our hypothesis in germinated pollen grains. The study revealed the downregulation of several genes responsible for actin polymerisation to be downregulated. Actin filaments serve as tracts for myosin dependent organelle movement during a directed growth as observed during pollen germination and pollen tube elongation (Duan and Tominaga, 2018). Profilins and villins are actin filament bundling proteins that play an important role in actin polymerization (Staiger and Hussey, 2004). PRF4 and VLN2 have been reported to regulate cytoskeletal structure by promoting the nucleation of f-actin monomers in pollen tubes (Liu et al., 2015; Zhao et al., 2020). We determined the expression of Profilin 4 (PRF4), Villin 2 (VLN2) and Villin-like 1 in wildtype and athmgb15 flowers. The q-RTPCR results indicated that the expression of PRF4, VLN2 and Villin-like 1 was significantly downregulated in athmgb15 cells. Previous studies have reported that downregulation of PRF4 lead to lower number of filamentous actin and also induced disorganization of apical factin, and reduced tip-directed vesicle transport in the pollen tube (Bubb et al., 2003; Liu et al., 2015). VLN2 functions with VLN3 in bundling of actin filaments during directional growth as observed in roots and pollen tubes (Huang et al., 2015; Qu et al., 2013; Zhao et al., 2020). VLN2 has also been reported to work with VLN5 and the *vln2vln5* double mutants have been reported to demonstrate normal pollen tube germination but retarded pollen tube elongation (Huang et al., 2015; Qu et al., 2013; Zhao et al., 2020).

To study actin distribution and polymerization during pollen tube growth, we used fluorescent rhodamine-phalloidin, which preferentially binds to f-actin in the pollen tube (Qu et al., 2020). The results indicate that, the fluorescence intensity of actin filaments in the apical and subapical regions of pollen tubes was greater in the wild type compared to that observed in *athmgb15*.

CHAPTER II: DISCUSSION

However, the actin arrangement is highly disorganized in the *athmgb15* pollen tube. There were fewer long actin fibers in the mutant than in the wild type. The rhodamine phalloidin stained f-actin appeared to be fragmented in *athmgb15* in comparison to the long actin fibers present in the wild type. To test whether actin polymerization is the main cause of defects in pollen tube growth in *athmg15*, we tested the effect of latrunculin B (LatB) treatment on pollen growth in the wild type and *athmgb15*. LatB affects actin polymerization and alters the f-actin level in the cell. The results indicated that after treatment with LatB (10 nM), actin filaments became fragmented in wildtype and in *athmgb15* pollen tubes; however, the effect was more pronounced in the *athmgb15* pollen tubes. The significant reduction in fluorescence post-LatB treatment suggested reduced f-actin formation in *athmgb15* pollen grains compared to that in the wild type.

Thus, collectively from our gene expression study and actin visualisation results, we speculate that the differential regulation of the actin binding genes in *athmgb15* might be an underlying factor for the disorganised f-actin distribution in the atypical pollen tube germination observed in *athmgb15* mutants.

AtHMGB15 interacts with ARP4 to regulate fertility in male gametes

AtHMGB15 is an architectural protein that has been established to coordinate higher order chromatin remodeling during transcription of developmental genes (Mallik et al., 2020). Our result indicate that AtHMGB15 interacts with ARP4 which is part of SWI/SNF chromatin remodelling complex (Travers, 2003). An independent study has shown that ARP4 interacts with S/MAR binding AT-hook containing nuclear localized protein AHL29/SOB3, indicating that ARP4 has an inherent property of interacting with AT rich binding proteins (Street et al., 2008). Dutkowski et al have predicted that AtHMGB15 interact with AtARP4 as a part of *Arabidopsis* SWI/SNF complex (Dutkowski and Tiuryn, 2009). The BiFC assay results also proved the AtHMGB15 and ARP4 interaction positive. Observations from previous studies by Kandaswamy et al., *atarp4* mutants showed phenotypes similar to *athmgb15* mutant related to anther and pollen development such as delayed anther dehiscence, shorter silique length, delayed flower senescence, lower seed content and reduced pollen viability (Kandasamy et al., 2005; Pawloski et al., 2006). Based on these findings we speculated that the interaction between the nuclear actin related protein ARP4 with the AT-rich binding proteins, AtHMGB15 is crucial for the regulation of transcription of several genes responsible for anther and pollen development.

CHAPTER II: DISCUSSION

The analysis unfolded from the comparison of *athmgb15* transcriptome (bud) with the published *atarp4* transcriptome by Nie et al., indicated differential regulation of genes responsible for sequestering of actin monomers and regulation of pollen tube growth in both *athmgb15* and *atarp4*. Our q-RTPCR study using homozygous lines of *arp4* mutant (CS876625) was also contingent with the transcriptome data. The microscopy data from TUNEL assay study also proved that tapetal PCD in *arp4* was prolonged although the delay was not as distinct as observed in *athmgb15*. The upregulation of *BI1* and *BI1 family protein* genes clearly indicates the possibility for the severity of defective tapetal PCD observed earlier in *athmgb15* compared to the tapetal cell death delay observed in *arp4*. Observations from rhodamine phalloidin staining showed presence of fragmented f-actin in the germinated pollen tubes of *arp4* that were consistent with the results from the transcriptome analysis.

Thus, AtHMGB15 being a transcriptional coactivator, regulates pollen development and pollen germination in *Arabidopsis*. HMG-box proteins have been shown to function as nuclear architectural proteins that orchestrate high order chromatin organization during transcription (Antosch et al., 2012; Thomas and Travers, 2001). In this chapter, we have conclusively shown that AtHMGB15 regulate transcription of actin related genes to regulate pollen tube growth. Our result also indicate that AtHMGB15 interacts with ARP4 which is part of SWI/SNF chromatin remodeling complex (Dutkowski and Tiuryn, 2009). Although it is not clear whether this interaction of AtHMGB15 with chromatin remodeling complex is an absolute requirement for the regulation of gene expression, further investigation is needed to unravel the regulatory network involved in pollen grains development in plants.

CHAPTER II: REFERENCES

REFERENCES:

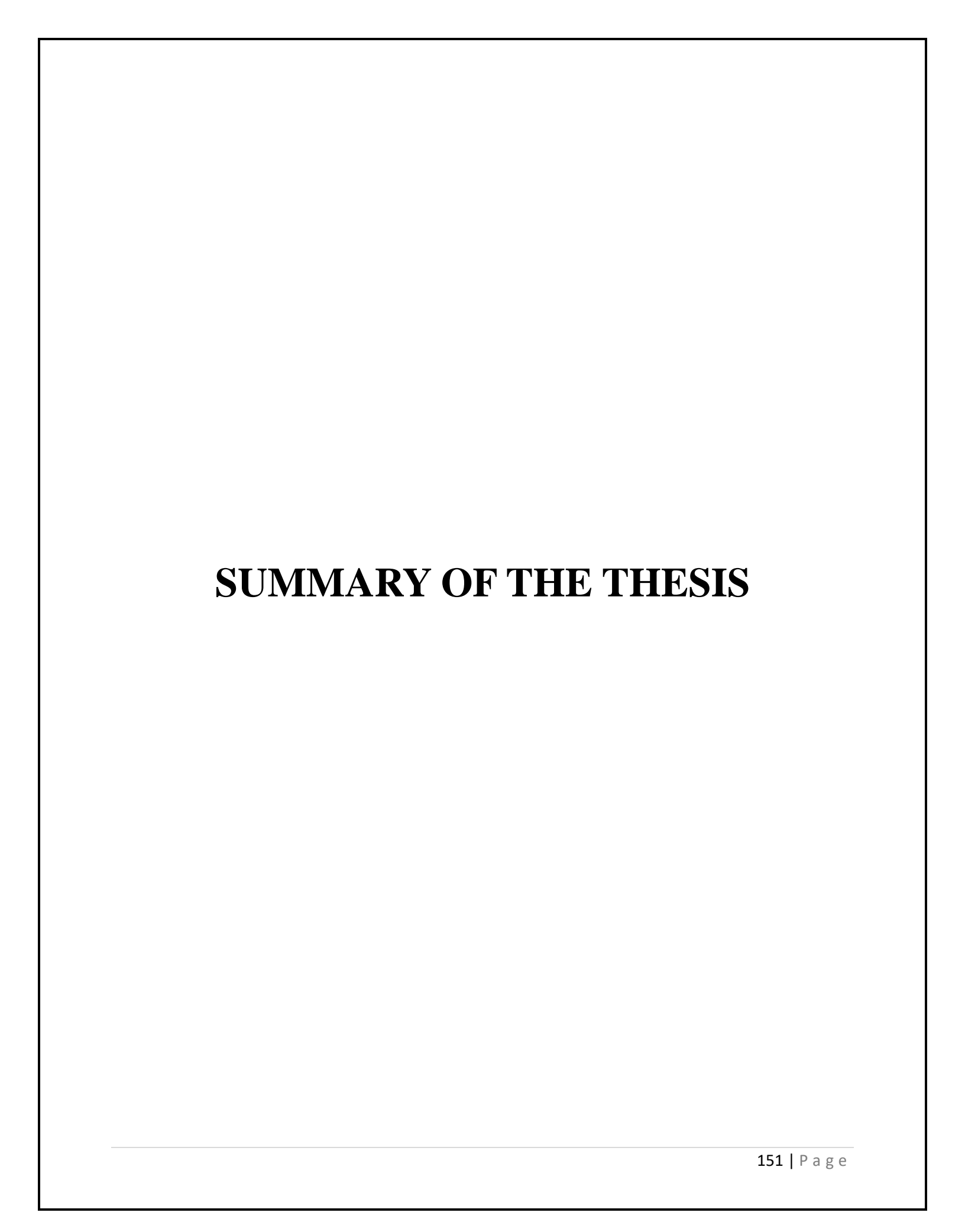
- 1. Antosch, M., Mortensen, S. A., and Grasser, K. D. (2012). Plant proteins containing high mobility group box DNA-binding domains modulate different nuclear processes. *Plant physiology* **159**, 875-883.
- 2. Bedinger, P. (1992). The remarkable biology of pollen. *The plant cell* **4**, 879.
- 3. Bedinger, P. A., Hardeman, K. J., and Loukides, C. A. (1994). Travelling in style: the cell biology of pollen. *Trends in cell biology* **4**, 132-138.
- 4. Breitsprecher, D., and Goode, B. L. (2013). Formins at a glance. *Journal of cell science* **126**, 1-7.
- 5. Bubb, M. R., Yarmola, E. G., Gibson, B. G., and Southwick, F. S. (2003). Depolymerization of actin filaments by profilin: effects of profilin on capping protein function. *Journal of Biological Chemistry* **278**, 24629-24635.
- 6. Chen, T., Teng, N., Wu, X., Wang, Y., Tang, W., Šamaj, J., Baluška, F., and Lin, J. (2007). Disruption of actin filaments by latrunculin B affects cell wall construction in Picea meyeri pollen tube by disturbing vesicle trafficking. *Plant and Cell Physiology* **48**, 19-30.
- 7. Duan, Z., and Tominaga, M. (2018). Actin–myosin XI: an intracellular control network in plants. *Biochemical and Biophysical Research Communications* **506**, 403-408.
- 8. Dutkowski, J., and Tiuryn, J. (2009). Phylogeny-guided interaction mapping in seven eukaryotes. *BMC bioinformatics* **10**, 1-19.
- 9. Farinati, S., Draga, S., Betto, A., Palumbo, F., Vannozzi, A., Lucchin, M., and Barcaccia, G. (2023). Current insights and advances into plant male sterility: new precision breeding technology based on genome editing applications. *Frontiers in Plant Science* 14.
- 10. Feng, H., Liu, C., Fu, R., Zhang, M., Li, H., Shen, L., Wei, Q., Sun, X., Xu, L., and Ni, B. (2019). LORELEI-LIKE GPI-ANCHORED PROTEINS 2/3 regulate pollen tube growth as chaperones and coreceptors for ANXUR/BUPS receptor kinases in Arabidopsis. *Molecular Plant* 12, 1612-1623.
- 11. Huang, S., Qu, X., and Zhang, R. (2015). Plant villins: versatile actin regulatory proteins. *Journal of integrative plant biology* **57**, 40-49.
- 12. Jiang, Y., Lu, Q., and Huang, S. (2022). Functional non-equivalence of pollen ADF isovariants in Arabidopsis. *The Plant Journal* **110**, 1068-1081.

CHAPTER II: REFERENCES

- 13. Jiang, Y., Zhang, M., and Huang, S. (2017). Analysis of actin-based intracellular trafficking in pollen tubes. *Plant Protein Secretion: Methods and Protocols*, 125-136.
- 14. Kandasamy, M. K., Deal, R. B., McKinney, E. C., and Meagher, R. B. (2005). Silencing the nuclear actin-related protein AtARP4 in Arabidopsis has multiple effects on plant development, including early flowering and delayed floral senescence. *The Plant Journal* 41, 845-858.
- 15. Lan, Y., Liu, X., Fu, Y., and Huang, S. (2018). Arabidopsis class I formins control membrane-originated actin polymerization at pollen tube tips. *PLoS Genetics* **14**, e1007789.
- 16. Liu, X., Qu, X., Jiang, Y., Chang, M., Zhang, R., Wu, Y., Fu, Y., and Huang, S. (2015). Profilin regulates apical actin polymerization to control polarized pollen tube growth. *Molecular Plant* **8**, 1694-1709.
- 17. Mallik, R., Prasad, P., Kundu, A., Sachdev, S., Biswas, R., Dutta, A., Roy, A., Mukhopadhyay, J., Bag, S. K., and Chaudhuri, S. (2020). Identification of genome-wide targets and DNA recognition sequence of the Arabidopsis HMG-box protein AtHMGB15 during cold stress response. *Biochimica et Biophysica Acta (BBA)-Gene Regulatory Mechanisms* 1863, 194644.
- 18. Marchant, D. B., and Walbot, V. (2022). Anther development—The long road to making pollen. *The Plant Cell* **34**, 4677-4695.
- 19. Pawloski, L. C., Kandasamy, M. K., and Meagher, R. B. (2006). The late pollen actins are essential for normal male and female development in Arabidopsis. *Plant molecular biology* **62**, 881-896.
- 20. Qu, X., Wang, Q., Wang, H., and Huang, S. (2020). Visualization of actin organization and quantification in fixed Arabidopsis pollen grains and tubes. *Bio-protocol* **10**, e3509-e3509.
- 21. Qu, X., Zhang, H., Xie, Y., Wang, J., Chen, N., and Huang, S. (2013). Arabidopsis villins promote actin turnover at pollen tube tips and facilitate the construction of actin collars. *The Plant Cell* **25**, 1803-1817.
- 22. Staiger, C. J., and Hussey, P. J. (2004). Actin and actin-modulating proteins. *The Plant Cytoskeleton in Cell Differentiation and Development. Blackwell Scientific Publications, Oxford*, 32-80.

CHAPTER II: REFERENCES

- 23. Street, I. H., Shah, P. K., Smith, A. M., Avery, N., and Neff, M. M. (2008). The AT-hook-containing proteins SOB3/AHL29 and ESC/AHL27 are negative modulators of hypocotyl growth in Arabidopsis. *The Plant Journal* **54**, 1-14.
- 24. Thomas, J. O., and Travers, A. A. (2001). HMG1 and 2, and related 'architectural' DNA-binding proteins. *Trends in biochemical sciences* **26**, 167-174.
- 25. Travers, A. A. (2003). Priming the nucleosome: a role for HMGB proteins? *EMBO reports* **4**, 131-136.
- 26. Xia, C., Wang, Y. J., Liang, Y., Niu, Q. K., Tan, X. Y., Chu, L. C., Chen, L. Q., Zhang, X. Q., and Ye, D. (2014). The ARID-HMG DNA-binding protein A t HMGB 15 is required for pollen tube growth in Arabidopsis thaliana. *The Plant Journal* **79**, 741-756.
- 27. Zhao, W., Qu, X., Zhuang, Y., Wang, L., Bosch, M., Franklin-Tong, V. E., Xue, Y., and Huang, S. (2020). Villin controls the formation and enlargement of punctate actin foci in pollen tubes. *Journal of cell science* **133**, jcs237404.
- 28. Nie WF, Wang J. Actin-Related Protein 4 Interacts with PIE1 and Regulates Gene Expression in *Arabidopsis*. Genes (Basel). 2021 Apr 2;12(4):520. doi: 10.3390/genes12040520. PMID: 33918349; PMCID: PMC8066076.



SUMMARY OF THE THESIS

The AtHMGB15 architectural protein interacts with the AT rich regions of the DNA and causes bends in the chromatin structure that facilitates the interaction of other transcription regulatory proteins with the DNA. The enriched expression of *AtHMGB15* transcript in young flower buds and pollen grains of *Arabidopsis* indicated its role in pollen grain development. Since development of the male germline is heavily reliant on the nourishment it receives from its adjacent layer of somatic cells called the tapetum, investigation of the effects of AtHMGB15 mutation on tapetum activity and development is crucial for the advancement of knowledge in pollen development. The broad aim of the thesis had been divided into two chapters. While the first chapter emphasises on the defects in gene expression and tapetum mediated development of the pollen grains in *athmgb15* with respect to wild type. The second chapter focuses on the abnormalities in the post developmental stage of pollen grains in *athmgb15* that is responsible for ensuing successful fertilization in flowering plants. The thesis thus concludes with a reflection on the advances made in programmed cell death of tapetal cells during the differentiation of pollen grains from the anther primordia (L2).

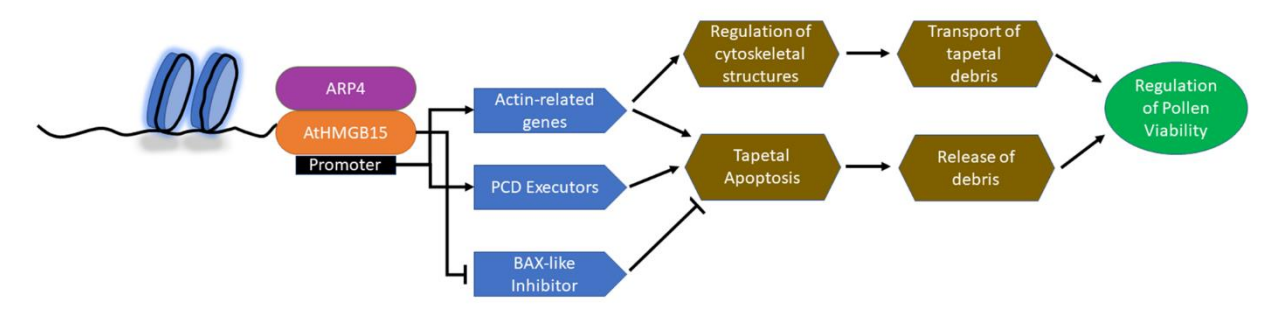
The flower transcriptome (stage 13) identified enrichment of biological processes terms related to programmed cell death, negative regulation of PCD, and pollen tube germination while the analysis of bud transcriptome (stage 8-11 of anther development) highlighted GO terms corresponding to actin binding along with programmed cell death, negative regulation of PCD, and pollen maturation. These findings were indicative of a defective pollen development and pollen tube germination pathway in athmgb15. The significantly lowered anther wax component in the mutant was the first experimental proof towards an abnormal tapetal function that was supported by the promoter study of phenylpropanoid pathway regulators MYB21 and MYB24 in presence of AtHMGB15. The prolonged tapetal degradation observed in athmgb15 from TUNEL assay, was also contingent with the downregulation of PCD executer genes like CEP1, MC9, RNS3 and BFN1 observed in the bud transcriptome and q-RTPCR validation studies. The ChIP data also shows a significant fold change in the occupancy of AtHMGB15 in the promoter region of the anti-apoptotic regulator Bax Inhibitor 1 and other PCD executer genes like CEP1, MC9, RNS3, inferring a regulatory role of AtHMGB15 in tapetal cell death. Interestingly, ROS is an evolutionarily conserved signal for PCD initiation, the lowered ROS content observed from the DCFH-DA study is a strong rationale for an inadequate cue to initiate PCD signalling in tapetal cells of athmgb15. With the initiation of PCD signalling, the cells release the PCD executers

SUMMARY OF THE THESIS

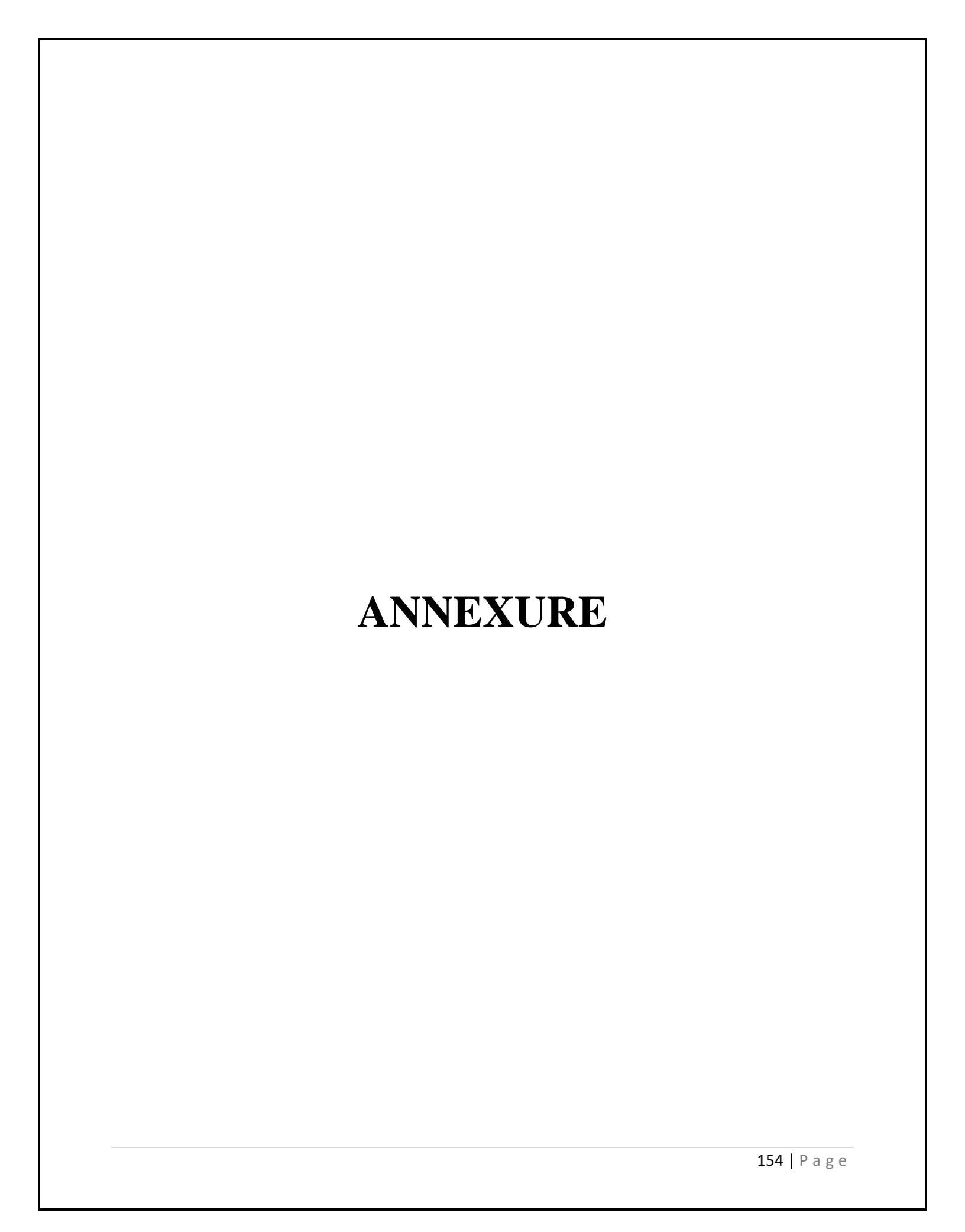
(enzymes). These enzymes like CEP1 and VPEs are mostly processed in vacuoles for storage and maturation, prior to their release. The vacuoles in the cells destined to undergo PCD exhibit a gradual increase in their size before rupturing their tonoplasts. The FM4-64FX staining results showed that the vacuoles in the tapetal cells of *athmgb15* did not show any significant change in their volume compared to wild type. However, actin cytoskeleton dynamics has been known to influence the change in vacuole shape and subsequent structural loss of the cells undergoing PCD. The timely breakdown of tapetal cells ensures normal pollen wall development and pollen maturation that is reflected in normal pollen tube germination and elongation.

The pollen tube germination study in *athmgb15* showed a retarded germination rate. Fascinatingly, rhodamine phalloidin stained actin filaments in germinated pollen tubes of *athmgb15* showed an inconsistent distribution of f-actin compared to the observations made in wild type. This study was further corroborated by the identification of another nuclear protein ARP4 that interacted with AtHMGB15 to regulate transcription of developmental genes and the loss of either proteins resulted in partial male sterility. The TUNEL assay performed in *arp4* mutants demonstrated prolonged tapetal PCD along with the downregulation of PCD genes from the q-RTPCR study. Finally, the f-actin visualisation in germinated pollen tubes of *arp4* also showed similar f-actin distribution as observed in *athmgb15*.

The thesis thus, summarises the instrumental role of AtHMGB15, a transcriptional co activator during the development, function and degradation of tapetal cells by interacting with different transcription factors and genes. The thesis also conclusively proves the effects of a defective tapetum function and degradation on the later stages of pollen and an outlook on its relevance to the study of sexual reproduction in plants.



Proposed model for the study elucidating the role of AtHMGB15 in the regulation of pollen viability mediated by tapetum.



Annexure 1

BUD NGS Validation primers Actin Myosin Binding Cluster

BUD NGS Validation primers		
Actin Myosin I	Binding Cluster	
GENE ID	GENE NAME	Sequence
AT2G33240	Myosin XI D	AGC TGC AAA GGG GAT GCT G
		GGA TCA AAA TGT ATC TCC AGA CGT G
AT2G31900	Myosin XI F	TGG TGT CTT CTC CAT TCC CTC TG
		CAA AAC ATG AGA AGA GAA GCT GC
AT4G29340	Profilin 4	CGC CAA CTT CCC TCA GTT C
		TTA TGC CTC CTG CTC CCT
AT2G41740	vilin 2	CTT CTT CAT CTT TTG CTT CCG TC
		TTA AAC GAA AGT CAC GAC GGC
AT2G29890	vilin like 1	ATG TGA GGT CGC GAC TAT CGA G
		ATG GAG TCT GAG TTT GTT CTT GGG
AT3G58160	Myosin XI J	AAG AAC AAT TCC AGC CG
		GAG GAG CAC ACA GG
AT5G59890	ADF4	TTG TTG CTG CTG CC
		CAT CAA GAT CCA TCT CAG TTG G
AT5G45280	Myosin 2	CAG CTT CAA ACC GTT CAA GG
		CGT ATT CGC GAC TGT GGG
AT3G19960	Myosin 1	GAA CTG ATA CTG CTG CTG G
		AGT TGA ATC CAA GAT TGC AGT ATC
AT3G50530	CDPK related	TAT TGT GTG GAA GCC GAC CG
	Kinase (CRK)	
	1000	AGT CCT TTA TCC ATG GAT GAC T
-	or and TC specfic T	
AT1G06280	LBD2	TCC CAA CCA ATG AGA GGC TG
151 C 1 12 T 2	1 (77) 10 /	ACG GTA CGT GAA GAG GAC C
AT1G14350	MYB124	GAC AAT CAA TTA TCT TGG AGG C
155 C 15100	D.1.1	TCA TCA GGA TTT TTC GGG ACG
AT5G47120	BI1	CGT TCA GAA TCA TCT TAA ACG GG
4F 4G 02 60 0	DII C II	AAG GAG GAC ATG AAA GGA GCC
AT4G02690	BII family	ATG TGC CTT CAC CAA TGG G
	protein	
Cnowen allenia	 biosynthesis genes	AAG GCG AAG AAA ATA AGC ACG G
AT2G29940	ABCG31	AGA TTG ATG CGT TTA TGA AGG C
A12U2994U	ADCUSI	AAC TCT TTT CCT TTG ACC TCC
AT5G40260	RUPTURED	ATC GAT TAC TAC GTC CTC GC
A13U4U2UU	POLLEN	ATO GAT TAC TAC GTC CTC GC
	GRAIN1	
	OIMIIVI	

	CTA AAC CCT CTC CGT AGC AG	
CYCLIN-	TTA TGG CCT CGT CAA AGG	
KINASE G1		
	ACG CTC TGT TAT CAA TGT TGG	
iosis and Mitosis	,	
CDK	TTG CTG ATT TTG GTC AGG C	
activating		
factor like AIC		
	TGA CCA TCA GAC CCT TGC	
CYCB1;5	TCC AAG AGA GAG TTG CAG G	
	AAG GAA GAC GTA TTG AGT CGG	
APC11	ATG GCA TGC AGT TGC TTC ATG	
	GTT GCA GGC TCC CCA AAT	
CDC20.5	ACC AGT TGC AAG CAA ACT CG	
	AGT CAA GAG TAG GAT CAT TGG C	
MEI2 like	AGA AGC ATC TTC GAA GTG TAC T	
protein 1		
•	AGG GTC ATT TGA CTC GCC	
CEP1	ACAATACAGAGCAGACATGG	
	ACAAGAGAAGAGCATTTGTC	
MC9	GCATTAATAAGTCAAGAGTAAGCC	
	GTGTTGTGGTTTTGGAGC	
RNS3	CAATGTTTTAGAGCTAGCCG	
	GAGAAACAAGGATCTTTAAGTGG	
BI 1	TAG ACG ATA TGA AAA TGT CCT TGG	
	AAT AAG AAT CAT CCA CGT GG	
CACC GTC GA	C ATG TAC GGC GGA GAT GAA GTG TCA GC	
CTGCAG TTA	AGG GCA TTT TCT CTG AAT GTA GG	
pecific conform	ation primers:	
GGA TTT CAG	TAT TTG TTC GGC TGT	
TACTCACTT	CGA GTT GTG GG	
	iosis and Mitosis CDK activating factor like AIC CYCB1;5 APC11 CDC20.5 ME12 like protein 1 CEP1 MC9 RNS3 BI 1 CACC GTC GA CTGCAG TTA A	

Annexure 2
List of differentially expressed genes in *athmgb15* bud transcriptome

At ID	Protein Name	log2FoldChange	p-value
AT1G02350	protoporphyrinogen oxidase-like protein	-2.086965321	0.029054753
AT1G02300	Cysteine proteinases superfamily protein	-8.574012166	0.018190667
AT1G03830	guanylate-binding family protein	-9.061124499	0.015587013
AT1G03905	P-loop containing nucleoside triphosphate hydrolases superfamily protein	-2.455851072	0.012968914
AT1G04170	eukaryotic translation initiation factor 2 gamma subunit	-3.052253629	0.002461215
AT1G04270	cytosolic ribosomal protein S15	-12.89076602	0.000968389
AT1G04650	holliday junction resolvase	-3.602914676	0.009202231
AT1G04640	lipoyltransferase 2	-2.286490324	0.049740903
AT1G04880	HMG (high mobility group) box protein with ARID/BRIGHT DNA-binding domain-containing protein	-6.424924679	0.000148984
AT1G05870	hypothetical protein (DUF1685)	-5.890625948	0.001876132
AT1G06148	hypothetical protein AT1G06148	-5.127579751	0.00122127
AT1G06630	F-box/RNI-like superfamily protein	-9.501588165	0.014966196
AT1G08630	threonine aldolase 1	-6.882353275	0.042053355
AT1G09470	myosin heavy chain, cardiac protein	-6.471093251	6.04528E-05
AT1G09880	Rhamnogalacturonate lyase family protein	-7.465481446	0.034098365
AT1G09880	Rhamnogalacturonate lyase family protein	-2.558492177	0.044538563
AT1G10670	ATP-citrate lyase A-1	-2.096161784	1.90851E-10
AT1G10920	NB-ARC domain-containing disease resistance protein	-8.755191176	0.019079434
AT1G11340	G-type lectin S-receptor-like Serine/Threonine-kinase	-6.193506163	0.003672184
AT1G11360	Adenine nucleotide alpha hydrolases-like superfamily protein	-6.941453801	0.040305646
AT1G11400	partner of Y14-MAGO	-5.010022318	0.012571242
AT1G12845	transmembrane protein	-4.313072366	8.18373E-08
AT1G13570	F-box/RNI-like superfamily protein	-3.048548841	0.03292591
AT1G14350	Duplicated homeodomain-like superfamily protein	-2.389285307	0.006656512
AT1G15240	phox (PX) domain-containing protein	-3.469775348	0.008063166
AT1G15250	Zinc-binding ribosomal protein family protein	-5.481820283	0.00137261
AT1G15400	hypothetical protein AT1G15400	-8.124542426	0.024619885
AT1G16240	syntaxin of plants 51	-2.610450338	0.005608603
AT1G16360	LEM3 (ligand-effect modulator 3) family protein / CDC50 family protein	-5.362877385	0.000123133
AT1G16710	histone acetyltransferase of the CBP family 12	-2.684037479	0.002377358
AT1G17350	NADH:ubiquinone oxidoreductase intermediate-associated protein 30	-8.369652912	0.02520769
AT1G17610	Disease resistance protein (TIR-NBS class)	-4.685258892	0.002228902
AT1G18670	Protein kinase superfamily protein	-2.688505162	0.010550207
AT1G18700	DNAJ heat shock N-terminal domain-containing protein	-3.435822543	0.006307242
AT1G18720	ER membrane protein, putative (DUF962)	-6.33265309	0.003380803
AT1G18750	AGAMOUS-like 65	-3.649108771	5.62966E-15
AT1G19210	Integrase-type DNA-binding superfamily protein	-2.215749701	2.54021E-06

AT1G20270	2-oxoglutarate (2OG) and Fe(II)-dependent oxygenase superfamily protein	-2.855380137	0.012749897
AT1G21470	hypothetical protein AT1G21470	-2.500833264	0.047354597
AT1G21560	hypothetical protein AT1G21560	-2.133660063	0.003958155
AT1G21780	BTB/POZ domain-containing protein	-12.25178057	0.001712859
AT1G22300	general regulatory factor 10	-6.179795946	3.83352E-05
AT1G24265	bZIP transcription factor, putative (DUF1664)	-3.083389941	0.00292525
AT1G25380	NAD+ transporter 2	-10.83270504	0.005560383
AT1G27170	transmembrane receptors / ATP binding protein	-4.401531009	0.017186486
AT1G27695	glycine-rich protein	-3.180572977	0.014029479
AT1G28280	VQ motif-containing protein	-3.489165477	0.000150677
AT1G28560	snRNA activating complex family protein	-9.123737536	1.21139E-07
AT1G29120	Hydrolase-like protein family	-3.689162775	0.023235898
AT1G29310	SecY protein transport family protein	-4.559355733	0.009901445
AT1G29330	ER lumen protein retaining receptor family protein	-3.051365814	0.033280898
AT1G29730	Leucine-rich repeat transmembrane protein kinase	-4.953159148	0.04038557
AT1G31200	phloem protein 2-A9	-2.089243986	0.046050049
AT1G32230	WWE protein-protein interaction domain protein family	-5.170237481	0.020193355
AT1G32230	WWE protein-protein interaction domain protein family	-2.122656641	0.003780303
AT1G33330	Class I peptide chain release factor	-7.130405611	2.98463E-07
AT1G33400	Tetratricopeptide repeat (TPR)-like superfamily protein	-6.705876568	0.047811701
AT1G33720	cytochrome P450, family 76, subfamily C, polypeptide 6	-6.834985009	0.042620482
AT1G33720	cytochrome P450, family 76, subfamily C, polypeptide 6	-2.686159243	0.002173769
AT1G34220	Regulator of Vps4 activity in the MVB pathway protein	-3.539926343	0.036367159
AT1G36070	Transducin/WD40 repeat-like superfamily protein	-3.669924716	0.005215152
AT1G44170	aldehyde dehydrogenase 3H1	-2.5129809	0.031089321
AT1G45545	WEAK CHLOROPLAST MOVEMENT UNDER BLUE LIGHT-like protein (DUF827)	-8.838000342	0.015868101
AT1G47330	methyltransferase, putative (DUF21)	-2.538111079	0.033056858
AT1G48030	mitochondrial lipoamide dehydrogenase 1	-2.85491883	0.000196134
AT1G48590	Calcium-dependent lipid-binding (CaLB domain) family protein	-3.848301341	0.000431652
AT1G49400	Nucleic acid-binding, OB-fold-like protein	-9.005479558	0.016584231
AT1G49980	DNA/RNA polymerases superfamily protein	-7.544833525	3.76123E-09
AT1G49980	DNA/RNA polymerases superfamily protein	-3.566411297	0.042785008
AT1G50690	Cystatin/monellin superfamily protein	-2.831959186	0.043477259
AT1G51340	MATE efflux family protein	-7.872005053	0.028375944
AT1G52315	Regulator of Vps4 activity in the MVB pathway protein	-5.208504	0.04490253
AT1G52870	Peroxisomal membrane 22 kDa (Mpv17/PMP22) family protein	-2.240128	0.04894366
AT1G53310	phosphoenolpyruvate carboxylase 1	-2.548795	4.37952E-11
AT1G53800	muscle M-line assembly protein	-4.447713	0.04892727
AT1G54650	Methyltransferase family protein	-2.751017	0.04409858
AT1G54730	Major facilitator superfamily protein	-2.258801	1.01067E-05
AT1G54730	Major facilitator superfamily protein	-2.13965	2.84798E-05
AT1G55540	Nuclear pore complex protein	-4.159657	0.0490913

AT1G58350	Putative serine esterase family protein	-2.61492	0.009615569
AT1G59560	E3 Ubiquitin ligase family protein	-2.790334	0.00911313
AT1G60640	stress response protein	-6.392472	0.000231758
AT1G61370	S-locus lectin protein kinase family protein	-2.098912	0.03288206
AT1G63010	Major Facilitator Superfamily with SPX (SYG1/Pho81/XPR1) domain-containing protein	-6.758447	0.04426702
AT1G63770	Peptidase M1 family protein	-5.116777	0.01381839
AT1G64253	DEK carboxy-terminal domain protein	-2.159698	0.03022028
AT1G65310	xyloglucan endotransglucosylase/hydrolase 17	-6.840695	0.04379677
AT1G67300	Major facilitator superfamily protein	-3.30708	0.04568711
AT1G67520	lectin protein kinase family protein	-2.787263	0.02050373
AT1G68526	hypothetical protein AT1G68526	-2.639448	0.03881626
AT1G69280	hypothetical protein AT1G69280	-2.026947	0.006507605
AT1G69310	WRKY DNA-binding protein 57	-2.093063	0.04532457
AT1G69820	gamma-glutamyl transpeptidase 3	-2.305081	0.01512362
AT1G69800	Cystathionine beta-synthase (CBS) protein	-7.296209	0.0340704
AT1G70490	Ras-related small GTP-binding family protein	-2.891451	3.5921E-05
AT1G71290	F-box associated ubiquitination effector family protein	-4.401283	0.001487066
AT1G72700	ATPase E1-E2 type family protein / haloacid dehalogenase-like hydrolase family protein	-8.394604	0.01979195
AT1G73130	mucin	-9.407476	0.01419184
AT1G73350	ankyrin repeat protein	-3.258691	0.003193066
AT1G77150	Pentatricopeptide repeat (PPR) superfamily protein	-4.595133	0.000715801
AT1G77170	Tetratricopeptide repeat (TPR)-like superfamily protein	-2.816637	0.01756971
AT1G77880	Galactose oxidase/kelch repeat superfamily protein	-3.089198	0.01115372
AT1G78730	FBD, F-box, Skp2-like and Leucine Rich Repeat domains containing protein	-3.748434	0.0273042
AT1G79520	Cation efflux family protein	-2.539219	6.23815E-07
AT1G79650	Rad23 UV excision repair protein family	-7.428711	0.03801671
AT2G01320	ABC-2 type transporter family protein	-11.14581	0.00433342
AT2G01320	ABC-2 type transporter family protein	-9.692861	0.01127936
AT2G01320	ABC-2 type transporter family protein	-8.509517	0.0190689
AT2G01320	ABC-2 type transporter family protein	-2.444345	0.01655602
AT2G01830	CHASE domain containing histidine kinase protein	-10.10039	3.58189E-13
AT2G02340	phloem protein 2-B8	-3.853646	0.008204863
AT2G02930	glutathione S-transferase F3	-3.760595	0.01033186
AT2G02960	RING/FYVE/PHD zinc finger superfamily protein	-6.6346	0.04946117
AT2G03140	alpha/beta-Hydrolases superfamily protein	-2.909118	0.02271438
AT2G03590	ureide permease 1	-7.419388	0.03193863
AT2G04040	MATE efflux family protein	-2.033871	0.003800627
AT2G04030	Chaperone protein htpG family protein	-28.16449	5.63101E-13
AT2G05440	GLYCINE RICH PROTEIN 9	-6.652318	0.00190713
AT2G10950	BSD domain-containing protein	-8.166436	0.0221482
AT2G16980	Major facilitator superfamily protein	-6.315279	1.5798E-06

AT2G16940	Splicing factor, CC1-like protein	-2.55745	0.01104499
AT2G17030	F-box SKIP23-like protein (DUF295)	-2.822255	0.002853413
AT2G17670	Tetratricopeptide repeat (TPR)-like superfamily protein	-6.904166	0.04358413
AT2G17850	Rhodanese/Cell cycle control phosphatase superfamily protein	-4.444143	0.002081429
AT2G18300	basic helix-loop-helix (bHLH) DNA-binding superfamily protein	-7.622117	4.89108E-06
AT2G18540	RmlC-like cupins superfamily protein	-7.828258	0.02875703
AT2G20940	transmembrane protein, putative (DUF1279)	-11.17864	8.78203E-05
AT2G21590	Glucose-1-phosphate adenylyltransferase family protein	-6.690065	0.04603256
AT2G21590	Glucose-1-phosphate adenylyltransferase family protein	-7.664128	0.02959671
AT2G23060	Acyl-CoA N-acyltransferases (NAT) superfamily protein	-3.710007	0.000157804
AT2G25290	Octicosapeptide/Phox/Bem1p (PB1) domain-containing protein / tetratricopeptide repeat (TPR)-containing protein	-7.275227	0.03449724
AT2G25470	receptor like protein 21	-6.91309	0.04105132
AT2G25530	AFG1-like ATPase family protein	-2.177417	0.002032884
AT2G26350	peroxin 10	-5.076946	0.006675453
AT2G26530	AR781, pheromone receptor-like protein (DUF1645)	-7.554986	0.03240155
AT2G27120	DNA polymerase epsilon catalytic subunit	-4.092564	0.03728484
AT2G27220	BEL1-like homeodomain 5	-8.565503	6.13828E-11
AT2G27930	PLATZ transcription factor family protein	-2.199345	0.00065477
AT2G28310	trimethylguanosine synthase (DUF707)	-8.295789	0.02333403
AT2G28470	beta-galactosidase 8	-2.696757	0.000679946
AT2G29300	NAD(P)-binding Rossmann-fold superfamily protein	-2.409941	0.02544849
AT2G29480	glutathione S-transferase tau 2	-2.862651	0.02249803
AT2G29890	villin-like 1	-4.331067	0.01760673
AT2G30480	hypothetical protein AT2G30480	-4.859394	0.04226052
AT2G30740	Protein kinase superfamily protein	-3.74932	0.003804839
AT2G31370	Basic-leucine zipper (bZIP) transcription factor family protein	-8.056477	0.02464786
AT2G31750	UDP-glucosyl transferase 74D1	-5.361338	0.000988029
AT2G31830	endonuclease/exonuclease/phosphatase family protein	-8.78907	0.0162565
AT2G31900	myosin-like protein XIF	-2.296391	0.04221411
AT2G32580	transmembrane protein, putative (DUF1068)	-3.828129	0.02508427
AT2G33240	myosin XI D	-7.439557	5.13799E-05
AT2G34450	HMG-box (high mobility group) DNA-binding family protein	-2.560313	1.03198E-14
AT2G35390	Phosphoribosyltransferase family protein	-9.952646	5.47207E-08
AT2G35840	Sucrose-6F-phosphate phosphohydrolase family protein	-8.607419	0.0177941
AT2G36290	alpha/beta-Hydrolases superfamily protein	-8.071715	0.0374304
AT2G36360	Galactose oxidase/kelch repeat superfamily protein	-4.540505	0.000988418
AT2G37860	reticulata-like protein, putative (DUF3411)	-7.160064	0.04631081
AT2G37860	reticulata-like protein, putative (DUF3411)	-6.902392	0.04340986
AT2G39300	CAP-gly domain linker	-7.987586	0.02564306
AT2G39320	Cysteine proteinases superfamily protein	-5.412369	1.76784E-05
AT2G39690	ternary complex factor MIP1 leucine-zipper protein (Protein of unknown function, DUF547)	-3.253762	0.004317195

AT2G39690	ternary complex factor MIP1 leucine-zipper protein (Protein of unknown function, DUF547)	-3.516769	0.01785941
AT2G39740	Nucleotidyltransferase family protein	-2.354292	0.02657943
AT2G39800	delta1-pyrroline-5-carboxylate synthase 1	-9.337773	0.01409276
AT2G40711	hypothetical protein AT2G40711	-2.127235	0.04304898
AT2G41070	Basic-leucine zipper (bZIP) transcription factor family protein	-4.973696	0.000340031
AT2G41510	cytokinin oxidase/dehydrogenase 1	-4.23398	2.40974E-08
AT2G41430	dehydration-induced protein (ERD15)	-7.553892	0.03320661
AT2G41740	villin 2	-9.757321	1.35802E-05
AT2G43710	Plant stearoyl-acyl-carrier-protein desaturase family protein	-3.609883	0.02360657
AT2G45290	Transketolase	-8.769967	3.39411E-13
AT2G45720	ARM repeat superfamily protein	-6.25626	0.02285966
AT2G46420	helicase with zinc finger protein	-2.437101	0.00257528
AT2G47350	HIT zinc finger and PAPA-1-like domain-containing protein	-6.766908	0.04829722
AT2G47650	UDP-xylose synthase 4	-3.562152	0.007157698
AT3G01345	Expressed protein	-2.315658	0.04982114
AT3G01810	EEIG1/EHBP1 protein amino-terminal domain protein	-5.22123	0.000248537
AT3G01990	ACT domain repeat 6	-5.439116	0.007441406
AT3G02875	Peptidase M20/M25/M40 family protein	-2.266105	0.004378788
AT3G02875	Peptidase M20/M25/M40 family protein	-2.64826	0.03166179
AT3G05250	RING/U-box superfamily protein	-2.78096	0.01193503
AT3G05760	C2H2 and C2HC zinc fingers superfamily protein	-7.028368	0.04370558
AT3G05870	anaphase-promoting complex/cyclosome 11	-6.819181	0.04541359
AT3G06630	protein kinase family protein	-4.989847	0.001384223
AT3G07330	Cellulose-synthase-like C6	-8.217457	0.0234663
AT3G07590	Small nuclear ribonucleoprotein family protein	-2.601426	0.02027601
AT3G07760	Sterile alpha motif (SAM) domain-containing protein	-8.213588	0.02185845
AT3G09020	alpha 1,4-glycosyltransferase family protein	-2.71261	0.000846876
AT3G10840	alpha/beta-Hydrolases superfamily protein	-6.386526	0.01389893
AT3G11040	Glycosyl hydrolase family 85	-2.456651	0.02288562
AT3G12080	GTP-binding family protein	-9.936105	0.009085705
AT3G12400	Ubiquitin-conjugating enzyme/RWD-like protein	-7.864718	0.0273802
AT3G12700	Eukaryotic aspartyl protease family protein	-7.262537	0.03496392
AT3G13065	STRUBBELIG-receptor family 4	-2.121642	0.008925066
AT3G13110	serine acetyltransferase 2;2	-3.366424	0.025236
AT3G13930	Dihydrolipoamide acetyltransferase, long form protein	-6.218507	5.23987E-06
AT3G15430	Regulator of chromosome condensation (RCC1) family protein	-2.546451	0.02227831
AT3G15840	post-illumination chlorophyll fluorescence increase	-2.835209	0.038561
AT3G17120	transmembrane protein	-8.675713	0.02328547
AT3G17970	translocon at the outer membrane of chloroplasts 64-III	-4.261394	0.01580314
AT3G18100	myb domain protein 4r1	-4.04682	0.03609517
AT3G18535	tubulin-tyrosine ligase	-2.396814	0.02494201
AT3G18535	tubulin-tyrosine ligase	-2.680907	0.009147303

AT3G18840	LOW protein: PPR containing-like protein	-3.194622	0.03182522
AT3G20380	TRAF-like family protein	-5.008368	0.000268887
AT3G20020	protein arginine methyltransferase 6	-2.244307	0.00478362
AT3G20320	trigalactosyldiacylglycerol2	-2.620839	0.000430949
AT3G22460	O-acetylserine (thiol) lyase (OAS-TL) isoform A2	-3.295753	0.03118403
AT3G23350	ENTH/VHS family protein	-2.304356	0.003763292
AT3G23490	cyanase	-2.494205	0.000030685
AT3G23540	alpha/beta-Hydrolases superfamily protein	-2.778185	0.0181047
AT3G24515	ubiquitin-conjugating enzyme 37	-2.376678	0.02885591
AT3G24590	plastidic type i signal peptidase 1	-2.106268	0.03814208
AT3G25530	glyoxylate reductase 1	-3.631713	0.00721444
AT3G25800	protein phosphatase 2A subunit A2	-2.686612	6.09634E-05
AT3G27010	TEOSINTE BRANCHED 1, cycloidea, PCF (TCP)-domain family protein 20	-9.542992	0.01106747
AT3G27440	uridine kinase-like 5	-4.805735	0.02130362
AT3G28770	transmembrane protein, putative (DUF1216)	-8.051549	0.02406699
AT3G29010	Biotin/lipoate A/B protein ligase family	-2.107511	0.000499048
AT3G44070	Glycosyl hydrolase family 35 protein	-6.069236	7.13671E-05
AT3G44350	NAC domain containing protein 61	-4.877605	0.000435503
AT3G44340	hypothetical protein AT3G44340	-4.724894	0.009283114
AT3G44340	hypothetical protein AT3G44340	-3.613928	0.006225457
AT3G45000	SNF7 family protein	-4.980791	0.001152625
AT3G45100	UDP-Glycosyltransferase superfamily protein	-2.067147	0.02113541
AT3G45440	Concanavalin A-like lectin protein kinase family protein	-2.598105	0.03612092
AT3G45140	lipoxygenase 2	-3.531815	0.03366272
AT3G46130	myb domain protein 48	-6.173763	0.000428888
AT3G46940	DUTP-PYROPHOSPHATASE-LIKE 1	-4.330012	0.02529628
AT3G47660	Regulator of chromosome condensation (RCC1) family protein	-7.329966	0.03350459
AT3G49870	ADP-ribosylation factor-like A1C	-2.5086	0.04369091
AT3G50040	hypothetical protein AT3G50040	-4.966581	0.000474845
AT3G50040	hypothetical protein AT3G50040	-8.337084	6.94746E-08
AT3G50420	Pentatricopeptide repeat (PPR) superfamily protein	-8.488068	0.0298565
AT3G50530	CDPK-related kinase	-10.67885	0.006185588
AT3G50790	esterase/lipase/thioesterase family protein	-2.401439	0.01256797
AT3G51150	ATP binding microtubule motor family protein	-2.484443	0.01511184
AT3G51580	transmembrane protein	-3.923325	0.006827339
AT3G52120	SWAP (Suppressor-of-White-APricot)/surp domain-containing protein / D111/G-patch domain-containing protein	-3.718702	0.002316014
AT3G52690	RNI-like superfamily protein	-5.083033	0.000113259
AT3G52990	Pyruvate kinase family protein	-2.987547	0.008742855
AT3G53570	serine/threonine-protein kinase AFC1	-3.929	0.04457061
AT3G53780	RHOMBOID-like protein 4	-7.026621	0.04198264
AT3G54830	Transmembrane amino acid transporter family protein	-6.021149	0.02831863
AT3G55510	Noc2p family	-4.346323	0.03349199

AT3G55630	DHFS-FPGS homolog D	-3.521605	0.007224539
AT3G56500	serine-rich protein-like protein	-2.131922	0.03357579
AT3G56510	RNA-binding (RRM/RBD/RNP motifs) family protein	-8.713296	0.01806895
AT3G57780	nucleolar-like protein	-7.056581	2.04974E-08
AT3G58290	TRAF-like superfamily protein	-3.244631	0.002022757
AT3G59210	F-box/RNI-like superfamily protein	-7.080996	0.04008387
AT3G59850	Pectin lyase-like superfamily protein	-7.518668	0.03241734
AT3G60330	0	-9.012418	0.01798069
AT3G60590	cytochrome P450 family protein	-3.852016	0.008444187
AT3G60590	cytochrome P450 family protein	-3.775252	0.009697076
AT3G60960	Tetratricopeptide repeat (TPR)-like superfamily protein	-10.66947	0.006317327
AT3G62150	P-glycoprotein 21	-10.407	1.92005E-13
AT3G62020	germin-like protein 10	-3.691093	0.0038843
AT4G00560	NAD(P)-binding Rossmann-fold superfamily protein	-4.427374	0.002915416
AT4G00670	Remorin family protein	-2.384397	0.04942676
AT4G00800	transducin family protein / WD-40 repeat family protein	-9.868126	0.01040656
AT4G00940	Dof-type zinc finger DNA-binding family protein	-9.43932	0.01276191
AT4G01100	adenine nucleotide transporter 1	-2.491838	1.26692E-05
AT4G01240	S-adenosyl-L-methionine-dependent methyltransferases superfamily protein	-5.039788	0.000913433
AT4G01450	nodulin MtN21 /EamA-like transporter family protein	-7.721149	0.0419135
AT4G01810	Sec23/Sec24 protein transport family protein	-7.530133	0.03218619
AT4G02140	hypothetical protein AT4G02140	-2.847072	0.01509601
AT4G02430	RNA-binding (RRM/RBD/RNP motifs) family protein	-2.793331	0.01906621
AT4G03505	hypothetical protein AT4G03505	-2.590479	0.00190332
AT4G08470	MAPK/ERK kinase kinase 3	-2.300876	0.01902078
AT4G09300	LisH and RanBPM domains containing protein	-2.946842	0.02643335
AT4G10430	TMPIT-like protein	-4.675285	0.001214222
AT4G11810	Major Facilitator Superfamily with SPX (SYG1/Pho81/XPR1) domain-containing protein	-2.780397	0.03629133
AT4G11900	S-locus lectin protein kinase family protein	-3.20099	0.006152626
AT4G12030	bile acid transporter 5	-7.063782	0.04100349
AT4G12250	UDP-D-glucuronate 4-epimerase 5	-11.53583	0.003150346
AT4G12990	transmembrane protein	-2.930482	0.02201531
AT4G13330	S-adenosyl-L-methionine-dependent methyltransferases superfamily protein	-7.620894	0.03077224
AT4G13572	hypothetical protein AT4G13572	-5.250764	0.001215542
AT4G13660	pinoresinol reductase 2	-6.952917	2.56423E-06
AT4G15563	F-box-like protein	-5.505215	0.00935141
AT4G15563	F-box-like protein	-5.635042	0.02774658
AT4G15955	alpha/beta-Hydrolases superfamily protein	-6.812333	2.95168E-06
AT4G16566	histidine triad nucleotide-binding 4	-5.20656	8.07515E-05
AT4G16920	Disease resistance protein (TIR-NBS-LRR class) family	-8.754508	0.000380823
AT4G19070	Putative membrane lipoprotein	-2.591208	0.03342599

17/1//20210	Peptidase M50 family protein	-6.887008	0.04474646
	cysteine-rich repeat secretory-like protein	-2.350001	1.16082E-08
	cysteine-rich repeat secretory-like protein	-2.329452	1.37739E-08
	cysteine-rich repeat secretory-like protein	-2.190329	2.06179E-06
		-2.571404	
	cysteine-rich repeat secretory-like protein		1.25153E-07
	cysteine-rich repeat secretory-like protein	-2.275128	0.000127084
	cysteine-rich repeat secretory-like protein (DUF26 and DUF1204)	-2.189737	1.04102E-05
	cysteine-rich repeat secretory-like protein (DUF26 and DUF1204)	-2.443356	5.51338E-06
	cysteine-rich repeat secretory-like protein (DUF26 and DUF1204)	-2.24476	3.58193E-05
	cysteine-rich repeat secretory-like protein (DUF26 and DUF1204)	-2.224754	8.30352E-06
	cysteine-rich repeat secretory-like protein (DUF26 and DUF1204)	-2.090103	9.58674E-05
	cysteine-rich receptor-like kinase	-2.361987	4.43473E-05
AT4G20670	cysteine-rich repeat secretory-like protein	-2.440535	3.90547E-06
AT4G20703	hypothetical protein AT4G20703	-4.011491	0.005920033
	vacuolar protein sorting-associated protein-like protein	-2.188436	0.000531648
AT4G23250	cysteine-rich receptor-like protein kinase 17	-4.266359	0.01945618
AT4G23460	Adaptin family protein	-5.007011	0.009557048
AT4G23570	phosphatase-like protein	-6.534913	0.01657936
AT4G24480	Protein kinase superfamily protein	-9.515765	6.44662E-11
	Rho GTPase activation protein (RhoGAP) with PH domain- containing protein	-9.171809	5.28677E-07
	phosphoglucose isomerase 1	-8.583146	0.02045854
AT4G24680	modifier of snc1	-2.466634	0.04343025
AT4G26520	Aldolase superfamily protein	-3.297426	0.0196045
AT4G26640	WRKY family transcription factor family protein	-2.003166	0.002745174
AT4G27590	Heavy metal transport/detoxification superfamily protein	-2.175669	0.004201442
AT4G27970	SLAC1 homologue 2	-7.701325	0.02875549
AT4G28070	AFG1-like ATPase family protein	-7.968861	0.02458314
AT4G28220	NAD(P)H dehydrogenase B1	-2.007649	0.000182627
AT4G28980	CDK-activating kinase 1AT	-8.158639	0.02250884
AT4G29340	profilin 4	-4.387608	1.69703E-06
AT4G30020	PA-domain containing subtilase family protein	-9.436412	0.01222596
AT4G30980	LJRHL1-like 2	-2.845675	0.00045684
	cyclin-dependent kinase-activating kinase assembly factor-related / CDK-activating kinase assembly factor-like protein	-2.429913	0.02805333
	Cyclophilin-like peptidyl-prolyl cis-trans isomerase family protein	-11.68613	0.002779237
	demeter-like protein 3	-7.441114	0.04264017
	alpha/beta-Hydrolases superfamily protein	-7.811101	0.02665485
	alpha/beta-Hydrolases superfamily protein	-7.653447	0.03269959
	GTP binding protein beta 1	-6.125698	1.21084E-05
	Protein kinase superfamily protein	-4.151074	0.04801196
	Plant regulator RWP-RK family protein	-8.429571	8.85571E-07
	phospholipase D delta	-9.431982	0.01578357
	aconitase 1	-2.213378	0.005794872

AT4G35920	PLAC8 family protein	-7.365623	0.03305191
AT4G37110	Zinc-finger domain of monoamine-oxidase A repressor R1	-3.867413	3.20846E-05
AT4G37680	heptahelical protein 4	-3.069993	0.01741255
AT4G39280	phenylalanyl-tRNA synthetase, putative / phenylalanine-tRNA ligase	-11.03252	0.004745749
AT4G39420	spatacsin carboxy-terminus protein	-7.395107	0.0496341
AT4G39830	Cupredoxin superfamily protein	-7.602523	0.03295137
AT5G02860	Pentatricopeptide repeat (PPR) superfamily protein	-4.264113	0.01448127
AT5G05000	translocon at the outer envelope membrane of chloroplasts 34	-7.288493	0.03968003
AT5G05590	phosphoribosylanthranilate isomerase 2	-2.69819	0.00211507
AT5G06800	myb-like HTH transcriptional regulator family protein	-4.813384	0.001744282
AT5G06800	myb-like HTH transcriptional regulator family protein	-6.397656	0.000730729
AT5G08110	UBQ, helicase-c and DEAD-like helicase domain-containing protein	-2.586337	2.73682E-05
AT5G08335	Isoprenylcysteine carboxyl methyltransferase (ICMT) family	-4.524314	0.001744886
AT5G09230	sirtuin 2	-2.456336	4.78835E-07
AT5G09900	26S proteasome regulatory subunit, putative (RPN5)	-4.683719	0.00058216
AT5G11350	DNAse I-like superfamily protein	-2.760089	0.000662328
AT5G14660	peptide deformylase 1B	-7.518984	0.03623059
AT5G14890	potassium transporter	-5.209593	0.007178521
AT5G15630	COBRA-like extracellular glycosyl-phosphatidyl inositol- anchored protein family	-3.153419	5.59666E-05
AT5G15900	TRICHOME BIREFRINGENCE-LIKE 19	-6.216091	1.53594E-05
AT5G16030	mental retardation GTPase activating protein	-2.326797	0.02554285
AT5G18500	Protein kinase superfamily protein	-2.764398	0.02700845
AT5G18810	SC35-like splicing factor 28	-2.26354	0.01048566
AT5G19110	Eukaryotic aspartyl protease family protein	-3.621784	0.000283561
AT5G19990	regulatory particle triple-A ATPase 6A	-10.09191	0.009796628
AT5G20360	Octicosapeptide/Phox/Bem1p (PB1) domain-containing protein / tetratricopeptide repeat (TPR)-containing protein	-9.845862	0.01008798
AT5G20570	RING-box 1	-2.777729	0.04799699
AT5G20660	Zn-dependent exopeptidases superfamily protein	-4.105267	0.00885648
AT5G20830	sucrose synthase 1	-9.973095	0.01069546
AT5G21222	protein kinase family protein	-2.040913	2.52282E-05
AT5G21900	RNI-like superfamily protein	-6.197029	7.21465E-08
AT5G23010	methylthioalkylmalate synthase 1	-3.073738	0.004460049
AT5G23010	methylthioalkylmalate synthase 1	-9.674069	5.35258E-12
AT5G24210	alpha/beta-Hydrolases superfamily protein	-7.519876	0.03593587
AT5G24270	Calcium-binding EF-hand family protein	-2.742799	0.02780637
AT5G24630	double-stranded DNA binding protein	-3.690566	0.02894371
AT5G25470	AP2/B3-like transcriptional factor family protein	-2.452268	0.006862986
AT5G25755	hypothetical protein AT5G25755	-4.38838	0.003361925
AT5G25880	NADP-malic enzyme 3	-2.044601	0.01164571
AT5G27860	hypothetical protein AT5G27860	-7.977045	0.000109985
AT5G28237	Pyridoxal-5\\'-phosphate-dependent enzyme family protein	-2.489633	0.004288749

AT5G28530	FAR1-related sequence 10	-7.486677	0.03405284
AT5G35680	Nucleic acid-binding, OB-fold-like protein	-8.667646	5.94646E-11
AT5G35930	AMP-dependent synthetase and ligase family protein	-10.4155	1.14662E-06
AT5G37770	EF hand calcium-binding protein family	-3.979999	0.008825665
AT5G40440	mitogen-activated protein kinase kinase 3	-2.176287	0.008497105
AT5G41610	cation/H+ exchanger 18	-2.006259	0.04455585
AT5G42820	Zinc finger C-x8-C-x5-C-x3-H type family protein	-5.199359	0.000168183
AT5G43730	Disease resistance protein (CC-NBS-LRR class) family	-8.518568	8.61534E-10
AT5G44120	RmlC-like cupins superfamily protein	-2.230064	0.03929974
AT5G44740	Y-family DNA polymerase H	-7.928306	2.61786E-05
AT5G45060	Disease resistance protein (TIR-NBS-LRR class) family	-5.099008	0.02446056
AT5G45500	RNI-like superfamily protein	-8.421997	0.000712593
AT5G45710	winged-helix DNA-binding transcription factor family protein	-8.272584	8.37127E-08
AT5G47300	F-box and associated interaction domains-containing protein	-2.975051	0.04303125
AT5G47710	Calcium-dependent lipid-binding (CaLB domain) family protein	-2.08316	0.01383965
AT5G48140	Pectin lyase-like superfamily protein	-3.972275	2.56474E-11
AT5G48120	ARM repeat superfamily protein	-5.38568	0.04480039
AT5G48370	Thioesterase/thiol ester dehydrase-isomerase superfamily protein	-9.641005	0.01174173
AT5G49940	NIFU-like protein 2	-5.653387	0.000189754
AT5G52230	methyl-CPG-binding domain protein 13	-7.93767	4.10947E-10
AT5G53440	LOW protein: zinc finger CCCH domain protein	-11.32552	0.003745635
AT5G54760	Translation initiation factor SUI1 family protein	-5.571657	0.03619313
AT5G54760	Translation initiation factor SUI1 family protein	-4.713731	0.007333178
AT5G55600	Agenet and bromo-adjacent homology (BAH) domain-containing protein	-7.684631	0.02916002
AT5G57110	autoinhibited Ca2+ -ATPase, isoform 8	-7.706118	0.02952494
AT5G58840	Subtilase family protein	-6.794254	0.04599679
AT5G60610	F-box/RNI-like superfamily protein	-2.034089	0.02059955
AT5G61960	MEI2-like protein 1	-3.280591	0.02999713
AT5G62850	Nodulin MtN3 family protein	-2.159851	1.87151E-14
AT5G63090	Lateral organ boundaries (LOB) domain family protein	-3.907084	0.02161217
AT5G63680	Pyruvate kinase family protein	-2.249505	0.04237108
AT5G65950	trafficking protein particle complex subunit-like protein	-4.729811	1.7973E-06
AT5G66070	RING/U-box superfamily protein	-2.199644	0.03262617
AT5G66550	Maf-like protein	-2.321721	0.04502384
AT5G66600	electron transporter, putative (Protein of unknown function, DUF547)	-3.078195	0.01326759
AT5G66640	DA1-related protein 3	-6.846938	0.04312853
AT5G67420	LOB domain-containing protein 37	-7.90907	0.02551384
AT1G30850	root hair specific 4	-5.546176	0.000354689
AT1G36920	hypothetical protein AT1G36920	-2.316042	0.04794717
AT1G44941	hypothetical protein AT1G44941	-3.281354	0.03083742
AT1G52390	hypothetical protein AT1G52390	-4.724095	0.004509358
AT1G56040	HEAT/U-box protein	-3.041313	0.01757725

AT1G59940	response regulator 3	-5.095131	0.000954528
AT1G60040	AGAMOUS-like 49	-4.645071	0.002977492
AT1G63245	CLAVATA3/ESR-RELATED 14	-2.827545	0.03882555
AT1G66420	DNA-binding storekeeper protein-related transcriptional regulator	-4.614648	0.002189282
AT1G67623	F-box family protein	-5.767576	0.000172075
AT2G19050	GDSL-like Lipase/Acylhydrolase superfamily protein	-5.116338	0.0004127
AT2G24696	transcriptional factor B3 family protein	-5.368502	0.001833493
AT3G21570	proline-rich nuclear receptor coactivator	-2.865857	0.04107484
AT3G22053	cysteine-rich repeat secretory protein	-2.995778	0.005835866
AT3G25577	hypothetical protein AT3G25577	-3.866582	0.006937104
AT3G30580	hypothetical protein AT3G30580	-3.368873	0.001906117
AT3G44235	transmembrane protein	-4.70988	0.000687096
AT3G47790	ABC2 homolog 7	-5.574201	0.000550008
AT3G55810	Pyruvate kinase family protein	-4.860198	0.000271886
AT3G63020	hypothetical protein (DUF3049)	-5.024003	0.000262735
AT4G08770	Peroxidase superfamily protein	-4.000638	0.006752462
AT4G16162	Leucine-rich repeat (LRR) family protein	-6.7999	0.000169998
AT4G23200	cysteine-rich RLK (RECEPTOR-like protein kinase) 12	-4.474634	0.000858802
AT5G14300	prohibitin 5	-5.965896	7.62923E-05
AT5G44380	FAD-binding Berberine family protein	-7.520727	0.03338975
AT5G44575	hypothetical protein AT5G44575	-5.055122	0.005345106
AT5G46930	Plant invertase/pectin methylesterase inhibitor superfamily protein	-2.799615	0.02353838
AT5G54150	hypothetical protein AT5G54150	-5.09882	0.001131249
AT1G01140	CBL-interacting protein kinase 9	6.523267604	0.000248673
AT1G01305	hypothetical protein AT1G01305	3.788747973	0.007515201
AT1G01700	RHO guanyl-nucleotide exchange factor 2	2.215827908	0.030478274
AT1G02080	transcription regulator	2.698049329	0.004963846
AT1G02310	Glycosyl hydrolase superfamily protein	3.592926009	0.017417906
AT1G02410	cytochrome c oxidase assembly protein CtaG / Cox11 family	2.062491524	9.55843E-05
AT1G02530	P-glycoprotein 12	2.509041408	0.000965316
AT1G03070	Bax inhibitor-1 family protein	5.539494071	0.004353484
AT1G03550	Secretory carrier membrane protein (SCAMP) family protein	2.204248898	0.003404564
AT1G03770	RING 1B	4.560233121	0.002589284
AT1G03920	Protein kinase family protein	3.184376995	0.014065721
AT1G05230	homeodomain GLABROUS 2	2.617589433	0.00762367
AT1G06960	RNA-binding (RRM/RBD/RNP motifs) family protein	5.020616223	0.000193524
AT1G07010	Calcineurin-like metallo-phosphoesterase superfamily protein	3.670747042	0.010346791
AT1G08810	myb domain protein 60	3.107639463	0.001736821
AT1G08820	vamp/synaptobrevin-associated protein 27-2	9.324883818	0.001005792
AT1G08820	vamp/synaptobrevin-associated protein 27-2	2.49632468	0.037958473
AT1G08970	nuclear factor Y, subunit C9	9.496868508	0.010877126
AT1G10170	NF-X-like 1	5.329059584	0.000428472
AT1G11120	CTTNBP 2 amino-terminal-like protein	3.065458074	0.023888232

AT1G11280	S-locus lectin protein kinase family protein	9.196220784	0.01269357
AT1G11362	Plant invertase/pectin methylesterase inhibitor superfamily protein	3.362527786	0.0453513
AT1G11400	partner of Y14-MAGO	5.723474653	6.16935E-06
AT1G11930	Putative pyridoxal phosphate-dependent enzyme, YBL036C type	5.038023529	0.041863327
AT1G12060	BCL-2-associated athanogene 5	2.493910585	0.004505361
AT1G12290	Disease resistance protein (CC-NBS-LRR class) family	2.991996162	0.000517518
AT1G12740	cytochrome P450, family 87, subfamily A, polypeptide 2	3.259038775	0.000886068
AT1G12900	glyceraldehyde 3-phosphate dehydrogenase A subunit 2	4.042469565	0.026492724
AT1G13320	protein phosphatase 2A subunit A3	4.057712876	0.000453394
AT1G13450	Homeodomain-like superfamily protein	3.377871747	0.00991029
AT1G14150	PsbQ-like 2	5.514930479	2.759E-05
AT1G14455	hypothetical protein AT1G14455	2.631532419	0.022795256
AT1G14640	SWAP (Suppressor-of-White-APricot)/surp domain-containing protein	2.351495774	0.042677595
AT1G15772	mediator of RNA polymerase II transcription subunit	2.176871888	0.001319284
AT1G16290	transglycosylase	2.48212011	0.003474084
AT1G16340	Aldolase superfamily protein	7.02729301	0.038815652
AT1G16570	UDP-Glycosyltransferase superfamily protein	6.86976928	0.014421271
AT1G18010	Major facilitator superfamily protein	3.883011135	0.006668709
AT1G18420	aluminum activated malate transporter family protein	7.118531533	0.035461756
AT1G18750	AGAMOUS-like 65	10.92502763	2.0323E-16
AT1G18750	AGAMOUS-like 65	8.537677492	4.06488E-06
AT1G18750	AGAMOUS-like 65	5.245362163	0.001981325
AT1G18860	WRKY DNA-binding protein 61	4.594130585	0.000780014
AT1G19520	pentatricopeptide (PPR) repeat-containing protein	2.578368745	0.02246677
AT1G20830	multiple chloroplast division site 1	2.344621286	0.007999277
AT1G20910	ARID/BRIGHT DNA-binding domain-containing protein	2.570791418	0.029769193
AT1G21000	PLATZ transcription factor family protein	3.987072035	0.012734674
AT1G21080	DNAJ heat shock N-terminal domain-containing protein	3.235040462	0.030304387
AT1G21600	plastid transcriptionally active 6	7.705337694	0.024476192
AT1G21970	Histone superfamily protein	4.586852652	0.001043233
AT1G22120	hypothetical protein AT1G22120	4.241593594	0.000940846
AT1G22530	PATELLIN 2	8.883148495	0.014663416
AT1G22720	Protein kinase superfamily protein	4.193117209	0.000928375
AT1G22920	COP9 signalosome 5A	3.117006808	0.005413872
AT1G23120	Polyketide cyclase/dehydrase and lipid transport superfamily protein	7.520157524	0.041777336
AT1G23090	sulfate transporter 91	2.156862823	0.00207837
AT1G23201	GCK domain protein	2.669853961	0.005464903
AT1G24267	bZIP transcription factor, putative (DUF1664)	2.593189129	0.001571512
AT1G25275	thionin-like protein	2.959336355	0.029311085
AT1G26260	cryptochrome-interacting basic-helix-loop-helix 5	2.487379095	0.013179378
AT1G26440	ureide permease 5	6.691143604	0.041551371
AT1G26796	Plant self-incompatibility protein S1 family	7.828888156	2.97577E-09
	John Marching protein of family	,.02000130	,,,,,,,,,,,,,,,,,,,,,,,,,,,,,,,,,,,,,

AT1G28090	Polynucleotide adenylyltransferase family protein	3.164503532	0.00583435
AT1G28327	E3 ubiquitin-protein ligase	6.963389745	6.41205E-06
AT1G29170	SCAR family protein	9.065936122	6.72737E-12
AT1G30620	NAD(P)-binding Rossmann-fold superfamily protein	2.903473301	0.000493507
AT1G31450	Eukaryotic aspartyl protease family protein	2.689825509	0.001834504
AT1G31540	Disease resistance protein (TIR-NBS-LRR class) family	7.165356611	0.038395612
AT1G32280	Bifunctional inhibitor/lipid-transfer protein/seed storage 2S albumin superfamily protein	3.665569797	0.000102039
AT1G32630	FAM50A-like protein	5.388294348	0.012592721
AT1G33500	tropomyosin	7.083449174	0.043708802
AT1G34120	inositol polyphosphate 5-phosphatase I	2.630673438	0.006148957
AT1G34460	CYCLIN B1;5	2.041819129	0.037559634
AT1G35530	DEAD/DEAH box RNA helicase family protein	9.562501278	3.37105E-06
AT1G36622	transmembrane protein	5.302517979	0.000403991
AT1G36160	acetyl-CoA carboxylase 1	5.136914158	0.011795857
AT1G37150	holocarboxylase synthetase 2	6.349180953	0.049769218
AT1G43130	like COV 2	2.015877015	0.034304824
AT1G43640	tubby like protein 5	9.361699745	0.013627071
AT1G44090	gibberellin 20-oxidase 5	3.225063483	0.028220944
AT1G45190	downregulated in DIF1 18	3.305886847	0.025156204
AT1G45215	ECA1 gametogenesis family protein (DUF784)	7.234413953	2.61307E-05
AT1G45221	Bifunctional inhibitor/lipid-transfer protein/seed storage 2S albumin superfamily protein	6.476290922	0.001124935
AT1G45223	ECA1 gametogenesis family protein (DUF784)	4.872256165	0.004396713
AT1G47450	prolamin-like protein (DUF784)	4.00166416	0.000725798
AT1G47470	ECA1 gametogenesis family protein (DUF784)	3.799379613	0.001419788
AT1G47603	purine permease 19	5.48172496	0.000904623
AT1G48210	Protein kinase superfamily protein	3.055516686	0.000803152
AT1G48360	zinc ion binding/nucleic acid binding/hydrolase	9.169084106	7.78824E-13
AT1G48770	hypothetical protein (DUF1639)	3.235023423	0.028690965
AT1G49160	Protein kinase superfamily protein	7.967864409	0.025320725
AT1G49770	basic helix-loop-helix (bHLH) DNA-binding superfamily protein	8.838787071	2.96814E-11
AT1G50290	hypothetical protein AT1G50290	3.938769376	0.025373215
AT1G50325	Plant invertase/pectin methylesterase inhibitor superfamily protein	4.508541507	0.023220527
AT1G50500	Membrane trafficking VPS53 family protein	2.179772226	0.000493666
AT1G50690	Cystatin/monellin superfamily protein	6.259947937	5.24616E-06
AT1G51270	vesicle-associated protein 1-4	6.320537191	0.047411765
AT1G51790	Leucine-rich repeat protein kinase family protein	2.445259138	0.016614261
AT1G52450	Ubiquitin carboxyl-terminal hydrolase-related protein	8.01811	0.0268995
AT1G52970	downregulated in DIF1 11	2.453634	0.04727139
AT1G53640	transmembrane protein	2.500094	0.01608222
AT1G54300	hypothetical protein AT1G54300	4.991733	0.001632828
AT1G54575	hypothetical protein AT1G54575	3.184926	0.01179361
AT1G54730	Major facilitator superfamily protein	2.113613	0.02626377

AT1G55030	RNI-like superfamily protein	5.982968	3.8115E-06
AT1G55320	acyl-activating enzyme 18	5.024019	9.20121E-05
AT1G55500	evolutionarily conserved C-terminal region 4	2.327307	0.04561782
AT1G55690	Sec14p-like phosphatidylinositol transfer family protein	2.239787	0.02128873
AT1G55915	zinc ion binding protein	2.835836	0.003167977
AT1G56100	Plant invertase/pectin methylesterase inhibitor superfamily protein	5.715225	0.007454224
AT1G56385	Plant self-incompatibility protein S1 family	5.426769	0.003125738
AT1G56415	Expressed protein	5.819068	0.002274704
AT1G57760	ECA1 gametogenesis family protein (DUF784)	6.179371	0.00355286
AT1G57777	ECA1 gametogenesis family protein (DUF784)	3.770673	0.03908623
AT1G58350	Putative serine esterase family protein	11.5534	0.003104996
AT1G58848	Disease resistance protein (CC-NBS-LRR class) family	2.896878	0.002347287
AT1G60200	splicing factor PWI domain-containing protein / RNA recognition motif (RRM)-containing protein	11.12271	1.43972E-13
AT1G60500	Dynamin related protein 4C	3.228465	0.006688375
AT1G61150	LisH and RanBPM domains containing protein	2.3283	0.01072813
AT1G61490	S-locus lectin protein kinase family protein	4.346612	0.02423247
AT1G61560	Seven transmembrane MLO family protein	2.195292	0.02805353
AT1G61970	Mitochondrial transcription termination factor family protein	2.069931	0.000131838
AT1G62290	Saposin-like aspartyl protease family protein	2.454803	0.04062856
AT1G62530	hypothetical protein (DUF863)	7.537682	2.82608E-08
AT1G62610	NAD(P)-binding Rossmann-fold superfamily protein	5.588837	0.03217699
AT1G63070	pentatricopeptide (PPR) repeat-containing protein	3.378107	0.04038891
AT1G63490	transcription factor jumonji (jmjC) domain-containing protein	2.456408	0.04929243
AT1G64480	calcineurin B-like protein 8	6.542664	0.0440438
AT1G65330	MADS-box transcription factor family protein	3.104721	0.04794914
AT1G65800	receptor kinase 2	10.04343	2.37162E-07
AT1G65990	type 2 peroxiredoxin-related / thiol specific antioxidant / mal allergen family protein	6.629767	0.000131982
AT1G66910	Protein kinase superfamily protein	7.232226	0.03313757
AT1G67420	Zn-dependent exopeptidases superfamily protein	2.133079	0.001792609
AT1G67570	zinc finger CONSTANS-like protein (DUF3537)	6.885316	0.03986333
AT1G67800	Copine (Calcium-dependent phospholipid-binding protein) family	6.738527	0.01551067
AT1G67800	Copine (Calcium-dependent phospholipid-binding protein) family	8.3284	0.02184926
AT1G67850	lysine ketoglutarate reductase trans-splicing protein (DUF707)	8.546937	0.01715234
AT1G67950	RNA-binding (RRM/RBD/RNP motifs) family protein	2.169134	2.79589E-16
AT1G67960	POLLEN DEFECTIVE IN GUIDANCE-like protein	11.38092	2.75453E-19
AT1G68140	zinc finger/BTB domain protein, putative (DUF1644)	3.426977	1.85193E-08
AT1G68570	Major facilitator superfamily protein	2.803925	0.008973358
AT1G68935	hypothetical protein AT1G68935	5.200068	0.006649762
AT1G69100	Eukaryotic aspartyl protease family protein	4.399078	0.01326197
AT1G69580	Homeodomain-like superfamily protein	3.267201	0.01156912
AT1G70290	trehalose-6-phosphatase synthase S8	9.90143	0.009035295
AT1G70740	Protein kinase superfamily protein	3.670341	0.01497502

AT1G71150	cyclin-D1-binding protein	2.731988	0.04658154
AT1G73607	low-molecular-weight cysteine-rich 65	3.637387	0.01570174
AT1G74040	2-isopropylmalate synthase 1	2.258034	0.03526008
AT1G74180	receptor like protein 14	7.904746	0.02462869
AT1G74810	HCO3- transporter family	7.157309	0.04185753
AT1G74810	HCO3- transporter family	8.007922	0.02497576
AT1G76750	egg cell-secreted-like protein (DUF1278)	3.216598	0.016877
AT1G77460	CELLULOSE SYNTHASE INTERACTIVE 3	10.71999	0.006074515
AT1G77655	hypothetical protein AT1G77655	2.215658	0.0130186
AT1G78590	NAD(H) kinase 3	3.801621	0.005293127
AT1G78955	camelliol C synthase 1	7.979485	9.31756E-06
AT1G80380	P-loop containing nucleoside triphosphate hydrolases superfamily protein	2.645994	0.03920856
AT1G80380	P-loop containing nucleoside triphosphate hydrolases superfamily protein	2.249408	0.03186719
AT2G01400	hypothetical protein AT2G01400	2.446223	0.002530242
AT2G01660	plasmodesmata-located protein 6	3.175886	0.02991409
AT2G02350	SKP1 interacting partner 3	2.304009	0.00399072
AT2G02490	transmembrane protein	3.158014	0.007275352
AT2G02410	yacP-like NYN domain protein	2.109837	0.0109301
AT2G03140	alpha/beta-Hydrolases superfamily protein	4.941973	0.006640217
AT2G04037	ECA1 gametogenesis family protein (DUF784)	4.106271	0.01119372
AT2G04041	ECA1 gametogenesis family protein (DUF784)	8.459863	0.000215142
AT2G12475	Defensin-like (DEFL) family protein	6.778214	0.000513687
AT2G13820	Bifunctional inhibitor/lipid-transfer protein/seed storage 2S albumin superfamily protein	3.175937	0.000343645
AT2G14610	pathogenesis-related protein 1	4.288589	0.02040851
AT2G14620	xyloglucan endotransglucosylase/hydrolase 10	2.432475	0.004355894
AT2G14680	myosin heavy chain-like protein	2.809449	0.03964337
AT2G16980	Major facilitator superfamily protein	6.907417	8.53423E-08
AT2G17442	hypothetical protein AT2G17442	4.339329	0.02283427
AT2G17780	PLAC8 family protein	2.614397	7.73127E-06
AT2G18240	Rer1 family protein	3.820338	0.04567033
AT2G19150	Pectin lyase-like superfamily protein	5.18822	0.000183368
AT2G19180	hypothetical protein AT2G19180	7.430569	0.02792589
AT2G19940	Putative N-acetyl-gamma-glutamyl-phosphate reductase	13.32175	0.000649924
AT2G20100	basic helix-loop-helix (bHLH) DNA-binding superfamily protein	7.664981	0.03173959
AT2G20500	hypothetical protein AT2G20500	3.52309	0.04710803
AT2G20540	mitochondrial editing factor 21	6.653542	0.04070904
AT2G20597	Plant thionin family protein	3.729242	0.01552774
AT2G20740	Tetraspanin family protein	7.530427	0.02918311
AT2G20815	QWRF motif protein (DUF566)	2.345014	0.0332094
AT2G21465	Defensin-like (DEFL) family protein	6.556391	0.002291439
AT2G21655	ECA1 gametogenesis family protein (DUF784)	4.225331	0.01533376

AT2G21727	ECA1 gametogenesis family protein (DUF784)	4.41582	0.001947819
AT2G21750	Egg cell-secreted protein (DUF1278)	3.393881	0.004586961
AT2G21740	Egg cell-secreted-like protein (DUF1278)	2.757887	0.03474336
AT2G21800	essential meiotic endonuclease 1A	7.669085	0.02964707
AT2G22250	aspartate aminotransferase	3.18978	5.83019E-05
AT2G22260	oxidoreductase, 2OG-Fe(II) oxygenase family protein	8.188696	0.03020862
AT2G22941	Defensin-like (DEFL) family protein	2.442406	3.67765E-09
AT2G23160	F-box family protein	2.140879	0.04748741
AT2G23660	LOB domain-containing protein 10	6.857431	0.03921609
AT2G23990	early nodulin-like protein 11	3.720567	0.02387948
AT2G24205	ECA1 gametogenesis related family protein	3.754762	0.04796415
AT2G24650	B3 domain-containing protein REM13	10.13123	1.37426E-10
AT2G24650	B3 domain-containing protein REM13	10.21865	2.76174E-10
AT2G25297	transmembrane protein	5.155783	0.000399318
AT2G25344	low-molecular-weight cysteine-rich 14	4.720754	0.006987432
AT2G25640	SPOC domain / Transcription elongation factor S-II protein	3.180234	0.02679277
AT2G25710	holocarboxylase synthase 1	2.165124	0.03527932
AT2G26400	acireductone dioxygenase 3	3.268349	0.00618143
AT2G27060	Leucine-rich repeat protein kinase family protein	9.237255	1.76003E-10
AT2G27315	egg cell-secreted-like protein (DUF1278)	3.153438	0.00704027
AT2G27580	A20/AN1-like zinc finger family protein	7.404774	0.001740782
AT2G28810	Dof-type zinc finger DNA-binding family protein	8.167118	0.01947837
AT2G28990	Leucine-rich repeat protein kinase family protein	5.642404	0.001136148
AT2G29320	NAD(P)-binding Rossmann-fold superfamily protein	3.842082	5.34566E-05
AT2G29890	villin-like 1	8.436991	0.01714016
AT2G30950	FtsH extracellular protease family	4.764008	0.001696004
AT2G32410	AXR1-like protein	8.028769	0.02446242
AT2G32780	ubiquitin-specific protease 1	2.711859	0.00423877
AT2G32560	F-box family protein	2.015639	0.01944036
AT2G33130	ralf-like 18	6.888436	0.000169814
AT2G33205	Serinc-domain containing serine and sphingolipid biosynthesis protein	7.389179	2.44338E-06
AT2G33350	CCT motif family protein	6.64586	0.04371465
AT2G34230	ubiquitin carboxyl-terminal hydrolase-like protein, putative (DUF627 and DUF629)	7.638201	3.68492E-09
AT2G34310	hypothetical protein AT2G34310	7.456653	0.02972137
AT2G34300	S-adenosyl-L-methionine-dependent methyltransferases superfamily protein	7.104472	0.0400577
AT2G34450	HMG-box (high mobility group) DNA-binding family protein	7.766298	0.03127563
AT2G34670	benzoyl-CoA reductase subunit C, putative (DUF630 and DUF632)	2.322546	0.005520117
AT2G35050	kinase superfamily with octicosapeptide/Phox/Bem1p domain- containing protein	9.022041	0.01484748
AT2G35615	Eukaryotic aspartyl protease family protein	3.115486	0.003897176
AT2G36325	GDSL-like Lipase/Acylhydrolase superfamily protein	2.951925	0.008900977

AT2G36480	pre-mRNA cleavage complex 2 Pcf11-like protein	4.398099	0.02009125
AT2G36900	membrin 11	2.09117	0.04808792
AT2G36960	TSL-kinase interacting protein 1	2.520406	0.000970771
AT2G37150	RING/U-box superfamily protein	2.037295	0.005749907
AT2G37930	hypothetical protein (DUF3527)	7.794191	3.0179E-06
AT2G38255	hypothetical protein (DUF239)	6.19827	0.001354097
AT2G38185	RING/U-box superfamily protein	2.771856	0.01091288
AT2G38580	Mitochondrial ATP synthase D chain-related protein	7.783126	0.02765271
AT2G39435	Phosphatidylinositol N-acetyglucosaminlytransferase subunit P-like protein	2.721594	0.006297523
AT2G39851	Proteinase inhibitor, propeptide	3.127696	0.01240736
AT2G39890	proline transporter 1	2.330027	0.02191415
AT2G39950	flocculation protein	9.266404	0.01182886
AT2G40960	Single-stranded nucleic acid binding R3H protein	5.197437	0.007581942
AT2G40995	Molecular chaperone Hsp40/DnaJ family protein	6.35498	0.000317907
AT2G41180	VQ motif-containing protein	20.84822	9.69679E-08
AT2G41830	Uncharacterized protein AT2G41830	2.518328	0.01763252
AT2G41920	Protein kinase superfamily protein	5.545227	8.99724E-05
AT2G42410	zinc finger protein 11	7.27082	0.03071243
AT2G43010	phytochrome interacting factor 4	2.476549	0.02956573
AT2G43480	Peroxidase superfamily protein	2.773626	0.009119469
AT2G43840	UDP-glycosyltransferase 74 F1	8.835969	6.06268E-08
AT2G44810	alpha/beta-Hydrolases superfamily protein	2.856945	0.01891382
AT2G45840	O-glucosyltransferase rumi-like protein (DUF821)	3.848732	0.03486845
AT2G46960	cytochrome P450, family 709, subfamily B, polypeptide 1	4.861241	0.009897822
AT2G47730	glutathione S-transferase phi 8	2.932178	0.006360798
AT3G01050	membrane-anchored ubiquitin-fold protein 1 precursor	7.027678	0.03470609
AT3G01085	Protein kinase superfamily protein	8.617143	8.78691E-05
AT3G01450	ARM repeat superfamily protein	4.38459	0.006901105
AT3G01900	cytochrome P450, family 94, subfamily B, polypeptide 2	7.544698	8.76736E-05
AT3G01990	ACT domain repeat 6	2.096772	0.03983875
AT3G02280	Flavodoxin family protein	2.008424	0.0475535
AT3G02370	tRNA-splicing endonuclease subunit	3.545243	0.001186123
AT3G02910	AIG2-like (avirulence induced gene) family protein	11.18439	0.004201033
AT3G02940	myb domain protein 107	2.6465	0.04047641
AT3G03800	syntaxin of plants 131	4.611457	0.04267397
AT3G04940	cysteine synthase D1	2.35428	0.01167857
AT3G05150	Major facilitator superfamily protein	7.521831	0.03429349
AT3G05155	Major facilitator superfamily protein	5.020868	3.03478E-05
AT3G05230	Signal peptidase subunit	4.744893	0.0112473
AT3G05460	sporozoite surface protein-like protein	3.465442	0.005855288
AT3G05520	Subunits of heterodimeric actin filament capping protein Capz superfamily	6.199163	0.01716263
AT3G05950	RmlC-like cupins superfamily protein	6.410327	4.74616E-06

AT3G06190	BTB-POZ and MATH domain 2	3.03696	1.62819E-05
AT3G06190	BTB-POZ and MATH domain 2	2.230162	0.01472467
AT3G06770	Pectin lyase-like superfamily protein	2.516798	0.001328913
AT3G08770	lipid transfer protein 6	11.46967	0.003327868
AT3G08960	ARM repeat superfamily protein	9.840956	1.4775E-13
AT3G09180	mediator of RNA polymerase II transcription subunit	2.311931	0.003215165
AT3G09600	Homeodomain-like superfamily protein	2.426177	0.006351625
AT3G09710	IQ-domain 1	4.247783	0.006185
AT3G10116	COBRA-like extracellular glycosyl-phosphatidyl inositol- anchored protein family	3.957107	0.01078789
AT3G10600	cationic amino acid transporter 7	2.136953	0.04681185
AT3G10880	tropomyosin	4.696737	0.009819432
AT3G10890	Glycosyl hydrolase superfamily protein	2.204199	0.01292966
AT3G11560	LETM1-like protein	9.293495	4.36253E-12
AT3G12020	P-loop containing nucleoside triphosphate hydrolases superfamily protein	8.409479	0.02031594
AT3G13060	evolutionarily conserved C-terminal region 5	2.675115	0.03150849
AT3G13062	Polyketide cyclase/dehydrase and lipid transport superfamily protein	2.588164	0.0250937
AT3G13430	RING/U-box superfamily protein	7.925853	0.02552505
AT3G13740	Ribonuclease III family protein	2.249259	0.007097017
AT3G14075	Mono-/di-acylglycerol lipase, N-terminal;Lipase, class 3	3.770957	0.01790211
AT3G15650	alpha/beta-Hydrolases superfamily protein	3.875963	0.00444267
AT3G16030	lectin protein kinase family protein	3.474824	0.001135127
AT3G16520	UDP-glucosyl transferase 88A1	9.537354	0.01439761
AT3G17150	Plant invertase/pectin methylesterase inhibitor superfamily protein	3.693962	0.003097566
AT3G17227	plant invertase/pectin methylesterase inhibitor superfamily protein	3.322877	0.04703072
AT3G17660	ARF-GAP domain 15	3.719318	0.001016955
AT3G18530	ARM repeat superfamily protein	3.380504	0.04131914
AT3G19270	cytochrome P450, family 707, subfamily A, polypeptide 4	2.551441	0.004310786
AT3G19830	Calcium-dependent lipid-binding (CaLB domain) family protein	2.200126	0.01307264
AT3G19930	sugar transporter 4	8.784144	0.01747809
AT3G19960	myosin 1	2.699865	0.01002342
AT3G20210	delta vacuolar processing enzyme	2.25428	0.02154154
AT3G21110	purin 7	2.302551	0.002963083
AT3G22810	auxin canalization protein (DUF828)	2.567461	0.007478287
AT3G22810	auxin canalization protein (DUF828)	2.556624	0.005039701
AT3G23380	ROP-interactive CRIB motif-containing protein 5	2.403065	0.02427561
AT3G23715	SCR-like 13	5.30613	0.000326042
AT3G23870	magnesium transporter NIPA (DUF803)	8.812693	0.01441842
AT3G24510	Defensin-like (DEFL) family protein	4.078752	0.001237613
AT3G24630	hypothetical protein AT3G24630	10.50178	0.006661438
AT3G24840	Sec14p-like phosphatidylinositol transfer family protein	2.030063	0.04870144
AT3G25013	Synaptobrevin family protein	2.580158	0.03387051

AT3G26150	cytochrome P450, family 71, subfamily B, polypeptide 16	3.554912	0.003219679
AT3G26060	Thioredoxin superfamily protein	2.067985	0.005325291
AT3G26510	Octicosapeptide/Phox/Bem1p family protein	2.226025	0.0482368
AT3G26720	Glycosyl hydrolase family 38 protein	5.286247	0.000368021
AT3G26890	meiosis chromosome segregation family protein	9.017713	0.0139105
AT3G26980	membrane-anchored ubiquitin-fold protein 4 precursor	2.927879	0.03828006
AT3G27460	SGF29 tudor-like domain-containing protein	2.817964	0.02512324
AT3G27650	LOB domain-containing protein 25	2.010803	0.008515707
AT3G27940	LOB domain-containing protein 26	5.122576	0.0433607
AT3G27930	beta-galactosidase	7.362403	0.0301154
AT3G28070	nodulin MtN21 /EamA-like transporter family protein	9.929491	0.0110456
AT3G28370	spindle assembly checkpoint component	8.224352	0.02286895
AT3G29797	ECA1 gametogenesis family protein (DUF784)	2.953232	0.03399402
AT3G29800	P-loop containing nucleoside triphosphate hydrolases superfamily protein	5.861207	1.45565E-05
AT3G30383	inhibitor/lipid-transfer protein/seed storage 2S albumin superfamily protein (DUF784)	7.481746	0.001049407
AT3G30385	inhibitor/lipid-transfer protein/seed storage 2S albumin superfamily protein (DUF784)	5.576984	0.009662641
AT3G30387	inhibitor/lipid-transfer protein/seed storage 2S albumin superfamily protein (DUF784)	5.614957	0.009456204
AT3G44006	hypothetical protein AT3G44006	6.682479	1.88248E-17
AT3G44690	hypothetical protein AT3G44690	8.009377	0.02239003
AT3G44790	TRAF-like family protein	2.339613	0.03939431
AT3G44540	fatty acid reductase 4	6.517702	0.04318477
AT3G44570	retrotransposon ORF-1 protein	2.518618	0.02783693
AT3G44920	cation/H+ exchanger 11	7.203013	1.59878E-06
AT3G45440	Concanavalin A-like lectin protein kinase family protein	4.532073	0.03795489
AT3G45870	nodulin MtN21 /EamA-like transporter family protein	2.692953	0.04688324
AT3G46020	RNA-binding (RRM/RBD/RNP motifs) family protein	2.535359	0.01296846
AT3G46060	RAB GTPase homolog 8A	5.22677	0.000291433
AT3G46616	hypothetical protein AT3G46616	5.524045	0.000102074
AT3G46870	Pentatricopeptide repeat (PPR) superfamily protein	5.414761	0.03553411
AT3G47890	Ubiquitin carboxyl-terminal hydrolase-related protein	7.784409	0.03453589
AT3G48120	serine/arginine-rich splicing factor	2.24796	0.01663252
AT3G48187	Serine/Threonine-kinase ATM	2.834465	1.64822E-07
AT3G48205	plant thionin family protein	5.731519	0.000128831
AT3G48840	RNA-binding (RRM/RBD/RNP motifs) family protein	2.893808	0.02718923
AT3G49070	transmembrane protein, putative (DUF677)	5.015094	3.71238E-05
AT3G49155	F-box/LRR protein	3.438737	0.009871545
AT3G49590	Autophagy-related protein 13	2.00017	0.001429537
AT3G49645	FAD-binding protein	2.101498	0.001460471
AT3G51150	ATP binding microtubule motor family protein	11.48132	0.003296008
AT3G52050	5\\'-3\\' exonuclease family protein	6.386161	0.04621471
AT3G53050	D-galactoside/L-rhamnose binding SUEL lectin protein	5.595355	9.39949E-05

AT3G53270	Small nuclear RNA activating complex (SNAPc), subunit SNAP43 protein	7.151198	0.03670986
AT3G54050	high cyclic electron flow 1	3.007597	0.04253135
AT3G54740	zein-binding protein (Protein of unknown function, DUF593)	7.560069	0.0150967
AT3G54740	zein-binding protein (Protein of unknown function, DUF593)	10.92963	0.004696185
AT3G54740	zein-binding protein (Protein of unknown function, DUF593)	7.824102	0.004052245
AT3G54970	D-aminoacid aminotransferase-like PLP-dependent enzymes superfamily protein	7.731118	0.02572942
AT3G55410	2-oxoglutarate dehydrogenase, E1 component	3.103176	0.02063482
AT3G55880	Alpha/beta hydrolase related protein	2.69052	0.003316559
AT3G57062	transmembrane protein	3.229335	1.75527E-05
AT3G57390	AGAMOUS-like 18	2.556495	8.38019E-16
AT3G57550	guanylate kinase	3.357851	0.01508094
AT3G57680	Peptidase S41 family protein	2.913097	0.000167007
AT3G58160	P-loop containing nucleoside triphosphate hydrolases superfamily protein	3.363827	3.54717E-05
AT3G58900	F-box/RNI-like superfamily protein	6.979622	0.03594953
AT3G59430	hypothetical protein AT3G59430	5.885611	0.01681265
AT3G59430	hypothetical protein AT3G59430	5.798451	0.0243351
AT3G59430	hypothetical protein AT3G59430	8.01811	0.0268995
AT3G61035	Cytochrome P450 superfamily protein	2.723395	0.02580962
AT3G61400	2-oxoglutarate (2OG) and Fe(II)-dependent oxygenase superfamily protein	6.177744	1.80185E-06
AT3G61400	2-oxoglutarate (2OG) and Fe(II)-dependent oxygenase superfamily protein	4.660635	0.009029078
AT3G61940	Cation efflux family protein	5.89988	9.13466E-05
AT4G00480	basic helix-loop-helix (bHLH) DNA-binding superfamily protein	6.812231	0.03759579
AT4G00550	digalactosyl diacylglycerol deficient 2	2.370648	0.006540022
AT4G01200	Calcium-dependent lipid-binding (CaLB domain) family protein	3.084989	0.04440704
AT4G02000	Tal1-like non-LTR retrotransposon	2.264837	0.04654052
AT4G02690	Bax inhibitor-1 family protein	2.724731	0.005583495
AT4G02830	hypothetical protein AT4G02830	6.919076	1.73912E-06
AT4G02760	RNI-like superfamily protein	2.523966	0.002475378
AT4G03298	transmembrane protein	5.804482	0.000158101
AT4G04190	transmembrane protein	5.58775	0.003875658
AT4G04480	F-box protein with a domain protein	2.07172	0.03836406
AT4G08025	ECA1 gametogenesis family protein (DUF784)	4.308397	0.01529849
AT4G05040	ankyrin repeat family protein	2.063039	0.01840664
AT4G08980	F-BOX WITH WD-40 2	8.535304	0.01618476
AT4G09010	ascorbate peroxidase 4	2.594838	0.01515761
AT4G09464	Carbohydrate-binding X8 domain superfamily protein	6.143908	0.001343513
AT4G09465	Carbohydrate-binding X8 domain superfamily protein	6.777143	0.001303377
AT4G09466	Carbohydrate-binding X8 domain superfamily protein	5.396885	0.005393225
AT4G09467	Carbohydrate-binding X8 domain superfamily protein	5.298235	0.006894376
AT4G09920	FBD, F-box and Leucine Rich Repeat domains containing protein	7.921417	0.02587756

AT4G10640	IQ-domain 16	2.535436	0.02187876
AT4G11653	RALF-like 29	5.071615	0.009658323
AT4G12740	HhH-GPD base excision DNA repair family protein	6.896624	0.03860534
AT4G13261	ECA1 gametogenesis family protein (DUF784)	3.687443	0.009385138
AT4G13263	ECA1 gametogenesis family protein (DUF784)	4.542668	0.000220106
AT4G13345	Serinc-domain containing serine and sphingolipid biosynthesis protein	3.739446	0.01601229
AT4G13410	Nucleotide-diphospho-sugar transferases superfamily protein	4.207216	0.02706232
AT4G13660	pinoresinol reductase 2	7.671484	1.07384E-07
AT4G13960	F-box/RNI-like superfamily protein	5.093827	0.000194541
AT4G14276	Defensin-like (DEFL) family protein	7.175129	0.000254721
AT4G14970	fanconi anemia group D2 protein	10.86999	0.004910576
AT4G15030	folate-sensitive fragile site protein	2.256207	0.04202687
AT4G15420	Ubiquitin fusion degradation UFD1 family protein	2.220214	0.04331292
AT4G15460	glycine-rich protein	2.445939	0.04828063
AT4G15530	pyruvate orthophosphate dikinase	20.02285	3.03943E-07
AT4G15750	Plant invertase/pectin methylesterase inhibitor superfamily protein	3.030562	0.04229983
AT4G15880	Cysteine proteinases superfamily protein	3.608043	0.02076164
AT4G16360	SNF1-related protein kinase regulatory subunit beta-2	2.073501	0.008994543
AT4G16566	histidine triad nucleotide-binding 4	6.711177	0.04171052
AT4G16765	2-oxoglutarate (2OG) and Fe(II)-dependent oxygenase superfamily protein	10.35862	3.39686E-08
AT4G16920	Disease resistance protein (TIR-NBS-LRR class) family	8.371185	0.006005619
AT4G17200	F-box and associated interaction domains-containing protein	3.593326	0.01839523
AT4G17990	hypothetical protein AT4G17990	2.905627	0.04482712
AT4G18960	K-box region and MADS-box transcription factor family protein, partial	2.779618	0.000468386
AT4G18975	Pentatricopeptide repeat (PPR) superfamily protein	2.801894	0.04322024
AT4G19810	Glycosyl hydrolase family protein with chitinase insertion domain- containing protein	10.27155	0.006803625
AT4G19990	FAR1-related sequence 1	7.256419	0.03330097
AT4G20320	CTP synthase family protein	2.318153	0.00643516
AT4G20350	oxidoreductase	3.296365	3.97828E-09
AT4G20920	double-stranded RNA-binding domain (DsRBD)-containing protein	3.228934	0.001989403
AT4G20940	Leucine-rich receptor-like protein kinase family protein	2.763202	0.000226131
AT4G21400	cysteine-rich RLK (RECEPTOR-like protein kinase) 28	2.031148	0.009454205
AT4G21400	cysteine-rich RLK (RECEPTOR-like protein kinase) 28	2.584888	0.02256351
AT4G21860	methionine sulfoxide reductase B 2	2.332298	0.001348911
AT4G22035	F-box only protein	3.348734	0.02807897
AT4G22120	ERD (early-responsive to dehydration stress) family protein	10.64576	0.005516784
AT4G22200	potassium transport 2/3	10.82904	6.5172E-09
AT4G22340	cytidinediphosphate diacylglycerol synthase 2	2.465582	0.04306647
AT4G22990	Major Facilitator Superfamily with SPX (SYG1/Pho81/XPR1) domain-containing protein	3.532491	3.76795E-05

A74G23350 transmembrane protein, putative (DUF239) 7.238348 0.000351881 A74G23882 Heavy metal transport/detoxification superfamily protein 2.471392 0.01381385 A74G24860 P-loop containing nucleoside triphosphate hydrolases superfamily protein 6.531491 0.0131295 A74G24860 P-loop containing nucleoside triphosphate hydrolases superfamily protein 6.362969 0.00022720; A74G25190 P-loop containing nucleoside triphosphate hydrolases superfamily protein 2.744982 0.00022720; A74G25190 Uridine kinase-like d 2.985334 0.0001677; A74G26520 Aldolase superfamily protein 4.676501 0.0005625-4 A74G267090 GDSL-like Lipase/Acybhydrolase superfamily protein 11.56159 5.23613E-0 A74G276700 proton pump interactor 1 2.435826 0.0373408 A74G276701 intracellular protein transporter 8.752428 0.01637089 A74G287610 intracellular protein transporter 8.752428 0.01637089 A74G287610 basic helix-loop-helix (bHLH) DNA-binding superfamily protein 4.881363 0.00372303 A74G287610 low-molecu				
A74G23882 Heavy metal transport/detoxification superfamily protein 2.471392 0.01383185 A74G24260 glycosyl hydrolase 9A3 6.531491 0.0131295 A74G24860 P-loop containing nucleoside triphosphate hydrolases superfamily protein 6.362969 0.0211525 A74G25310 2-oxoglutarate (2OG) and Fe(II)-dependent oxygenase superfamily protein 2.744982 0.00022720 A74G25310 Haloacid dehalogenase-like hydrolase (HAD) superfamily protein 8.65407 0.0161253 A74G26520 uridine kinase-like Aldolase superfamily protein 4.676501 0.00065625-4 A74G26520 GDSL-like Lipase/Acylhydrolase superfamily protein 11.56159 5.23613E-08 A74G26790 GDSL-like Lipase/Acylhydrolase superfamily protein 11.56159 5.23613E-08 A74G27500 myb domain protein 97 2.617339 0.01558095 A74G27700 heat shock protein transporter 8.725428 0.01637089 A74G28780 LORELEI-LIKE-GPI ANCHORED PROTEIN 3 2.441354 0.00218301 A74G38070 low-molecular-weight cysteine-rich 63 3.80992 0.01718615 A74G30074 low-molecular-weight cystei	AT4G23210	cysteine-rich RLK (RECEPTOR-like protein kinase) 13	7.120748	0.03578656
AT4G24260 glycosyl hydrolase 9A3 6.531491 0.0131295 AT4G24860 P-loop containing nucleoside triphosphate hydrolases superfamily protein 6.362969 0.0211525 AT4G25310 2-oxoglutarate (2OG) and Fe(II)-dependent oxygenase superfamily protein 2.744982 0.00022720; superfamily protein AT4G26190 Haloacid dehalogenase-like hydrolase (HAD) superfamily protein 8.65407 0.0161253 AT4G26510 urdine kinase-like 4 2.985334 0.00041077 AT4G26520 Aldolase superfamily protein 4.676501 0.0065625- AT4G26930 myb domain protein 97 2.617739 0.01558095 AT4G27600 proton pump interactor 1 2.435826 0.0373408 AT4G276701 intracellular protein transporter 8.725428 0.01637089 AT4G28280 LORELEI-LIKE-GPI ANCHORED PROTEIN 3 2.441354 0.002183012 AT4G38070 low-molecular-weight cysteine-rich 3 3.89092 0.01718615 AT4G30074 low-molecular-weight cysteine-rich 19 4.551994 0.0189251 AT4G30090 low-molecular-weight cysteine-rich 19 4.55194 0.01295302 <td>AT4G23350</td> <td>transmembrane protein, putative (DUF239)</td> <td>7.238348</td> <td>0.000351881</td>	AT4G23350	transmembrane protein, putative (DUF239)	7.238348	0.000351881
AT4G24860 P-loop containing nucleoside triphosphate hydrolases superfamily protein 6.362969 0.0211525 AT4G25310 P-loop containing nucleoside triphosphate hydrolases superfamily protein 2.744982 0.000227202 AT4G26190 Haloacid dehalogenase-like hydrolase (HAD) superfamily protein 8.65407 0.01612533 AT4G26510 uridine kinase-like 4 2.985334 0.00041077 AT4G26520 Aldolase superfamily protein 4.676501 0.00065625-4 AT4G26790 GDSL-like Lipase/Acylhydrolase superfamily protein 11.56159 5.23613E-06 AT4G27500 myb domain protein 97 2.617739 0.01588095 AT4G27700 beat shock protein 21 2.435826 0.0373408 AT4G27670 leat shock protein 21 2.51831 0.00418301 AT4G28790 basic helix-loop-helix (BHLH) DNA-binding superfamily protein 4.881363 0.00373203 AT4G30007 low-molecular-weight cysteine-rich 19 4.551994 0.0189823 AT4G31073 hypothetical protein AT4G31073 3.987072 0.01273467 AT4G31080 integral membrane metal-binding family protein (DUF2296) 6.316782 <td>AT4G23882</td> <td>Heavy metal transport/detoxification superfamily protein</td> <td>2.471392</td> <td>0.01383185</td>	AT4G23882	Heavy metal transport/detoxification superfamily protein	2.471392	0.01383185
Protein	AT4G24260	glycosyl hydrolase 9A3	6.531491	0.0131295
AT4G26190 Haloacid dehalogenase-like hydrolase (HAD) superfamily protein 8.65407 0.01612553 AT4G26510 uridine kinase-like 4 2.985334 0.000410777 AT4G26520 Aldolase superfamily protein 4.676501 0.00065625-6 AT4G26790 GDSL-like Lipase/Acylhydrolase superfamily protein 11.56159 5.23613E-0s AT4G26930 myb domain protein 97 2.617739 0.01558095 AT4G27670 broton pump interactor 1 2.438526 0.0373408 AT4G27670 beat shock protein 21 2.51831 0.004400887 AT4G28280 LORELEI-LIKE-GPI ANCHORED PROTEIN 3 2.441354 0.002183012 AT4G28790 basic helix-loop-helix (bHLH) DNA-binding superfamily protein 4.881363 0.00373203 AT4G30074 low-molecular-weight cysteine-rich 63 3.80992 0.01718615 AT4G30075 low-molecular-weight cysteine-rich 19 4.551994 0.01889251 AT4G30070 how-molecular-weight cysteine-rich 19 4.51994 0.01889251 AT4G30300 hon-intrinsic ABC protein 15 3.380792 0.01273467 AT4G310390 <t< td=""><td>AT4G24860</td><td></td><td>6.362969</td><td>0.0211525</td></t<>	AT4G24860		6.362969	0.0211525
AT4G26510 uridine kinase-like 4 2.985334 0.000410777 AT4G26520 Aldolase superfamily protein 4.676501 0.000656254 AT4G26790 GDSL-like Lipase/Acylhydrolase superfamily protein 11.56159 5.23613E-08 AT4G267300 myb domain protein 97 2.617739 5.2613E-08 AT4G275700 proton pump interactor 1 2.435826 0.0337408 AT4G27670 heat shock protein 21 2.51831 0.00400883 AT4G28790 basic helix-loop-helix (bHLH) DNA-binding superfamily protein 4.881363 0.00372030 AT4G38007 low-molecular-weight cysteine-rich 63 3.80992 0.01718615 AT4G30074 low-molecular-weight cysteine-rich 19 4.551994 0.01889251 AT4G30074 low-molecular-weight cysteine-rich 19 4.551994 0.01889251 AT4G31030 low-molecular-weight cysteine-rich 19 4.713083 0.002353351 AT4G31073 hypothetical protein AT4G31073 3.987072 0.01273467 AT4G31080 integral membrane metal-binding family protein (DUF2296) 6.316782 5.13857E-06 AT4G321080 <	AT4G25310	superfamily protein	2.744982	0.000227202
AT4G26520 Aldolase superfamily protein 4.676501 0.000656254 AT4G26790 GDSL-like Lipase/Acylhydrolase superfamily protein 11.56159 5.23613E-08 AT4G26930 myb domain protein 97 2.617739 0.01558095 AT4G27500 proton pump interactor 1 2.435826 0.0373408 AT4G27670 heat shock protein 21 2.51831 0.004400887 AT4G27670 heat shock protein 21 2.51831 0.004400887 AT4G2880 LORELEI-LIKE-GPI ANCHORED PROTEIN 3 2.441354 0.002183012 AT4G30067 low-molecular-weight cysteine-rich 63 3.80992 0.01718615 AT4G30074 low-molecular-weight cysteine-rich 19 4.51594 0.01889251 AT4G30070 non-intrinsic ABC protein 15 4.713083 0.002353751 AT4G31073 hypothetical protein AT4G31073 3.987072 0.01273467 AT4G32180 hS12-like 1 3.39758 0.00151615 AT4G32378 pectin lyase-like superfamily protein 8.687519 1.72573E-08 AT4G32379 pectin lyase-like superfamily protein 9.374159 2	AT4G26190	Haloacid dehalogenase-like hydrolase (HAD) superfamily protein	8.65407	0.01612553
AT4G26790 GDSL-like Lipase/Acylhydrolase superfamily protein 11.56159 5.23613E-08 AT4G26930 myb domain protein 97 2.617739 0.01558095 AT4G27500 proton pump interactor 1 2.435826 0.0373408 AT4G27670 heat shock protein transporter 8.725428 0.01637089 AT4G27670 heat shock protein 21 2.51831 0.004400887 AT4G28280 LORELEI-LIKE-GPI ANCHORED PROTEIN 3 2.441354 0.002183012 AT4G30074 low-molecular-weight cysteine-rich 63 3.80992 0.01718615 AT4G30075 low-molecular-weight cysteine-rich 19 4.551994 0.01889251 AT4G30090 12.56841 0.00129302 AT4G30190 0 12.56841 0.00129302 AT4G31073 hypothetical protein AT4G31073 3.987072 0.01273467 AT4G320100 HSI2-like 1 3.397758 0.009151615 AT4G322100 HSI2-like 1 3.397758 0.00168537 AT4G32290 Pectin lyase-like superfamily protein 8.687519 1.72573E-08 AT4G32350 Pectin phosph	AT4G26510		2.985334	0.000410777
AT4G26930 myb domain protein 97 2.617739 0.01558095 AT4G27500 proton pump interactor 1 2.435826 0.0373408 AT4G27610 intracellular protein transporter 8.725428 0.01637089 AT4G27670 heat shock protein 21 2.51831 0.004400887 AT4G28790 basic helix-loop-helix (bHLH) DNA-binding superfamily protein 4.881363 0.00372303 AT4G30067 low-molecular-weight cysteine-rich 63 3.80992 0.01718615 AT4G30190 0 12.56841 0.001293302 AT4G30300 non-intrinsic ABC protein 15 4.713083 0.002353751 AT4G31073 hypothetical protein AT4G31073 3.987072 0.01273467 AT4G321080 integral membrane metal-binding family protein (DUF2296) 6.316782 5.13857E-06 AT4G322101 HSI2-like 1 3.397758 0.009151615 AT4G323275 Pectin lyase-like superfamily protein 4.732327 8.28746E-06 AT4G323275 Pectin lyase-like superfamily protein 4.732327 8.28746E-06 AT4G332500 potassium channel protein 9.374159	AT4G26520	Aldolase superfamily protein	4.676501	0.000656254
A74G27500 proton pump interactor 1 2.435826 0.0373408 A74G27610 intracellular protein transporter 8.725428 0.01637089 A74G27670 heat shock protein 21 2.51831 0.004400883 A74G28280 LORELEI-LIKE-GPI ANCHORED PROTEIN 3 2.441354 0.002183012 A74G28790 basic helix-loop-helix (bHLH) DNA-binding superfamily protein 4.881363 0.00372303 A74G30074 low-molecular-weight cysteine-rich 63 3.80992 0.01718615 A74G30190 0 12.56841 0.0189251 A74G30300 non-intrinsic ABC protein 15 4.713083 0.002353751 A74G31073 hypothetical protein A74G31073 3.987072 0.01273467 A74G31080 integral membrane metal-binding family protein (DUF2296) 6.316782 5.13857E-06 A74G32010 HSI2-like 1 3.397588 0.009151615 A74G32280 pantothenate kinase 2 2.038836 0.01068537 A74G32590 2Fe-2S ferredoxin-like superfamily protein 8.687519 1.72573E-08 A74G32590 Protein phosphatase 2C family protein 2.056	AT4G26790	GDSL-like Lipase/Acylhydrolase superfamily protein	11.56159	5.23613E-08
AT4G27610 intracellular protein transporter 8.725428 0.01637089 AT4G27670 heat shock protein 21 2.51831 0.004400887 AT4G27670 heat shock protein 21 2.51831 0.004400887 AT4G28790 basic helix-loop-helix (bHLH) DNA-binding superfamily protein 4.881363 0.00373803 AT4G30067 low-molecular-weight cysteine-rich 63 3.80992 0.01718615 AT4G30190 0 12.56841 0.01295302 AT4G30300 non-intrinsic ABC protein 15 4.713083 0.002353751 AT4G31073 hypothetical protein AT4G31073 3.987072 0.01273467 AT4G31080 integral membrane metal-binding family protein (DUF2296) 6.316782 5.13887E-06 AT4G32010 HS12-like 1 3.397758 0.001551615 AT4G32280 pantothenate kinase 2 2.038836 0.01068537 AT4G32590 2Fe-2S ferredoxin-like superfamily protein 8.687519 1.72573E-08 AT4G32590 potassium channel protein 9.374159 2.31269E-16 AT4G33050 calmodulin-binding family protein 2.05631	AT4G26930	myb domain protein 97	2.617739	0.01558095
AT4G27670 heat shock protein 21 2.51831 0.004400887 AT4G28280 LORELEI-LIKE-GPI ANCHORED PROTEIN 3 2.441354 0.002183012 AT4G38790 basic helix-loop-helix (bHLH) DNA-binding superfamily protein 4.881363 0.00372303 AT4G30067 low-molecular-weight cysteine-rich 63 3.80992 0.011880251 AT4G30074 low-molecular-weight cysteine-rich 19 4.551994 0.01889251 AT4G30190 0 12.56841 0.001295302 AT4G30300 non-intrinsic ABC protein 15 4.713083 0.002537515 AT4G31073 hypothetical protein AT4G31073 3.987072 0.01273467 AT4G32010 HSI2-like 1 3.397758 0.009151615 AT4G32375 Pectin lyase-like superfamily protein 8.687519 1.72573E-08 AT4G32375 Pectin lyase-like superfamily protein 4.732327 8.28746E-06 AT4G32590 Protein phosphatase 2C family protein 9.374159 2.31269E-10 AT4G33550 Bifunctional inhibitor/lipid-transfer protein/seed storage 2S albumin superfamily protein 2.352356 0.04922457 AT4G35165	AT4G27500	proton pump interactor 1	2.435826	0.0373408
AT4G28280 LORELEI-LIKE-GPI ANCHORED PROTEIN 3 2.441354 0.002183012 AT4G28790 basic helix-loop-helix (bHLH) DNA-binding superfamily protein 4.881363 0.00372303 AT4G30067 low-molecular-weight cysteine-rich 63 3.80992 0.0118615 AT4G30190 10 4.551994 0.01889251 AT4G30300 non-intrinsic ABC protein 15 4.713083 0.002353751 AT4G31073 hypothetical protein AT4G31073 3.987072 0.01273467 AT4G32010 HS12-like 1 3.397758 0.009151615 AT4G32180 pantothenate kinase 2 2.038836 0.01068537 AT4G32375 Pectin lyase-like superfamily protein 8.687519 1.72573E-08 AT4G32590 2Fe-2S ferredoxin-like superfamily protein 4.732327 8.28746E-06 AT4G32590 Protein phosphatase 2C family protein 2.05631 0.02562415 AT4G33500 Protein phosphatase 2C family protein 2.311602 0.00397325 AT4G33500 Protein phosphatase 2C family protein 2.35631 0.02562415 AT4G35165 egg cell-secreted-like protein (DUF1278)	AT4G27610	intracellular protein transporter	8.725428	0.01637089
AT4G28790 basic helix-loop-helix (bHLH) DNA-binding superfamily protein 4.881363 0.00372303 AT4G30067 low-molecular-weight cysteine-rich 63 3.80992 0.01718615 AT4G30074 low-molecular-weight cysteine-rich 19 4.551994 0.01889251 AT4G30109 0 12.56841 0.001295302 AT4G31073 hypothetical protein AT4G31073 3.987072 0.01273467 AT4G31080 integral membrane metal-binding family protein (DUF2296) 6.316782 5.13857E-06 AT4G32010 HSI2-like 1 3.397758 0.009151615 AT4G32180 pantothenate kinase 2 2.038836 0.01068537 AT4G32590 Pectin lyase-like superfamily protein 8.687519 1.72573E-08 AT4G32590 potassium channel protein 9.374159 2.31269E-10 AT4G32950 Protein phosphatase 2C family protein 2.05631 0.02562415 AT4G33050 calmodulin-binding family protein 2.311602 0.00397325 AT4G33500 Edifunctional inhibitor/lipid-transfer protein/seed storage 2S albumin superfamily protein 2.352356 0.04922457 AT4G36380<	AT4G27670	heat shock protein 21	2.51831	0.004400887
A74G30067 low-molecular-weight cysteine-rich 63 3.80992 0.01718615 A74G30074 low-molecular-weight cysteine-rich 19 4.551994 0.01889251 A74G30190 0 12.56841 0.001295302 A74G30300 non-intrinsic ABC protein 15 4.713083 0.002353751 A74G31073 hypothetical protein AT4G31073 3.987072 0.01273467 A74G32108 integral membrane metal-binding family protein (DUF2296) 6.316782 5.13857E-06 A74G32101 HSI2-like 1 3.397758 0.009151615 A74G32375 Pectin lyase-like superfamily protein 8.687519 1.72573E-08 A74G32375 Pectin lyase-like superfamily protein 4.732327 8.28746E-06 A74G32590 2Fe-2S ferredoxin-like superfamily protein 9.374159 2.31269E-10 A74G32950 Protein phosphatase 2C family protein 2.05631 0.02562415 A74G33050 calmodulin-binding family protein 2.311602 0.0397325 A74G33550 Bifunctional inhibitor/lipid-transfer protein/seed storage 2S albumin superfamily protein 2.3216695 0.04922457 A74G35290	AT4G28280	LORELEI-LIKE-GPI ANCHORED PROTEIN 3	2.441354	0.002183012
A74G30074 low-molecular-weight cysteine-rich 19 4.551994 0.01889251 A74G30190 0 12.56841 0.001295302 A74G30300 non-intrinsic ABC protein 15 4.713083 0.002353751 A74G31073 hypothetical protein AT4G31073 3.987072 0.01273467 A74G32010 HSI2-like 1 3.397758 0.009151615 A74G322180 pantothenate kinase 2 2.038836 0.01068537 A74G32375 Pectin lyase-like superfamily protein 8.687519 1.72573E-08 A74G32590 2Fe-2S ferredoxin-like superfamily protein 4.732327 8.28746E-06 A74G32650 potassium channel protein 9.374159 2.31269E-16 A74G32950 Protein phosphatase 2C family protein 2.05631 0.02562415 A74G33050 calmodulin-binding family protein 2.311602 0.00397325 A74G33505 Bifunctional inhibitor/lipid-transfer protein/seed storage 2S 2.352356 0.04922457 A74G35165 egg cell-secreted-like protein (DUF1278) 2.821173 0.03612151 A74G36380 Cytochrome P450 superfamily protein	AT4G28790	basic helix-loop-helix (bHLH) DNA-binding superfamily protein	4.881363	0.00372303
AT4G30190 0 12.56841 0.001295302 AT4G30300 non-intrinsic ABC protein 15 4.713083 0.002353751 AT4G31073 hypothetical protein AT4G31073 3.987072 0.01273467 AT4G31080 integral membrane metal-binding family protein (DUF2296) 6.316782 5.13857E-06 AT4G32010 HS12-like 1 3.397758 0.009151615 AT4G32180 pantothenate kinase 2 2.038836 0.01068537 AT4G32375 Pectin lyase-like superfamily protein 8.687519 1.72573E-08 AT4G32590 2Fe-2S ferredoxin-like superfamily protein 4.732327 8.28746E-06 AT4G32650 potassium channel protein 9.374159 2.31269E-10 AT4G32950 Protein phosphatase 2C family protein 2.05631 0.02562415 AT4G33050 calmodulin-binding family protein 2.311602 0.00397325 AT4G33550 Bifunctional inhibitor/lipid-transfer protein/seed storage 2S albumin superfamily protein 2.352356 0.04922457 AT4G35165 egg cell-secreted-like protein (DUF1278) 2.821173 0.03612151 AT4G3680 Cytochr	AT4G30067	low-molecular-weight cysteine-rich 63	3.80992	0.01718615
AT4G30300 non-intrinsic ABC protein 15 4.713083 0.002353751 AT4G31073 hypothetical protein AT4G31073 3.987072 0.01273467 AT4G31080 integral membrane metal-binding family protein (DUF2296) 6.316782 5.13857E-06 AT4G32010 HS12-like 1 3.397758 0.009151615 AT4G32180 pantothenate kinase 2 2.038836 0.01068537 AT4G32375 Pectin lyase-like superfamily protein 8.687519 1.72573E-08 AT4G32590 2Fe-2S ferredoxin-like superfamily protein 4.732327 8.28746E-06 AT4G32650 potassium channel protein 9.374159 2.31269E-10 AT4G32950 Protein phosphatase 2C family protein 2.05631 0.02562415 AT4G33050 calmodulin-binding family protein 2.311602 0.00397325 AT4G33550 Bifunctional inhibitor/lipid-transfer protein/seed storage 2S albumin superfamily protein 2.352356 0.04922457 AT4G35165 egg cell-secreted-like protein (DUF1278) 2.821173 0.03612151 AT4G36380 Cytochrome P450 superfamily protein 3.696886 0.03634587	AT4G30074	low-molecular-weight cysteine-rich 19	4.551994	0.01889251
AT4G31073 hypothetical protein AT4G31073 3.987072 0.01273467 AT4G31080 integral membrane metal-binding family protein (DUF2296) 6.316782 5.13857E-06 AT4G32010 HSI2-like 1 3.397758 0.009151615 AT4G32180 pantothenate kinase 2 2.038836 0.01068537 AT4G32375 Pectin lyase-like superfamily protein 8.687519 1.72573E-08 AT4G32590 2Fe-2S ferredoxin-like superfamily protein 4.732327 8.28746E-06 AT4G32950 Potein phosphatase 2C family protein 9.374159 2.31269E-10 AT4G32950 Protein phosphatase 2C family protein 2.05631 0.02562415 AT4G33050 calmodulin-binding family protein 2.311602 0.00397325 AT4G33550 Bifunctional inhibitor/lipid-transfer protein/seed storage 2S albumin superfamily protein 2.352356 0.04922457 AT4G35165 egg cell-secreted-like protein (DUF1278) 2.821173 0.03612151 AT4G36380 Cytochrome P450 superfamily protein 3.696886 0.03634587 AT4G36400 FAD-linked oxidases family protein 2.33057 0.04908833 <t< td=""><td>AT4G30190</td><td>0</td><td>12.56841</td><td>0.001295302</td></t<>	AT4G30190	0	12.56841	0.001295302
AT4G31080 integral membrane metal-binding family protein (DUF2296) 6.316782 5.13857E-06 AT4G32010 HSI2-like 1 3.397758 0.009151615 AT4G32180 pantothenate kinase 2 2.038836 0.01068537 AT4G32375 Pectin lyase-like superfamily protein 8.687519 1.72573E-08 AT4G32590 2Fe-2S ferredoxin-like superfamily protein 4.732327 8.28746E-06 AT4G32550 potassium channel protein 9.374159 2.31269E-10 AT4G32950 Protein phosphatase 2C family protein 2.05631 0.02562415 AT4G33050 calmodulin-binding family protein 2.311602 0.00397325 AT4G33550 Bifunctional inhibitor/lipid-transfer protein/seed storage 2S albumin superfamily protein 2.352356 0.04922457 AT4G35165 egg cell-secreted-like protein (DUF1278) 2.821173 0.03612151 AT4G36380 Cytochrome P450 superfamily protein 3.696886 0.03634587 AT4G37970 cinnamyl alcohol dehydrogenase 6 5.543145 0.006092639 AT4G39120 PHD finger family protein / bromo-adjacent homology (BAH) domain-containing protein 2.488647	AT4G30300	non-intrinsic ABC protein 15	4.713083	0.002353751
AT4G32010 HSI2-like 1 3.397758 0.009151615 AT4G32180 pantothenate kinase 2 2.038836 0.01068537 AT4G32375 Pectin lyase-like superfamily protein 8.687519 1.72573E-08 AT4G32590 2Fe-2S ferredoxin-like superfamily protein 4.732327 8.28746E-06 AT4G32650 potassium channel protein 9.374159 2.31269E-10 AT4G32950 Protein phosphatase 2C family protein 2.05631 0.02562415 AT4G33050 calmodulin-binding family protein 2.311602 0.00397325 AT4G33550 Bifunctional inhibitor/lipid-transfer protein/seed storage 2S albumin superfamily protein 2.352356 0.04922457 AT4G35165 egg cell-secreted-like protein (DUF1278) 2.821173 0.03612151 AT4G35290 glutamate receptor 2 5.216695 0.04591054 AT4G36380 Cytochrome P450 superfamily protein 3.696886 0.03634587 AT4G37970 cinnamyl alcohol dehydrogenase 6 5.543145 0.006092639 AT4G39120 phD finger family protein / bromo-adjacent homology (BAH) domain-containing protein 2.488647 6.45774E-07	AT4G31073	hypothetical protein AT4G31073	3.987072	0.01273467
AT4G32180 pantothenate kinase 2 2.038836 0.01068537 AT4G32375 Pectin lyase-like superfamily protein 8.687519 1.72573E-08 AT4G32590 2Fe-2S ferredoxin-like superfamily protein 4.732327 8.28746E-06 AT4G32650 potassium channel protein 9.374159 2.31269E-10 AT4G32950 Protein phosphatase 2C family protein 2.05631 0.02562415 AT4G33050 calmodulin-binding family protein 2.311602 0.00397325 AT4G33550 Bifunctional inhibitor/lipid-transfer protein/seed storage 2S albumin superfamily protein 2.352356 0.04922457 AT4G35165 egg cell-secreted-like protein (DUF1278) 2.821173 0.03612151 AT4G35290 glutamate receptor 2 5.216695 0.04591054 AT4G36380 Cytochrome P450 superfamily protein 3.696886 0.03634587 AT4G37970 cinnamyl alcohol dehydrogenase 6 5.543145 0.006092639 AT4G39100 PHD finger family protein / bromo-adjacent homology (BAH) domain-containing protein 2.386542 0.03723632 AT5G01570 plectin-like protein 2.488647 6.45774E-07	AT4G31080	integral membrane metal-binding family protein (DUF2296)	6.316782	5.13857E-06
AT4G32375 Pectin lyase-like superfamily protein 8.687519 1.72573E-08 AT4G32590 2Fe-2S ferredoxin-like superfamily protein 4.732327 8.28746E-06 AT4G32650 potassium channel protein 9.374159 2.31269E-10 AT4G32950 Protein phosphatase 2C family protein 2.05631 0.02562415 AT4G33050 calmodulin-binding family protein 2.311602 0.00397325 AT4G33550 Bifunctional inhibitor/lipid-transfer protein/seed storage 2S albumin superfamily protein 2.352356 0.04922457 AT4G35165 egg cell-secreted-like protein (DUF1278) 2.821173 0.03612151 AT4G35290 glutamate receptor 2 5.216695 0.04591054 AT4G36380 Cytochrome P450 superfamily protein 3.696886 0.03634587 AT4G36400 FAD-linked oxidases family protein 2.333057 0.04908833 AT4G39100 PHD finger family protein / bromo-adjacent homology (BAH) domain-containing protein 2.386542 0.03723632 AT4G39120 inositol monophosphatase family protein 2.488647 6.45774E-07 AT5G01570 plectin-like protein 2.466711 <th< td=""><td>AT4G32010</td><td>HSI2-like 1</td><td>3.397758</td><td>0.009151615</td></th<>	AT4G32010	HSI2-like 1	3.397758	0.009151615
AT4G32590 2Fe-2S ferredoxin-like superfamily protein 4.732327 8.28746E-06 AT4G32650 potassium channel protein 9.374159 2.31269E-10 AT4G32950 Protein phosphatase 2C family protein 2.05631 0.02562415 AT4G33050 calmodulin-binding family protein 2.311602 0.00397325 AT4G33550 Bifunctional inhibitor/lipid-transfer protein/seed storage 2S albumin superfamily protein 2.352356 0.04922457 AT4G35165 egg cell-secreted-like protein (DUF1278) 2.821173 0.03612151 AT4G35290 glutamate receptor 2 5.216695 0.04591054 AT4G36400 FAD-linked oxidases family protein 3.696886 0.03634587 AT4G37970 cinnamyl alcohol dehydrogenase 6 5.543145 0.006092639 AT4G39100 PHD finger family protein / bromo-adjacent homology (BAH) domain-containing protein 2.386542 0.03723632 AT4G39120 inositol monophosphatase family protein 2.488647 6.45774E-07 AT5G01570 plectin-like protein 2.716811 0.006230382 AT5G02180 Transmembrane amino acid transporter family protein 20.02285	AT4G32180	pantothenate kinase 2	2.038836	0.01068537
AT4G32650 potassium channel protein 9.374159 2.31269E-10 AT4G32950 Protein phosphatase 2C family protein 2.05631 0.02562415 AT4G33050 calmodulin-binding family protein 2.311602 0.00397325 AT4G33550 Bifunctional inhibitor/lipid-transfer protein/seed storage 2S albumin superfamily protein 2.352356 0.04922457 AT4G35165 egg cell-secreted-like protein (DUF1278) 2.821173 0.03612151 AT4G35290 glutamate receptor 2 5.216695 0.04591054 AT4G36380 Cytochrome P450 superfamily protein 3.696886 0.03634587 AT4G36400 FAD-linked oxidases family protein 2.333057 0.04908833 AT4G37970 cinnamyl alcohol dehydrogenase 6 5.543145 0.006092639 AT4G39100 PHD finger family protein / bromo-adjacent homology (BAH) domain-containing protein 2.386542 0.03723632 AT5G01570 plectin-like protein 2.716811 0.006230382 AT5G02180 Transmembrane amino acid transporter family protein 2.02285 3.03943E-07	AT4G32375	Pectin lyase-like superfamily protein	8.687519	1.72573E-08
AT4G32950 Protein phosphatase 2C family protein 2.05631 0.02562415 AT4G33050 calmodulin-binding family protein 2.311602 0.00397325 AT4G33550 Bifunctional inhibitor/lipid-transfer protein/seed storage 2S albumin superfamily protein 2.352356 0.04922457 AT4G35165 egg cell-secreted-like protein (DUF1278) 2.821173 0.03612151 AT4G35290 glutamate receptor 2 5.216695 0.04591054 AT4G36380 Cytochrome P450 superfamily protein 3.696886 0.03634587 AT4G36400 FAD-linked oxidases family protein 2.333057 0.04908833 AT4G39700 cinnamyl alcohol dehydrogenase 6 5.543145 0.006092639 AT4G39100 PHD finger family protein / bromo-adjacent homology (BAH) 2.386542 0.03723632 AT5G01570 plectin-like protein 2.488647 6.45774E-07 AT5G01570 plectin-like protein 2.466711 0.04261023 AT5G02180 Transmembrane amino acid transporter family protein 20.02285 3.03943E-07	AT4G32590	2Fe-2S ferredoxin-like superfamily protein	4.732327	8.28746E-06
AT4G33050 calmodulin-binding family protein 2.311602 0.00397325 AT4G33550 Bifunctional inhibitor/lipid-transfer protein/seed storage 2S albumin superfamily protein 2.352356 0.04922457 AT4G35165 egg cell-secreted-like protein (DUF1278) 2.821173 0.03612151 AT4G35290 glutamate receptor 2 5.216695 0.04591054 AT4G36380 Cytochrome P450 superfamily protein 3.696886 0.03634587 AT4G37970 cinnamyl alcohol dehydrogenase 6 5.543145 0.006092639 AT4G39100 PHD finger family protein / bromo-adjacent homology (BAH) domain-containing protein 2.386542 0.03723632 AT5G01570 plectin-like protein 2.716811 0.006230382 AT5G01570 plectin-like protein 2.466711 0.04261023 AT5G02180 Transmembrane amino acid transporter family protein 20.02285 3.03943E-07	AT4G32650	potassium channel protein	9.374159	2.31269E-10
AT4G33550 Bifunctional inhibitor/lipid-transfer protein/seed storage 2S albumin superfamily protein 2.352356 0.04922457 AT4G35165 egg cell-secreted-like protein (DUF1278) 2.821173 0.03612151 AT4G35290 glutamate receptor 2 5.216695 0.04591054 AT4G36380 Cytochrome P450 superfamily protein 3.696886 0.03634587 AT4G36400 FAD-linked oxidases family protein 2.333057 0.04908833 AT4G37970 cinnamyl alcohol dehydrogenase 6 5.543145 0.006092639 AT4G39100 PHD finger family protein / bromo-adjacent homology (BAH) domain-containing protein 2.386542 0.03723632 AT5G01570 plectin-like protein 2.716811 0.006230382 AT5G01570 plectin-like protein 2.466711 0.04261023 AT5G02180 Transmembrane amino acid transporter family protein 20.02285 3.03943E-07	AT4G32950	Protein phosphatase 2C family protein	2.05631	0.02562415
albumin superfamily protein 2.821173 0.03612151 AT4G35165 egg cell-secreted-like protein (DUF1278) 2.821173 0.03612151 AT4G35290 glutamate receptor 2 5.216695 0.04591054 AT4G36380 Cytochrome P450 superfamily protein 3.696886 0.03634587 AT4G36400 FAD-linked oxidases family protein 2.333057 0.04908833 AT4G37970 cinnamyl alcohol dehydrogenase 6 5.543145 0.006092639 AT4G39100 PHD finger family protein / bromo-adjacent homology (BAH) domain-containing protein 2.386542 0.03723632 AT4G39120 inositol monophosphatase family protein 2.488647 6.45774E-07 AT5G01570 plectin-like protein 2.716811 0.006230382 AT5G01570 plectin-like protein 2.466711 0.04261023 AT5G02180 Transmembrane amino acid transporter family protein 20.02285 3.03943E-07	AT4G33050	calmodulin-binding family protein	2.311602	0.00397325
AT4G35290 glutamate receptor 2 5.216695 0.04591054 AT4G36380 Cytochrome P450 superfamily protein 3.696886 0.03634587 AT4G36400 FAD-linked oxidases family protein 2.333057 0.04908833 AT4G37970 cinnamyl alcohol dehydrogenase 6 5.543145 0.006092639 AT4G39100 PHD finger family protein / bromo-adjacent homology (BAH) domain-containing protein 2.386542 0.03723632 AT4G39120 inositol monophosphatase family protein 2.488647 6.45774E-07 AT5G01570 plectin-like protein 2.716811 0.006230382 AT5G01570 plectin-like protein 2.466711 0.04261023 AT5G02180 Transmembrane amino acid transporter family protein 20.02285 3.03943E-07	AT4G33550	albumin superfamily protein	2.352356	0.04922457
AT4G36380 Cytochrome P450 superfamily protein 3.696886 0.03634587 AT4G36400 FAD-linked oxidases family protein 2.333057 0.04908833 AT4G37970 cinnamyl alcohol dehydrogenase 6 5.543145 0.006092639 AT4G39100 PHD finger family protein / bromo-adjacent homology (BAH) domain-containing protein 2.386542 0.03723632 AT4G39120 inositol monophosphatase family protein 2.488647 6.45774E-07 AT5G01570 plectin-like protein 2.716811 0.006230382 AT5G02180 Transmembrane amino acid transporter family protein 20.02285 3.03943E-07	AT4G35165		2.821173	0.03612151
AT4G36400 FAD-linked oxidases family protein 2.333057 0.04908833 AT4G37970 cinnamyl alcohol dehydrogenase 6 5.543145 0.006092639 AT4G39100 PHD finger family protein / bromo-adjacent homology (BAH) domain-containing protein 2.386542 0.03723632 AT4G39120 inositol monophosphatase family protein 2.488647 6.45774E-07 AT5G01570 plectin-like protein 2.716811 0.006230382 AT5G02180 Transmembrane amino acid transporter family protein 20.02285 3.03943E-07	AT4G35290	glutamate receptor 2	5.216695	0.04591054
AT4G37970 cinnamyl alcohol dehydrogenase 6 5.543145 0.006092639 AT4G39100 PHD finger family protein / bromo-adjacent homology (BAH) domain-containing protein 2.386542 0.03723632 AT4G39120 inositol monophosphatase family protein 2.488647 6.45774E-07 AT5G01570 plectin-like protein 2.716811 0.006230382 AT5G01570 plectin-like protein 2.466711 0.04261023 AT5G02180 Transmembrane amino acid transporter family protein 20.02285 3.03943E-07	AT4G36380	Cytochrome P450 superfamily protein	3.696886	0.03634587
AT4G39100 PHD finger family protein / bromo-adjacent homology (BAH) domain-containing protein 2.386542 0.03723632 AT4G39120 inositol monophosphatase family protein 2.488647 6.45774E-07 AT5G01570 plectin-like protein 2.716811 0.006230382 AT5G01570 plectin-like protein 2.466711 0.04261023 AT5G02180 Transmembrane amino acid transporter family protein 20.02285 3.03943E-07	AT4G36400	FAD-linked oxidases family protein	2.333057	0.04908833
domain-containing protein 2.488647 6.45774E-07 AT4G39120 inositol monophosphatase family protein 2.488647 6.45774E-07 AT5G01570 plectin-like protein 2.716811 0.006230382 AT5G01570 plectin-like protein 2.466711 0.04261023 AT5G02180 Transmembrane amino acid transporter family protein 20.02285 3.03943E-07	AT4G37970	cinnamyl alcohol dehydrogenase 6	5.543145	0.006092639
AT4G39120 inositol monophosphatase family protein 2.488647 6.45774E-07 AT5G01570 plectin-like protein 2.716811 0.006230382 AT5G01570 plectin-like protein 2.466711 0.04261023 AT5G02180 Transmembrane amino acid transporter family protein 20.02285 3.03943E-07	AT4G39100	domain-containing protein	2.386542	0.03723632
AT5G01570 plectin-like protein 2.466711 0.04261023 AT5G02180 Transmembrane amino acid transporter family protein 20.02285 3.03943E-07	AT4G39120		2.488647	6.45774E-07
AT5G02180 Transmembrane amino acid transporter family protein 20.02285 3.03943E-07	AT5G01570	plectin-like protein	2.716811	0.006230382
	AT5G01570	plectin-like protein	2.466711	0.04261023
ATT CONTENT 1 1 1 1 2	AT5G02180	Transmembrane amino acid transporter family protein	20.02285	3.03943E-07
A15G03570 iron regulated 2 2.971391 0.007952118	AT5G03570	iron regulated 2	2.971391	0.007952118

AT5G03790	homeobox 51	2.503521	0.03495556
AT5G04130	DNA GYRASE B2	2.318108	0.02361126
AT5G04347	Plant self-incompatibility protein S1 family	3.21431	0.02128419
AT5G04620	biotin F	3.122892	0.003802821
AT5G04980	DNAse I-like superfamily protein	2.070487	0.000531153
AT5G05080	ubiquitin-conjugating enzyme 22	2.270938	0.02292832
AT5G05380	prenylated RAB acceptor 1.B3	3.192314	0.04089586
AT5G05410	DRE-binding protein 2A	10.46146	0.007416999
AT5G05940	ROP guanine nucleotide exchange factor 5	2.066371	0.003127197
AT5G06710	homeobox leucine zipper protein	3.041735	0.01252243
AT5G06780	Emsy N Terminus (ENT)/ plant Tudor-like domains-containing protein	4.588196	3.11375E-08
AT5G07850	HXXXD-type acyl-transferase family protein	5.445164	0.005902726
AT5G08180	Ribosomal protein L7Ae/L30e/S12e/Gadd45 family protein	8.590748	0.01759076
AT5G08315	Defensin-like (DEFL) family protein	4.70752	0.009725877
AT5G08420	RNA-binding KH domain-containing protein	2.847352	0.03912502
AT5G08750	RING/FYVE/PHD zinc finger superfamily protein	3.351176	1.04778E-14
AT5G08650	Small GTP-binding protein	3.407278	1.1925E-15
AT5G09690	magnesium transporter 7	2.098169	0.009870869
AT5G10150	UPSTREAM OF FLC protein (DUF966)	2.184128	0.002120284
AT5G10190	Major facilitator superfamily protein	2.719847	0.000799594
AT5G10630	Translation elongation factor EF1A/initiation factor IF2gamma family protein	2.69144	0.005515907
AT5G10690	pentatricopeptide (PPR) repeat-containing protein / CBS domain-containing protein	10.413	0.006536895
AT5G11210	glutamate receptor 2.5	7.178178	0.03707997
AT5G11940	Subtilase family protein	3.274113	0.008511817
AT5G13640	phospholipid:diacylglycerol acyltransferase	4.020392	0.002140603
AT5G13950	nuclear factor kappa-B-binding protein	10.56848	0.0068319
AT5G16030	mental retardation GTPase activating protein	2.066766	0.02567592
AT5G16470	zinc finger (C2H2 type) family protein	10.00067	0.004345995
AT5G16690	origin recognition complex subunit 3	2.185364	0.01264199
AT5G16660	Low-density receptor-like protein	7.395254	0.03328362
AT5G17100	Cystatin/monellin superfamily protein	2.109871	0.000634358
AT5G19380	CRT (chloroquine-resistance transporter)-like transporter 1	4.390983	0.006797042
AT5G19410	ABC-2 type transporter family protein	2.011236	0.04866233
AT5G18680	tubby like protein 11	2.752784	0.006635486
AT5G20220	zinc knuckle (CCHC-type) family protein	2.461945	0.008334353
AT5G20720	chaperonin 20	5.233929	0.00059707
AT5G22040	ubiquitin carboxyl-terminal hydrolase	8.355556	0.01869164
AT5G22460	alpha/beta-Hydrolases superfamily protein	3.110812	0.002765485
AT5G22620	phosphoglycerate/bisphosphoglycerate mutase family protein	3.303551	0.02298083
AT5G22970	hypothetical protein AT5G22970	3.810316	0.005504879
AT5G23010	methylthioalkylmalate synthase 1	3.284597	3.1858E-06

AT5G23020	2-isopropylmalate synthase 2	3.299066	0.03513006
AT5G23260	K-box region and MADS-box transcription factor family protein	6.96135	0.03506018
AT5G23260	K-box region and MADS-box transcription factor family protein	6.771545	5.34379E-06
AT5G23250	Succinyl-CoA ligase, alpha subunit	5.047549	2.1478E-05
AT5G23490	hypothetical protein AT5G23490	8.660064	0.02221849
AT5G23520	smr (Small MutS Related) domain-containing protein	2.663034	0.01721618
AT5G23570	XS domain-containing protein / XS zinc finger domain-containing protein-like protein	2.337864	1.24766E-14
AT5G24316	proline-rich family protein	3.801463	0.02386052
AT5G25320	ACT-like superfamily protein	4.893512	3.15184E-05
AT5G25756	hypothetical protein AT5G25756	3.095449	0.0387529
AT5G26250	Major facilitator superfamily protein	7.213707	4.42688E-08
AT5G26920	Cam-binding protein 60-like G	2.623633	0.03717272
AT5G27570	cell division cycle 20.2, cofactor of APC complex-like protein	2.728015	0.02127468
AT5G27560	DUF1995 domain protein, putative (DUF1995)	8.959069	0.00017367
AT5G28020	cysteine synthase D2	8.240651	0.02017029
AT5G28020	cysteine synthase D2	9.532273	0.01158415
AT5G33340	Eukaryotic aspartyl protease family protein	2.58636	0.007120511
AT5G33390	glycine-rich protein	2.951136	0.01469662
AT5G34905	ECA1 gametogenesis family protein (DUF784)	3.685747	0.03561875
AT5G36310	ECA1 gametogenesis related family protein	2.557503	0.04086488
AT5G37340	ZPR1 zinc-finger domain protein	3.391809	0.01648891
AT5G37470	hypothetical protein (DUF577)	5.457034	0.001195537
AT5G37370	PRP38 family protein	2.831797	0.01269259
AT5G38330	low-molecular-weight cysteine-rich 80	7.817552	0.000349115
AT5G38690	Zinc-finger domain of monoamine-oxidase A repressor R1 protein	6.494276	0.000573506
AT5G39365	Defensin-like (DEFL) family protein	4.244029	0.000402633
AT5G40440	mitogen-activated protein kinase kinase 3	6.158912	4.63748E-07
AT5G40720	C3H4 type zinc finger protein (DUF23)	8.143575	0.02306152
AT5G40840	Rad21/Rec8-like family protein	2.87035	8.76529E-07
AT5G40820	Ataxia telangiectasia-mutated and RAD3-like protein	10.6514	0.006407471
AT5G41150	Restriction endonuclease, type II-like superfamily protein	2.537833	0.02339098
AT5G41680	Protein kinase superfamily protein	2.311096	0.002074033
AT5G42940	RING/U-box superfamily protein	2.538216	9.96586E-06
AT5G43350	phosphate transporter 1;1	6.195555	4.14641E-06
AT5G43360	phosphate transporter 1;3	6.916509	8.62695E-05
AT5G43285	Putative membrane lipoprotein	2.113548	0.01680572
AT5G43513	Putative membrane lipoprotein	3.632255	0.008216056
AT5G43518	Putative membrane lipoprotein	5.33776	0.012759
AT5G43560	TRAF-like superfamily protein	3.60037	3.85046E-14
AT5G43695	hypothetical protein AT5G43695	6.024621	3.81969E-06
AT5G43880	methyl-coenzyme M reductase II subunit gamma, putative (DUF3741)	8.094009	0.02215769
AT5G44582	hypothetical protein AT5G44582	2.866038	0.03512479

	6.32175E-05
AT5G44785 organellar single-stranded DNA binding protein 3 3.30303 0.	
	0.009754743
1	0.02572372
	0.02501006
	0.02954482
7	0.00037729
1 / 11	0.003858945
· · · · · · · · · · · · · · · · · · ·	0.04496195
	0.01748343
	0.005400103
	0.005129289
	0.005279587
AT5G51490 Plant invertase/pectin methylesterase inhibitor superfamily 4.263824	0.02848893
AT5G51450 RPM1 interacting protein 3 3.723372 0.	0.009417514
AT5G51810 gibberellin 20 oxidase 2 2.070847 0.	0.009361799
AT5G53030 hypothetical protein AT5G53030 3.368876 0	0.01151923
AT5G53080 Tetratricopeptide repeat (TPR)-like superfamily protein 2.595434 0	0.02014616
AT5G53120 spermidine synthase 3 2.378596 0	0.002456869
AT5G54280 myosin 2 2.596438 9	9.16834E-08
AT5G55400 Actin binding Calponin homology (CH) domain-containing protein 10.7394 0.	0.005212511
	0.02135325
AT5G55132 Defensin-like (DEFL) family protein 6.937922	0.04520022
AT5G55250 IAA carboxylmethyltransferase 1 7.198779	0.04959308
AT5G56190 Transducin/WD40 repeat-like superfamily protein 8.038624 0.	0.000212046
AT5G56250 hapless 8 9.277401 0	0.01113334
AT5G56260 Ribonuclease E inhibitor RraA/Dimethylmenaquinone 6.705865 4 methyltransferase	4.63563E-07
AT5G56700 FBD / Leucine Rich Repeat domains containing protein 5.725686 2	2.13275E-05
AT5G57270 Core-2/I-branching beta-1,6-N-acetylglucosaminyltransferase family protein 4.756178	0.01339303
AT5G57380 Fibronectin type III domain-containing protein 2.120101	0.02773449
1 11	0.01162721
AT5G57565 Protein kinase superfamily protein 4.826486 0	0.01127007
AT5G57860 Ubiquitin-like superfamily protein 3.802636 0	0.02039239
AT5G58100 transmembrane protein 6.599035 0	0.04747833
AT5G58412 Putative membrane lipoprotein 3.338609 0	0.002106889
AT5G58610 PHD finger transcription factor 8.176388 0	0.02790395
AT5G59890 actin depolymerizing factor 4 6.524879 0	0.04597661
AT5G60000 transmembrane protein 4.807255 2	2.83108E-06
AT5G60060 F-box SKIP23-like protein (DUF295) 4.219472 2	2.38086E-08
AT5G60470 C2H2 and C2HC zinc fingers superfamily protein 6.017235 9	9.74109E-05
AT5G60964 ECA1 gametogenesis related family protein 6.719014 0.	0.000895139
AT5G60950 COBRA-like protein 5 precursor 2.920025 0	0.02267707

AT5G61250	glucuronidase 1	7.02805	0.000210427
AT5G61530	small G protein family protein / RhoGAP family protein	2.911455	0.008666472
AT5G62100	BCL-2-associated athanogene 2	3.116207	0.000542565
AT5G62460	RING/FYVE/PHD zinc finger superfamily protein	10.70767	0.005746759
AT5G63063	Plant thionin family protein	3.600878	0.01866349
AT5G63090	Lateral organ boundaries (LOB) domain family protein	5.969538	0.000581401
AT5G63880	SNF7 family protein	2.484142	0.00172384
AT5G63890	histidinol dehydrogenase	2.796675	2.06486E-13
AT5G63990	Inositol monophosphatase family protein	2.631314	0.003630511
AT5G65070	K-box region and MADS-box transcription factor family protein	2.036235	0.04016269
AT5G65090	DNAse I-like superfamily protein	8.179654	0.02439139
AT5G65100	Ethylene insensitive 3 family protein	2.708501	0.03104386
AT5G65640	beta HLH protein 93	10.78789	0.005760317
AT5G66610	DA1-related protein 7	2.442641	0.000989416
AT5G66640	DA1-related protein 3	7.643911	0.02987537
AT5G66675	transmembrane protein, putative (DUF677)	9.591263	0.00136008
AT3G01331	ECA1 gametogenesis related family protein	6.742179	0.04172564
AT3G04540	Cysteine-rich protein	7.167094	0.04183759
AT4G39760	Galactose oxidase/kelch repeat superfamily protein	6.798376	0.04165194
AT5G25410	transmembrane protein, putative (DUF239)	6.358511	0.04713127
AT5G42232	Defensin-like (DEFL) family protein	7.486243	0.04671478

Annexure 3
List of genes unique to *athmgb15* buds

At ID	Protein name	log2FoldChange	p-value
AT3G23715	SCR-like 13	5.30613	0.000326
AT1G18750	AGAMOUS-like 65	8.537677492	4.06E-06
AT1G26796	Plant self-incompatibility protein S1 family	7.828888156	2.98E-09
AT1G47603	purine permease 19	5.48172496	0.000905
AT2G12475	Defensin-like (DEFL) family protein	6.778214	0.000514
AT4G14276	Defensin-like (DEFL) family protein	7.175129	0.000255
AT4G32650	potassium channel protein	9.374159	2.31E-10
AT3G11560	LETM1-like protein	9.293495	4.36E-12
AT3G30383	inhibitor/lipid-transfer protein/seed storage 2S albumin superfamily protein (DUF784)	7.481746	0.001049
AT4G03298	transmembrane protein	5.804482	0.000158
AT4G09465	Carbohydrate-binding X8 domain superfamily protein	6.777143	0.001303
AT5G60964	ECA1 gametogenesis related family protein	6.719014	0.000895
AT1G16570	UDP-Glycosyltransferase superfamily protein	6.86976928	0.014421
AT1G21000	PLATZ transcription factor family protein	3.987072035	0.012735
AT1G29170	SCAR family protein	9.065936122	6.73E-12
AT1G62530	hypothetical protein (DUF863)	7.537682	2.83E-08
AT5G43695	hypothetical protein AT5G43695	6.024621	3.82E-06
AT3G05520	Subunits of heterodimeric actin filament capping protein Capz superfamily	6.199163	0.017163
AT3G46616	hypothetical protein AT3G46616	5.524045	0.000102
AT1G35530	DEAD/DEAH box RNA helicase family protein	9.562501278	3.37E-06
AT2G27580	A20/AN1-like zinc finger family protein	7.404774	0.001741
AT4G31080	integral membrane metal-binding family protein (DUF2296)	6.316782	5.14E-06
AT1G08820	vamp/synaptobrevin-associated protein 27-2	9.324883818	0.001006
AT1G18750	AGAMOUS-like 65	10.92502763	2.03E-16
AT1G18750	AGAMOUS-like 65	5.245362163	0.001981
AT1G48360	zinc ion binding/nucleic acid binding/hydrolase	9.169084106	7.79E-13
AT1G50690	Cystatin/monellin superfamily protein	6.259947937	5.25E-06
AT1G55030	RNI-like superfamily protein	5.982968	3.81E-06
AT1G60200	splicing factor PWI domain-containing protein / RNA recognition motif (RRM)-containing protein	11.12271	1.44E-13
AT1G65800	receptor kinase 2	10.04343	2.37E-07
AT1G78955	camelliol C synthase 1	7.979485	9.32E-06
AT2G16980	Major facilitator superfamily protein	6.907417	8.53E-08
AT2G19150	Pectin lyase-like superfamily protein	5.18822	0.000183
AT2G24650	B3 domain-containing protein REM13	10.13123	1.37E-10
AT2G25297	transmembrane protein	5.155783	0.000399
AT2G24650	B3 domain-containing protein REM13	10.21865	2.76E-10
AT2G27060	Leucine-rich repeat protein kinase family protein	9.237255	1.76E-10

AT2G33205	Serinc-domain containing serine and sphingolipid biosynthesis protein	7.389179	2.44E-06
AT2G40995	Molecular chaperone Hsp40/DnaJ family protein	6.35498	0.000318
AT3G01085	Protein kinase superfamily protein	8.617143	8.79E-05
AT3G08960	ARM repeat superfamily protein	9.840956	1.48E-13
AT3G10116	COBRA-like extracellular glycosyl-phosphatidyl inositol-anchored protein family	3.957107	0.010788
AT3G45440	Concanavalin A-like lectin protein kinase family protein	4.532073	0.037955
AT3G48205	plant thionin family protein	5.731519	0.000129
AT3G61400	2-oxoglutarate (2OG) and Fe(II)-dependent oxygenase superfamily protein	4.660635	0.009029
AT4G04190	transmembrane protein	5.58775	0.003876
AT4G13960	F-box/RNI-like superfamily protein	5.093827	0.000195
AT4G22200	potassium transport 2/3	10.82904	6.52E-09
AT4G31073	hypothetical protein AT4G31073	3.987072	0.012735
AT4G32375	Pectin lyase-like superfamily protein	8.687519	1.73E-08
AT4G37970	cinnamyl alcohol dehydrogenase 6	5.543145	0.006093
AT5G27560	DUF1995 domain protein, putative (DUF1995)	8.959069	0.000174
AT5G56190	Transducin/WD40 repeat-like superfamily protein	8.038624	0.000212
AT5G56700	FBD / Leucine Rich Repeat domains containing protein	5.725686	2.13E-05
AT5G60470	C2H2 and C2HC zinc fingers superfamily protein	6.017235	9.74E-05
AT1G21970	Histone superfamily protein	4.586852652	0.001043
AT1G28327	E3 ubiquitin-protein ligase	6.963389745	6.41E-06
AT1G49770	basic helix-loop-helix (bHLH) DNA-binding superfamily protein	8.838787071	2.97E-11
AT1G54300	hypothetical protein AT1G54300	4.991733	0.001633
AT1G65990	type 2 peroxiredoxin-related / thiol specific antioxidant / mal allergen family protein	6.629767	0.000132
AT1G67960	POLLEN DEFECTIVE IN GUIDANCE-like protein	11.38092	2.75E-19
AT3G01900	cytochrome P450, family 94, subfamily B, polypeptide 2	7.544698	8.77E-05
AT3G05950	RmlC-like cupins superfamily protein	6.410327	4.75E-06
AT3G29800	P-loop containing nucleoside triphosphate hydrolases superfamily protein	5.861207	1.46E-05
AT3G44920	cation/H+ exchanger 11	7.203013	1.6E-06
AT3G53050	D-galactoside/L-rhamnose binding SUEL lectin protein	5.595355	9.4E-05
AT3G61400	2-oxoglutarate (2OG) and Fe(II)-dependent oxygenase superfamily protein	6.177744	1.8E-06
AT3G61940	Cation efflux family protein	5.89988	9.13E-05
AT4G02830	hypothetical protein AT4G02830	6.919076	1.74E-06
AT4G13660	pinoresinol reductase 2	7.671484	1.07E-07
AT4G23350	transmembrane protein, putative (DUF239)	7.238348	0.000352
AT4G30300	non-intrinsic ABC protein 15	4.713083	0.002354
AT5G26250	Major facilitator superfamily protein	7.213707	4.43E-08
AT5G38330	low-molecular-weight cysteine-rich 80	7.817552	0.000349

AT5G43350	phosphate transporter 1;1	6.195555	4.15E-06
AT5G43360	phosphate transporter 1;3	6.916509	8.63E-05
AT2G28990	Leucine-rich repeat protein kinase family protein	5.642404	0.001136
AT2G33130	ralf-like 18	6.888436	0.00017
AT2G34230	ubiquitin carboxyl-terminal hydrolase-like protein, putative (DUF627 and DUF629)	7.638201	3.68E-09
AT2G41920	Protein kinase superfamily protein	5.545227	9E-05
AT2G04041	ECA1 gametogenesis family protein (DUF784)	8.459863	0.000215
AT1G68935	hypothetical protein AT1G68935	5.200068	0.00665
AT4G26790	GDSL-like Lipase/Acylhydrolase superfamily protein	11.56159	5.24E-08
AT4G16765	2-oxoglutarate (2OG) and Fe(II)-dependent oxygenase superfamily protein	10.35862	3.4E-08
AT2G38255	hypothetical protein (DUF239)	6.19827	0.001354
AT5G61250	glucuronidase 1	7.02805	0.00021
AT5G63090	Lateral organ boundaries (LOB) domain family protein	5.969538	0.000581
AT2G43840	UDP-glycosyltransferase 74 F1	8.835969	6.06E-08
AT5G23260	K-box region and MADS-box transcription factor family protein	6.771545	5.34E-06

Annexure 4
TFs Differentially regulated in bud transcriptome:

Categories	At ID	log2FoldChange	p-value
	AT1G14350	-2.389285307	0.006656512
	AT3G18100	-4.04682	0.03609517
	AT3G46130	-6.173763	0.000428888
	AT3G27810	-0.3656374	0.6799984
MYB	AT5G40350	0.09722783	0.8498625
	AT1G08810	3.107639463	0.001736821
	AT3G02940	2.6465	0.04047641
	AT2G36960	2.520406	0.000970771
	AT3G09600	2.426177	0.006351625
	AT4G26930	2.617739	0.01558095
	AT1G18750	-3.649108771	5.62966E-15
M-type MADS	AT1G60040	-4.645071	0.002977492
WI-type_WIADS	AT1G65330	3.104721	0.04794914
	AT1G18750	10.92502763	5.62966E-15
ERF	AT1G19210	-2.215749701	2.54021E-06
	AT1G69310	-2.093063	0.04532457
WRKY	AT4G26640	-2.003166	0.002745174
	AT1G18860	4.594130585	0.000780014
	AT2G18300	-7.622117	4.89108E-06
	AT4G30980	-2.845675	0.00045684
	AT1G26260	2.487379095	0.013179378
bHLH	AT1G49770	8.838787071	2.96814E-11
	AT4G00480	6.812231	0.03759579
	AT4G28790	4.881363	0.00372303
	AT5G65640	10.78789	0.005760317
TALE	AT2G27220	-8.565503	6.13828E-11
	AT2G31370	-8.056477	0.02464786
bZIP	AT2G41070	-4.973696	0.000340031
TCP	AT3G27010	-9.542992	0.01106747
NAC	AT3G44350	-4.877605	0.000435503
Dof	AT4G00940	-9.43932	0.01276191
	AT2G28810	8.167118	0.01947837
Nin-like	AT4G35270	-8.429571	8.85571E-07
G2-like	AT5G06800	-4.813384	0.001744282
	AT5G25470	-2.452268	0.006862986
В3	AT2G24696	-5.368502	0.001833493
D 3	AT2G24650	10.13123	1.37426E-10
	AT4G32010	3.397758	0.009151615
FAR1	AT5G28530	-7.486677	0.03405284

HSF	AT5G45710	-8.272584	8.37127E-08
	AT5G63090	-3.907084	0.02161217
LDD	AT2G23660	6.857431	0.03921609
LBD	AT3G27650	2.010803	0.008515707
	AT3G27940	5.122576	0.0433607
GeBP	AT1G66420	-4.614648	0.002189282
	AT1G05230	2.617589433	0.00762367
HD-ZIP	AT5G06710	3.041735	0.01252243
	AT5G03790	2.503521	0.03495556
NF-YC	AT1G08970	9.496868508	0.010877126
NF-X1	AT1G10170	5.329059584	0.000428472
NF-YB	AT1G21970	4.586852652	0.001043233
	AT5G47670	3.207655	0.04496195
Trihelix	AT1G13450	3.377871747	0.00991029
G2-like	AT1G69580	3.267201	0.01156912
C2H2	AT2G42410	7.27082	0.03071243
	AT5G60470	6.017235	9.74109E-05
	AT3G57390	2.556495	8.38019E-16
	AT4G18960	2.779618	0.000468386
	AT5G23260	6.96135	0.03506018
MIKC MADS	AT5G65070	2.036235	0.04016269
	AT4G19990	7.256419	0.03330097
	AT5G05410	10.46146	0.007416999
	AT5G45980	2.772443	0.02954482
	AT5G65100	2.708501	0.03104386

Annexure 5

Common genes between *athmgb15* flower and *athmgb15* bud transcriptome

At ID	ProteinName	Fold change in bud	Fold change in flower	
AT2G29320	NAD(P)-binding Rossmann-fold superfamily protein;(source:Araport11)	3.842082	0.801975	
AT2G21655	ECA1 gametogenesis family protein (DUF784);(source:Araport11)	4.225331	1.20976	
AT5G66675	transmembrane protein, putative (DUF677);(source:Araport11)	9.591263	-0.913368	
AT2G03140	Eukaryotic aspartyl protease family protein;(source:Araport11)	4.941973	0.389798	
AT4G32375	Pectin lyase-like superfamily protein;(source:Araport11)	8.687519	4.26237	
AT1G69100	Eukaryotic aspartyl protease family protein	4.399078	1.96584	
AT2G19050	GDSL-like Lipase/Acylhydrolase superfamily protein	-5.116338	-2.62033	
AT5G16030	mental retardation GTPase activating protein	-2.326797	0.756119	
AT3G05155	Major facilitator superfamily protein	5.020868	3.43576	
AT5G60000	transmembrane protein	4.807255	1.21185	
AT3G01085	Protein kinase superfamily protein	8.617143	-0.97598	
AT4G13263	ECA1 gametogenesis family protein (DUF784)	4.542668	1.30062	
AT2G04037	ECA1 gametogenesis family protein (DUF784)	4.106271	1.48599	
AT2G36325	GDSL-like Lipase/Acylhydrolase superfamily protein	2.951925	1.5747	
AT4G08025	ECA1 gametogenesis family protein (DUF784)	4.308397	1.18515	
AT2G21727	ECA1 gametogenesis family protein (DUF784)	4.41582	1.29335	
AT5G04347	Plant self-incompatibility protein S1 family	3.21431	1.92656	
AT2G02960	RING/FYVE/PHD zinc finger superfamily protein	-6.6346	-0.348282	
AT1G22120	hypothetical protein AT1G22120	4.2415936	4.45617	
AT2G30950	FtsH extracellular protease family	4.764008	0.969073	
AT3G05950	RmlC-like cupins superfamily protein	6.410327	3.16873	
AT5G28237	Pyridoxal-5\\'-phosphate-dependent enzyme family protein	-2.489633	-0.887339	
AT5G07850	HXXXD-type acyl-transferase family protein	5.445164	5.02023	
AT1G57760	ECA1 gametogenesis family protein (DUF784)	6.179371	0.963326	
AT4G25310	2-oxoglutarate (2OG) and Fe(II)-dependent oxygenase superfamily protein	2.744982	6.6129	
AT1G67623	F-box family protein	-5.767576	-5.46929	
AT2G43010	phytochrome interacting factor 4	2.476549	0.875968	
AT1G47470	ECA1 gametogenesis family protein (DUF784)	3.7993796	1.38214	
AT5G39365	Defensin-like (DEFL) family protein	4.244029	4.06995	
AT3G01990	ACT domain repeat 6	2.096772	-1.15969	
AT1G28327	E3 ubiquitin-protein ligase	6.9633897	6.08527	
AT5G02860	Pentatricopeptide repeat (PPR) superfamily protein	-4.264113	0.74117	
AT1G26796	Plant self-incompatibility protein S1 family	7.8288882	4.45052	
AT1G79520	Cation efflux family protein	-2.539219	0.736653	
AT2G24205	ECA1 gametogenesis related family protein	3.754762	1.47908	
AT5G03570	iron regulated 2	2.971391	2.32284	
AT3G05150	Major facilitator superfamily protein	7.521831	-0.991899	
AT2G44810	alpha/beta-Hydrolases superfamily protein (DAD1)	2.856945	-2.01128	

AT2G27930	PLATZ transcription factor family protein	-2.199345	0.730954
AT3G17660	ARF-GAP domain 15	3.719318	-0.893387
AT3G28770	transmembrane protein, putative (DUF1216)	-8.051549	1.5938
AT2G02490	transmembrane protein	3.158014	1.65572
AT3G17120	transmembrane protein	-8.675713	-1.08609
AT2G16980	Major facilitator superfamily protein	6.907417	2.42239
AT3G21570	proline-rich nuclear receptor coactivator	-2.865857	-3.8023
AT1G62530	hypothetical protein (DUF863)	7.537682	3.85821
AT5G19110	Eukaryotic aspartyl protease family protein	-3.621784	-2.47383
AT1G63770	Peptidase M1 family protein	-5.116777	0.721723
AT4G16920	Disease resistance protein (TIR-NBS-LRR class) family	-8.754508	0.723942
AT3G29797	ECA1 gametogenesis family protein (DUF784)	2.953232	1.01026
AT5G48140	Pectin lyase-like superfamily protein	-3.972275	-3.51014
AT2G26530	AR781, pheromone receptor-like protein (DUF1645)	-7.554986	-1.8603
AT3G44006	hypothetical protein AT3G44006	6.682479	6.59466
AT1G31450	Eukaryotic aspartyl protease family protein	2.6898255	2.67288
AT2G35615	Eukaryotic aspartyl protease family protein	3.115486	2.78515
AT1G19210	Integrase-type DNA-binding superfamily protein	3.113460	-2.00442
ATTGT9210	integrase-type DNA-binding superfamily protein	2.2157497	-2.00442
AT5G13950	nuclear factor kappa-B-binding protein	10.56848	0.434289
AT3G19830	Calcium-dependent lipid-binding (CaLB domain) family protein	2.200126	-1.25076
AT4G11810	Major Facilitator Superfamily with SPX (SYG1/Pho81/XPR1) domain- containing protein	-2.780397	-3.35056
AT5G51490	Plant invertase/pectin methylesterase inhibitor superfamily	4.263824	5.21488
AT5G24210	alpha/beta-Hydrolases superfamily protein	-7.519876	2.22488
AT4G23570	phosphatase-like protein	-6.534913	-0.89162
AT5G42820	Zinc finger C-x8-C-x5-C-x3-H type family protein	-5.199359	0.935247
AT5G66070	RING/U-box superfamily protein	-2.199644	-1.10798
AT3G57390	AGAMOUS-like 18	2.556495	-0.809947
AT1G04880	HMG (high mobility group) box protein with ARID/BRIGHT DNA-binding domain-containing protein	6.4249247	-3.5488
AT1G01140	CBL-interacting protein kinase 9	6.5232676	-0.943833
AT4G20320	CTP synthase family protein	2.318153	-0.589523
AT1G33720	cytochrome P450, family 76, subfamily C, polypeptide 6	-6.834985	2.06455
AT3G01900	cytochrome P450, family 94, subfamily B, polypeptide 2	7.544698	3.53445
AT2G39800	delta1-pyrroline-5-carboxylate synthase 1	-9.337773	1.3749
AT5G05410	DRE-binding protein 2A	10.46146	-0.725328
AT2G21750	Egg cell-secreted protein (DUF1278)	3.393881	2.47106
AT5G60060	F-box SKIP23-like protein (DUF295)	4.219472	5.68772
AT4G22035	F-box only protein	3.348734	4.25939
AT4G30190	HA2	12.56841	0.514665
AT5G53440	LOW protein: zinc finger CCCH domain protein	-11.32552	0.51825
AT4G27670	heat shock protein 21	2.51831	-1.59294
AT3G54050	high cyclic electron flow 1	3.007597	0.654754

AT5G06710	homeobox leucine zipper protein	3.041735	-0.996617
AT2G18300	basic helix-loop-helix (bHLH) DNA-binding superfamily protein	-7.622117	2.27855
AT2G31830	endonuclease/exonuclease/phosphatase family protein	-8.78907	-1.10485
AT3G27650	LOB domain-containing protein 25	2.010803	3.30339
AT5G67420	LOB domain-containing protein 37	-7.90907	1.12637
AT1G73607	low-molecular-weight cysteine-rich 65	3.637387	1.21718
AT3G26980	membrane-anchored ubiquitin-fold protein 4 precursor	2.927879	-1.2974
AT5G52230	methyl-CPG-binding domain protein 13	-7.93767	0.660271
AT5G23010	methylthioalkylmalate synthase 1	3.284597	1.95405
AT4G24680	modifier of snc1	-2.466634	0.369864
AT1G51340	MATE efflux family protein	- 7.8720051	-0.674899
AT4G26930	myb domain protein 97	2.617739	1.65475
AT1G68570	Major facilitator superfamily protein	2.803925	0.974254
AT3G15840	post-illumination chlorophyll fluorescence increase	-2.835209	0.851463
AT4G32650	potassium channel protein	9.374159	1.7653
AT1G74810	HCO3- transporter family	7.157309	1.99744
AT1G49770	basic helix-loop-helix (bHLH) DNA-binding superfamily protein	8.8387871	4.03216
AT3G13110	serine acetyltransferase 2;2	-3.366424	-0.932595
AT2G27580	A20/AN1-like zinc finger family protein	7.404774	-1.15069
AT5G26250	Major facilitator superfamily protein	7.213707	2.11502
AT3G03800	syntaxin of plants 131	4.611457	-1.48533
AT5G37770	EF hand calcium-binding protein family	-3.979999	-0.924126
AT1G70290	trehalose-6-phosphatase synthase S8	9.90143	0.785327
AT3G16520	UDP-glucosyl transferase 88A1	9.537354	0.7221
AT3G45870	nodulin MtN21 /EamA-like transporter family protein	2.692953	1.55453
AT3G07760	Sterile alpha motif (SAM) domain-containing protein	-8.213588	-0.657802
AT1G18860	WRKY DNA-binding protein 61	4.5941306	5.23186
AT5G45980	WUSCHEL related homeobox 8	2.772443	3.41964

Annexure 6

Overlapping genes between *athmgb15* bud transcriptomes and *athmgb15* pollen microarray data by Xia et al.

Sl. no	At ID	Gene Name	Expression in athmgb15 pollen	Expression in athmgb15 bud
1	AT1G18750	AGAMOUS-like 65	Up	Down
2	AT1G48030	mitochondrial lipoamide dehydrogenase 1	Up	Down
3	AT1G51340	MATE efflux family protein	Up	Down
4	AT3G27440	uridine kinase-like 5	Up	Down
5	AT5G45710	winged-helix DNA-binding transcription factor family protein	Down	Down
6	AT1G67623	F-box family protein	Down	Down
7	AT2G19050	GDSL-like Lipase/Acylhydrolase superfamily protein	Down	Down
8	AT3G21570	proline-rich nuclear receptor coactivator	Down	Down
9	AT2G20740	Tetraspanin family protein	Down	Up
10	AT2G27580	A20/ANI-like zinc finger family protein	Down	Up
11	AT2G47730	glutathione S-transferase phi 8	Up	Up
12	AT3G05150	Major facilitator superfamily protein	Down	Up
13	AT3G05520	Subunits of heterodimeric actin filament capping protein Capz superfamily	Up	Up
14	AT3G23870	magnesium transporter NIPA (DUF803)	Down	Up
15	AT3G27930	beta-galactosidase	Up	Up
16	AT3G61400	2-oxoglutarate (20G) and Fe(II)-dependent oxygenase superfamily protein	Up	Up
17	AT5G03570	iron regulated 2	Up	Up
18	AT5G59890	actin depolymerizing factor 4	Up	Up
19	AT5G61530	small G protein family protein / RhoGAP family protein	Down	Up

20	AT5G25410	transmembrane protein, putative (DUF239)	Up	Up
21	AT1G01140	CBL-interacting protein kinase 9	Up	Up
22	AT1G03550	Secretory carrier membrane protein (SCAMP) family protein	Up	Up
23	AT1G04170	eukaryotic translation initiation factor 2 gamma subunit	Down	Down
24	AT1G04880	HMG (high mobility group) box protein with ARID/BRIGHT DNA-binding domain-containing protein	Down	Down
25	AT1G16360	LEM3 (ligand-effect modulator 3) family protein / CDC50 family protein	Up	Down
26	AT1G18860	WRKY DNA-binding protein 61	Up	Up
27	AT1G21080	DNAJ heat shock N-terminal domain-containing protein	Up	Up
28	AT1G22300	general regulatory factor 10	Up	Down
29	AT1G29330	ER lumen protein retaining receptor family protein	Up	Down
30	AT1G34120	inositol polyphosphate 5-phosphatase I	Up	Up
31	AT1G64480	calcineurin B-like protein 8	Up	Up
32	AT1G68140	zinc finger/BTB domain protein, putative (DUF1644)	Up	Up
33	AT1G69100	Eukaryotic aspartyl protease family protein	Up	Up
34	AT2G25530	AFG1-like ATPase family protein	Up	Down
35	AT2G33350	CCT motif family protein	Up	Up
36	AT2G36290	alpha/beta-Hydrolases superfamily protein	Up	Down
37	AT2G45290	Transketolase	Up	Down
38	AT3G07330	Cellulose-synthase-like C6	Down	Down
39	AT3G07760	Sterile alpha motif (SAM) domain-containing protein	Up	Down
40	AT3G13930	Dihydrolipoamide acetyltransferase, long form protein	Up	Down

41	AT3G51150	ATP binding microtubule motor family protein	Down	Down
42	AT3G58160	P-loop containing nucleoside triphosphate hydrolases superfamily protein	Up	Up
43	AT4G24680	modifier of snc l	Up	Down
44	AT4G32375	Pectin lyase-like superfamily protein	Up	Up
45	AT5G20830	sucrose synthase 1	Up	Down
46	AT5G22620	phosphoglycerate/bisphosphoglycerate mutase family protein	Up	Up
47	AT5G42940	RING/U-box superfamily protein	Down	Up
48	AT5G48140	Pectin lyase-like superfamily protein	Down	Down
49	AT5G49870	Mannose-binding lectin superfamily protein	Up	Up
50	AT5G62460	RING/FYVE/PHD zinc finger superfamily protein	Down	Up
51	AT5G66550	Maf-like protein	Up	Down
52	AT1G21970	Histone superfamily protein	Up	Up
53	AT1G28327	E3 ubiquitin-protein ligase	Up	Up
54	AT1G50500	Membrane trafficking VPS53 family protein	Up	Up
55	AT1G70290	trehalose-6-phosphatase synthase S8	Up	Up
56	AT1G70490	Ras-related small GTP-binding family protein	Up	Down
57	AT1G74810	HCO3- transporter family	Up	Up
58	AT2G19180	hypothetical protein AT2G19180	Down	Up
59	AT2G19940	Putative N-acetyl-gamma-glutamyl-phosphate reductase	Up	Up
60	AT2G43710	Plant stearoyl-acyl-carrier-protein desaturase family protein	Up	Down
61	AT3G01900	cytochrome P450, family 94, subfamily B, polypeptide 2	Up	Up
62	AT3G13060	evolutionarily conserved C-terminal region 5	Up	Up

63	AT3G13110	serine acetyltransferase 2;2	Up	Down
64	AT3G45870	nodulin MtN21 /EamA-like transporter family protein	Up	Up
65	AT3G55410	2-oxoglutarate dehydrogenase, E1 component	Up	Up
66	AT3G57390	AGAMOUS-like 18	Down	Up
67	AT4G02140	hypothetical protein AT4G02140	Up	Down
68	AT4G15420	Ubiquitin fusion degradation UFD1 family protein	Down	Up
69	AT4G23460	Adaptin family protein	Up	Down
70	AT4G24620	phosphoglucose isomerase I	Up	Down
71	AT4G29340	profilin 4	Up	Down
72	AT4G32180	pantothenate kinase 2	Up	Up
73	AT5G09230	sirtuin 2	Up	Down
74	AT5G25880	NADP-malic enzyme 3	Up	Down
75	AT5G26250	Major facilitator superfamily protein	Up	Up
76	AT5G55400	Actin binding Calponin homology (CH) domain- containing protein	Down	Up

Annexure 7

Genes overlapping between *athmgb15* bud transcriptome and *arp4* seedling transcriptome by Nie et al.

Sl. No.	At ID	Gene name	Expression in arp4	Expression in athmgb15
1	AT1G33720	Cytochrome P450, family 76, subfamily C, polypeptide 6	Up	Down
2	AT5G24210	Alpha/beta-Hydrolases superfamily protein	Up	Down
3	AT4G33550		Up	Up
4	AT5G53030	Uncharacterized protein At5g53030	Up	Up
5	AT1G65330	MADS-box transcription factor PHERES 1	Up	Up
6	AT3G06630	Protein kinase family protein	Up	Down
7	AT4G29340	Profilin-3	Up	Down
8	AT4G28280	LLG3	Up	Up
9	AT1G37150	holocarboxylase synthetase 2	Up	Up
10	AT1G06148	Unknown gene	Up	Down
11	AT3G05950	Germin-like protein subfamily 1 member 7	Up	Up
12	AT4G02140		Up	Down
13	AT5G56700	FBD / Leucine Rich Repeat domains containing protein	Up	Up
14	AT2G36325	GDSL esterase/lipase At2g36325	Up	Up
15	AT2G41510	cytokinin oxidase/dehydrogenase 1	Down	Down
16	AT2G26400	acireductone dioxygenase 3	Up	Up
17	AT5G65070	K-box region and MADS-box transcription factor family protein	Up	Up
18	AT3G47790	ABC transporter A family member 8	Up	Down
19	AT4G13410	Probable glucomannan 4-beta- mannosyltransferase 15	Up	Up

20	AT1G48590	Protein C2-DOMAIN ABA-RELATED 5	Up	Down
21	AT2G33205	Serinc-domain containing serine and sphingolipid biosynthesis protein	Up	Up
22	AT3G44350	NAC domain containing protein 61	Up	Down
23	AT1G53640	unknown protein	Up	Up
24	AT1G34460	CYCLIN B1;5	Up	Up
25	AT2G02930	Glutathione S-transferase F3	Up	Down
26	AT1G02350	Glutathione S-transferase F3	Up	Down
27	AT3G05155	Major facilitator superfamily protein	Up	Up
28	AT5G44575		Up	Down
29	AT5G26920	Calmodulin-binding protein 60 G	Up	Up
30	AT1G02310	MANI	Up	Up
31	AT3G02940		Up	Up
32	AT1G64480	Calcineurin B-like protein 8	Down	Up

Annexure table 8

Overlapping set of genes common in *arp4* (seedling), athmgb15 (bud) transcriptomes and AtHMGB15 ChIP-chip data by Mallik et al.

Sl. No.	At ID	Gene name	Expression in arp4	Expression in athmgb15
1	AT1G33720	Cytochrome P450, family 76, subfamily C, polypeptide 6	Up	Down
2	AT5G24210	Alpha/beta-Hydrolases superfamily protein	Up	Down
3	AT4G33550		Up	Up
4	AT5G53030	Uncharacterized protein At5g53030	Up	Up
5	AT1G65330	MADS-box transcription factor PHERES 1	Up	Up
6	AT3G06630	Protein kinase family protein	Up	Down
7	AT4G29340	Profilin-3	Up	Down
8	AT4G28280	LLG3	Up	Up
9	AT1G37150	holocarboxylase synthetase 2	Up	Up
10	AT1G06148	Unknown gene	Up	Down
11	AT3G05950	Germin-like protein subfamily 1 member 7	Up	Up
12	AT4G02140		Up	Down
13	AT5G56700	FBD / Leucine Rich Repeat domains containing protein	Up	Up
14	AT2G36325	GDSL esterase/lipase At2g36325	Up	Up
15	AT2G41510	cytokinin oxidase/dehydrogenase 1	Down	Down
16	AT2G26400	acireductone dioxygenase 3	Up	Up
17	AT5G65070	K-box region and MADS-box transcription factor family protein	Up	Up
18	AT3G47790	ABC transporter A family member 8	Up	Down
19	AT4G13410	Probable glucomannan 4-beta- mannosyltransferase 15	Up	Up
20	AT1G48590	Protein C2-DOMAIN ABA-RELATED 5	Up	Down
21	AT2G33205	Serinc-domain containing serine and sphingolipid biosynthesis protein	Up	Up
22	AT3G44350	NAC domain containing protein 61	Up	Down
23	AT1G53640	unknown protein	Up	Up

24	AT1G34460	CYCLIN B1;5	Up	Up
25	AT2G02930	Glutathione S-transferase F3	Up	Down
26	AT1G02350	Glutathione S-transferase F3	Up	Down
27	AT3G05155	Major facilitator superfamily protein	Up	Up
28	AT5G44575		Up	Down
29	AT5G26920	Calmodulin-binding protein 60 G	Up	Up
30	AT1G02310	MANI	Up	Up
31	AT3G02940		Up	Up
32	AT1G64480	Calcineurin B-like protein 8	Down	Up

WORK PRESENTED

- 1) **Talk.** The role of a novel plant exclusive ARID-HMG protein in uncovering F- Actin dynamics in *Arabidopsis* pollen grain development.
 - Students Symposium: Recent Trends in Natural Sciences, Bose Institute, India 2023
- 2) **Poster.** Unravelling the role of a novel plant exclusive ARID-HMG protein in early stages of pollen grain development.

EMBL conference: From 3D light to 3D electron microscopy, EMBL Heidelberg, Germany 2022

LIST OF PUBLICATIONS

1) Identification of genome wide targets and DNA recognition sequence of the Arabidopsis HMG- box protein AtHMGB15 during cold stress response.

Mallik, R., Prasad, P., Kundu, A., Sachdev, S., Biswas, R., Dutta, A., Roy, A., Mukhopadhyay, J., Bag, S. K., and Chaudhuri, S. (2020) BBA - Gene Regulatory Mechanisms

https://doi.org/10.1016/j.bbagrm.2020.194644

2) The Arabidopsis ARID-HMG DNA-BINDING PROTEIN 15 modulates JA signalling by regulating MYC2 during pollen development.

Sachdev, S., Biswas, R., Roy, A., Nandi, A., Roy, V., Basu, S., and Chaudhuri, S. (2024). Plant Physiology.

https://doi.org/10.1093/plphys/kiae355

3) AtHMGB15 regulates tapetal apoptosis in pollen development and actin dynamics during pollen germination in Arabidopsis.

Biswas, R., Chaudhuri, S. (2024). Plant Reproduction.

http://dx.doi.org/10.1007/s00497-024-00505-x

4) From anther walls to pollen wall: the tale of tapetum.

Biswas, R., Chaudhuri, S. (2024) The Nucleus.

(Article accepted and is being formatted)

SHORT COMMUNICATION



AtHMGB15 regulates tapetal apoptosis in pollen development and actin dynamics during pollen germination in arabidopsis

Ruby Biswas¹ · Shubho Chaudhuri¹

Received: 12 February 2024 / Accepted: 11 June 2024 © The Author(s), under exclusive licence to Springer-Verlag GmbH Germany, part of Springer Nature 2024

Key message ARID-HMG DNA binding protein, AtHMGB15, regulates pollen development and pollen germination in Arabidopsis.

Abstract Previous studies have shown that ARID-HMG DNA binding protein, AtHMGB15 regulate pollen development and pollen germination in *Arabidopsis*. Here, we performed transcriptome and cytological studies to understand the role of AtHMGB15 in regulating pollen wall morphology and the pollen tube germination rate. Our result showed abnormal vacuolization in the tapetal cells during anther maturation and prolonged PCD in AtHMGB15 loss-of-function mutant. The tapetum has the ability to perform both secretory and biosynthetic activities critical for pollen maturation and pollen viability. Interestingly, expression of PCD executer genes *CEP1*, *MC9* and *RNS3* were significant down-regulation of in *athmgb15-4*. The growth of pollen tubes is regulated by the actin cytoskeleton dynamics. To address the defect in pollen tube growth of *athmgb15*, we monitored the actin network in growing pollen tubes of wildtype and *athmgb15-4* using Rhodamine-phalloidin fluorescence. Our results indicate a highly fragmented actin distribution in *athmgb15-4* pollen tubes with a lesser number of long actin fibers and significantly low f-actin concentration at the apex. q-RTPCR further indicates significant downy-regulation of actin regulatory proteins *VLN2* and *PRF4*. Collectively, our results suggest that AtHMGB15 being a nuclear architectural protein orchestrates high-order chromatin organization to promote the transcription of genes responsible for pollen development and pollen germination.

 $\textbf{Keywords} \ \ ARID\text{-}HMG \cdot Tapetum \cdot Vacuolation \cdot Programmed cell \ death \cdot Actin \ cytoskeleton \cdot Pollen \ tube$

Introduction

In angiosperm, the development of healthy male gametes in the anther depends upon the timely degradation of tapetal cells through programmed cell death (PCD) (Chapman 1987; Echlin 1971b; Lavania et al. 2014; Lei and Liu 2020; Varnier et al. 2005; Zhang and Yang 2014). Tapetal cells that nourishes microsporocytes at the early stage of pollen development, is also involved in the secretion of callases to release microspores from tetrad and later undergo degradation to release cellular constituents for the formation of the pollen cell wall (Echlin 1971a; El-Ghazaly 1999; Hsieh and Huang

Communicated by Prem L Bhalla.

Published online: 21 June 2024

2004; Hsieh and Huang 2007). The tapetal secretory system plays an important role in delivering nutrients, enzymes, metabolites and pollen cell materials during microsporogenesis (Gotelli et al. 2023; Pacini and Juniper 1979; Quilichini et al. 2014). Tapetal cell vacuoles play a significant role in programmed cell death as they provide enzymes for degrading tetrad walls to release microspores (Wan et al. 2010). Also, in later stages of anther development, the vacuole membrane ruptures, collapsing the vacuole and releasing vacuolar processing enzyme (VPE) in the cytoplasm that activates a cascade of proteolytic activity leading to PCD (Cheng et al. 2020; Cheng et al. 2019). Altering the timing of PCD often leads to male sterility, which has been used in crop breeding to control gene flow (Chen and Liu 2014; Tao et al. 2023). Thus, genes that control tapetal PCD can be important agronomic targets (Tao et al. 2023).

After the release of pollen grains from anthers, the pollen germinates and the growing pollen tube passes through the style tissue to deliver two nonmotile sperm cells to the female gametophyte for successful fertilization. The success



Shubho Chaudhuri shubho@jcbose.ac.in

Department of Biological Sciences, Bose Institute, Unified Academic Campus, EN 80, Sector V, Bidhan Nagar, Kolkata, West Bengal 700091, India

of this event depends upon the growth and structure of the tube for proper penetration (Johnson et al. 2019). Pollen tube grows via the tip growth mechanism with a continuous supply of cell wall materials to the tip of the tube (Cai and Cresti 2009; Ruan et al. 2021; Wang et al. 2020). This requires a highly efficient intracellular trafficking system that continuously transports materials to the tip of the tube for its growth and elongation (Cai and Cresti 2009; Fu et al. 2001; Onelli et al. 2015; Onelli and Moscatelli 2013; Ruan et al. 2021; Selinski and Scheibe 2014). Thus, the cytoplasmic trafficking processes in growing pollen tube are essential for the redistribution of organelles and the movement of secretory vesicles to the apical region of the pollen tube (Zhang et al. 2023). The transport of secretory vesicles to deliver the necessary materials for the synthesis of cell wall to the tip of the tube is regulated by actin cytoskeleton dynamics (Jiang et al. 2017; Qu et al. 2015; Vidali and Hepler 2001; Vidali et al. 2001; Zhu et al. 2017). The actin filaments are arranged in the pollen tube in such a way as to provide directionality to the cytoplasmic streaming (Zhang et al. 2023). Actin filaments at the cortex of the tube have their barbed end facing toward the tip, while actin filaments at the inner region of the tube have barbed ends facing away from the tip. This arrangement of actin filaments in the subapical region is required to prevent organelle trafficking to the apex and facilitate their reverse movement toward the core (Jiang et al. 2017). Actin regulatory proteins like Villins, fimbrins, LIMS, and formins acts at different stages of actin assembly and/or disassembly (Campellone and Welch 2010). These regulatory proteins contribute at the nucleation stage of actin polymerization, capping of the barbed end of actin filament, severing and bundling of the filaments (Campellone and Welch 2010). Profilin is another multifunctional actin regulatory protein that interacts with actin monomers in a 1:1 stoichiometry (Liu et al. 2015). Studies have shown that Profilin binds with G-actin and actin-profilin complex binds to growing barbed end of actin, thus promoting actin polymerization (Liu et al. 2021, Pollard 2016). Profilin, however, is also proposed to promote actin depolymerization by binding to actin monomers and sequestering them in a calcium dependent manner, maintaining low filamentous actin in the cell (Pollard 2016). Actin-depolymerizing factor (ADF) is a small molecular weight actin binding protein that regulates actin turnover in the cell (Inada 2017). ADF preferentially binds to ADP-G actin and inhibit ADP- to ATP- nucleotide

Previous studies from our group have shown that loss of function of Arabidopsis ARID-HMG protein, AtHMGB15, is exhibited as defects in pollen morphology, exine wall patterning, pollen viability, pollen tube germination rate and defect in hormone signaling (Sachdev et al. 2022; Xia et al. 2014). athmgb15 mutants also exhibit reduced filament length, silique length and a reduced seed set

(Sachdev et al. 2022). AtHMGB15 interacts with two AtMIKC transcription factors, AGL66 and AGL104, which are responsible for pollen maturation and pollen tube growth (Xia et al. 2014).

In this study, we attempt to determine the underlying cause of abnormal pollen wall morphology and retarded pollen tube germination rate exhibited by the AtHMGB15 loss of function mutants. Transcriptome analysis of athmgb15-4 bud (corresponding to stages 8-11) revealed that genes belonging to programmed cell death (PCD), pollen development, pollen tube growth, actin filament binding and organization were differentially regulated in the mutant. Gene Ontology analysis of the transcriptome reported the enrichment of GO term likes actin binding, vesicle transport along actin filament, and actin filamentbased movement. To assess the defective pollen wall morphology, we observed the developmental stages of tapetal cells in wild type and athmgb15-4. The vacuolation pattern in tapetal cells from FM4-64FX stained images showed abnormal vacuolation pattern while the TUNEL assay data showed prolonged tapetal PCD in the athmgb15-4 mutants. Expression study of genes indicated downregulation of key PCD executer genes like CEP1, MC9 and RNS3 in athmgb15-4 mutant whereas upregulation of the antiapoptotic genes like BI1 and BI1 like family protein. To further understand the abnormal elongation of the pollen tube in athmgb15, actin organization was studied during pollen tube elongation. The results indicated that the actin organization in germinated pollen tubes showed fragmentated f-actin in the athmgb15-4 mutant compared to the continuous f-actin observed in wild type. These observations lie in tandem with the significant down-regulation of actin-binding proteins viz VLN2, PRF4 and VLN1 in athmgb15-4 mutant. Our studies collectively suggest a role of AtHMGB15 in the regulation of pathways involved during pollen grain development and pollen tube germination.

Materials and methods

Plant lines and growth conditions

The Arabidopsis thaliana ecotype Columbia-0 (Col-0) used in this study was referred to as the wild type. The T-DNA insertion line of AtHMGB15 (GABI_351D08) was obtained from the Eurasian Arabidopsis Stock Centre (uNASC). The seeds were plated on Murashige and Skoog agar plates at 22 °C under 16 h light ($\sim 150 \pm 10 \mu mol m^{-2}$) and 8 h dark cycle in the plant growth chamber. After 20 days, the plants were transferred to soil pots in a greenhouse maintaining 60–70% relative humidity at 22 °C.



FM4-64FX staining of anther sections

The staining of the samples with FM4-64FX were performed according to Jeli'nkova et al. with some modifications (Jelínková et al. 2019). The flower buds corresponding to different anther developmental stages were collected and treated with xylene before being embedded in paraffin wax and the samples were subsequently sectioned into 5 µm transverse sections as described by Chang et al. (2014). The samples on the slides were deparaffinized and rehydrated to finally stain with 0.5 µM FM4-64FX. This was followed by fixation in 4% formaldehyde in phosphate buffered saline (PBS) for 30 min to visualize the vacuoles in the tapetal cells. The sample was washed in PBS thrice before visualization. Fluorescence of FM 4-64FX was stimulated with laser line at 514 nm and the fluorescence emission was obtained above 575 nm. Imaging was done using a Leica STELLARIS confocal laser scanning microscope.

Toluidine blue staining

Mutant and wild type flower buds were fixed overnight in FAA (50% ethanol, 5.0% gla cial acetic acid, 3.7% formal-dehyde), dehydrated in a graded ethanol series, embedded in paraffin wax, and sectioned into 5 µm transverse sections using a microtome as described by Chang et al. (2014). The samples on the slides were deparaffinized and rehydrated to finally stain with 1% toluidine blue at room temperature for 2 min followed by washing for 5 min in water. Bright-field photographs of the anther cross-sections were taken using a digital camera mounted on a compound microscope (Nikon ECLIPSE Ni, Tokyo, Japan) and processed with NIS-Elements software (Nikon, Tokyo, Japan).

TUNEL assay

The 5- μ m paraffin sections from different stages of anther development were then assessed with a TUNEL apoptosis detection kit (DeadEnd Fluorometric TUNEL system; Promega) according to the manufacturer's instructions. The excitation wavelength to stimulate the propidium iodide fluorescence was ~535 nm whereas for the fluorescein-12-UTP was ~496 nm. The sections were photographed using a Leica STELLARIS confocal laser scanning microscope.

Actin filament visualization and quantification analyses in pollen tubes

Actin filaments were visualized and quantified in fixed and unfixed pollen tubes from germinated pollen grains according to a previously published method (Qu et al. 2020). Briefly, after being cultured on the surface of solid pollen germination media (GM) for 3 h, they were subjected to

treatment with 300 µmol L⁻¹ m-maleimidobenzoyl-Nhydroxysuccinimide ester in liquid GM for 1 h. After treatment with 0.05% NP-40 in liquid GM for 10 min, pollen grains and pollen tubes were washed with TBSS (50 mmol L⁻¹ Tris-HCl, pH 7.5, 200 mmol L⁻¹ NaCl, and 400 mmol L⁻¹ sucrose) three times. The treated samples were subsequently incubated with 200 nmol L⁻¹ Rhodamine phalloidin at 4 °C for overnight. The samples were then observed using a Leica STELLARIS confocal laser scanning microscope excited with a 535 nm laser with the emission wavelength set at 550-600 nm. The fluorescence intensity of Rhodamine phalloidin-staining was measured to reflect the amount of actin filaments as described previously (Jiang et al. 2019). The effects of LatB treatment on the actin cytoskeleton in pollen grains were determined by including 10 nmol L⁻¹ of LatB in the pollen GM and incubated for 30 min.

Sample collection, illumina sequencing, and data processing for RNA sequencing

Total RNA was isolated from 200 mg of young buds (anther stage 8–11) of wildtype and athmgb15-4 mutant using RNASure® Mini Kit (Nucleopore-Genetix). NEBNext® Ultra II Directional RNA library Prep Kit was used to prepare high quality libraries, according to manufacturer's protocols and paired end sequencing reads of read length 151 bp was generated with Ilumina HiSeq-X sequencing platform. Raw reads were checked individually by using FASTQC. Quality control and per-processing of FASTQ files are essential to providing clean data for downstream analysis. Fastp, an ultra-fast FASTQ pre-processor with useful quality control and data-filtering features was used. It performs quality control, adapter trimming, quality filtering, per-read quality pruning and many other operations with a single scan of the FASTQ data. This tool is developed in C + + and has multi-threading support. A cutoff of 30 was set for the quality phred score and only high-quality reads were retained. High quality reads were aligned against NCBI Reference of Arabidopsis thaliana (assembly TAIR10.1) by using ultrafast, splice-ware aligner Hisat2. To understand the alignment quality, we checked several parameters including mapping percentage of reads. Details of mapping read percentage per sample given billow. Mapped reads were further considered for transcript assembly and quantification of transcript abundance by using stringtie. Transcript count, obtain from each sample were further used for analysis of differential expression of transcripts between alternate conditions by using DESeq2. A p value cutoff of 0.05 and less was used to identify the significantly expressed transcripts. Genes with absolute values of fold change (FC) > 2 were considered to be differentially expressed. An FC>2 was considered as significant upregulation, while FC < -2 was considered as significant downregulation.



Identification and analysis of differentially expressed genes

Significantly up- and downregulated genes from each experiment were selected for GO enrichment analysis by using the DAVID web platform. The gene enrichment process clustered genes in 3 Gene Ontology (GO) groups, viz., biological process (BP), molecular function (MF) and cellular component (CC), along with the KEGG pathway. The top significant GO terms were selected by using the *p* value. The functional annotation clustering and KEGG pathway analyses were performed for the significant differentially expressed genes (DEGs) via DAVID v6.2. The heatmaps were generated using MeV.

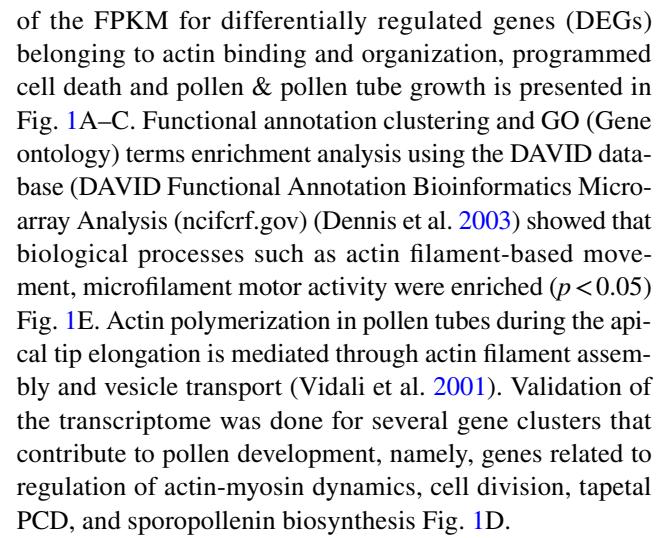
RT-PCR and q-RTPCR

q-RTPCR was performed as described previously (Mallik et al. 2020). The relative fold change in the gene of interest was calculated with respect to the transcript level of the housekeeping gene AtEF1 α (AT1G07920) using the $2^{-\Delta\Delta CT}$ method. The significance of the results was analyzed by paired two-tailed Student's t test ($P \le 0.05$) using three independent biological replicates. The primers used in the analysis are listed in Supplementary Table S2.

Results and discussion

Deletion of AtHMGB15 function causes differential regulation of genes related to PCD and actin dynamics during early stage of pollen development

Previous studies from our group and Xia et al. have established the role of AtHMGB15 (At1g04880) in pollen development (Xia et al. 2014). Our studies show that the loss of function mutant of AtHMGB15 (athmgb15-4) shows defective pollen morphology, delayed pollen tube germination and loss of pollen viability (Sachdev et al. 2022). Further analysis indicated that numbers of cell wall biosynthesis genes were significantly down-regulated in athmgb15-4 mutant compared to wildtype (Sachdev et al. 2022). In order to gain additional insight in the developmental events of athmgb15 mutant anthers, we performed a comparative transcriptome to classify the genes differentially regulated by AtHMGB15 in the bud (stages 8–11) of anther development. Three biological replicates were used to confirm statistical significance of the results and reduce errors. We have identified 1049 genes that are significantly regulated (log₂ fold change ≥ 2 for upregulated transcripts and ≤ 2 for downregulated transcripts and P value ≤ 0.05) at bud stage. Among them, 434 genes were significantly downregulated and 615 genes were upregulated in athmgb15 mutant. A heatmap



Furthermore comparison our transcriptome with the microarray data of Xia et al. (2014), resulted in an overlap of 76 genes that were differentially regulated by AtHMGB15 in pollen, and bud tissue, is represented in the Venn diagram as shown in (Fig. 1F and supplementary Table S1). Functional annotation clustering of the overlapping genes reported that the cluster responsible for actin binding was the most enriched in the dataset.

Loss of AtHMGB15 causes abnormal vacuolation and prolonged PCD in tapetal cells

The rupture of vacuoles and release of lytic enzyme into the anther locule is an important step in tapetal PCD (Cheng et al. 2019). Therefore, monitoring the change in vacuole morphology is an effective approach to understand the progress of PCD. Semi-thin Sects. (5 µm) of anthers from different developmental stages (5, 7 and 12) of the wild type and athmgb15-4 anthers were stained with FM4-64FX to visualize the vacuoles of tapetum cells during tapetal degradation. The results indicated that with the advancement of anther development in athmgb15-4, there were fewer enlarged vacuoles in the tapetum cell cytoplasm than observed in the wild type (Fig. 2A). Since vacuole enlargement is followed by the rupture of the tonoplast to release the enzymes is a pre requisite for the tapetal degradation to proceed (Parish and Li 2010), our observation suggested that degradation of the tapetum is compromised in the AtHMGB15 mutant.

To test whether loss of function of AtHMGB15 significantly affects the temporal regulation of the onset and execution of programmed cell death in the tapetum, we investigated tapetal PCD in wild-type and *athmgb15-4* mutant anthers using a terminal deoxynucleotidyl transferase-mediated dUTP nick-end labeling (TUNEL) assay. The results of the TUNEL assay indicated that fragmentation of the tapetum was initiated at stage 10 in the wild-type anthers (Fig. 2B). At stage 10, we observed a TUNEL-positive



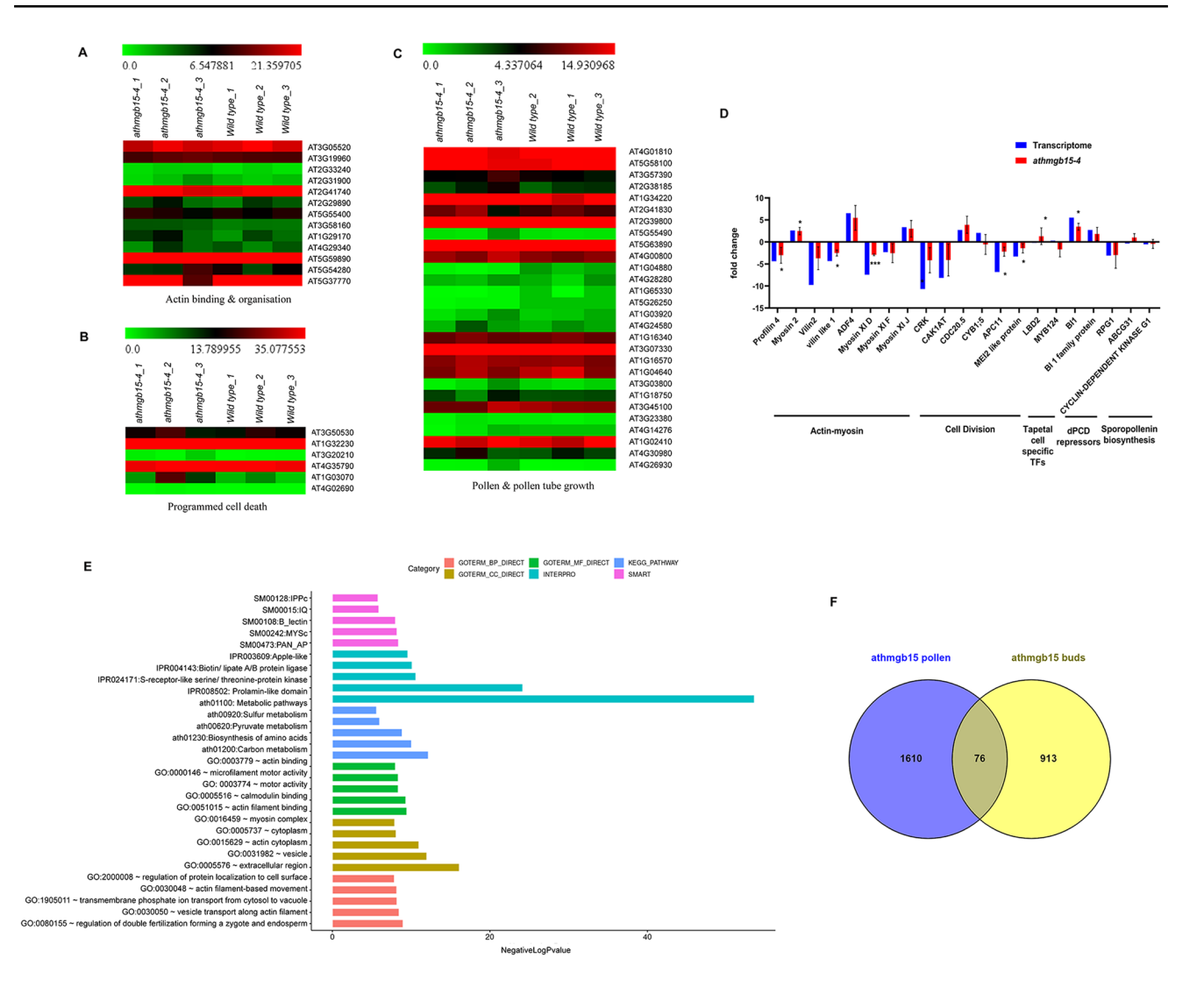


Fig. 1 AtHMGB15 deletion affects actin dynamics and PCD pathway during pollen development. (A, B, C) Heatmap of the FPKM values of genes from biological processes corresponding to actin binding & organization (A), programmed cell death (B) and pollen & pollen tube growth (C) in *athmgb15-4* and wildtype. The data set is a representation of the significant (p < 0.05) differentially expressed genes from three biological replicates. D Validation of the transcriptome using q-RTPCR. The bar represents the mean \pm SD

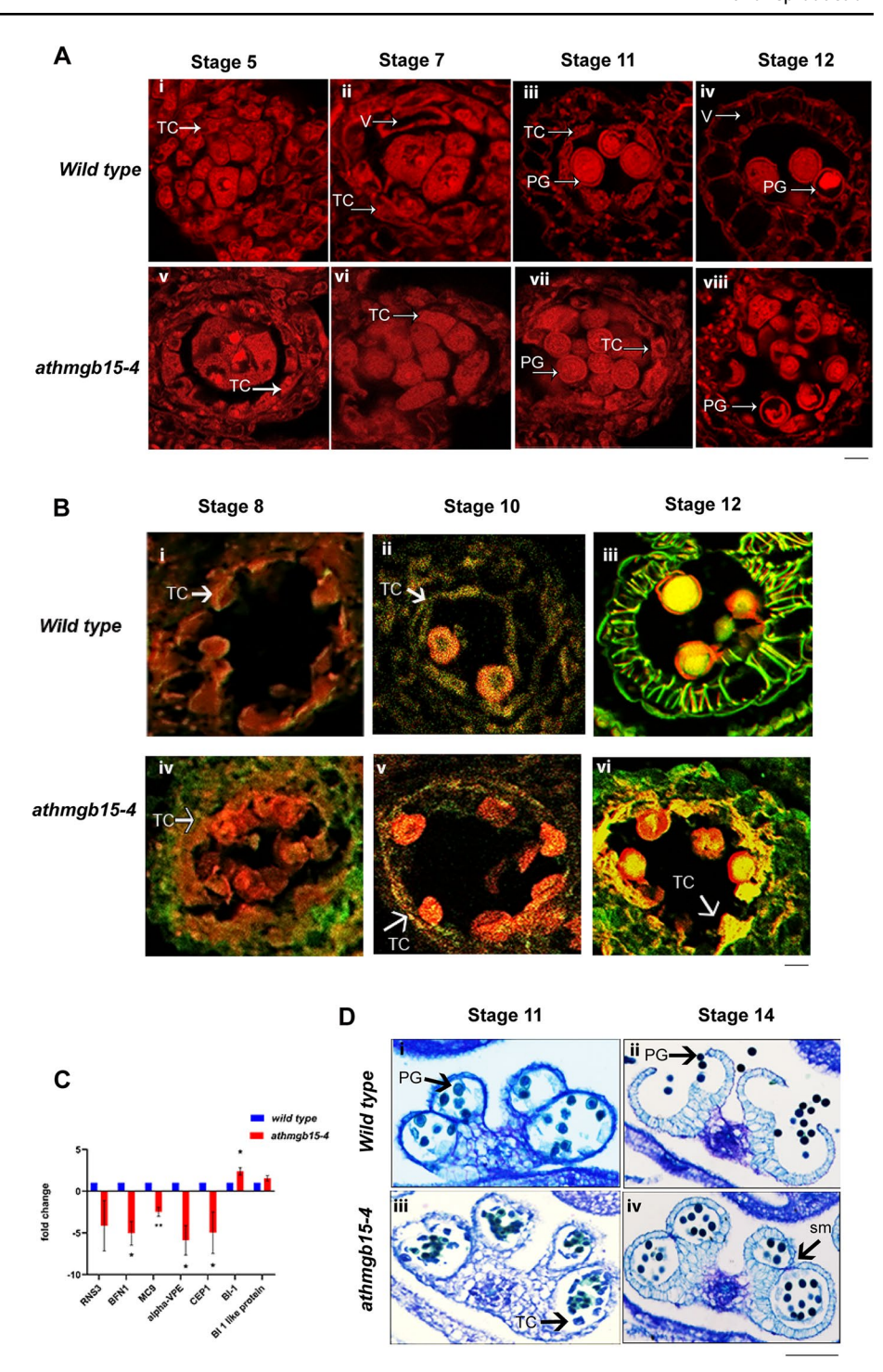
(n=3). The significance of the data was calculated using students t-test. *, ** and *** denote significant change p < 0.05, p < 0.005 and p < 0.0005respectively. E Gene ontology analysis of the most enriched gene clusters. The enriched clusters were then classified into major GO categories of Biological Process (BP), Molecular function (MF) and Cellular component (CC). F Venn diagram representing the overlapping genes common in transcriptome of athmgb15 bud and pollen (Xia et al. 2014)

signal from both wildtype and *athmgb15-4* anthers, indicating that most of the tapetal nuclei underwent PCD during this stage. No TUNEL-positive signals were observed at stage 12 or later in the wild-type anther, signifying the completion of PCD of tapetal cells. However, TUNEL-positive signal continued to be distinctly visible even at stage 12 in *athmgb15-4*, indicating that tapetal nuclei degeneration was not completed by stage 12. TUNEL assays suggest that tapetal cell degeneration may be prolonged in the *athmgb15-4* mutants compared to wild type. The well-timed PCD of tapetal cells is crucial for proper maturation of the pollen grains and their viability.

We further studied the expression of certain PCD genes that are responsible for tapetum degradation. Transcriptome and q-RTPCR revealed that *CEP1*, *MC9*, *BFN1*, α-*VPE* and *RNS3* were significantly downregulated in *athmgb15-4* buds (Fig. 2C). *CEP1* and *RNS3* have been previously shown to be highly expressed during tapetal-PCD (Guo et al. 2022; Zhang et al. 2014). The expression of the *Bax inhibitor BI1* which is known as anti-PCD that inhibits ROS-mediated cell death (Ishikawa et al. 2011) is significantly higher in the *athmgb15-4* mutant. The cysteine protease CEP1 is a key executor of tapetal PCD that participates directly in tetrad cell wall hydrolysis in *Arabidopsis* (Zhang et al. 2014). *cep1*



Fig. 2 Abnormal vacuolation and prolonged tapetal PCD in the athmgb15-4 mutant. A Anther sections from stages 5, 7, 11, and 12 of wild type (i-iv) and athmgb15-4 were (v-viii) stained with FM4-64FX. V, vacuoles; PG, pollen grains; and T, tapetum. The scale bar represents 10 µm. B TUNEL assay showing the progression of tapetal PCD in wild-type (i-iii) and athmgb15-4 anthers (iv-vi) from anther stages 8, 10 and 12. The yellow fluorescence denotes the TUNEL positive signal. The scale bar represents 10 µm. C q-RTPCR of PCD-related genes in the wild type and athmgb15-4. The bars represent the means $\pm (n=3)$. The significance of the data was calculated using students t-test. * and ** denotes significant change p < 0.05 and p < 0.005 respectively. **D** Light microscope images of anthers sections from stage 11 and 14 stained with 1% toluidine blue. The scale bar represents 50 µM. PG—pollen grains, TC—tapetal cells and sm-septum



mutants have aborted PCD causing abnormal exine and low fertility rate (Zhang et al. 2014).

Microscopic observations of semi-thin anther sections were analyzed to characterize the anther dehiscence in the wild-type and *athmgb15-4* mutant. Stage 11 of anther development in wild type *Arabidopsis* is identified by the binucleation of microspores and expansion of the endothecium (Fig. 2D). The septum is still present, the tapetal

layer has almost fully degraded, and the pollen grains begin to acquire their characteristic elliptical shape. This continues until stage 12, at which point the microspores contain a vegetative nucleus as well as two generative nuclei (Gómez et al. 2015; Sanders et al. 1999). In the *athmgb15-4* mutant, however, the stage 11 anther exhibited a perceptible increase in size along its major axis even though developmental progress marking the onset



of the next stage is not observed. The pollen grains had not yet acquired their final shape, unlike the wild type. This is consistent with the prolonged tapetal PCD. By the end of stage 14 of anther development, septum of the wild type *Arabidopsis* exhibits complete disintegration, and dehiscence of the anther. In case of *athmgb15-4*, however, the septum is still intact in stage 14 and no signs of anther dehiscence are detected, indicating an abnormally delayed anther dehiscence in the mutant. Collectively, our results indicate that abnormal vacuolation, prolonged tapetal degeneration, significant down-regulation of PCD genes and delayed anther dehiscense in *athmgb15-4* might be a rationale for low viability and deformed pollen wall morphology in the *athmgb15-4* pollen grains as reported in previous studies (Xia et al. 2014).

Defective f-actin organization in the *athmgb15-4* mutant during pollen tube growth

To study actin distribution and polymerization during pollen tube growth, we used fluorescent rhodamine-phalloidin, which preferentially binds to f-actin in the pollen tube (Qu et al. 2020). The results indicate that the fluorescence intensity of actin filaments in the apical and subapical regions of pollen tubes was greater in the wild type compared to that observed in *athmgb15-4* (Fig. 3A). However, the actin arrangement is highly disorganized in the *athmgb15-4* pollen tube. There were fewer long actin fibers in the mutant than in the wild type. The rhodamine phalloidin stained f-actin appeared to be fragmented in *athmgb15-4* in comparison with the long actin fibers present in the wild type. To test whether actin polymerization is the main cause of defects in pollen tube growth in *athmg15-4*, we tested the

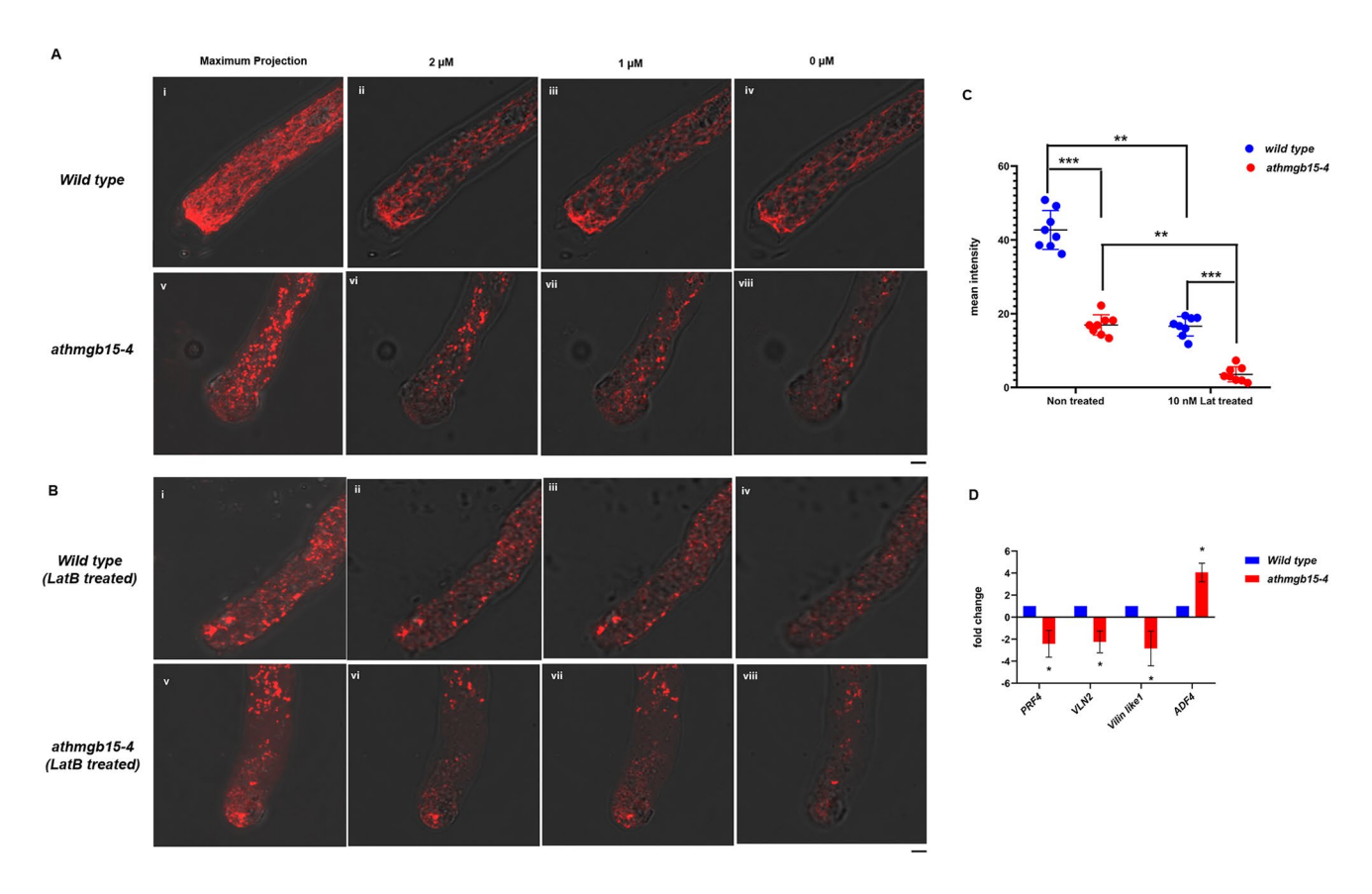


Fig. 3 F-actin distribution in germinated pollen tubes of wild-type and *athmgb15-4* pollen grains. **A** Optical Z-slice (0.5 μm) images of a elongating pollen tube of wild type (i–iv) and *athmgb15-4* (v–viii). The F-actin distribution in germinating pollen tube was stained using rhodamine phalloidin, and the maximum intensity projected pollen tubes are shown in (i–v). The scale bar represents 5 μm. **B** Optical Z-slice (0.5 μm) images of a pollen tube of wild type (i–iv) and *athmgb15-4* (v–viii) treated with 10 nM LatB. F-actin was distributed in germinating pollen tube germination LatB treatment was stained using rhodamine phalloidin, and the maximum intensity projected

pollen tubes are shown in (i–v). The scale bar represents 5 µm. **C** Graphical representation of the rhodamine-phalloidin fluorescence intensity in control and LatB-treated pollen tubes of wildtype and *athmgb15-4*. The bars represent the means $\pm (n=8)$ and significance was calculated using Student's t test. ** denotes p < 0.005 and *** denotes p < 0.0005. **D** q-RTPCR of genes expressing actin-binding proteins in the wild type and *athmgb15-4*. The bars represent the means $\pm (n=3)$. * Indicates a significant change with respect to the wild type (p < 0.05) according to Student's t test



effect of latrunculin B (LatB) treatment on pollen growth in the wild type and *athmgb15-4*. LatB affects actin polymerization and alters the f-actin level in the cell (Chen et al. 2007). The results indicated that after treatment with LatB (10 nM), actin filaments became fragmented in wildtype and in *athmgb15-4* pollen tubes (Fig. 3B); however, the effect was more pronounced in the *athmgb15-4* pollen tubes. The significant reduction in fluorescence post-LatB treatment suggested reduced f-actin formation in *athmgb15-4* pollen grains compared to that in the wild type (Fig. 3C).

Actin filaments serve as tracts for myosin dependent organelle movement during a directed growth as observed during pollen germination and pollen tube elongation. Profilins and villins are actin filament bundling proteins that play an important role in actin polymerization (Bubb et al. 2003; Huang et al. 2015; Liu et al. 2015; Qu et al. 2013; Zhao et al. 2020). PRF4 and VLN2 have been reported to regulate cytoskeletal structure by promoting the nucleation of f-actin monomers in pollen tubes (Qu et al. 2013). We determined the expression of Profilin 4 (PRF4), Villin 2 (VLN2) and Villin-like 1 in wildtype and athmgb15-4 flowers. The q-RTPCR results indicated that the expression of PRF4, VLN2 and Villin-like 1 was significantly downregulated in athmgb15-4 cells (Fig. 3D). Previous studies have reported that downregulation of PRF4 lead to lower number of filamentous actin and also induced disorganization of apical f-actin, and reduced tip-directed vesicle transport in the pollen tube (Liu et al. 2015). VLN2 functions with VLN3 in bundling of actin filaments during directional growth as observed in roots and pollen tubes (Thomas 2012). VLN2 has also been reported to work with VLN5 and the vln2vln5 double mutants have been reported to demonstrate normal pollen tube germination but retarded pollen tube elongation (Qu et al. 2015). From our gene expression study, we speculate that the differential regulation of the actin binding genes in athmgb15 might be an underlying factor for the disorganized f-actin distribution in pollen tubes of athmgb15-4.

In summary, AtHMGB15 is a transcriptional coactivator that regulates pollen development and pollen germination in Arabidopsis (Xia et al. 2014). HMG-box proteins have been shown to function as nuclear architectural proteins that orchestrate high-order chromatin organization during transcription (Hansen et al. 2008). In this work, we have shown that AtHMGB15 regulates the transcription of actinrelated genes to regulate pollen tube growth. AtHMGB15 also regulates the expression of genes responsible for programmed cell death in tapetal cells, which is a vital step in the formation of viable pollen grains with proper exine ornamentation. Although actin dynamics are not known to play an important role in vacuole organization and vesicle transport post-tapetal degradation, understanding these dynamics could lead to increased understanding of the PCD process during the development of pollen grains. Whether AtHMGB15 interacts with the chromatin remodeling complex or transcription factors during pollen development is not known and need further investigation.

Author contribution statement SC conceptualized the idea and supervised the project. SC wrote and reviewed the manuscript. RB performed all the investigations and wrote and reviewed the manuscript. All the authors have agreed with this final draft for submission. Fund acquisition was contributed by SC.

Supplementary Information The online version contains supplementary material available at https://doi.org/10.1007/s00497-024-00505-x.

Acknowledgements Dr. Shubho Chaudhuri and Ruby Biswas would like to sincerely acknowledge the Bose Institute for providing institutional support and infrastructure for experiments and data analysis. This work was supported by the Department of Science and Technology, Government of India. This work was funded by the SERB (SERB/2017/000768), Department of Science & Technology, Government of India.

Funding Science and Engineering Research Board, SERB/2017/000768, Shubho Chaudhuri.

Data availability The datasets generated during this current study are available in the NCBI Sequence Read Archive PRJNA1019630.

Declarations

Conflict of interest The authors declare no conflicts of interest.

References

- Bubb MR, Yarmola EG, Gibson BG, Southwick FS (2003) Depolymerization of actin filaments by profilin: effects of profilin on capping protein function. J Biol Chem 278(27):24629–24635
- Cai G, Cresti M (2009) Organelle motility in the pollen tube: a tale of 20 years. J Exp Bot 60(2):495–508
- Campellone KG, Welch MD (2010) A nucleator arms race: cellular control of actin assembly. Nat Rev Mol Cell Biol 11(4):237–251
- Chang F, Zhang Z, Jin Y, Ma H (2014) Cell biological analyses of anther morphogenesis and pollen viability in Arabidopsis and rice. Methods Mol Biol 1110:203–216
- Chapman G (1987) The tapetum. International review of cytology, vol. 107. Elsevier, Amsterdam, pp 111–125.
- Chen L, Liu Y-G (2014) Male sterility and fertility restoration in crops. Annu Rev Plant Biol 65:579–606
- Chen T, Teng N, Wu X, Wang Y, Tang W, Šamaj J, Baluška F, Lin J (2007) Disruption of actin filaments by latrunculin B affects cell wall construction in Picea meyeri pollen tube by disturbing vesicle trafficking. Plant Cell Physiol 48(1):19–30
- Cheng Z, Zhang J, Yin B, Liu Y, Wang B, Li H, Lu H (2019) γVPE plays an important role in programmed cell death for xylem fiber cells by activating protease CEP1 maturation in Arabidopsis thaliana. Int J Biol Macromol 137:703–711
- Cheng Z, Guo X, Zhang J, Liu Y, Wang B, Li H, Lu H (2020) βVPE is involved in tapetal degradation and pollen development by activating proprotease maturation in Arabidopsis thaliana. J Exp Bot 71(6):1943–1955



- Dennis G, Sherman BT, Hosack DA, Yang J, Gao W, Lane HC, Lempicki RA (2003) DAVID: database for annotation, visualization, and integrated discovery. Genome Biol 4(9):1–11
- Echlin P (1971a) Production of sporopollenin by the tapetum. Sporopollenin. Elsevier, Amsterdam, pp 220–247
- Echlin P (1971b) The role of the tapetum during microsporogenesis of angiosperms. Pollen, Elsevier, Amsterdam, pp 41–61
- El-Ghazaly G (1999) Tapetum and orbicules (Ubisch bodies): development, morphology and role of pollen grains and tapetal orbicules in allergenicity. Fertilization in higher plants: molecular and cytological aspects. Springer, New York, pp 157–173
- Fu Y, Wu G, Yang Z (2001) Rop GTPase-dependent dynamics of tiplocalized F-actin controls tip growth in pollen tubes. J Cell Biol 152(5):1019–1032
- Gómez JF, Talle B, Wilson ZA (2015) Anther and pollen development: a conserved developmental pathway. J Integr Plant Biol 57(11):876–891
- Gotelli M, Lattar E, Zini LM, Rosenfeldt S, Galati B (2023) Review on tapetal ultrastructure in angiosperms. Planta 257(6):100
- Guo X, Li L, Liu X, Zhang C, Yao X, Xun Z, Zhao Z, Yan W, Zou Y, Liu D (2022) MYB2 is important for tapetal PCD and pollen development by directly activating protease expression in Arabidopsis. Int J Mol Sci 23(7):3563
- Hansen FT, Madsen CK, Nordland AM, Grasser M, Merkle T, Grasser KD (2008) A novel family of plant DNA-binding proteins containing both HMG-box and AT-rich interaction domains. Biochemistry 47(50):13207–13214
- Hsieh K, Huang AH (2004) Endoplasmic reticulum, oleosins, and oils in seeds and tapetum cells. Plant Physiol 136(3):3427–3434
- Hsieh K, Huang AH (2007) Tapetosomes in Brassica tapetum accumulate endoplasmic reticulum–derived flavonoids and alkanes for delivery to the pollen surface. Plant Cell 19(2):582–596
- Huang S, Qu X, Zhang R (2015) Plant villins: versatile actin regulatory proteins. J Integr Plant Biol 57(1):40–49
- Inada N (2017) Plant actin depolymerizing factor: actin microfilament disassembly and more. J Plant Res 130:227–238
- Ishikawa T, Watanabe N, Nagano M, Kawai-Yamada M, Lam E (2011) Bax inhibitor-1: a highly conserved endoplasmic reticulum-resident cell death suppressor. Cell Death Differ 18(8):1271–1278
- Jelínková A, Malínská K, Petrášek J (2019) Using FM dyes to study endomembranes and their dynamics in plants and cell suspensions. Plant cell morphogenesis: methods and protocols. Springer, New York, pp 173–187
- Jiang Y, Zhang M, Huang S (2017) Analysis of actin-based intracellular trafficking in pollen tubes. Plant protein secretion: methods and protocols. Springer, New York, pp 125–136
- Jiang Y, Chang M, Lan Y, Huang S (2019) Mechanism of CAP1-mediated apical actin polymerization in pollen tubes. Proc Nat Acad Sci 116(24):12084–12093
- Johnson MA, Harper JF, Palanivelu R (2019) A fruitful journey: pollen tube navigation from germination to fertilization. Annu Rev Plant Biol 70:809–837
- Lavania UC, Basu S, Kushwaha JS, Lavania S (2014) Seasonal temperature variations influence tapetum mitosis patterns associated with reproductive fitness. Genome 57(9):517–521
- Lei X, Liu B (2020) Tapetum-dependent male meiosis progression in plants: increasing evidence emerges. Front Plant Sci 10:1667
- Liu X, Qu X, Jiang Y, Chang M, Zhang R, Wu Y, Fu Y, Huang S (2015) Profilin regulates apical actin polymerization to control polarized pollen tube growth. Mol Plant 8(12):1694–1709
- Liu C, Zhang Y, Ren H (2021) Profilin promotes formin-mediated actin filament assembly and vesicle transport during polarity formation in pollen. Plant Cell 33(4):1252–1267
- Mallik R, Prasad P, Kundu A, Sachdev S, Biswas R, Dutta A, Roy A, Mukhopadhyay J, Bag SK, Chaudhuri S (2020) Identification of genome-wide targets and DNA recognition sequence of the

- Arabidopsis HMG-box protein AtHMGB15 during cold stress response. Biochimica Et Biophysica Acta Gene Regul Mech 1863(12):194644
- Onelli E, Moscatelli A (2013) Endocytic pathways and recycling in growing pollen tubes. Plants 2(2):211–229
- Onelli E, Idilli AI, Moscatelli A (2015) Emerging roles for microtubules in angiosperm pollen tube growth highlight new research cues. Front Plant Sci 6:51
- Pacini E, Juniper B (1979) The ultrastructure of pollen-grain development in the olive (olea europaea). 2. Secretion by the tapetal cells. New Phytol 83(1):165–174
- Parish RW, Li SF (2010) Death of a tapetum: a programme of developmental altruism. Plant Sci 178(2):73–89
- Pollard TD (2016) Actin and actin-binding proteins. Cold Spring Harb Perspect Biol 8(8):a018226
- Qu X, Zhang H, Xie Y, Wang J, Chen N, Huang S (2013) Arabidopsis villins promote actin turnover at pollen tube tips and facilitate the construction of actin collars. Plant Cell 25(5):1803–1817
- Qu X, Jiang Y, Chang M, Liu X, Zhang R, Huang S (2015) Organization and regulation of the actin cytoskeleton in the pollen tube. Front Plant Sci 5:786
- Qu X, Wang Q, Wang H, Huang S (2020) Visualization of actin organization and quantification in fixed Arabidopsis pollen grains and tubes. Bio-Protoc 10(1):e3509-e3509
- Quilichini TD, Douglas CJ, Samuels AL (2014) New views of tapetum ultrastructure and pollen exine development in *Arabidopsis* thaliana. Ann Bot 114(6):1189–1201
- Ruan H, Li J, Wang T, Ren H (2021) Secretory vesicles targeted to plasma membrane during pollen germination and tube growth. Front Cell Develop Biol 8:615447
- Sachdev S, Biswas R, Roy A, Chaudhuri S (2022) The Arabidopsis ARID-HMG protein AtHMGB15 modulates JA signalling by regulating MYC2 during pollen development. bioRxiv 2010:515973
- Sanders PM, Bui AQ, Weterings K, McIntire K, Hsu Y-C, Lee PY, Truong MT, Beals T, Goldberg R (1999) Anther developmental defects in *Arabidopsis thaliana* male-sterile mutants. Sex Plant Reprod 11(6):297–322
- Selinski J, Scheibe R (2014) Pollen tube growth: where does the energy come from? Plant Signal Behav 9(12):e977200
- Tao Y, Chen H, Zou T, Ye Q, Han Y, Yuan W, Wang K, Liu J, Peng K, Liu H (2023) Manipulation of tapetal degradation provides a dominant male-sterility system for pyramiding breeding in rice. Plant Physiol 193:2282–2286
- Thomas C (2012) Bundling actin filaments from membranes: some novel players. Front Plant Sci 3:188
- Varnier A-L, Mazeyrat-Gourbeyre F, Sangwan RS, Clément C (2005) Programmed cell death progressively models the development of anther sporophytic tissues from the tapetum and is triggered in pollen grains during maturation. J Struct Biol 152(2):118–128
- Vidali L, Hepler P (2001) Actin and pollen tube growth. Protoplasma 215:64–76
- Vidali L, McKenna ST, Hepler PK (2001) Actin polymerization is essential for pollen tube growth. Mol Biol Cell 12(8):2534–2545
- Wan L, Xia X, Hong D, Li J, Yang G (2010) Abnormal vacuolization of the tapetum during the tetrad stage is associated with male sterility in the recessive genic male sterile *Brassica napus* L. Line 9012A. J Plant Biol 53:121–133
- Wang X, Sheng X, Tian X, Zhang Y, Li Y (2020) Organelle movement and apical accumulation of secretory vesicles in pollen tubes of *Arabidopsis thaliana* depend on class XI myosins. Plant J 104(6):1685–1697
- Xia C, Wang YJ, Liang Y, Niu QK, Tan XY, Chu LC, Chen LQ, Zhang XQ, Ye D (2014) The ARID-HMG DNA-binding protein A t HMGB 15 is required for pollen tube growth in *Arabidopsis thaliana*. Plant J 79(5):741–756



- Zhang D, Yang L (2014) Specification of tapetum and microsporocyte cells within the anther. Curr Opin Plant Biol 17:49–55
- Zhang D, Liu D, Lv X, Wang Y, Xun Z, Liu Z, Li F, Lu H (2014) The cysteine protease CEP1, a key executor involved in tapetal programmed cell death, regulates pollen development in Arabidopsis. Plant Cell 26(7):2939–2961
- Zhang R, Xu Y, Yi R, Shen J, Huang S (2023) Actin cytoskeleton in the control of vesicle transport, cytoplasmic organization and pollen tube tip growth. Plant Physiol 193(1):9–25
- Zhao W, Qu X, Zhuang Y, Wang L, Bosch M, Franklin-Tong VE, Xue Y, Huang S (2020) Villin controls the formation and enlargement of punctate actin foci in pollen tubes. J Cell Sci 133(6):jcs237404
- Zhu J, Nan Q, Qin T, Qian D, Mao T, Yuan S, Wu X, Niu Y, Bai Q, An L (2017) Higher-ordered actin structures remodeled by Arabidopsis actin-depolymerizing factor5 are important for pollen germination and pollen tube growth. Mol Plant 10(8):1065–1081

Publisher's Note Springer Nature remains neutral with regard to jurisdictional claims in published maps and institutional affiliations.



Plant Physiology®

https://doi.org/10.1093/plphys/kiae355 Advance access publication 26 June 2024 Research Article

The Arabidopsis ARID-HMG DNA-BINDING PROTEIN 15 modulates jasmonic acid signaling by regulating MYC2 during pollen development

Sonal Sachdev, 10 Ruby Biswas, 10 Adrita Roy, 1 Ayantika Nandi, 10 Vishal Roy, 10 Sabini Basu, 10 and Shubho Chaudhuri 1.* 10

The author responsible for distribution of materials integral to the findings presented in this article in accordance with the policy described in the Instructions for Authors (https://academic.oup.com/plphys/pages/General-Instructions) is Shubho Chaudhuri.

Abstract

The intricate process of male gametophyte development in flowering plants is regulated by jasmonic acid (JA) signaling. JA signaling initiates with the activation of the basic helix-loop-helix transcription factor (TF), MYC2, leading to the expression of numerous JA-responsive genes during stamen development and pollen maturation. However, the regulation of JA signaling during different stages of male gametophyte development remains less understood. This study focuses on the characterization of the plant ARID-HMG DNA-BINDING PROTEIN 15 (AtHMGB15) and its role in pollen development in Arabidopsis (Arabidopsis thaliana). Phenotypic characterization of a T-DNA insertion line (athmgb15-4) revealed delayed bolting, shorter siliques, and reduced seed set in mutant plants compared to the wild type. Additionally, AtHMGB15 deletion resulted in defective pollen morphology, delayed pollen germination, aberrant pollen tube growth, and a higher percentage of nonviable pollen grains. Molecular analysis indicated the downregulation of JA biosynthesis and signaling genes in the athmgb15-4 mutant. Quantitative analysis demonstrated that JA and its derivatives were ~10-fold lower in athmgb15-4 flowers. Exogenous application of methyl jasmonate could restore pollen morphology and germination, suggesting that the low JA content in athmgb15-4 impaired JA signaling during pollen development. Furthermore, our study revealed that AtHMGB15 hybrically interacts with MYC2 to form a transcription activation complex. This complex promotes the transcription of key JA signaling genes, the R2R3-MYB TFS MYB21 and MYB24, during stamen and pollen development. Collectively, our findings highlight the role of AtHMGB15 as a positive regulator of the JA pathway, controlling the spatiotemporal expression of key regulators involved in Arabidopsis stamen and pollen development.

Introduction

The development of male gametophytes in angiosperms is a highly coordinated process, requiring the integration of various plant hormone signaling pathways (Mascarenhas 1990; Wilson and Zhang 2009; Marciniak and Przedniczek 2019). The spatiotemporal activity of key hormone signaling factors regulates the pollen maturation, anther dehiscence, release of pollen grains to the surface of the stigma, and pollen tube germination, for successful fertilization. The differentiation of sporogenous cells (pollen mother cell) in the anther gives rise to haploid microspores through meiosis. Subsequent development involves mitotic divisions and the formation of the pollen cell wall through programmed cell death of the tapetum layer (McCormick 2004; Zhang et al. 2007). The degeneration of the tapetum layer is essential for anther dehiscence and the release of mature pollen. In selfpollinating plants, anther dehiscence and the release of pollen onto the stigma depend upon the appropriate length of the stamen filament. The anthers in these self-pollinating plants are positioned at an equivalent height or above the stigma papillae, ensuring efficient pollen transfer and fertilization. Any abnormalities during pollen maturation, stamen elongation, or anther dehiscence can lead to reduced fertility or complete male sterility.

Plant hormone jasmonic acid (JA) and its derivatives are indispensable for the development of stamen and male gametophyte

maturation (Huang et al. 2017b). Arabidopsis (Arabidopsis thaliana) mutants deficient in JA biosynthesis, viz. FATTY ACID DESATURASE 3/7/8 (fad3fad7fad8), DEFECTIVE IN ANTHER DEHISENCE 1 (dad1), LIPOOXYGENASE 3/4 (lox3-lox4), ALLENE OXIDE SYNTHASE (aos), and 12-OXOPHYTODIENOIC ACID REDUCTASE 3 (opr3), exhibit male sterility due to arrested stamen development at anthesis (McConn and Browse 1996; Stintzi and Browse 2000; Ishiguro et al. 2001; Park et al. 2002; Caldelari et al. 2011). These mutants have indehiscent anthers or short filaments that fail to reach the stigma surface. Although the pollen grain from these mutants initially develops normally to produce tricellular gametophyte, they lose viability during later stages (Acosta and Przybyl 2019). However, the application of exogenous JA can restore fertility in these JA biosynthesis-deficient mutants (Park et al. 2002). CORONATINE INSENSITIVE1 (COI1), an F-box protein is a part of SKP1-CULLIN1-F-box-type (SCF) E3 ubiquitin ligase complex SCF^{COI1} and a crucial component of JA signaling, forms a complex with transcriptional repressors Jasmonate ZIM-domain (JAZ) in the presence of JA-isoleucine (JA-Ile) derivative. The 26S proteasome mediates the degradation of JAZ repressor and releases the MYC transcription factor (TF) for the expression of JA-responsive genes (Xie et al. 1998; Devoto et al. 2002; Chini et al. 2007; Thines et al. 2007; Zhai et al. 2015). coi1 mutants exhibit impaired stamen maturation and male sterility. However, unlike JA biosynthesis-deficient

¹Department of Biological Sciences, Bose Institute, Unified Academic Campus, EN 80, Sector V, Kolkata 700091, WB, India

^{*}Author for correspondence: shubho@jcbose.ac.in (S.C.)

mutants, exogenous application of JA fails to rescue fertility in coil mutants (Feys et al. 1994; Xu et al. 2002).

The MYC2 TF, a member of the basic helix-loop-helix family, is a central regulator of the JA response. MYC2 activates the transcription of JA-responsive genes by binding to G-box motifs present in their promoter regions (Dombrecht et al. 2007; Pozo et al. 2008; Figueroa and Browse 2012; Kazan and Manners 2013). Previous studies have shown that MYC2 along with MYC3, MYC4, and MYC5 redundantly regulates stamen development and seed production (Qi et al. 2015; Gao et al. 2016). While the single and double mutants showed no defect in stamen development, the triple mutants myc2myc3myc4, myc2myc4myc5, and myc3myc4myc5 exhibited delayed stamen development (Dombrecht et al. 2007; Schweizer et al. 2013). The anthers of these triple mutants fail to dehisce at the floral stage 13, and pollen grains are unable to germinate in vitro; however, anther dehiscence and pollen maturation occur at $the \, later \, stage \, of \, flower \, development. \, Quadruple \, mutants, in \, com$ parison with triple mutants, exhibit more severe defects in stamen development, characterized by short stamen filaments, indehiscent anthers, and nonviable pollen grains (Qi et al. 2015).

MYC2 TF coordinates JA signaling through R2R3-type MYB TFs, specifically MYB21 and MYB24, during stamen maturation (Song et al. 2011). MYB21 and MYB24 physically interact with MYC2 forming the MYC-MYB complex for transcription activation while also interacting with JAZ to attenuate their activity (Yang et al. 2020; Zhang et al. 2021). The phytohormone gibberellin (GA) has been shown to regulate the expression of MYB21/24 and promote stamen growth (Cheng et al. 2009). Studies indicate that DELLA inhibits JA biosynthesis by suppressing the expression of DAD1 and LOX1. DELLA also interacts with MYB21/24 in the absence of GA and represses their transcriptional activity (Cheng et al. 2009). GA triggers the ubiquitination of DELLA and upregulates the expression of JA biosynthesis genes DAD1 and LOX1 (Huang et al. 2020). The increased concentration of JA will induce the expression of MYB21 and MYB24 (Vera-Sirera et al. 2016; Huang et al. 2020). Thus, GA and JA signaling synergistically modulate stamen elongation by regulating MYC-MYB signaling (Song et al. 2014; Chini et al. 2016). myb21 mutants have short filaments that are unable to reach the pistil's stigma resulting in complete male sterility (Mandaokar et al. 2006). However, myb21 pollen grains are viable. myb24 mutants are completely fertile, whereas the myb21myb24 double mutants exhibit impaired stamen development and complete sterility highlighting the essential role of MYB21 in filament elongation and MYB24 in pollen viability and anther dehiscence (Mandaokar et al. 2006; Mandaokar and Browse 2009; Song et al. 2011; Huang et al. 2017b).

AtHMGB15 belongs to a unique group of nuclear architectural proteins, containing 2 DNA-binding domains, namely ARID and HMG-box (Štros et al. 2007). Biochemical analysis shows that ARID-HMG proteins bind to different DNA topological structures preferably in the AT-rich region (Hansen et al. 2008; Roy et al. 2016). Previous research has demonstrated the involvement of AtHMGB15 in pollen tube growth (Xia et al. 2014). Approximately 10% of the pollen grains of the Ds insertion line of AtHMGB15 (athmgb15-1) have defective morphology. Comparative transcriptome analysis between wild-type and athmgb15-1 pollen showed alteration of genes specific for pollen. Additionally, AtHMGB15 was found to interact with two MIKC* TFs, namely AGL66 and AGL104. However, the mechanistic role of AtHMGB15 in pollen development remained unclear. In this study, we characterized the T-DNA insertion mutant of AtHMGB15 (athmgb15-4), where the insertion is in the first exon. Our findings demonstrate that ~30% of pollen grains from athmqb15-4 plants exhibit defective morphology, characterized by a round shape, and disrupted reticulate ornamentation. Transcriptome analysis revealed substantial repression of JA biosynthesis and signaling in athmgb15-4 flowers. Collectively, our results provide comprehensive insights into the mechanistic role of the ARID-HMG protein AtHMGB15 in pollen development, specifically in regulating key master regulators of the JA pathway.

Results

Isolation and characterization of athmgb15-4 mutant lines

The athmqb15-4 mutant was identified from a screening of the T-DNA insertion line of Arabidopsis ecotype Col-0 from the GABI-Kat collection (GABI_351D08). GABI_351D08 has the T-DNA insertion annotated at exon 1 of the gene At1q04880 (Fig. 1A, i). The T-DNA insertion carries a sulfadiazine-resistant marker. The homozygous athmgb15-4 lines were generated through the selfcrossing of heterozygous athmgb15-4 plants followed by the selection of sulfadiazine resistance progeny. The homozygous lines were confirmed by PCR (Fig. 1A, ii), and the T-DNA insertion was validated through Southern blot (Supplementary Fig. S1). RT-qPCR analysis demonstrated a significant downregulation of AtHMGB15 expression in the athmgb15-4 mutant plants (Fig. 1A, iii). Previously, our group had reported the absence of the AtHMGB15 protein in the same mutant line (Mallik et al. 2020). Homozygous seeds were collected for subsequent investigations.

At the rosette stage, athmqb15-4 plants did not exhibit any phenotypic differences compared to wild-type plants, except for a shorter primary root length in athmgb15-4 (Fig. 1B, i and Supplementary Fig. S2). Additionally, athmqb15-4 plants showed a significant delay in flowering compared to wild type (Fig. 1B, ii and Supplementary Fig. S3). Under regular growth conditions (long days), the number of rosette leaves at bolting for wild type was 14 compared to 20 for athmgb15-4. Further, athmgb15-4 takes around 37 days for flowering compared to 27 days for wild-type plants (Fig. 1B, iv, v). Approximately 45% ($P \le 0.05$) of seedlings of wild type initiated bolting after 30 days post-germination (dpg), whereas only 8% (P \leq 0.05) of athmgb15-4 plants exhibited bolting (Fig. 1B, iii). The seeds of athmgb15-4 mutant plants showed no marked difference when compared with wild type; they were viable and exhibited normal germination, like the wild type. However, mutant siliques were shorter in length compared to wild type (Fig. 1C, i, ii, iv) and contained fewer fertilized ovules, resulting in reduced seed yield compared to wild-type plants (Fig. 1C, iii, v).

Comparative transcriptome between wild type and athmgb15-4 showed differential regulation of genes belonging to pollen development, cell wall, and hormone pathways

Earlier studies have shown that expression of AtHMGB15 is highly tissue-specific with maximum expression observed in pollen grain (Xia et al. 2014). To gain insights into the role of AtHMGB15 in pollen development, we conducted a comparative transcriptome analysis between wild-type and athmqb15-4 flowers of stage 13 (Sanders et al. 1999). The gene ontology (GO) term enrichment analysis using differentially expressed genes (DEGs) revealed enrichment of pollen tube development, cell growth and its regulation, cell wall development, biogenesis and organization, hormone-mediated signaling pathway and response, response to JA, and biosynthetic and metabolic process for biological process

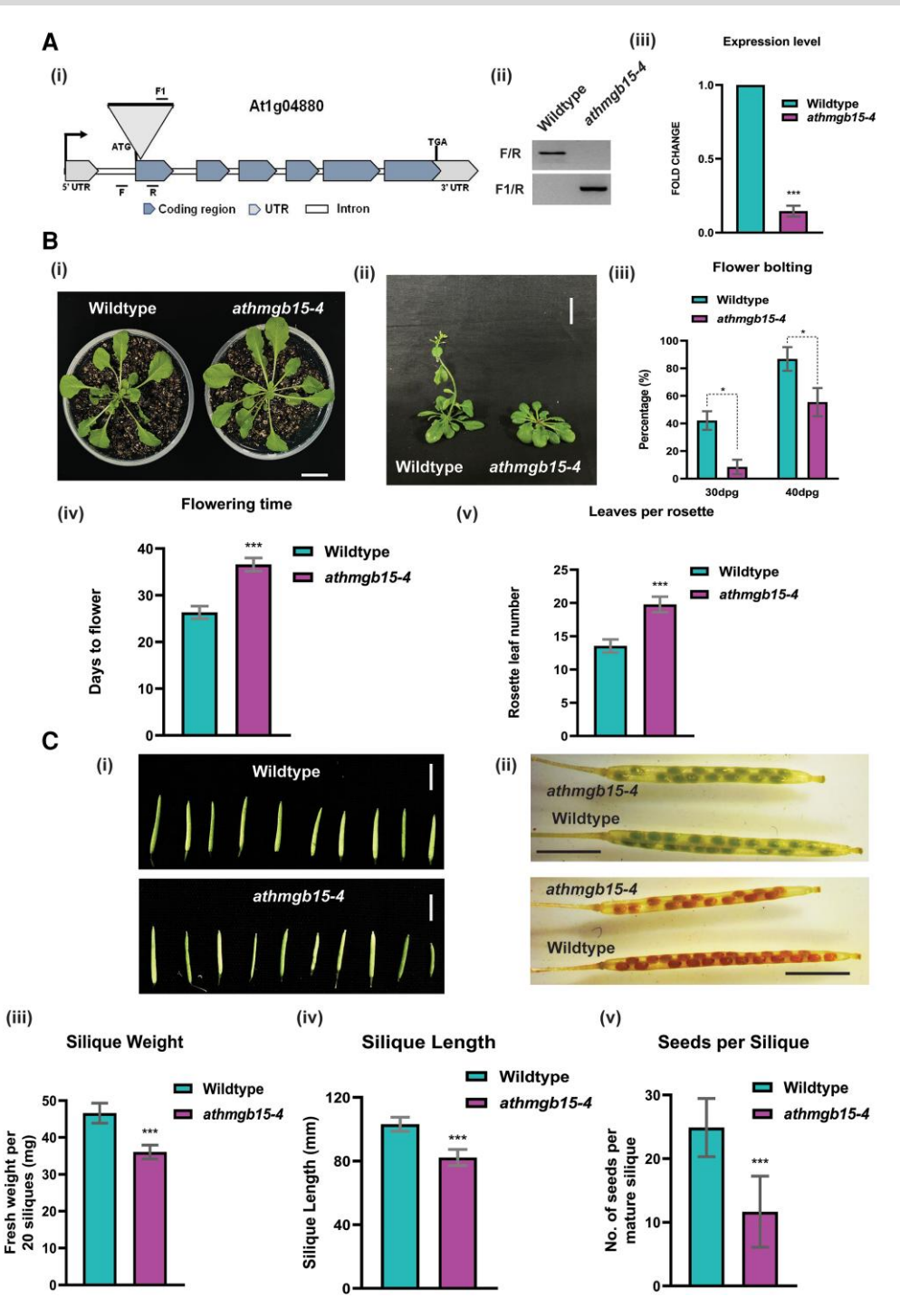


Figure 1. Phenotypic characterization of athmgb15-4 mutant. A) (i) Schematic showing the position of T-DNA insertion in the 1st exon of AtHMGB15 (At1g04880) and the position of PCR primers used for mutant screening. Black arrow indicates the transcription start site. (ii) PCR confirmation of athmqb15-4 homozygous line. (iii) RT-qPCR showing significant reduction of AtHMGB15 transcript in athmqb15-4 lines. The fold change was represented with respect to wild type. Error bars represent mean \pm SD (n=3); significance was calculated by paired two-tailed Student's t-test. Asterisks represent significant differences between wild type and athmgb15-4, ***P < 0.001. B) (i) Wild type and athmgb15-4 at the rosette stage. Scale bar = 2 cm. (ii) Delayed flowering of athmgb15-4 compared to wild type. Scale bar = 2 cm. (iii) Quantitative analysis of flower bolting between athmgb15-4 and wild type. The experiments were done from seeds of 4 to 5 independent harvests. Data were collected from 100 plants of each batch. Error bars represent mean ± SD (n = 400), and significance was calculated by paired two-tailed Student's t-test. Asterisks represent significant differences between wild type and athmgb15-4, *P < 0.05. dpg, days post-germination. (iv) Days from germination to flowering. Error bars represent mean \pm SD (n = 27), and significance was calculated by paired two-tailed Student's t-test. Asterisks represent significant differences between wild type and athmgb15-4, ***P < 0.001. (v) Number of rosette leaves at bolting. Error bars $represent\ mean\ \pm\ SD\ (n=27), and\ significance\ was\ calculated\ by\ paired\ two-tailed\ Student's\ t-test.\ Asterisks\ represent\ significant\ differences\ between\ wild$ type and athmgb15-4, ***P < 0.001. C) (i) Comparative silique length of wild type and athmgb15-4. Scale bar = 5 mm. (ii) Comparison of seed set between wild type and athmgb15-4. Scale bar = 2.5 mm. (iii) Quantitative silique fresh weight between athmgb15-4 and wild type. Measurement was taken using 20 siliques for each observation. Error bars represent mean \pm SD (n=20). (iv) Quantitative silique length between athmgb15-4 and wild type. Measurement was taken using 20 siliques for each observation. Error bars represent mean \pm SD (n = 20). (v) Seed numbers were counted from mature siliques of wild type and athmqb15-4. Error bar represents mean \pm SD (n=30). The significance of all these results was analyzed by paired two-tailed Student's t-test Asterisks represent significant differences between wild type and athmgb15-4, ***P < 0.001.

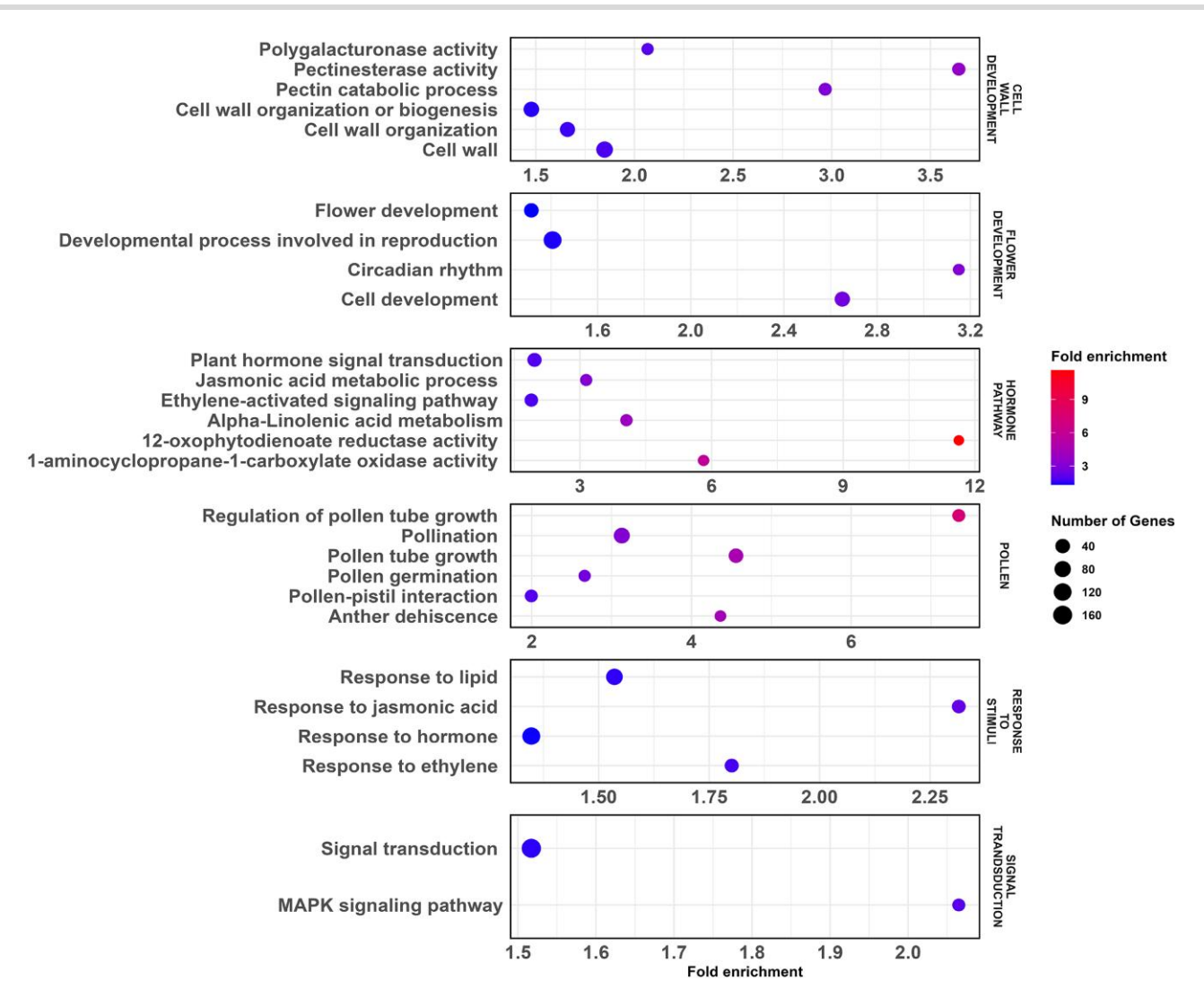


Figure 2. The GO and KEGG enrichment analysis. Bubble plot showing the enriched terms from the biological process, molecular function, cell component, and KEGG pathways between wild-type and *athmgb*15-4 DEG datasets. The significantly enriched terms are plotted using the False Discovery Rate enrichment and number of genes and are categorized under 6 subcategories relevant to our study, namely, cell wall development, hormone pathway, response to stimuli, flower development, pollen, and signal transduction.

(Fig. 2 and Supplementary Fig. S4). Additionally, Kyoto Encyclopedia of Genes and Genomes (KEGG) analysis highlighted the enrichment of α -linolenic acid metabolism, carotenoid biosynthesis, and biosynthesis of secondary metabolites as some of the pathways enriched in our dataset (Supplementary Fig. S5). To validate our result, we selected candidate genes and performed RT-qPCR analysis (Supplementary Fig. S6).

Previously published microarray data from Xia et al. using athmgb15-1 and wild-type pollen grains have shown genes responsible for cell growth, pollen development, and pollen tube growth, cell wall synthesis, and cellular transport as some of the important ones that are differentially enriched. We next compared our transcriptome with Xia et al. and found 171 DEGs common in both the datasets. Of these, 111 DEGs represent downregulated, and 60 represent upregulated. Further analysis showed that these 111 downregulated genes represent GO biological processes such as pollen tube growth and development, pollination, cell growth, and protein phosphorylation. Notably, there was no GO enrichment related to the JA pathway except the LOX4 gene which was found downregulated even in Xia

et al. dataset (Supplementary Fig. S7A to C and Tables S1 and S2). This discrepancy can be attributed to the difference in tissue types used for the transcriptome studies; Xia et al. used pollen grains, while we used stage 13 flower. Nevertheless, previous studies have established the role of jasmonate during the initiation of pollen development particularly during anther development at around stages 12 to 13 of flower development (Sanders et al. 1999).

In our previous study, we conducted a whole-genome ChIP-on-chip assay using 14-day-old Arabidopsis seedlings to identify the targets of AtHMGB15. Comparing our DEGs with the ChIP-on-chip data, we identified ~1,090 common loci between the 2 datasets. GO analysis of these common loci unveiled the significant enrichment of genes belonging to stress response, response to JA, and pollen development in terms of biological processes (Supplementary Fig. S7 D to F and Tables S3 and S4). Collectively, our transcriptome analysis and previous findings indicate that AtHMGB15 directly or indirectly regulates the transcription of genes involved in the pollen development pathway, possibly by modulating hormone signaling.

athmqb15-4 plants have defective pollen morphology and delayed pollen germination rate

To investigate the role of AtHMGB15 on pollen development, we initially studied pollen grain morphology of athmqb15-4 mutants and wild-type plants using scanning electron microscopy (SEM). Our observations revealed that wild-type pollen grains exhibited an ellipsoidal shape (Fig. 3A), while athmqb15-4 pollen grains displayed a mixture of shapes, including ~25% to 30% with circular or irregular shapes (Fig. 3B and Supplementary Fig. S8A). Additionally, the outermost exine wall of wild-type pollen grains had a typical reticulate pattern of ornamentation, which was completely absent in the defective pollen grains of mutant plants. To gain further insights into the abnormal cell wall morphology of athmqb15-4 plants, we analyzed the transcriptome data for genes associated with cell wall biosynthesis. Our RNA-seq analysis revealed significant downregulation of genes involved in cell wall biosynthesis in athmqb15-4 flowers, including pectin lyase, cellulose synthase, pectin methylesterase, and extensin, which are known to play crucial roles in pollen development (Fig. 3C and Supplementary Fig. S6C). Interestingly, most of the cell wall validated genes, viz. pectin lyase (At5g48140 and At3g07850), pectin methyltransferase (At4g15980), cellulose synthase (At2g33100), and xyloglucan endotransglucosylase (AT4G30280), showed AtHMGB15 binding as per our ChIP-on-chip data (Mallik et al. 2020) (Supplementary Table S3).

Subsequently, we examined the pollen germination rate of wild-type and athmgb15-4 pollen grains. The time kinetics of in vitro pollen tube germination shows that within 4 h, more than 50% of pollen grains ($P \le 0.005$) were germinated for wild-type pollen grains and by 6 h almost 80% (P ≤ 0.005) germination was achieved (Fig. 3D, i, iii). Interestingly, only 40% (P≤0.005) germination of athmgb15-4 pollen grains was observed after 24 h in pollen germination media (Fig. 3D, ii, iii). These results indicate that the mutation of AtHMGB15 leads to severe defects in pollen morphology and causes significant delays in the germination rate of pollen tubes. Some of the pollen grains from athmgb15-4 that show tube growth comparable to wild type may be considered normal ellipsoidal in shape (like wild type). However, this percentage is less in the mutant compared to the wild type, based on our in vitro germination assay (Supplementary Fig. S8B). To assess the viability of athmgb15-4 pollen grains compared to wild type, we performed fluorescein diacetate (FDA) and propidium iodide (PI) staining. While FDA is permeable to the cell membrane and can stain live cells, PI is impermeable and can stain DNA only when the cell integrity is compromised. Thus, PI-stained cells are considered dead cells. Comparison of the staining patterns revealed a higher percentage of nonviable pollen grains (55%, $P \le 0.005$) in athmgb15-4 mutants compared to wild type (30%, $P \le 0.05$) (Fig. 3E), justifying the lower germination rate observed in the mutant plants. Thus, our data strongly indicate that the AtHMGB15 function is essential for the development of viable pollen grains in Arabidopsis.

AtHMGB15 regulates the expression of genes involved in the JA pathway during flower development

KEGG analysis of RNA-seq data has identified enrichment of the α-linolenic acid metabolism pathway from the differential expressed gene pool (Fig. 2, and Supplementary Fig. S5). α-Linolenic acid is the precursor of the plant phytohormone, JA. JA and its derivatives have been shown to regulate many developmental processes including stamen and flower development (Wasternack and Hause 2013; Jang et al. 2020). We examined the expression of JA biosynthesis and signaling genes in athmqb15-4 flowers using RT-qPCR. As shown in Fig. 4, A, the relative fold change for genes involved in JA biosynthesis and JA signaling was significantly downregulated in athmqb15-4 flowers compared to wild type. Furthermore, the expression levels of JA-related genes were moderately downregulated in another T-DNA mutant of AtHMGB15 (SALK_057612C_9 and SALK_057612C_15) (Supplementary Fig. S9). These athmgb15 mutants harbor T-DNA insertion in the promoter region. Collectively, the transcriptome and RT-qPCR analyses suggested the transcriptional activator role of AtHMGB15 for the expression of JA biosynthesis and signaling genes during flower development. Comparing our transcriptome and earlier published ChIP-on-chip data (Mallik et al. 2020), it was observed that most of the validated genes associated with JA response, viz. LOX3, AOS, DAD1, AOC3, JAR1, JAZ1, JAZ3, JAZ8, and MYC2, have AtHMGB15-binding site (Supplementary Table S3).

To further establish the regulation of AtHMGB15 in JA signaling during pollen development, we raised complementation lines using 35S::AtHMGB15 in athmqb15-4 background. Stable homozygous lines were selected (athmqb15-4-OEA4), and the expression of AtHMGB15 was analyzed using RT-qPCR (Fig. 4B, iii). These complementation lines were stable and recovered the delayed bolting and small silique size phenotype of athmgb15-4 mutant (Fig. 4B, i, ii). Moreover, a comparison of pollen tube germination rates showed a significantly higher population of germinated pollen grains in the athmgb15-4-OEA4 compared to athmgb15-4 (Fig. 4C, i, ii). Additionally, more than 95% ($P \le 0.05$) of pollen grains in athmqb15-4-OEA4 exhibited an ellipsoidal shape, indicating complete recovery of pollen morphology (Fig. 4D). RT-qPCR results revealed higher expression of JA biosynthesis and signaling genes in the complementation line compared to the mutant (Fig. 4E). The expression of JA biosynthesis genes in the complementation line was comparable to wild type; however, the expression of JA signaling genes was higher than wild type. The molecular and phenotypic analyses of complementation lines strongly demonstrate that AtHMGB15 is essential in JA-regulated signaling events during pollen development.

athmgb15 flowers showed low levels of JA and its derivatives

The downregulation of JA biosynthesis genes in athmgb15-4 mutants suggests a low intrinsic level of JA and its derivatives. To assess the hormone level, we next estimated the in vivo level of jasmonate in the flowers of wild-type, athmgb15-4, and athmgb15-4-OE_{A4} lines. As shown in Fig. 5A, the levels of JA along with two of its derivatives, namely methyl jasmonate (MeJA) and JA-Ile, are almost 10-fold (P \leq 0.05) lower in athmgb15-4 flowers compared to wild type. Remarkably, the low level of JA and its derivatives were restored in athmgb15-4-OEA4 complementation lines.

Considering the reduced JA levels in athmgb15-4 flowers, the effect of exogenous MeJA application on these flowers was examined by evaluating the pollen tube germination post-48 h treatment. The result revealed that the application of exogenous treatment of MeJA on buds and young flowers restores the pollen tube germination of athmgb15-4 pollen grains, and the rate is equivalent to that of wild-type pollen grains (Fig. 5B and C). We checked the expression of JA biosynthesis and signaling genes post-exogenous MeJA application in the young flowers. Our results indicate that there was a significant increase in the expression of AOS, OPR3, MYC2, JAZ1, and JAZ10

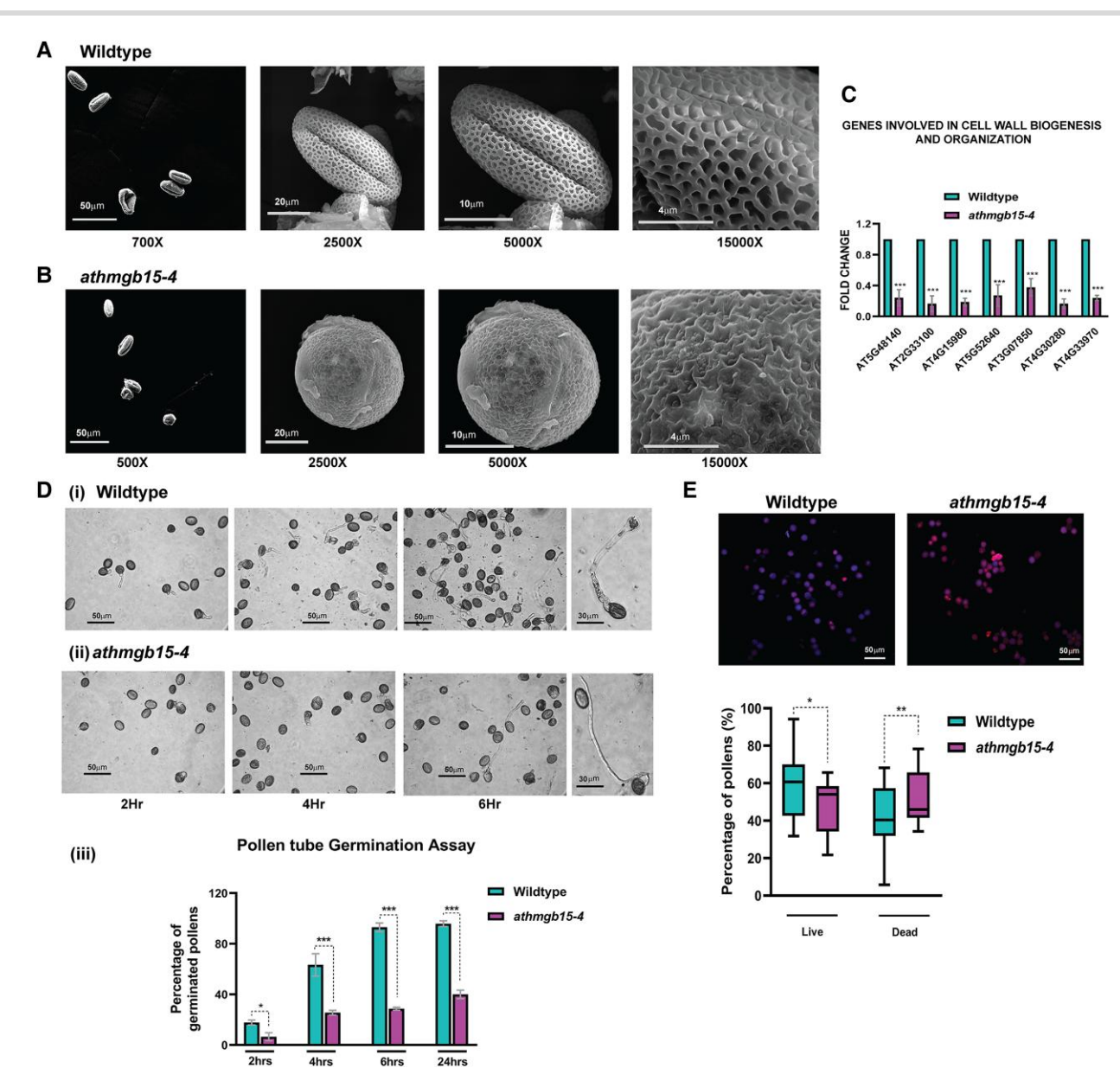


Figure 3. Defective pollen morphology and pollen germination rate of athmgb15-4 compared to wild type. **A)** SEM of pollen grains isolate from wild type showing ellipsoidal shape with reticulate ornamentations. **B)** Representation of defective pollen morphology of athmgb15-4 mutant having a circular shape with irregular ornamentation. The experiment was repeated at least 10 times with pollen grains isolated from different batches of wild type and athmgb15-4. **C)** Expression of differentially regulated cell wall biosynthesis genes between wild type and athmgb15-4 using RT-qPCR. The fold change was represented with respect to wild type. Error bars represent mean \pm SD (n=8). The significance was analyzed by paired two-tailed Student's t-test. Asterisks represent significant differences between wild type and athmgb15-4, ***P < 0.001. **D)** Freshly isolated pollen grains from (i) wild type and athmgb15-4 were subjected to in vitro germination for different time periods. (iii) Graphical representation of rate of pollen germination of wild type and athmgb15-4 at the given time points. Error bars represent mean \pm SD (n=10). The significance was analyzed by paired two-tailed Student's t-test. Asterisks represent significant differences between wild type and athmgb15-4, *P < 0.05, ***P < 0.001. **E)** Pollen viability was measured using FDA and PI. FDA-stained cells are blue denoting live pollen grains, the PI-stained cells are red denoting dead pollen grains, and the purple-colored pollen grains are sterile in nature. The excitation wavelength used for the fluorescence microscope to observe PI was 535 nm, with an exposure duration of 100 ms and the gain at 1x. The excitation wavelength for FDA was 488 nm, with an exposure duration of 200 ms and the gain at 1.5x. Box plot representation of pollen viability between wild type and athmgb15-4. Whiskers represent mean \pm SD (n=12). The significance was analyzed by paired two-tailed Student's t-test. Asterisks represent significant differences as in

(Fig. 5D and Supplementary Fig. S10) in wild-type and athmgb15-4 flowers after exogenous MeJA application. Thus, restoration of mutant pollen phenotype and induction of JA signaling genes by exogenous MeJA application indicates that the low endogenous level of JA in athmgb15-4 plants is responsible for the reduced expression of JA signaling genes during pollen development.

AtHMGB15 acts as a transcription activator for the expression of MYC2

Transcriptome and RT-qPCR analyses revealed the downregulation of the key TFs of JA signaling, viz. MYC2, MYB21, and MYB24, in *athmgb*15-4 mutant flowers. We next aimed to investigate whether AtHMGB15 acts as a transcription activator for the expression of these genes.

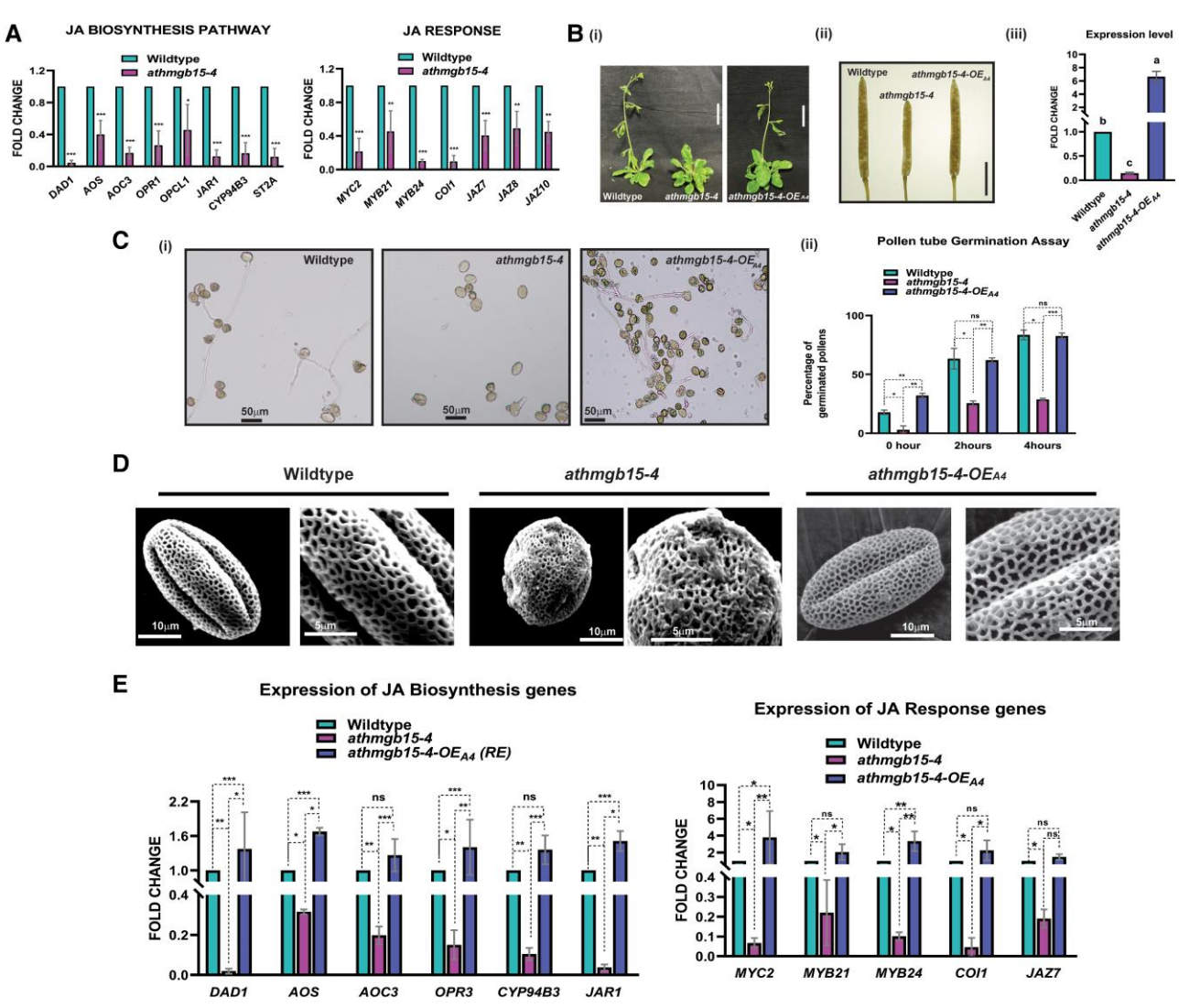


Figure 4. Complementation of athmgb15-4 mutant line with AtHMGB15 restores pollen morphology and pollen tube germination. A) Expression of differentially regulated JA biosynthesis and signaling genes was analyzed between wild type and athmqb15-4 using RT-qPCR. The fold change was represented with respect to wild type. Error bars represent mean \pm SD (n=6). The significance for each gene was analyzed by paired two-tailed Student's t-test. Asterisks represent significant differences between wild type and athmqb15-4, *P < 0.05, **P < 0.01, ***P < 0.001, *B) (i) Comparative flower bolting between wild type, athmgb15-4, and athmgb15-4-OE_{A4}. Scale bar = 2 cm. (ii) Silique length of wild type, athmgb15-4, and athmgb15-4-OE_{A4}. Scale bar = 4 mm. (iii) RT-qPCR to check AtHMGB15 transcript level in wild type, athmgb15-4, and athmgb15-4-OEA4. The fold change was represented with respect to wild type. Error bars represent mean ± SD (n = 6). Letters indicate significant differences according to a one-way ANOVA with Tukey's post hoc test (P < 0.05). C) (i) Comparative in vitro pollen germination between wild type, athmgb15-4, and athmgb15-4-OEA4. (ii) Quantification of the rate of pollen germination. Error bars represent mean \pm SD (n=6). The significance for each time point was analyzed by one-way ANOVA with Fisher's LSD post hoc test. Asterisks represent significant differences as indicated (*P < 0.05, **P < 0.01, ***P < 0.001, ns, not significant). D) SEM analysis of pollen morphology. E) Expression of JA biosynthesis and signaling genes in wild-type, athmgb15-4, and athmgb15-4-OE_{A4} flowers. The fold change for each gene was represented with respect to wild type. Error bars represent mean \pm SD (n=8). The significance for each gene was analyzed by one-way ANOVA with Tukey's post hoc test. Asterisks represent significant differences as indicated (*P < 0.05, **P < 0.01, ***P < 0.001, ns, not significant).

AtHMGB15 occupancy at the upstream region of MYC2, MYB21, and MYB24

To explore the potential interaction between AtHMGB15 and the upstream regions of these genes, a ChIP assay was performed using the custom-made (Thermo Scientific, India) affinitypurified anti-AtHMGB15 antibody and the immunoprecipitated DNA was subjected to qPCR. It is noteworthy that the antibody that was used for ChIP analysis was previously validated in the whole-genome ChIP-on-chip study (Mallik et al. 2020). However, we have further performed a western blot with flower samples of stage 13 to further revalidate the antibody (Supplementary Fig. S11). All our ChIP data were normalized with 2 loci, namely At1g01840 and At1g01310, showing no AtHMGB15 occupancy from our

previous study (Mallik et al. 2020). The primers were designed from in silico analysis of promoter/upstream region of MYC2, MYB21, and MYB24 that contain AtHMGB15-binding site A(A/C)-ATA-(A/T)(A/T) (Mallik et al. 2020). The qPCR analysis showed AtHMGB15 occupancy at the promoter/upstream region of MYC2, MYB21, as well as MYB24 (Fig. 6A). To test whether AtHMGB15 directly binds to the promoter/upstream region of MYC2, MYB21, and MYB24, we performed an electrophoretic mobility shift assay (EMSA) using the same 200-bp DNA fragments that were used for ChIP validation of AtHMGB15 binding. EMSA experiments confirmed the direct binding of AtHMGB15 protein at the promoter regions of MYC2, MYB21, and MYB24 (Fig. 6B). There was no binding with the 200-bp DNA fragment corresponding to At1g01310

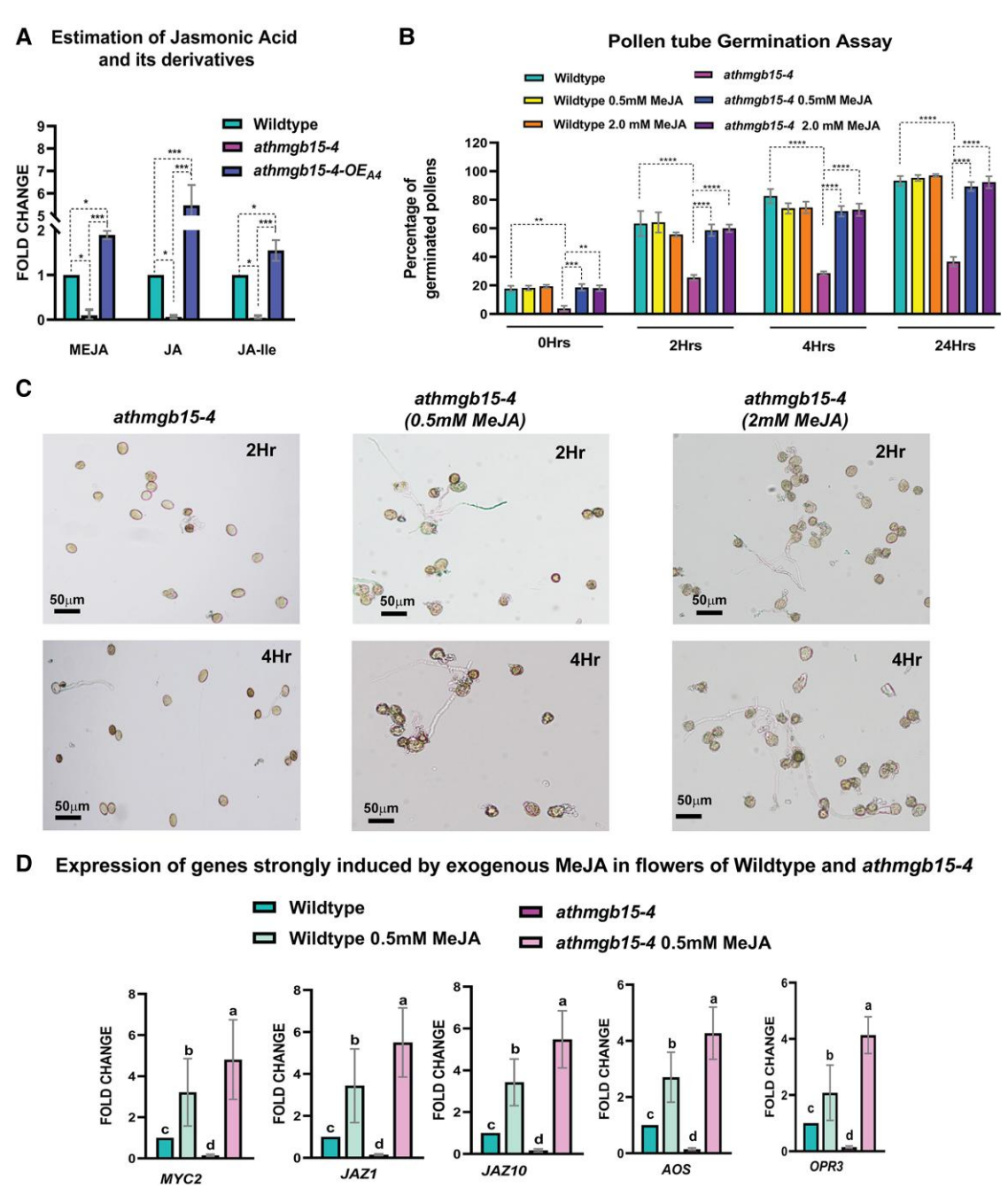


Figure 5. athmgb15-4 mutants have reduced levels of JA and its derivatives. A) JA and its derivatives were measured from the flowers of wild type, athmgb15-4, and athmgb15-4-0EA4 and represented as fold change with respect to wild type. Error bars represent mean \pm SD (n=3). The significance was analyzed by one-way ANOVA with Fisher's LSD post hoc test. Asterisks represent significant differences as indicated (*P < 0.05 and ***P < 0.001). JA, jasmonic acid; MeJA, methyl jasmonate; JA-Ile, jasmonic acid isoleucine. B) Quantification of the rate of pollen tube germination in the presence of different concentrations of methyl jasmonate. Error bars represent mean \pm SD (n=3). The significance was analyzed by two-way ANOVA with Tukey's post hoc test. Asterisks represent significant differences as indicated (**P < 0.01, ***P < 0.001, and ****P < 0.0001). C) Restoration of in vitro pollen germination of athmgb15-4 on treatment with exogenous MeJA (0.5 and 2 mM). D) Expression of genes strongly induced by exogenous MeJA (0.5 mM) in flowers of wild type and athmgb15-4. The fold change was represented with respect to wild type. Error bars represent mean \pm SD (n=6). Letters indicate significant differences according to a one-way ANOVA with Tukey's post hoc test (P<0.05).

(negative control). Furthermore, site-directed mutagenesis (SDM) causing mutation of the AT-rich binding motif resulted in a significant reduction in AtHMGB15 binding, with binding observed only at high protein concentrations (Supplementary Fig. S12). Moreover, previous ChIP-on-chip data also supported the presence of AtHMGB15 at the MYC2 and MYB24 loci, further suggesting its role in regulating the transcription of JA signaling genes.

AtHMGB15 activates the transcription of MYC2

The binding of AtHMGB15 at the promoter/upstream region of MYC2 prompted us to investigate whether AtHMGB15 regulates the transcription of MYC2. For this, ~2-kb promoter/upstream region of MYC2 was cloned in pCambia1304 replacing 35S promoter to generate pMYC2::GUS reporter construct. The constructs were infiltrated into Nicotiana benthamiana plants to examine the promoter activity (pMYC2) by measuring GUS activity in the absence

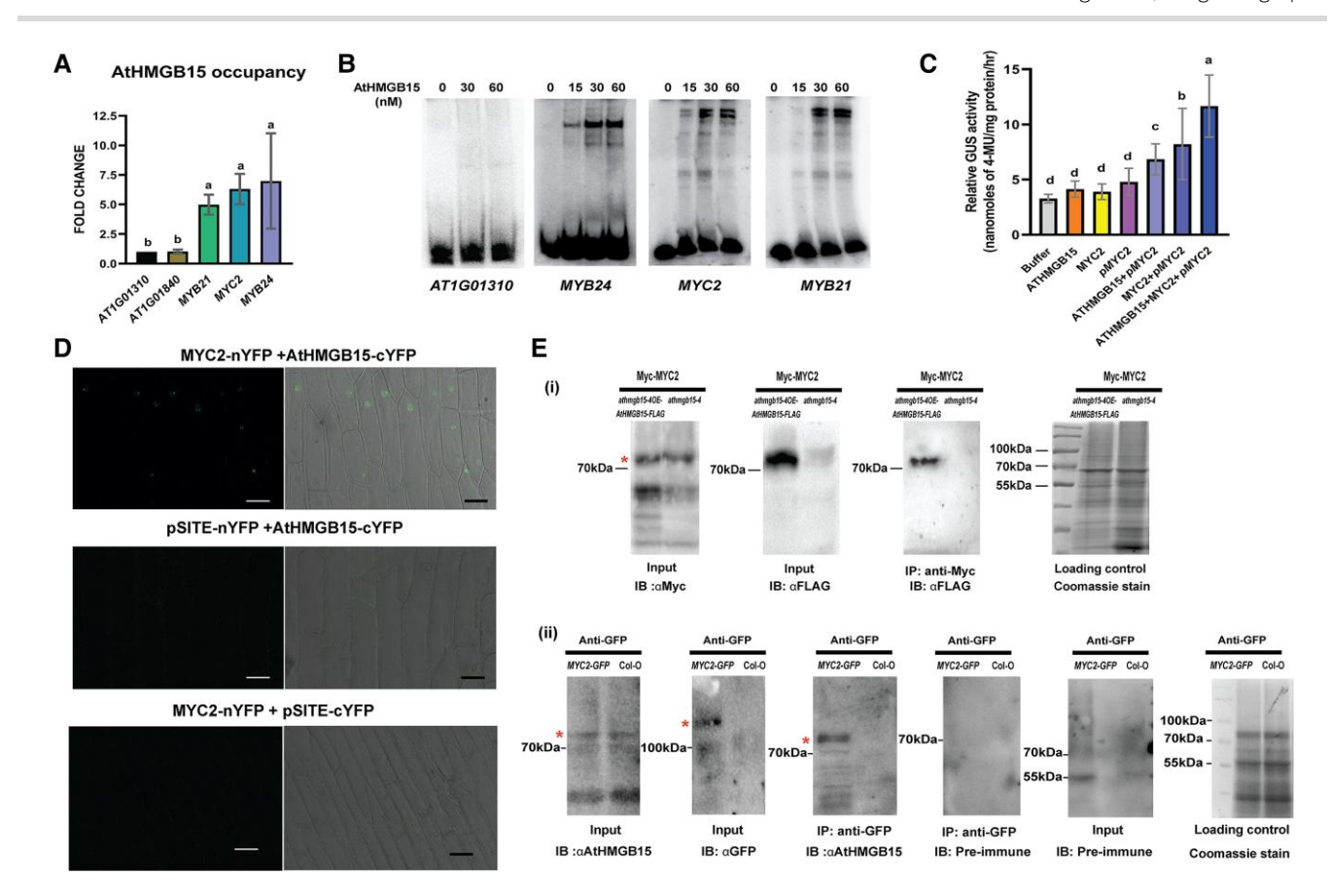


Figure 6. AtHMGB15 acts as a transcriptional activator for the expression of MYC2. A) ChIP analysis shows AtHMGB15 occupancy at the promoter/ upstream of MYC2, MYB21, and MYB24. The data were normalized with no binding regions corresponding to At1g01310. Error bars represent mean ± SD (n=5). Letters indicate significant differences according to a one-way ANOVA with Tukey's post hoc test (P < 0.05). **B)** EMSA was performed using ³²P-labeled DNA fragments of At1g01310, MYB24, MYC2, and MYB21 and increasing concentration of recombinant AtHMGB15 (15 to 60 nm). **C)** 2 kb promoter region of MYC2 (pMYC2) was cloned with GUS reporter, and Agrobacterium-mediated infiltration was done with 35S::AtHMGB15, and 35S:: MYC2 in Nicotiana tabacum. GUS reporter gene assay was done after 48 h using MUG. Error bars represent mean ± SD (n = 15). Letters indicate significant differences between the represented datasets according to a one-way ANOVA with Tukey's post hoc test (P < 0.05). D) BiFC confirming the interaction between AtHMGB15 and MYC2 in onion epidermal cells using split Yellow Fluorescent Protein (YFP). AtHMGB15-cYFP+pSITE-nYFP-C1 and MYC2-nYFP+ pSITE-cYFP-N1 were used as control. Scale bar = 50 µm. E) (i) Co-immunoprecipitation (co-IP) assay confirming interaction of AtHMGB15 and MYC2. Total protein from leaves of athmgb15-40EA4-FLAG and athmgb15-4 transiently expressing Myc-MYC2 was extracted and subjected to immunoprecipitation with anti-Myc antibody, followed by immunoblot analysis with anti-FLAG (IB: αFLAG) antibodies to detect AtHMGB15-Flag and anti-Myc (IB: αMyc) $antibodies \ to \ detect\ Myc-MYC2.\ Extract\ of\ athmgb 15-4\ leaves\ only\ expressing\ Myc-MYC2\ was\ used\ as\ a\ control.\ Coomassie\ blue\ staining\ for\ Rubisco\ was$ used to ascertain even protein loading in each lane. (ii) Co-immunoprecipitation (co-IP) assay confirming interaction of AtHMGB15 and MYC2 in vivo. Total protein from seedlings of MYC2-GFP was extracted and immunoprecipitated with anti-GFP magnetic beads, followed by immunoblot analysis with anti-AtHMGB15 (IB: αAtHMGB15) and anti-GFP (IB: αGFP) antibodies and preimmune sera. Extract of wild-type seedlings was used as control. Coomassie blue staining for Rubisco was used to ensure even protein loading in each lane (* indicates the band of interest).

and presence of AtHMGB15. AtHMGB15 is not a TF but can modulate transcription when associated with a TF. Moreover, previous studies have identified the MYC2-binding site at the promoter of MYC2 gene (Zander et al. 2020). Thus, we presumed that AtHMGB15 is a coactivator coupled with the TF MYC2 to regulate transcription. To test this hypothesis, we measured the promoter activity of MYC2 in the presence of both the proteins, namely MYC2 and AtHMGB15. As shown in Fig. 6C, the promoter activity was higher in the presence of AtHMGB15 (pMYC2 + AtHMGB15) compared to the control (pMYC2). Similarly, we have observed an increase in pMYC2 activity in the presence of MYC2 (pMYC2+MYC2) compared to the control, supporting the earlier finding that MYC2 regulates its transcription. Interestingly, the pMYC2 activity increased significantly in the presence of both MYC2 and AtHMGB15 protein (pMYC2+MYC2 +AtHMGB15) compared to when measured with individual proteins. The increase of pMYC2 activity in the presence of both the proteins, namely AtHMGB15 and MYC2, indicates that AtHMGB15 along with MYC2 TF positively activates the transcription of MYC2.

AtHMGB15 interacts with MYC2 protein to form the activator complex

To further explore the physical interaction between AtHMGB15 and MYC2, a BiFC assay was conducted using co-infiltration of Agrobacterium carrying MYC2-nYFP and AtHMGB15-cYFP constructs into the onion epidermis. The results revealed reconstitution of the Yellow Fluorescent Protein (YFP) signal in the nucleus, particularly in the nucleolus, indicating the physical interaction between AtHMGB15 and MYC2 in planta (Fig. 6D). No YFP fluorescence was observed in the control combinations.

To further validate this physical interaction, we performed a transient co-immunoprecipitation using Myc-tagged MYC2 and C-terminal Flag-tagged AtHMGB15. We raised transgenic Arabidopsis overexpressing AtHMGB15-flag in athmqb15-4 background. These transgenic plants were used for Agrobacterium infiltration using the Myc-MYC2 construct. As a control, Myc-MYC2 constructs were infiltrated in *athmgb15-4* plants. The complex was immunoprecipitated using an anti-Myc antibody and detected with an anti-flag antibody. The Western blot analysis indicates that Myc-tagged MYC2 immunoprecipitated AtHMGB15-Flag (Fig. 6E). Alternatively, we infiltrated Myc-MYC2 into the leaves of AtHMGB15-Flag and performed immunoprecipitation assay with anti-FLAG affinity beads to pull down the protein complex. To detect its interactors, we used an anti-Myc antibody. We infiltrated pGWB618 (empty vector) in the leaves of AtHMGB15-Flag as control (Supplementary Fig. S13).

To confirm the interaction between MYC2 and AtHMGB15 in planta, co-immunoprecipitation assay was performed using transgenic plants expressing MYC2-GFP. The complex was pulled down with anti-GFP magnetic beads, and AtHMGB15 was detected in the precipitated complex using AtHMGB15 antibody (Mallik et al. 2020). The results confirmed positive interaction between MYC2 and AtHMGB15, in vivo. Arabidopsis Col-0 was used as control in this assay (Fig. 6E, ii). These experimental findings indicate the physical interaction of AtHMGB15 with MYC2 protein to form an activator complex to promote the transcription of the MYC2 TF.

AtHMGB15 promotes the transcription of MYBs

MYC2 has been shown to interact with R2R3-MYB TFs, MYB21, and MYB24 to regulate anther and pollen development in a JA-dependent manner (Goossens et al. 2017). Our RT-qPCR analysis confirmed the expression of MYB21 and MYB24 is downregulated in athmqb15 mutants. Additionally, the in silico analysis revealed the presence of MYC2-binding sites at the promoter region of MYB24. Since AtHMGB15 and MYC2 form a transcription activator complex, we next investigated whether this complex regulates the transcription of R2R3-MYB TFs. To explore this possibility, we examined the expression of MYB21 and MYB24 in the flowers of 2 previously characterized myc2 knockout lines, namely myc2-2 and jin1-2 (Boter et al. 2004; Lorenzo et al. 2004). Our results demonstrated a significant downregulation of MYB21 and MYB24 expression in these myc2 mutant lines (Fig. 7A, i). Furthermore, the expression of JA biosynthesis gene OPR3, which was previously shown to be MYC2-dependent (Mandaokar et al. 2006), was downregulated in these mutants. We analyzed the JA content of myc2 mutants and observed a significant reduction in jasmonate levels (Fig. 7A, ii).

Subsequently, we investigated the promoter activity of MYB21 and MYB24 in the presence of AtHMGB15 and MYC2 TFs. The promoter activity of pMYB24 was significantly upregulated in the

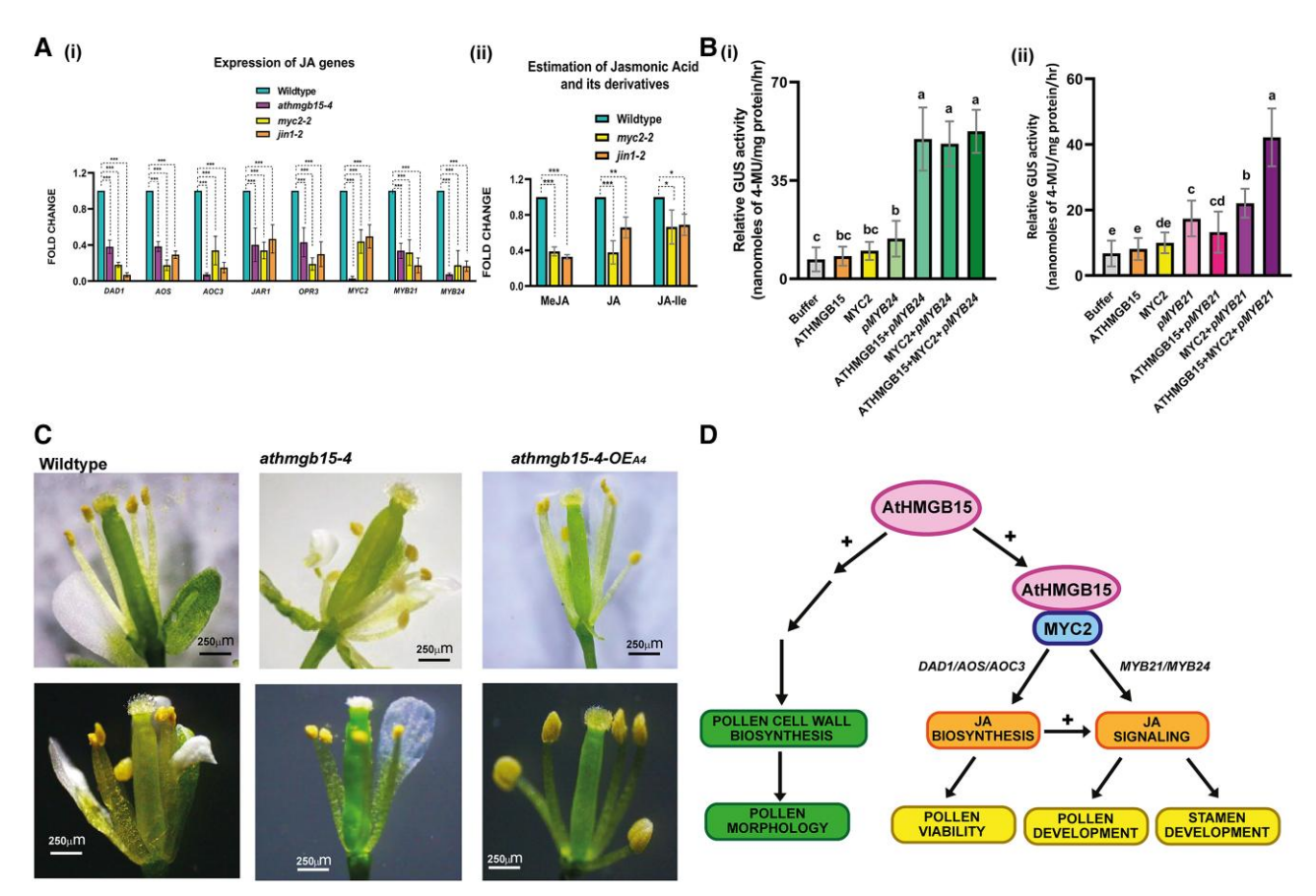


Figure 7. AtHMGB15 promotes transcription of MYBs. **A)** (i) Expression of JA genes in MYC2 knockout mutants myc2-2 and jin1-2, and athmgb15-4 using RT-qPCR. The fold change was represented with respect to wild type. Error bars represent mean \pm SD (n=4). The significance for each gene was analyzed by one-way ANOVA with Tukey's post hoc test. Asterisks represent significant differences as indicated (***P < 0.001). (ii) Comparative JA and its derivatives content in flowers of wild type and MYC2 knockout mutants myc2-2 and jin1-2. Error bars represent mean \pm SD (n=3). The fold change for each gene was represented with respect to wild type. The significance for each gene was analyzed by one-way ANOVA with Tukey's post hoc test. Asterisks represent significant differences as indicated (*P < 0.05, **P < 0.01, and ***P < 0.001). **B)** (i and ii) 2-kb promoter regions of MYB21 (pMYB21) and MYB24 (pMYB24) were cloned with GUS reporter and Agrobacterium-mediated infiltration was done with 35S::AtHMGB15 and 35S::MYC2 in N. tabacum. GUS reporter gene assay was done after 48 h using MUG. Error bars represent mean \pm SD (n=15). Letters indicate significant differences between the represented datasets according to a one-way ANOVA with Tukey's post hoc test (P < 0.05). **C)** Comparison of stamen phenotype between wild type, athmgb15, and athmgb15-4-OEA4. Scale bar = 250 μ m. **D)** Proposed model elucidating the role of AtHMGB15 in activating the JA pathways by forming an activation complex with MYC2 to regulate stamen and pollen development.

presence of AtHMGB15 and MYC2 independently; however, in the presence of both proteins, there was no additional increase in promoter activity (Fig. 7B, i). For pMYB21, an increase in promoter activity was observed only in the presence of MYC2 protein (Fig. 7B, ii). There was no increase in promoter activity in the presence of AtHMGB15, although strong DNA-binding activity of AtHMGB15 was observed in the promoter region. Interestingly, the activity of pMYB21 increased significantly in the presence of both AtHMGB15 and MYC2, suggesting the formation of an activation complex between these 2 proteins to activate pMYB21.

Since R2R3 TFs were needed for the elongation of stamen during flower development, we further analyzed the flower morphology of athmgb15-4 and compared it to wild-type Arabidopsis flower. Our observation suggests that around 30% of athmgb15-4 flowers have shorter stamen filaments compared to wild type (Fig. 7C and Supplementary Fig. S14). This may be one of the reasons for poor fertilization and low seed yield in athmgb15 mutants. The complementation lines on the other hand showed a similar stamen phenotype as compared to wild type. Taken together, these findings suggest that AtHMGB15 regulates the transcription of R2R3-MYB TFs during flower development, thereby regulating the growth and development of stamens and pollen grains.

Discussion

AtHMGB15 insertion mutants have defective pollen morphology

Optimal pollen development and functional floral organs are crucial for efficient pollination and genetic diversity. These complex processes are precisely regulated by endogenous cues. In this study, we have investigated the role of the Arabidopsis ARID/ HMG group of transcriptional regulators, AtHMGB15, in pollen development. A previous study by Xia et al. (2014) using a Ds insertion line and our study using another T-DNA mutant allele of AtHMGB15 similarly showed defective pollen morphology and retarded pollen growth in mutant plants. These allelic mutants of athmqb15 have a significant reduction in the seed set. Given the impaired pollen morphology and viability resulting from the absence of functional AtHMGB15, we aimed to explore its involvement in pollen formation and maturation during Arabidopsis floral development. Pollen development initiates after meiosis of sporogenous cells corresponding to stage 10 of floral development and continues through stages 12 to 13 till the completion of the pollen cell wall (Sanders et al. 1999). Subsequently, filament elongation and anther dehiscence occur, enabling the release of viable pollen grains for germination (Goldberg et al. 1993; Scott et al. 2004). In this investigation, we initially examined the differential gene expression between wild type and athmgb15-4 mutant during the early stages of flower development, to identify AtHMGB15-regulated targets involved in the pollen development process. Our findings revealed the downregulation of genes responsible for pollen cell wall development in the athmqb15 mutant. The reduced expression of cell wall-related genes provides a plausible explanation for the defective morphology and distorted cell wall architecture observed in athmgb15 pollen grains.

AtHMGB15 regulates JA biosynthesis and signaling during pollen development

A significant finding in our study is the differential expression of genes responsible for α -linolenic acid metabolism and response to JA. As previously mentioned, α -linolenic acid serves as a precursor of plant phytohormone, JA. Our RT-qPCR data showed

significant downregulation of genes responsible for JA biosynthesis and response pathways in athmgb15 mutant flowers. This downregulation of JA biosynthesis genes leads to a substantial decrease in jasmonate levels in the athmgb15-4 mutant. Interestingly, the complementation of athmgb15-4 with full-length AtHMGB15 or exogenous application of jasmonate completely restores impaired JA signaling and pollen morphology of athmgb15-4, indicating that the defect lies in JA biosynthesis for this phenotype.

Previous studies have established that phytohormone JA is one of the major plant hormones required for different stages of flower development, including regulation of anther development, stamen elongation, dehiscence, flower opening, and pollen development (McConn and Browse 1996; Ishiguro et al. 2001; Mandaokar et al. 2006; Mandaokar and Browse 2009; Qi et al. 2015; Huang et al. 2017a, 2017b; Huang et al. 2020). Mutants, deficient in JA biosynthesis and signaling, were found to have reduced fertility or are male sterile (Feys et al. 1994; Xie et al. 1998; Ishiguro et al. 2001; Park et al. 2002; Cheng et al. 2009). Collectively, the low jasmonate content observed in *athmgb15-4* indicates that AtHMGB15 plays a crucial role in regulating the JA pathway for the development of viable pollen grains in *Arabidopsis*.

AtHMGB15-mediated regulation of JA signaling in athmgb15-4 plants

Attenuation of JA signaling at specific developmental stages is crucial for the proper growth and fitness of plants. This regulation involves intricate interactions between JA biosynthesis and signaling through positive and negative feedback loops (Wasternack and Hause 2013; Wasternack 2019; Zander et al. 2020). Positive feedback stimulates JA biosynthesis to activate JA signaling, while the negative loop controls the activity of TFs such as MYC2 by inducing the expression of negative repressors like JAZ or JAZ splice variants (Chini et al. 2007; Pauwels and Goossens 2011; Song et al. 2011, 2014; Chini et al. 2016). The basic helix-loop-helix TF MYC2 serves as the master regulator of JA signaling (Kazan and Manners 2013). The transcriptional activity of MYC2, responsible for JA-responsive gene expression, is tightly controlled by the SCFCOI1–JAZ complex. The physical interaction of JAZ1 with MYC2 attenuates the transcriptional activity of MYC2 (Xu et al. 2002; Chini et al. 2007; Acosta and Przybyl 2019), which is released by jasmonate-induced SCFCOI1-dependent proteasomal degradation of JAZ (Devoto et al. 2002; Thines et al. 2007; Kazan and Manners 2008). Intriguingly, MYC2 targets its own promoter, as well as the promoters of JAZ genes, during jasmonate response, indicating that MYC2 activates its own transcription and that of its negative regulator, JAZ (Dombrecht et al. 2007; Kazan and Manners 2013; Zander et al. 2020). This tight regulation leads to a negative feedback loop in JA signaling where JA-dependent destruction of MYC2 repressor followed by MYC2-dependent activation of JAZ repressor regulates the appropriate amplitude of JA signaling during various development processes (Chini et al. 2007).

Our findings demonstrate that AtHMGB15 directly binds to the promoter of MYC2 and interacts with MYC2 to form the activator complex that positively regulates the transcription of MYC2. Since the expression of MYC2 is compromised in *athmgb*15 mutant, expression of most of the *JAZ* genes (*JAZ*1, 5,6,7,8, and 10) was found to be downregulated in these plants (Supplementary Fig. S6). The downregulation of both MYC2 and *JAZ* suggests that fine-tuning of *JA* signaling is severely affected in *athmgb*15 mutants.

Regulation of JA biosynthesis

Studies have revealed that JA biosynthesis is regulated by a positive feedback loop through the SCFCOI1-JAZ regulatory module in the presence of jasmonate derivative (Devoto et al. 2002). The JA-dependent release of MYC2 binds to JA-responsive elements (G-box) present in the promoters of JA biosynthesis genes such as AOS, AOC3, OPR3, OPRL1, LOX3, and LOX4 to promote their transcription (Dombrecht et al. 2007; Pozo et al. 2008; Figueroa and Browse 2012; Kazan and Manners 2013). Additionally, a previous transcriptome study has shown the downregulation of JA biosynthesis genes in MYC2 mutant jin1-8 plants (Lorenzo et al. 2004), further supporting the role of MYC2 in the transcription of JA biosynthesis genes. In this study, we have observed a decrease in the expression of JA biosynthesis genes and low jasmonate content in MYC2 mutants myc2-2 and jin1-2, supporting that MYC2 regulates transcription of JA biosynthesis. Since AtHMGB15 positively regulates the MYC2 expression, we reasoned that the low expression of JA biosynthesis genes is due to the downregulation of MYC2 gene expression in athmqb15-4. Our data align with previous studies showing MYC2 controls JA biosynthesis genes through a positive feedback loop (Van Moerkercke et al. 2019).

DAD1 is a chloroplastic phospholipase A1 lipase that is involved in the initial step of JA biosynthesis for the formation of α -linolenic acid. The dad1 mutants were defective in anther dehiscence, pollen maturation, and flower bud development (Ishiguro et al. 2001; Peng et al. 2013). The expression of DAD1 is regulated by the homeotic protein AGAMOUS and the auxinresponsive factors ARF6 and ARF8 (Nagpal et al. 2005; Tabata et al. 2010). Our study shows a small change in the expression of ARF6 but no change in the expression of AGAMOUS or ARF8. However, the expression of COI1 was found to be severely repressed in athmgb15 mutants. A previous study has shown that wound-induced DAD1 expression is lower in JA biosynthesis mutants as and opr3, and completely abolished in coi1, suggesting that DAD1 expression is regulated by both coronatine insensitive (COI)-dependent and independent mechanisms (Hyun et al. 2008; Ruduś et al. 2014). Considering the repression of COI1 in athmgb15-4, we propose that the transcription of DAD1 is possibly COI1-dependent during the pollen development process.

JAR1, CYP94B3, and ST2A are JA catabolic enzymes required for the formation of JA derivatives JA-Ile, 12-hydroxy-JA-Ile, and 12-HSO4-JA, respectively (Ruan et al. 2019; Wasternack 2019). JA serves as the substrate for JA-Ile formation by JAR1. Similarly, JA-Ile is hydroxylated by CYP94B3, and STA2 uses 12-OH-JA for sulfated derivate (Wasternack and Hause 2013). In each case, it appears that the biosynthesis of JA catabolites depends upon the availability of its substrate and the level of these derivatives through positive feedback. Consistent with these findings, we propose that the low level of JA derivatives is due to the reduced JA content in athmgb15-4 plants. Consequently, the expression of genes responsible for the formation of JA derivatives was found repressed in athmqb15 mutants. Furthermore, Koo et al. have demonstrated that the expression of CYP94B3 is dependent on COI1, as the expression is completely diminished in the coi1 mutant. Therefore, reduced expression of CYP94B3 in athmqb15 mutant may be due to downregulation of COI1 gene expression and substrate availability (Koo et al. 2011). These collective observations establish the significance of AtHMGB15-mediated regulation in maintaining an appropriate jasmonate concentration during pollen development.

Repression of JA biosynthesis and signaling resulted in downregulation of JA-responsive TF MYB21 and MYB24 in athmgb15 mutant

The R2R3-MYB TFs, MYB21 and MYB24, are considered a critical regulator of JA signaling during stamen development (Huang et al. 2017b, 2020; Yang et al. 2020). In this study, we observed a downregulation of MYB21 and MYB24 expression in the athmgb15-4 mutant. Additionally, we found that AtHMGB15 binds to the promoter of MYB24 and MYB21 to activate their transcription. There may be 2 possible reasons for the repression of MYBs in the athmgb15-4 mutant. Firstly, repression of JA biosynthesis in athmqb15-4 causes downregulation of MYB21 and MYB24 expression, as previously shown in opr3 mutants (Song et al. 2011; Huang et al. 2020). Furthermore, the absence of functional AtHMGB15 may contribute to the downregulation of MYB21 and MYB24, as AtHMGB15 transcriptionally activates their expression. Genetic analysis has indicated that MYB21 and MYB24 are indispensable for stamen growth and development and myb21myb24 double mutant is completely male sterile with short filaments, delayed anther dehiscence, and nonviable pollen grains (Huang et al. 2020). Consistently, we have observed short filaments in around 30% of athmqb15-4 flowers. The short filaments may be one possible reason for having defective pollination as anthers fail to reach stigma leading to lower seed yields in athmqb15-4 mutant.

AtHMGB15 and MYC2 form the activator complex for regulating JA-responsive transcription

Our study reveals an intriguing finding regarding the interaction between the AtHMGB15 protein and the MYC2 TF. We provide evidence demonstrating that AtHMGB15, in conjunction with MYC2, activates the transcription of MYC2. Interestingly, previous research by Zander et al. has identified that MYC2 binds many targets that do not have canonical G-box DNA sequence motifs. This suggests that MYC2 may indirectly bind to numerous targets through its interaction with the partner protein AtHMGB15. Our study indicates that AtHMGB15 acts as a necessary partner for MYC2 activity. The interaction between MYC2 and AtHMGB15 suggests that these 2 proteins form a transcriptional activator complex for MYC2-dependent gene expression during JA signaling.

In this study, we provide mechanistic insights into the role of ARID/HMG group nuclear proteins in pollen development. We identify the involvement of AtHMGB15 in the formation of pollen cell wall by positively regulating the expression of cell wall genes. Moreover, we demonstrate the contribution of AtHMGB15 to JA signaling by forming an activator complex with the MYC2 TF, thereby activating JA-dependent gene expression during pollen development (Fig. 7D). Our findings shed light on the physiological roles of plant ARID/HMGs, particularly in gene regulation and chromatin remodeling. The present study shall be a step forward in this direction and establish a role of AtHMGB15 in transcription activation other than being an HMG-box group of nuclear architectural protein.

Materials and methods

Plant materials and growth conditions

Arabidopsis (A. thaliana) ecotype Columbia-O (Col) was used in this study. All the mutants and over-expression lines used in this study were in the Col background. The T-DNA insertion line of AtHMGB15 (GABI_351D08) was obtained from the Eurasian Arabidopsis Stock Centre (NASC), and the T-DNA insertion line of AtHMGB15 (SALK057612C) was obtained from the Arabidopsis Biological Resource Centre (ABRC). SALK_083483 (atmyc2-2) and SALK_061267 (atjin1-2) and 35S:MYC2-GFP lines were also procured for the study. The seeds were grown on Murashige and Skoog agar plates at 22 °C under 16-h:8-h light (~150 \pm 10 μ mol m $^{-2}$ s $^{-1}$) and dark cycles in the growth chamber. 20-day-old seedlings were transferred to soil pots in the greenhouse with 60% relative humidity. Freshly opened flowers were collected every day between 9:00 am and 11:00 am IST during the flowering stage (flowering stage 13) for downstream experiments. Pictures of wild-type, athmgb15-4 mutant, and athmgb15-4-OE_A4 (RE) plants at various growth stages (rosette, inflorescence bolting, fully mature plant with flower and silique stage) were taken using a digital camera. Individual organs such as the flowers and siliques were isolated and investigated for Leica stereo-zoom microscope S9i.

Generation of transgenic plants

The coding sequence of AtHMGB15 was cloned under 35S in pMDC84 using the gateway cloning system (Invitrogen). This construct was used to generate complementation lines constructed in the athmgb15-4 mutant background. Plant transformation was performed by Agrobacterium tumefaciens-mediated floral dip method, and transgenic plants (Zhang et al. 2006) were selected by hygromycin selection. The complementation lines were confirmed by PCR for insertion and RT-qPCR for expression. The plants were progressed to the T3 generation before they were used for analysis. The list of primers used for this study is presented in Supplementary Table S5.

RNA extraction, Illumina sequencing, and RT-qPCR

Total RNA was isolated from 200 mg of young flowers (flowering stages 12 to 13) of wild type and athmgb15-4 mutant using RNASure Mini Kit (Nucleopore-Genetix). RNA isolated from three such replicates was pooled and used for Illumina NextSeq 500 sequencing at Eurofins Genomics India Pvt. Ltd. using 2×75 bp chemistry generating 30 million paired end reads per sample. Processing of raw read, adaptor removal using Trimmomatic v0.35, and mapping of read to Arabidopsis genome (TAIR10) using TopHat v2.1.1 were performed. The differential gene expression analysis was carried out using Cufflink v1.3.0 where threshold fold change was set (FC) values >0 along with P value threshold of 0.05 and threshold fold change was set (FC) values >± 1 with P value cutoff filter of 0.05, which were considered as differentially expressed genes. The data are available in the NCBI Sequence Read Archive repository under the accession ID: PRJNA874885.

For the replicates, total RNA was isolated from 200 mg of young as mentioned above. RNA quality was measured using an Agilent Tape station (RIN>7) by Theomics International Pvt. Ltd. Total RNA integrity was checked by Agilent Bioanalyzer 2100, and samples with clean rRNA peaks only were used for further investigation. Libraries for RNA-seg were prepared according to the KAPA stranded RNA-seq kit with RiboErase (KAPA Biosystems, Wilmington, MA, USA) system. Final library quality and quantity were analyzed by Agilent Bioanalyzer 2100 and Life Technologies Qubit3.0 Fluorometer, respectively. The libraries were size selected for 140 bp \pm 10% fragments and sequenced on Illumina Novoseq 6000 to an average depth of 20 million reads using 2x 150 bp chemistry. Mapping of reads to Arabidopsis genome (TAIR10) was performed as mentioned earlier. The data are available in NCBI Sequence Read Archive repository under the accession ID: PRJNA974968.

RT-qPCR was performed, and relative fold change for the gene of interest was calculated with respect to housekeeping gene AtEF1 α transcript (At1g07920) level using the $2^{-\Delta \Delta CT}$ method. The primers used in the analysis are enlisted in Supplementary Table S5.

Bioinformatics analysis

The ShinyGO v0.77 program was used for the GO annotation analysis of DEGs in terms of Biological Process, Molecular Function, and Cellular Components ontologies. Significantly enriched GO and KEGG pathways of the differentially expressed genes were carried out using ShinyGO v0.77 program. Venny v2.0. was used to generate Venn diagrams for comparison between various datasets. The promoter sequence of MYC2, MYB24, and MYB21 was analyzed using PlantPAN 3.0.

Chromatin immunoprecipitation and ChIP-qPCR

Nuclei from the 700 mg of wild-type flower tissue were isolated using the Plant Nuclei isolation kit (Sigma #CELLYTPN1) using the manufacturer's protocol. The chromatin immunoprecipitation assay was performed as described previously by Mallik et al. (2020), and immunoprecipitated DNA was analyzed by ChIP-qPCR. The data were normalized with respect to input, and fold change was calculated against previously characterized 2 loci At1g01840 and At1g01310 using the $2^{-\Delta\Delta CT}$ method. Three independent biological replicate samples were used for qPCR experiments, where each sample was collected from $\geq\!80$ wild-type plants in the flowering stage. The primer list for the ChIP study is attached in Supplementary Table S5.

Electrophoretic mobility shift assay

EMSA was performed using the protocol described previously (Roy et al. 2016; Mallik et al. 2020). The DNA binding studies were done with PCR fragments obtained from the selected genes by ChIP-qPCR study. The DNA fragments (200 bp) from the promoter/upstream region of MYC2, MYB21, and MYB24 containing previously identified AtHMGB15-binding site "A(A/C)-ATA-(A/T) (A/T)" were PCR amplified, and fragments were end labeled with γ^{32} P ATP (3,500 Ci/mmol) using T4 polynucleotide kinase (Thermo Scientific, #EK0031) and purified. 5×10^4 cpm γ^{32} P-labeled DNA (~7 fmol) was mixed with increasing concentrations (15 to 60 nm) of the full-length AtHMGB15 in the presence of 1x EMSA buffer containing 10 mm Tris-HCl (pH 7.5), 5 mm NaCl, 0.1 mm EDTA, 0.5 mm MgCl₂, 0.1 mm DTT, 5% (v/v) glycerol, and 1.25 µg/ml poly dI-dC. The DNA-protein mixture was incubated for 1 h on ice and analyzed by 5% (v/v) native PAGE supplemented with 5% (v/v) glycerol in 0.5× TBE at 4 °C.

Site-directed mutagenesis

SDM was done according to the protocol described previously (Roy et al. 2016). Two synthetic partial overlapping primers containing the desired mutation were designed (Supplementary Table S5 and Fig. S12) and extended using Pfu turbo, thereby generating mutated plasmids. The PCR products were treated with 1 μ l of DpnI endonuclease (10 U/ μ l, Agilent) at 37 °C for 1 to 2 h and transformed into competent DH5 α cells. The mutation was verified by sequencing. The mutated fragments of MYC2, MYB21, and MYB24 were then amplified from the clones, and EMSA was performed as described earlier.

Scanning electron microscopy

Pollen grains were isolated from anthers of dried flowers of wild type, athmgb15-4 mutant, and athmgb15-4-OE $_{\rm A4}$ (RE) and refined by passing them through a series of fine mesh with decreasing porosity. The pollen grains were brushed onto the brass stub with a carbon tape and subjected to gold coating in Edward gold sputter coater. The coated samples were visualized in SEM (FEI 200) under an accelerating voltage of 5, 10, and 20 kV.

Pollen germination and viability assay

Pollen germination assay was done as described previously (Li 2011). Pollen was isolated from mature wild-type, athmgb15-4, and athmqb15-4-OE_{A4} (RE) flowers by drying them and then suspending them in a pollen germination medium containing 20% (w/v) sucrose, 100 mm boric acid, 1 m CaCl₂, 200 mm Tris-MES, 1 м MgSO₄, 30% (w/v) PEG 4000, and 500 mм KCl of pH 5.6 to 6. Pollen germination was observed after 2, 4, 6, and 24 h and visualized by a microscope (Nikon ECLIPSE Ni). Double staining with FDA and PI was performed using the method described earlier (Chang et al. 2014). A drop containing the stained pollen grains was viewed under a fluorescence microscope (Nikon ECLIPSE Ni). FDA-stained cells are blue denoting live pollen grains, the PI-stained cells are red denoting dead pollen grains, and the purple-colored pollen grains are sterile in nature. The excitation wavelength used for the fluorescence microscope to observe PI was 535 nm, with an exposure duration of 100 ms and the gain at 1x. The excitation wavelength for FDA was 488 nm, with an exposure duration of 200 ms and the gain at 1.5x.

Hormone estimation

JA content was estimated using electron spray ionization coupled with mass spectroscopy (ESI-MS) as described previously (Liu et al. 2010). 500 mg of fresh flower tissue from wild-type, athmgb15-4, and athmgb15-4-OEA4 (RE) plants along with myc2-2 and jin1-2 was homogenized in liquid N2 and extracted overnight with methanol (HPLC grade) at 4 °C. The homogenates were centrifuged, diluted with water (HPLC grade), and subjected to the Sep-Pak C18 cartridge (Pierce #89870). SPE cartridge was washed with 20% (v/v) and 30% (v/v) methanol and finally eluted with 100% (v/v) methanol. The eluant was 10 times diluted with methanol and analyzed by ESI-MS. Analytical standards of MeJA (Sigma #392707), JA (Sigma #J2500), and JA-Ile (Cayman Chemical #10740) were used. The relative abundance of all three derivatives in the wild-type, athmgb15-4, and athmgb15-4-OEA4 (RE) samples was obtained and expressed as fold change with respect to wild type.

Hormone treatment

For MeJA treatment, the wild-type and athmgb15-4 plants were grown in soil. At the onset of flowering, 0.5 and 2 mm MeJA (Sigma #392707) was sprayed directly onto the flower buds twice a day for 2 consecutive days. The treated flowers were harvested and used for pollen germination assay (Park et al. 2002). RNA isolation, cDNA synthesis, and RT-qPCR were performed with flowers treated with exogenous MeJA (0.5 mm) and harvested at 4 h post-treatment.

GUS assay

GUS assay was performed as described previously (Bedi and Nag Chaudhuri 2018). 2-kb promoter regions of MYC2, MYB21, and MYB24 were cloned into pKGWFS7 vector, containing GUS as the reporter gene, by the Gateway cloning (Invitrogen). Similarly, the

full-length coding sequence of AtHMGB15 and MYC2 was cloned in pMDC84 and pCambia1304, respectively. Overnight culture of Agrobacterium tumefaciens strain EHA105 containing pMYC2, pMYB21, and pMYB24 was mixed individually with different combinations of Agrobacterium strain containing 35S::AtHMGB15 and 35S::MYC2 at OD $_{600}$ 0.8 and infiltrated into the leaves of 6-wk-old N. benthamiana plants. The leaf samples were incubated for 48 h and homogenized, and GUS activity was measured using 1 mm 4-Methylumbelliferyl- β -D-glucuronide (MUG) at fluorescence at 455 nm (excitation at 365 nm) in a fluorimeter (Thermo Scientific Varioskan Flash). The total protein concentration of extracted leaf samples was measured by the Bradford method at 595 nm. GUS activity was represented as nanomoles of 4-MU produced per mg of protein, and the total data were obtained from 15 sets of biological repeats.

BiFC

For BiFC assay, the full-length coding sequences of AtHMGB15 and MYC2 were cloned through Gateway cloning system (Invitrogen) into the binary vector pSITE-cEYFP-N1 (CD3-1651) and pSITE-nEYFP-C1 (CD3-1648), respectively. Agrobacterium strain (EHA105) transformed with the cloned vectors along with the empty vectors as control was infiltrated into the onion epidermis as done previously (Roy et al. 2019). The inner epidermal peels were isolated and subjected to wash with 1x PBS for 16 h, mounted on a slide, and observed for interaction under the confocal microscope (Stellaris 5, Leica). The laser used for the fluorescence microscopy was 488 nm with a collection bandwidth of 513 to 560 nm. The gain was set at 86 with 2% intensity.

Co-immunoprecipitation and immunoblotting

Co-immunoprecipitation was followed as previously described with experimental modifications (Nie et al. 2021). Full-length CoDing Sequence of MYC2 was cloned into pGWB618 having Myc tag. The positive clone was transformed into the A. tumefaciens strain EHA105. The bacterial cells were pelleted and resuspended to at final OD_{600} at 0.3, in resuspension buffer (10 mm MgCl₂, 10 mm MES, 200 μM acetosyringone, pH 5.7) in the dark for 3 h at room temperate prior to infiltration. The resuspended cells were infiltrated in the leaves of athmgb15-4 (control) and athmqb15-4-OEA4-FLAG. Infected leaves were harvested at 48 h after infiltration and frozen in liquid nitrogen. Total proteins were extracted from infected leaves using extraction buffer (3 ml/g of leaf) containing 50 mm Tris-HCl (pH 7.4), 1 mm EDTA, 150 mm NaCl, 5% (v/v) glycerol, 0.5% (v/v) Triton X-100, 1 mm PMSF, and 1x Protease Inhibitor Cocktail Tablets (Roche). After centrifugation at 20,000 g for 30 min, the extracts were precleared with protein A^{plus} agarose beads (BB#-PA001PD) to reduce nonspecific interactions. The input sample was collected from pre-cleaned extract. The complex was immunoprecipitated using Anti-Myc antibody (abcam #9E10) overnight at 4 °C and pulled down using Magna ChIP Protein A+G Magnetic beads (Millipore #16-663). The co-immunoprecipitated protein samples were extracted from the beads using 2x SDS sample buffer, boiled, and separated in a 10% (v/v) SDS-PAGE followed by transfer to a PVDF membrane. The co-immunoprecipitation was detected using anti-FLAG M2 antibody (Sigma-Aldrich #F1804) and anti-Myc antibody (abcam #9E10). The blot was detected with Enhanced Chemiluminescence substrate (Bio-Rad).

Alternatively, in the leaves of athmgb15-4- OE_{A4^-FLAG} , the Myc-MYC2 and PGWB618 (control) were infiltrated. The procedure was followed as above; instead, the complex was pulled down

against Anti-FLAG Affinity beads (abcam #270704) and detected against anti-Myc antibody and anti-FLAG M2 antibody (control).

Co-immunoprecipitation was carried out with Arabidopsis over-expressing MYC2-GFP lines and Col-0 plants (control). The total protein was extracted as described above. The extract was pulled down using anti-GFP nanobody Magnetic beads (Antibodies.com #A310039), and the AtHMGB15 was detected using custom-made affinity-purified anti-AtHMGB15 (Thermo Scientific) antibody. MYC2-GFP was detected using anti-GFP (Plant specific) antibody (Antibodies.com #A50024). Western blot using preimmune Sera was used as experimental controls. The co-immunoprecipitation experiments were repeated at least 3 times.

Quantification and statistical analysis

Statistical analysis was performed using GraphPad Prism8 (GraphPad Software) and IBM SPSS Statistics (v29.0.2.0). The values shown in the figures are either means of 3 or more experimental replicates or means of 3 or more independent experiments as specified in each figure caption. Student's t-test and one-way and two-way analysis of variance (ANOVAs) were performed in GraphPad Prism and IBM SPSS Statistics. Details of statistical tests are indicated in each figure legend.

Accession numbers

Sequence data from this article can be found in The Arabidopsis Information Resource (TAIR) under the accession numbers AtHMGB15 (AT1G04880), MYC2 (AT1G32640), MYB24 (AT5G40350), MYB21 (AT3G27810), and EF1 (AT1G07920). The accession numbers of genes are mentioned in Supplementary Table S5.

Acknowledgments

The authors sincerely thank Dr Sreeramaiah Gangappa (IISER, Kolkata) for the seeds of SALK_083483 (atmyc2-2), SALK_061267 (atjin1-2), 35S:MYC2-GFP line, and pGWB618 vector and Dr Anindita Seal (Department of Biotechnology, University of Calcutta) for BiFC vectors.

Author contributions

S.C. conceptualized the idea, supervised the project, and was involved in funding acquisition. S.S. performed all the experiments related to raising transgenic and morphological studies, RT-qPCR, pollen germination assay, ChIP, EMSA, SDM, BiFC, Co-immunoprecipitation assay and immunoblotting, SEM, hormone estimation, preparation of samples for RNA-seq, analysis of RNA-seq data (accession ID: PRJNA874885 and PRJNA974968), promoter assay, hormone treatment, and screening of SALK_057612C_15 and SALK_057612C_9 mutants. R.B. performed the experiments on pollen viability, pollen germination, promoter assay, and flower morphology and assisted S.S. in EMSA, SEM, ChIP, and analyzing RNA-seq (accession ID: PRJNA874885). A.R. screened athmgb15-4 mutant line, standardization of pollen SEM, and prepared samples for RNA-seq. A.N. assisted S.S. in screening of SALK_057612C_15 and SALK_057612C_9 mutants and assisted R.B. in flower morphology. V.R. assisted S.S. in analyzing RNA-seq data (accession ID: PRJNA974968). S.B. assisted S.S. in EMSA. S.S. contributed to the critical revision of the manuscript. S.C. wrote the original draft, and all the authors read, edited, and reviewed it.

Supplementary data

The following materials are available in the online version of this article.

Supplementary Table S1. Summary of 111 downregulated genes common to athmgb15-1 and athmgb15-4 mutants.

Supplementary Table S2. Summary of 60 upregulated genes common to *athmqb*15-1 and *athmqb*15-4 mutants.

Supplementary Table S3. Summary of downregulated genes common to *athmgb*15-4 flowers (RNA-seq) vs wild-type seedlings (ChIP-on-chip).

Supplementary Table S4. Summary of upregulated genes common to *athmgb*15-4 flowers (RNA-seq) vs wild-type seedlings (ChIP-on-chip).

Supplementary Table S5. List of primers.

Supplementary Figure S1. Confirmation of *athmgb*15-4 homozygous line was done by Southern blot.

Supplementary Figure S2. *athmgb*15-4 mutant shows retarded primary root growth.

Supplementary Figure S3. *athmgb*15-4 shows delayed flowering compared to wild type.

Supplementary Figure S4. Gene ontology analysis of differentially enriched genes.

Supplementary Figure S5. KEGG ontology analysis of differentially enriched genes.

Supplementary Figure S6. Analysis of transcriptome data and validation of selected genes.

Supplementary Figure S7. Comparative analysis of DEGs (flower tissue) with Xia et al. (2014) (pollen tissue) and Mallik et al. (2020) (seedling tissue) datasets.

Supplementary Figure S8. Representative pollen grains isolated from wild type and the *athmqb*15-4 mutant.

Supplementary Figure S9. Isolation and characterization of the homozygous line of AtHMGB15 from SALK_057612C.

Supplementary Figure S10. Relative expression of JA biosynthesis and JA signaling genes post-MeJA treatment of the athmgb15-4 mutant.

Supplementary Figure S11. Western blot using total protein from flower tissue of wild type and *athmqb*15-4.

Supplementary Figure S12. DNA binding analysis of MYC2, MYB24, and MYB21 using recombinant AtHMGB15 protein.

Supplementary Figure S13. Co-immunoprecipitation (co-IP) assay confirming interaction of AtHMGB15 and MYC2.

Supplementary Figure S14. Representative flowers isolated from wild type, athmgb15-4, and athmgb15-4-OE $_{\rm A4}$ lines (RE).

Funding

This work was supported by the Science and Engineering Research Board (SERB), Department of Science and Technology, Government of India (SERB/2017/000768 and CRG/2022/001524). S.S. sincerely acknowledges the University Grants Commission (UGC), Government of India, for her fellowship [UGC-Ref. No.: 749/(CSIR-UGC NET DEC. 2016)]. The authors sincerely acknowledge the Bose Institute for institutional support.

Conflict of interest statement. The authors declared no conflict of interest.

Data availability

The datasets generated during this current study are available in the NCBI Sequence Read Archive repository (https://www.ncbi.nlm.nih.gov/sra/PRJNA874885) under the accession ID:

PRJNA874885. The replicates are available in the NCBI Sequence Read Archive repository (https://www.ncbi.nlm.nih.gov/sra/PRJNA974968) under the accession ID: PRJNA974968.

References

- Acosta IF, Przybyl M. Jasmonate signaling during Arabidopsis stamen maturation. Plant Cell Physiol. 2019:60(12):2648–2659. https://doi.org/10.1093/pcp/pcz201
- Bedi S, Nag Chaudhuri R. Transcription factor ABI 3 auto-activates its own expression during dehydration stress response. FEBS Lett. 2018:592(15):2594–2611. https://doi.org/10.1002/1873-3468.13194
- Boter M, Ruíz-Rivero O, Abdeen A, Prat S. Conserved MYC transcription factors play a key role in jasmonate signaling both in tomato and Arabidopsis. *Genes Dev.* 2004:18(13):1577–1591. https://doi.org/10.1101/gad.297704
- Caldelari D, Wang G, Farmer EE, Dong X. Arabidopsis lox3 lox4 double mutants are male sterile and defective in global proliferative arrest. Plant Mol Biol. 2011:75(1-2):25–33. https://doi.org/10.1007/s11103-010-9701-9
- Chang F, Zhang Z, Jin Y, Ma H. Cell biological analyses of anther morphogenesis and pollen viability in Arabidopsis and rice. In: Riechmann JL, Wellmer F, editors. Flower development: methods and protocols. New York (NY): Springer; 2014. p. 203–216
- Cheng H, Song S, Xiao L, Soo HM, Cheng Z, Xie D, Peng J. Gibberellin acts through jasmonate to control the expression of MYB21, MYB24, and MYB57 to promote stamen filament growth in Arabidopsis. PLoS Genet. 2009:5(3):e1000440. https://doi.org/10.1371/journal.pgen.1000440
- Chini A, Fonseca S, Fernandez G, Adie B, Chico J, Lorenzo O, García-Casado G, López-Vidriero I, Lozano F, Ponce M. The JAZ family of repressors is the missing link in jasmonate signalling. *Nature*. 2007:448(7154):666–671. https://doi.org/10.1038/nature06006
- Chini A, Gimenez-Ibanez S, Goossens A, Solano R. Redundancy and specificity in jasmonate signalling. *Curr Opin Plant Biol.* 2016:33: 147–156. https://doi.org/10.1016/j.pbi.2016.07.005
- Devoto A, Nieto-Rostro M, Xie D, Ellis C, Harmston R, Patrick E, Davis J, Sherratt L, Coleman M, Turner JG. COI1 links jasmonate signalling and fertility to the SCF ubiquitin–ligase complex in Arabidopsis. Plant J. 2002:32(4):457–466. https://doi.org/10.1046/j. 1365-313X.2002.01432.x
- Dombrecht B, Xue GP, Sprague SJ, Kirkegaard JA, Ross JJ, Reid JB, Fitt GP, Sewelam N, Schenk PM, Manners JM, et al. MYC2 differentially modulates diverse jasmonate-dependent functions in Arabidopsis. Plant Cell. 2007:19(7):2225–2245. https://doi.org/10.1105/tpc.106.048017
- Feys BJ, Benedetti CE, Penfold CN, Turner JG. Arabidopsis mutants selected for resistance to the phytotoxin coronatine are male sterile, insensitive to methyl jasmonate, and resistant to a bacterial pathogen. Plant Cell. 1994:6(5):751–759. https://doi.org/10.2307/3869877
- Figueroa P, Browse J. The Arabidopsis JAZ2 promoter contains a G-Box and thymidine-rich module that are necessary and sufficient for jasmonate-dependent activation by MYC transcription factors and repression by JAZ proteins. Plant Cell Physiol. 2012:53(2):330–343. https://doi.org/10.1093/pcp/pcr178
- Gao C, Qi S, Liu K, Li D, Jin C, Li Z, Huang G, Hai J, Zhang M, Chen M. MYC2, MYC3, and MYC4 function redundantly in seed storage protein accumulation in Arabidopsis. Plant Physiol Biochem. 2016:108:63–70. https://doi.org/10.1016/j.plaphy.2016.07.004
- Goldberg RB, Beals TP, Sanders PM. Anther development: basic principles and practical applications. *Plant Cell*. 1993:5(10):1217. https://doi.org/10.1105/tpc.5.10.1217

- Goossens J, Mertens J, Goossens A. Role and functioning of bHLH transcription factors in jasmonate signalling. *J Exp Bot.* 2017:68(6):1333–1347. https://doi.org/10.1093/jxb/erw440
- Hansen FT, Madsen CK, Nordland AM, Grasser M, Merkle T, Grasser KD. A novel family of plant DNA-binding proteins containing both HMG-box and AT-rich interaction domains. *Biochemistry*. 2008:47(50):13207–13214. https://doi.org/10.1021/bi801772k
- Huang H, Gao H, Liu B, Qi T, Tong J, Xiao L, Xie D, Song S. Arabidopsis MYB24 regulates jasmonate-mediated stamen development. Front Plant Sci. 2017a:8:1525. https://doi.org/10.3389/fpls.2017. 01525
- Huang H, Gong Y, Liu B, Wu D, Zhang M, Xie D, Song S. The DELLA proteins interact with MYB21 and MYB24 to regulate filament elongation in Arabidopsis. BMC Plant Biol. 2020:20(1):1–9. https://doi.org/10.1186/s12870-020-2274-0
- Huang H, Liu B, Liu L, Song S. Jasmonate action in plant growth and development. *J Exp Bot*. 2017b:68(6):1349–1359. https://doi.org/10.1093/jxb/erw495
- Hyun Y, Choi S, Hwang H-J, Yu J, Nam S-J, Ko J, Park J-Y, Seo YS, Kim EY, Ryu SB. Cooperation and functional diversification of two closely related galactolipase genes for jasmonate biosynthesis. Dev Cell. 2008:14(2):183–192. https://doi.org/10.1016/j.devcel. 2007.11.010
- Ishiguro S, Kawai-Oda A, Ueda J, Nishida I, Okada K. The DEFECTIVE IN ANTHER DEHISCENCE1 Gene Encodes a Novel Phospholipase A1 catalyzing the initial step of jasmonic acid biosynthesis, which synchronizes pollen maturation, anther dehiscence, and flower opening in Arabidopsis. Plant Cell. 2001:13(10):2191–2209. https://doi.org/10.1105/tpc.010192
- Jang G, Yoon Y, Choi YD. Crosstalk with jasmonic acid integrates multiple responses in plant development. Int J Mol Sci. 2020:21(1):305. https://doi.org/10.3390/ijms21010305
- Kazan K, Manners JM. Jasmonate signaling: toward an integrated view. Plant Physiol. 2008:146(4):1459–1468. https://doi.org/10.1104/pp.107.115717
- Kazan K, Manners JM. MYC2: the master in action. *Mol Plant*. 2013:6(3):686–703. https://doi.org/10.1093/mp/sss128
- Koo AJ, Cooke TF, Howe GA. Cytochrome P450 CYP94B3 mediates catabolism and inactivation of the plant hormone jasmonoyl-Lisoleucine. Proc Natl Acad Sci. 2011:108(22):9298–9303. https://doi. org/10.1073/pnas.1103542108
- Li X. Arabidopsis pollen tube germination. *Bio Protoc.* 2011:1(10):e73. https://doi.org/10.21769/BioProtoc.73
- Liu X, Yang Y, Lin W, Tong J, Huang Z, Xiao L. Determination of both jasmonic acid and methyl jasmonate in plant samples by liquid chromatography tandem mass spectrometry. Chin Sci Bull. 2010:55(21): 2231–2235. https://doi.org/10.1007/s11434-010-3194-4
- Lorenzo O, Chico JM, Saénchez-Serrano JJ, Solano R. JASMONATE-INSENSITIVE1 encodes a MYC transcription factor essential to discriminate between different jasmonate-regulated defense responses in Arabidopsis. Plant Cell. 2004:16(7): 1938–1950. https://doi.org/10.1105/tpc.022319
- Mallik R, Prasad P, Kundu A, Sachdev S, Biswas R, Dutta A, Roy A, Mukhopadhyay J, Bag SK, Chaudhuri S. Identification of genomewide targets and DNA recognition sequence of the Arabidopsis HMG-box protein AtHMGB15 during cold stress response. Biochim Biophys Acta (BBA)-Gene Regulatory Mech. 2020:1863(12): 194644. https://doi.org/10.1016/j.bbagrm.2020.194644
- Mandaokar A, Browse J. MYB108 acts together with MYB24 to regulate jasmonate-mediated stamen maturation in Arabidopsis. Plant Physiol. 2009:149(2):851–862. https://doi.org/10.1104/pp.108. 132597

- Mandaokar A, Thines B, Shin B, Markus Lange B, Choi G, Koo YJ, Yoo YJ, Choi YD, Choi G, Browse J. Transcriptional regulators of stamen development in Arabidopsis identified by transcriptional profiling. *Plant J.* 2006:46(6):984–1008. https://doi.org/10.1111/j. 1365-313X.2006.02756.x
- Marciniak K, Przedniczek K. Comprehensive insight into gibberellinand jasmonate-mediated stamen development. *Genes (Basel)*. 2019:10(10):811. https://doi.org/10.3390/genes10100811
- Mascarenhas JP. Gene activity during pollen development. Ann Rev Plant Biol. 1990:41(1):317–338. https://doi.org/10.1146/annurev.pp.41.060190.001533
- McConn M, Browse J. The critical requirement for linolenic acid is pollen development, not photosynthesis, in an Arabidopsis mutant. Plant Cell. 1996:8(3):403–416. https://doi.org/10.2307/3870321
- McCormick S. Control of male gametophyte development. Plant Cell. 2004:16(suppl_1):S142–S153. https://doi.org/10.1105/tpc.016659
- Nagpal P, Ellis CM, Weber H, Ploense SE, Barkawi LS, Guilfoyle TJ, Hagen G, Alonso JM, Cohen JD, Farmer EE. Auxin response factors ARF6 and ARF8 promote jasmonic acid production and flower maturation. *Development*. 2005:132(18):4107–4118. https://doi. org/10.1242/dev.01955
- Nie J, Zhou W, Liu J, Tan N, Zhou JM, Huang L. A receptor-like protein from Nicotiana benthamiana mediates VmE02 PAMP-triggered immunity. New Phytolog. 2021:229(4):2260–2272. https://doi.org/10.1111/nph.16995
- Park JH, Halitschke R, Kim HB, Baldwin IT, Feldmann KA, Feyereisen R. A knock-out mutation in allene oxide synthase results in male sterility and defective wound signal transduction in Arabidopsis due to a block in jasmonic acid biosynthesis. *Plant J.* 2002:31(1): 1–12. https://doi.org/10.1046/j.1365-313X.2002.01328.x
- Pauwels L, Goossens A. The JAZ proteins: a crucial interface in the jasmonate signaling cascade. Plant Cell. 2011:23(9):3089–3100. https://doi.org/10.1105/tpc.111.089300
- Peng YJ, Shih CF, Yang JY, Tan CM, Hsu WH, Huang YP, Liao PC, Yang CH. A RING-type E 3 ligase controls anther dehiscence by activating the jasmonate biosynthetic pathway gene DEFECTIVE IN ANTHER DEHISCENCE 1 in Arabidopsis. Plant J. 2013:74(2): 310–327. https://doi.org/10.1111/tpj.12122
- Pozo MJ, Van Der Ent S, Van Loon L, Pieterse CM. Transcription factor MYC2 is involved in priming for enhanced defense during rhizobacteria-induced systemic resistance in Arabidopsis thaliana. New Phytol. 2008:180(2):511–523. https://doi.org/10.1111/j. 1469-8137.2008.02578.x
- Qi T, Huang H, Song S, Xie D. Regulation of jasmonate-mediated stamen development and seed production by a bHLH-MYB complex in Arabidopsis. *Plant Cell*. 2015:27(6):1620–1633. https://doi.org/10.1105/tpc.15.00116
- Roy D, Chakrabarty J, Mallik R, Chaudhuri S. Rice Trithorax factor ULTRAPETALA 1 (OsULT1) specifically binds to "GAGAG" sequence motif present in Polycomb response elements. Biochim Biophys Acta Gene Regul Mech. 2019:1862(5):582–597.
- Roy A, Dutta A, Roy D, Ganguly P, Ghosh R, Kar RK, Bhunia A, Mukhopadhyay J, Chaudhuri S. Deciphering the role of the AT-rich interaction domain and the HMG-box domain of ARID-HMG proteins of Arabidopsis thaliana. Plant Mol Biol. 2016:92(3):371–388. https://doi.org/10.1007/s11103-016-0519-y
- Ruan J, Zhou Y, Zhou M, Yan J, Khurshid M, Weng W, Cheng J, Zhang K. Jasmonic acid signaling pathway in plants. Int J Mol Sci. 2019:20-(10):2479. https://doi.org/10.3390/ijms20102479
- Ruduś I, Terai H, Shimizu T, Kojima H, Hattori K, Nishimori Y, Tsukagoshi H, Kamiya Y, Seo M, Nakamura K. Wound-induced expression of DEFECTIVE IN ANTHER DEHISCENCE1 and DAD1-like lipase genes is mediated by both CORONATINE

- INSENSITIVE1-dependent and independent pathways in Arabidopsis thaliana. Plant Cell Rep. 2014:33(6):849–860. https://doi.org/10.1007/s00299-013-1561-8
- Sanders PM, Bui AQ, Weterings K, McIntire K, Hsu Y-C, Lee PY, Truong MT, Beals T, Goldberg R. Anther developmental defects in Arabidopsis thaliana male-sterile mutants. Sex Plant Reprod. 1999:11(6):297–322. https://doi.org/10.1007/s004970050158
- Schweizer F, Fernández-Calvo P, Zander M, Diez-Diaz M, Fonseca S, Glauser G, Lewsey MG, Ecker JR, Solano R, Reymond P. Arabidopsis basic helix-loop-helix transcription factors MYC2, MYC3, and MYC4 regulate glucosinolate biosynthesis, insect performance, and feeding behavior. Plant Cell. 2013:25(8):3117–3132. https://doi.org/10.1105/tpc.113.115139
- Scott RJ, Spielman M, Dickinson H. Stamen structure and function. Plant Cell. 2004:16(suppl_1):S46–S60. https://doi.org/10.1105/tpc. 017012
- Song S, Qi T, Huang H, Ren Q, Wu D, Chang C, Peng W, Liu Y, Peng J, Xie D. The jasmonate-ZIM domain proteins interact with the R2R3-MYB transcription factors MYB21 and MYB24 to affect jasmonate-regulated stamen development in Arabidopsis. Plant Cell. 2011;23(3):1000–1013. https://doi.org/10.1105/tpc.111.083089
- Song S, Qi T, Wasternack C, Xie D. Jasmonate signaling and crosstalk with gibberellin and ethylene. *Curr Opin Plant Biol.* 2014:21: 112–119. https://doi.org/10.1016/j.pbi.2014.07.005
- Stintzi A, Browse J. The Arabidopsis male-sterile mutant, opr3, lacks the 12-oxophytodienoic acid reductase required for jasmonate synthesis. Proc Natl Acad Sci. 2000:97(19):10625–10630. https://doi.org/10.1073/pnas.190264497
- Štros M, Launholt D, Grasser KD. The HMG-box: a versatile protein domain occurring in a wide variety of DNA-binding proteins. Cell Mol Life Sci. 2007:64(19-20):2590–2606. https://doi.org/10.1007/s00018-007-7162-3
- Tabata R, Ikezaki M, Fujibe T, Aida M, Tian C-e, Ueno Y, Yamamoto KT, Machida Y, Nakamura K, Ishiguro S. Arabidopsis auxin response factor6 and 8 regulate jasmonic acid biosynthesis and floral organ development via repression of class 1 KNOX genes. Plant Cell Physiol. 2010:51(1):164–175. https://doi.org/10.1093/pcp/pcp176
- Thines B, Katsir L, Melotto M, Niu Y, Mandaokar A, Liu G, Nomura K, He S, Howe G, Browse J. JAZ repressor proteins are targets of the SCF (COI1) complex during jasmonate signalling. *Nature*. 2007:448(7154):661–665. https://doi.org/10.1038/nature05960
- Van Moerkercke A, Duncan O, Zander M, Šimura J, Broda M, Vanden Bossche R, Lewsey MG, Lama S, Singh KB, Ljung K, et al. A MYC2/ MYC3/MYC4-dependent transcription factor network regulates water spray-responsive gene expression and jasmonate levels. Proc Natl Acad Sci. 2019:116(46):23345–23356. https://doi.org/10. 1073/pnas.1911758116
- Vera-Sirera F, Gomez MD, Perez-Amador MA. DELLA proteins, a group of GRAS transcription regulators that mediate gibberellin signaling. In: Gonzalez D, editor. Plant transcription factors. USA: Elsevier; 2016. p. 313–328. https://doi.org/10.1016/B978-0-12-800854-6.00020-8
- Wasternack C. Termination in jasmonate signaling by MYC2 and MTBs. Trends Plant Sci. 2019:24(8):667–669. https://doi.org/10.1016/j.tplants.2019.06.001
- Wasternack C, Hause B. Jasmonates: biosynthesis, perception, signal transduction and action in plant stress response, growth and development. An update to the 2007 review in Annals of Botany. Ann Bot. 2013:111(6):1021–1058. https://doi.org/10.1093/aob/mct067
- Wilson ZA, Zhang D-B. From Arabidopsis to rice: pathways in pollen development. *J Exp Bot.* 2009:60(5):1479–1492. https://doi.org/10.1093/jxb/erp095

- Xia C, Wang YJ, Liang Y, Niu QK, Tan XY, Chu LC, Chen LQ, Zhang XQ, Ye D. The ARID-HMG DNA-binding protein A t HMGB 15 is required for pollen tube growth in Arabidopsis thaliana. *Plant J.* 2014:79(5):741–756. https://doi.org/10.1111/tpj.12582
- Xie D-X, Feys BF, James S, Nieto-Rostro M, Turner JG. COI1: an Arabidopsis gene required for jasmonate-regulated defense and fertility. Science. 1998:280(5366):1091–1094. https://doi.org/10.1126/science.280.5366.1091
- Xu L, Liu F, Lechner E, Genschik P, Crosby WL, Ma H, Peng W, Huang D, Xie D. The SCFCOI1 ubiquitin-ligase complexes are required for jasmonate response in Arabidopsis. *Plant Cell*. 2002:14(8): 1919–1935. https://doi.org/10.1105/tpc.003368
- Yang Z, Li Y, Gao F, Jin W, Li S, Kimani S, Yang S, Bao T, Gao X, Wang L. MYB21 interacts with MYC2 to control the expression of terpene synthase genes in flowers of *Freesia hybrida* and *Arabidopsis thaliana*. *J Exp Bot*. 2020:71(14):4140–4158. https://doi.org/10.1093/jxb/eraa184
- Zander M, Lewsey MG, Clark NM, Yin L, Bartlett A, Saldierna Guzmán JP, Hann E, Langford AE, Jow B, Wise A. Integrated multi-omics

- framework of the plant response to jasmonic acid. Nat Plants. 2020:6(3):290-302. https://doi.org/10.1038/s41477-020-0605-7
- Zhai Q, Zhang X, Wu F, Feng H, Deng L, Xu L, Zhang M, Wang Q, Li C. Transcriptional mechanism of jasmonate receptor COI1-mediated delay of flowering time in Arabidopsis. Plant Cell. 2015:27(10): 2814–2828. https://doi.org/10.1105/tpc.15.00619
- Zhang X, He Y, Li L, Liu H, Hong G. Involvement of the R2R3-MYB transcription factor MYB21 and its homologs in regulating flavonol accumulation in Arabidopsis stamen. *J Exp Bot.* 2021:72(12): 4319–4332. https://doi.org/10.1093/jxb/erab156
- Zhang X, Henriques R, Lin S-S, Niu Q-W, Chua N-H. Agrobacterium-mediated transformation of Arabidopsis thaliana using the floral dip method. *Nat Protocols*. 2006:1(2):641–646. https://doi.org/10.1038/nprot.2006.97
- Zhang ZB, Zhu J, Gao JF, Wang C, Li H, Li H, Zhang HQ, Zhang S, Wang DM, Wang QX. Transcription factor AtMYB103 is required for anther development by regulating tapetum development, callose dissolution and exine formation in Arabidopsis. *Plant J.* 2007:52(3): 528–538. https://doi.org/10.1111/j.1365-313X.2007.03254.x



Biochimica et Biophysica Acta (BBA) - Gene Regulatory Mechanisms

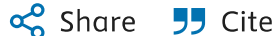
Volume 1863, Issue 12, December 2020, 194644

Research paper

Identification of genome-wide targets and DNA recognition sequence of the Arabidopsis HMG-box protein AtHMGB15 during cold stress response

Rwitie Mallik ^a, Priti Prasad ^{b c 1}, Anindya Kundu ^{a 1}, Sonal Sachdev ^a, Ruby Biswas ^a, Arkajyoti Dutta ^d , Adrita Roy ^a, Jayanta Mukhopadhyay ^d, Sumit K. Bag ^{b c}, Shubho Chaudhuri ^a 🖰 🖾

Show more V





https://doi.org/10.1016/j.bbagrm.2020.194644 7 Get rights and content 7

Highlights

- AtHMGB15 is a novel plant ARID-HMG group of protein
- DNase I footprinting assays has identified A(A/C)--ATA---(A/T)(A/T) as AtHMGB15 binding motif
- Expression of AtHMGB15 increases in response to cold stress response
- AtHMGB15 targets belonging to abiotic stress response, cold response and root development during cold stress

• Expression of several cold response genes decreases in *athmgb15* knockout plants

Abstract

AtHMGB15 belongs to a group of ARID-HMG proteins which are plant specific. The presence of two known DNA binding domains: AT rich interacting domain (ARID) and High Mobility Group (HMG)-box, in one polypeptide, makes this protein intriguing. Although proteins containing individual HMG and ARID domains have been characterized, not much is known about the role of ARID-HMG proteins. Promoter analysis of AtHMGB15 showed the presence of various stress responsive cis regulatory elements along with MADS-box containing transcription factors. Our result shows that the expression of AtHMGB15 increased significantly upon application of cold stress. Using ChIP-chip approach, we have identified 6128 and 4689 significantly enriched loci having AtHMGB15 occupancy under control and cold stressed condition respectively. GO analysis shows genes belonging to abiotic stress response, cold response and root development were AtHMGB15 targets during cold stress. DNA binding and footprinting assays further identified A(A/C)--ATA---(A/T)(A/T) as AtHMGB15 binding motif. The enriched probe distribution in both control and cold condition shows a bias of AtHMGB15 binding towards the transcribed (gene body) region. Further, the expression of cold stress responsive genes decreased in athmgb15 knockout plants compared to wild-type. Taken together, binding enrichment of AtHMGB15 to the promoter and upstream to stress loci suggest an unexplored role of the protein in stress induced transcription regulation.

Introduction

Plants are subjected to various kinds of adverse environmental stresses throughout their lifespan. Being sessile organisms, plants can cope with such conditions by changing the cellular processes within themselves through reprogramming of the transcriptome. These stress dependent changes in plants are needed to act against adverse environmental condition for maintaining the overall stability during stress situations. However, the compact chromatin structure in eukaryotic cell imposes various constraints to many DNA dependent processes such as transcription, replication, repair, recombination and transposition. This problem is overcome by the unique aspect of plasticity present in the eukaryotic chromatin. Even though the DNA is very tightly packed, it is rendered accessible for carrying out various DNA dependent processes. This dynamicity of the genome

architecture is extremely fascinating and has become one of the most studied aspects in chromatin biology in the last few decades.

Preliminary DNA packaging begins with the coiling of DNA with the aid of the histone octamer where it forms the bead on the string arrangement [1]. Following this, the DNA undergoes rounds of supercoiling to finally attain the condensed form of the chromatin [2,3]. DNA binding proteins that aid in stabilizing the DNA structure during this packaging form the 'Architectural group of proteins' that promotes wrapping, bending and bridging [4]. Similarly, to make the packaged DNA accessible for different nuclear factors, alteration of compact chromatin structure to a more open configuration is required. This plasticity is achieved through chromatin remodelling mainly through three methods: by i) modulation of interactions between an architectural protein and DNA [5], ii) modulating the higherorder folding of the genome by antagonizing or cooperative action of architectural proteins [[6], [7], [8]] and iii) energy dependent displacement of DNA wrappers [9,10]. The High Mobility Group of proteins are the group of architectural proteins involved in modulating chromatin structure and organizing the efficient participation of other proteins in various nuclear activities such as transcription, replication and DNA repair [[11], [12], [13], [14]]. Based on the type of DNA binding domain, HMG proteins are grouped into three distinct classes HMGA, HMGB and HMGN [12]. In plants, with the exception of HMGN, proteins belonging to both HMGA and HMGB families have been characterized [15]. Other than classical HMGB type proteins, plants have three more types of HMG-box containing proteins a) structure-specific recognition protein1 (SSRP1), b) proteins containing three copies of HMG-box (3xHMG) and c) proteins with both AT-rich interaction domain and HMG-box domain (ARID-HMG) [16]. Among the different types of the HMG proteins, the 3xHMG box proteins and the ARID HMG proteins are found exclusively in plants. Interestingly, the presence of two DNA binding domains: ARID and HMG in ARID-HMG group make it a unique member among the plant HMGB-box proteins.

The ARID domain was first identified in Bright, a mouse B-cell-specific transcription factor [17] and DRI gene of Drosophila [18]. Initially characterized as the AT-rich DNA binding domain; subsequent studies have revealed that many ARID domain containing proteins can bind DNA in a non-sequence specific manner [19]. The ARID domain containing proteins have been implicated in a wide variety of roles, including chromatin remodelling, transcription, and cell growth [20]. In *Arabidopsis*, 7 ARID domain containing proteins have been identified and have been grouped into the ARID transcription factor family (https://agris-knowledgebase.org/AtTFDB/ ¬). Among these 7 proteins, 4 members belong to the novel ARID-HMG group namely AtHMGB9, AtHMGB10, AtHMGB11 and AtHMGB15. Molecular characterization indicates that ARID-HMG protein can bind to various DNA

structures and facilitate DNA bending [21,22]. It is likely that the presence of two DNA binding motifs in ARID-HMG proteins can promote transcription either by modulating the chromatin accessibility or by acting as transcription activators.

Previous studies of plant ARID-HMG group were focused mainly on the biochemical properties of the protein. However, there was less information available to understand the physiological role of this group of proteins. Only a recent study has shown that one member of Arabidopsis ARID-HMG family, AtHMGB15, is highly expressed in pollen and plays a significant role in pollen tube growth [23]; however, the milieu of roles that might be played by this protein remains unexplored. The advent of ChIP coupled with microarray or sequencing techniques, revolutionized detection of transcription factor binding sites, and aided greatly in gaining insights into their functional roles. In this paper, we are reporting for the first time, about a genome-wide DNA binding study of AtHMGB15. In-silico sequence analysis revealed the presence of stress-responsive element about 500bp upstream of the transcription start site of AtHMGB15 gene. Expression analysis showed that AtHMGB15 is upregulated during various stresses condition, with the maximum upregulation during cold stress. The genome-wide DNA binding study indicates that 6128 loci were significantly enriched in the control data set, whereas 4689 loci were enriched during cold stress response. The genome-wide distribution of AtHMGB15 shows that its occupancy is highly enriched in the euchromatin region with maximum enrichment in gene bodies. Further, in vitro and in vivo DNA binding studies show that AtHMGB15 prefers to bind AT rich sequence with a motif A(A/C)--ATA---(A/T)(A/T). Further, the integration of gene expression data with the AtHMGB15 ChIP-chip results led to the identification of target genes that were differentially regulated under cold stress. Moreover, transcription studies have shown that expression of many known cold responsive genes that have AtHMGB15 occupancy were differentially regulated in AtHMGB15 knockout mutants. Collectively, the genome-wide analysis of AtHMGB15 targets during cold stress response and integration with gene expression led us to the unravelling of previously unexplored aspects of the protein.

Section snippets

Plant material and treatment condition

Arabidopsis thaliana ecotype Columbia (Col-0) seeds, after cold (4°C) stratification, were germinated under 16h light (\sim 150±10 μ molm⁻²s⁻¹) and 8h dark at 22°C on MS Agar plates. 22days old Arabidopsis seedlings were subjected to various stress treatment such as cold, salinity, ABA treatment and dehydration for different time period, according to Yamaguchi-

Shinozaki et al. [24] with some modifications. Briefly, for cold stress treatment, Arabidopsis seedlings were subjected to 4°C...

Expression of AtHMG15 increase during cold stress

AtHMGB15 is an ARID-HMG protein that belongs to the plant HMG-box family. Previous studies from our group have shown that ARID-HMG proteins can bind different DNA topologies through ARID-domain [21]. Expression analysis has indicated that *AtHMGB15* transcripts were highly enriched in flowering tissues, especially in pollen. The tissue specific expression was supported by the presence of multiple binding sites of homeobox transcription factors responsible for flower development at the...

Discussion

AtHMGB15 is a novel plant specific protein containing two DNA binding domains, ARID domain and HMG domain, in a single polypeptide. Recent studies from Xia et al. have elucidated the biological role of AtHMGB15 in pollen biology [23]. The Ds mutant line of AtHMGB15 showed defective pollen morphology and retarded pollen tube growth, indicating a unique niche of the protein in the plant development. To delve deeper into the function of AtHMGB15 *in vivo* and to identify the spectrum of targets...

Data availability

The microarray data sets are available from GEO (Gene Expression Omnibus) under accession number GSE140593....

CRediT authorship contribution statement

SC designed this research; RM performed the ChIP experiments. RM and AK performed DNA binding and footprinting experiments. PP, RM, AK, and SB analysed the ChIP-chip data. AD, RM, JM performed and analysed fluorescence anisotropy data. SC and RM wrote the manuscript. All the authors reviewed and approved the final version of this manuscript....

Declaration of competing interest

The authors have no conflict of interest to declare....

Acknowledgement

The authors would like to thank Dr. Pallob Kundu for showing his generosity by gifting the SELEX library and Dr. Supriyo Chowdhury for his academic inputs for SELEX experiment....

Funding

This work was supported by Council of Scientific & Industrial Research (CSIR), Government of India; Grant Numbers [38(1245)/10/EMR-II] and [38(1365)/13/EMR-II]; Science and Engineering Research Board (SERB), Government of India; Grant Numbers EMR/2017/000768 and Bose Institute, India....

Recommended articles

References (54)

D.J. Tremethick

Higher-order structures of chromatin: the elusive 30 nm fiber Cell (2007)

M.E. Bianchi et al.

HMG proteins: dynamic players in gene regulation and differentiation Curr. Opin. Genet. Dev. (2005)

C.S. Malarkey et al.

The high mobility group box: the ultimate utility player of a cell Trends Biochem. Sci. (2012)

R. Reeves

High mobility group (HMG) proteins: modulators of chromatin structure and DNA repair in mammalian cells

DNA Repair (Amst) (2015)

D. Roy et al.

Rice Trithorax factor ULTRAPETALA 1 (OsULT1) specifically binds to "GAGAG" sequence motif present in Polycomb response elements

Biochim. Biophys. Acta Gene Regul. Mech. (2019)

R. Reeves

Nuclear functions of the HMG proteins

Biochim. Biophys. Acta (2010)

D.L. Lildballe et al.

The expression level of the chromatin-associated HMGB1 protein influences growth, stress tolerance, and transcriptome in Arabidopsis

J. Mol. Biol. (2008)

1. Mizoi et al.

AP2/ERF family transcription factors in plant abiotic stress responses

Biochim. Biophys. Acta (2012)

K. Yen et al.

Genome-wide nucleosome specificity and directionality of chromatin remodelers Cell (2012)

K. Luger et al.

Crystal structure of the nucleosome core particle at 2.8 A resolution Nature (1997)



View more references

Cited by (7)

Whole genome resequencing unveils low-temperature stress tolerance specific genomic variations in jute (Corchorus sp.)

2024, Journal of Genetic Engineering and Biotechnology

Show abstract ✓

AtHMGB15 regulates tapetal apoptosis in pollen development and actin dynamics during pollen germination in arabidopsis ¬

2024, Plant Reproduction

The Functional Analysis of High Mobility Group MsHMG-Y Involved in Flowering Regulation in Medicago sativa L. ¬

HES5-mediated repression of LIGHT transcription may contribute to apoptosis in hepatocytes ¬

2021, Cell Death Discovery

A KDM4-DBC1-SIRT1 Axis Contributes to TGF-b Induced Mesenchymal Transition of Intestinal Epithelial Cells 7

2021, Frontiers in Cell and Developmental Biology

Choline Kinase Alpha Is a Novel Transcriptional Target of the Brg1 in Hepatocyte: Implication in Liver Regeneration ¬

2021, Frontiers in Cell and Developmental Biology



View all citing articles on Scopus ↗

1 Equal contribution.

View full text

© 2020 Elsevier B.V. All rights reserved.



All content on this site: Copyright © 2024 Elsevier B.V., its licensors, and contributors. All rights are reserved, including those for text and data mining, AI training, and similar technologies. For all open access content, the Creative Commons licensing terms apply.

